YCRETS 2023
YOUNG CONCRETE RESEARCHERS, ENGINEERS & TECHNOLOGISTS SYMPOSIUM

CEMENT & CONCRETE SA

PROCEEDINGS OF THE
YOUNG CONCRETE RESEARCHERS, ENGINEERS & TECHNOLOGIST SYMPOSIUM (YCRETS)

Hosted by:

Stellenbosch
UNIVERSITY
IYUNIVESITHI
UNIVERSITEIT

12 – 14 JULY 2023

Young Concrete Researchers,
Engineers and Technologist Symposium (YCRETS)
Proceedings

July, 2023

Edited by:
AJ Babafemi, R Combrinck and W de Villiers

Published by:
Cement & Concrete SA
Tel: +27 (0)11 315 0300
Website: https://www.cemcon-sa.org.za/
Info: info@cemcon-sa.org.za

ISBN: 978-0-9922176-5-5

Following the success of the Young Concrete Researchers, Engineers and Technologist Symposium (YCRETS 2021), which was held virtually due to COVID-19 with 24 published papers, these proceedings contain papers presented at the YCRETS 2023 held at the Jan Mouton Lecture Hall, Neelsie Student Centre, Victoria Street, Stellenbosch University from the 13th to 14th of July, 2023. The purpose of the symposium was to provide a platform for young researchers to discuss recent developments and applications in concrete and cement-based materials in South Africa, and Southern Africa at large. The overaching theme for the conference was Circularity, covering a wide range of sub-themes including innovation (additive manufacturing, artificial intelligence, BIM, etc.), cement-based materials, design (sustainable renovation, repurposing of concrete structures, etc.), analysis (structural analysis of various elements or structures), and durability aspects of concrete structures.

Only selected papers were accepted for presentation at the Symposium. All the papers published in the proceedings with ISBN 978-0-9922176-5-5 were subjected to independent peer review by members of the scientific committee before being accepted. A summary of the technical paper contributions by the participating institutions were as follows: Stellenbosch University 35%; University of Pretoria 13%; University of the Witwatersrand 9%; University of Cape Town 4%; University of KwaZulu-Natal 4%; Joint South African Institutions 17%; Joint South African and International Institutions 13%, Industry 4%.

In addition to the selected technical paper presentations, two guest lectures were also presented at the Symposium. The first lecture, titled "What are we measuring?", was presented by Professor Elsabe Kearsley from the University of Witwatersrand. The second lecture, titled "Waste reuse for sustainable concrete production", was presented by Emeritus Professor Leslie Petrik from the University of the Western Cape.

Special thanks goes to the Local Organsing Committee (LOC), who worked tirelessly to make the Symposium a success. The members of the LOC are:

Gideon Van Zijl - Symposium Chair
John Babafemi - Organising Committee Chair
Wibke De Villiers - Scientific Committee
Riaan Combrinck – Proceedings
Humaira Fataar - Travel & Accommodation
Tata van Rooyen - Conference Day Leader
Hanlie Turner - Marketing & Finance
Natasja Pols - Marketing & Finance

Further, sincere thanks to the Scientific Committee for reviewing and ensuring a high quality of papers. The support of Hanlie Turner and Natasja Pols in planning and organising the symposium is invalauable; thank you so much. Special thanks go to Cement and Concrete SA, the custodians of this event. A special acknowledgement is also extended to the authors and presenters who contributed to the proceedings and the success of the Symposium.

Prof. John Babafemi
Conference Chair
Associate Professor, Department of Civil Engineering
Stellenbosch University, South Africa

Southern Africa has a rich history in concrete materials research and construction, and world leading scholars have emanated from our midst. It is a privilege to gather their and visiting international research students, graduates, young practicing engineers and technicians to subject their findings to scrutiny and debate at the 2023 edition of YCRETS.

This Proceedings contains research, technical and review paper contributions by authors from sixteen universities and industries in Southern, West and East Africa. The contributions reflect that circularity in construction is a common vision within the symposium themes of innovation, materials, durability and design. Innovative tests, materials, construction methods and reliability considerations are presented not only for the sake of novelty, but with the intention of enabling maximum inclusion of materials from waste streams as filler, binder, precursor and activator materials. In the Materials theme, the use of waste streams is proposed and appropriate cement-based material technology is presented for the use of construction and demolition waste in concrete and masonry units, and nanotechnology for treatment of waste water as mixing water in concrete. The durability theme comprises of contributions on permeation reducing admixtures, carbonation prediction and chloride-induced corrosion monitoring, and principles of durable over high strength concrete repair materials. Anchor system design, consideration of sustainability in structural reliability design, and a case study of a large concrete hydro power plant structure are presented under the design theme.

All the papers included in the Proceedings have been blind reviewed by members of the Scientific Committee, representing an international panel of academic and industry experts.

The Chairperson of the first YCRETS in 2021, Professor Yunus Ballim, remarked that "cement-based materials will continue to be of dominant use in infrastructure construction. However, this does not mean that these materials can continue to be used in the same manner, mainly because of their significant negative environmental impacts". The young author contributions of YCRETS 2023 heed his assertion in exploiting vast waste streams, confirming their potential status as commodities in a circular economy and greening of concrete. This demands multi-disciplinary research collaboration, reflected in this Proceedings by co-authorship from subject fields in chemical, civil, environmental, fire, mechanical and aeronautical, mining and structural engineering and information technology. Key fields of chemistry and civil engineering are represented by keynote speakers Emeritus Professor Leslie Petrik of the Department of Chemistry at the University of the Western Cape, and Professor Elsabe Kearsley of the Department of Civil Engineering at the University of Pretoria.

Professor Gideon van Zijl, July 2023

Prof Mark Alexander – UCT

Prof John Babafemi – SU

Prof Yunus Ballim – Wits

Prof Hans Beushausen – UCT

Prof Billy Boshoff – UP

Prof Suvash Chandra Paul – International University of Business, Agriculture and Technology, Bangladesh

Dr Seung Cho – SU

Prof Riaan Combrinck – SU

Dr Wibke de Villiers – SU

Dr Grizelda du Toit – AfriSam

Prof George Fanourakis – UJ

Dr Humaira Fataar – SU

Dr Reza Hassanli – UNISA

Miss Janina Kanjee – Wits

Dr Muzafalu Kayondo – Uganda Electricity Generation Company

Prof Elsabe Kearsley – UP

Dr John Kolawole – Loughborough University, UK

Dr Jacques Kruger – SU

Mr Mike McDonald – AfriSam

Dr Christina McLeod – UKZN

Prof Mike Otieno – WITS

Mr Bryan Perrie – CCSA

Prof Leslie Petrik – UWC

Prof Manu Santhanam – Indian Institute of Technology, Madras

Dr Tata van Rooyen – SU

Prof Gideon van Zijl – SU

YCRETS 2023
YOUNG CONCRETE RESEARCHERS, ENGINEERS & TECHNOLOGISTS SYMPOSIUM
CEMENT & CONCRETE SA

A proposed pendulum impact test method for UHPFRC

Jurie F. Adendorff (1), Elsabe P. Kearsley (1) and Abrie J. Oberholster (2)

(1) Department of Civil Engineering, University of Pretoria

(2) Department of Mechanical and Aeronautical Engineering, University of Pretoria

Abstract

The present study aims to develop a pendulum impact test method to determine the impact resistance of Ultra-High-Performance Fibre-Reinforced Concrete (UHPFRC). Different impact test methods were investigated, and their shortcomings were identified. These shortcomings include, but are not limited to, energy absorbed by the test instrument and inertial effects of the test specimen. The proposed test method has been designed to address these shortcomings in determining the impact resistance of UHPFRC. Measuring equipment was used to further extend the capabilities of the test method. An accelerometer was used to record an acceleration time-history of the impact event at 96 kHz. Furthermore, high-speed photography (7 600 fps) was used for motion tracking and Digital Image Correlation (DIC).

Keywords: Impact resistance, Loading rate, Pendulum impact, Test method, UHPFRC

1. INTRODUCTION AND BACKGROUND

Ultra-High-Performance Fibre-Reinforced Concrete (UHPFRC) is known for its enhanced mechanical properties [1] and is therefore considered a potential option for the construction of structures subjected to severe loading conditions such as vehicular impacts due to its ability to absorb energy and remain ductile [1]. Despite this and the fact that it has long been known that concrete is a strain-rate sensitive material [2], the dynamic mechanical properties of UHPFRC is not yet well understood [2]. This stems from a lack of standardised test methods [2] which hinders the progress in understanding the dynamic mechanical properties of UHPFRC. It is therefore important to develop relevant test methods that enable standardisation and promote research progress.

Existing test methods developed to test materials at different strain rates are shown in Figure 1, along with their strain rate ranges and associated real-life applications. Different test methods are used to apply rapid loads (impacts) to test specimens. These methods include the use of gravity through drop-weight and pendulum impact tests, hydraulic machines and stress waves using the Split-Hopkinson Pressure Bar (SHPB).

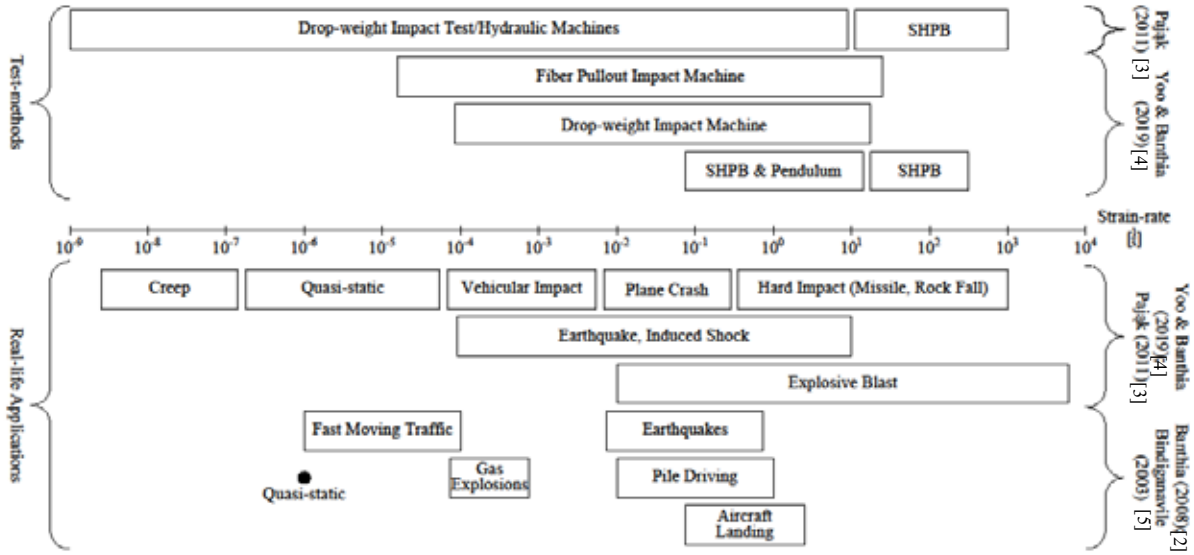

Figure 1: Strain rates of impact testing methods and their associated real-life applications (adapted from [6])

The drop-weight impact test method is the most common impact test method and makes use of a free-falling mass to rapidly apply a load to a test specimen. A comparison of the number of drops required to attain a predetermined failure criterion can be used to interpret the data. It is also possible to install instrumentation on the mass, test specimen, and supports [10, 11]. The rate of load application is directly proportional to the height from which the mass is allowed to fall.

The advantages of this test method are attributed to its simplicity, which facilitates its implementation and makes it less expensive than other testing methods [7]. ACI Committee 544 has recognized the drop-weight impact test method described in ACI 544.2R-89 as a standardized test method for the impact testing of Fibre-Reinforced Concrete (FRC) [8]. However, the simplicity of the test method introduces some limitations, the primary being the rebound effect, which generates a secondary impact when the test specimen does not fail under the initial impact [13, 14]. Without instrumentation, the additional load caused by the secondary impact cannot be measured. Furthermore, when failure of the test specimen occurs it is difficult to determine the amount of energy absorbed by the test specimen without instrumentation, since the free-falling weight retains residual energy after impact. Furthermore, Abid et al. [7] found that a minimum of 55 test specimens are required for the ACI 544-2R test procedure to gain a 90 % level of confidence in the test results. Finally, the ACI 544-2R test procedure is not practically suited for testing FRC and UHPFRC since an excess of 1 000 blows may be needed for a test specimen to reach the “first-crack” [9] or failure criteria [7, 9, 12]. Ramakrishnan et al. [9] discarded further attempts to test fibre-reinforced shotcrete test specimens (thickness of 76 mm) until failure due to the large number of blows needed to reach the “first-crack” criteria. Other limitations include the influence of boundary conditions and inertial resistance of the test specimen which may lead to over-estimations of the impact resistance [10].

Another common impact test method is the pendulum impact test method which involves a weighted hammer attached to an arm that moves in a circular motion prior to striking the test specimen. Similar to the drop-weight impact test method, the rate of load application is directly proportional to the height from which the mass is allowed to fall. Although this test method was originally intended for testing metals, several authors have successfully used modified versions of these tests on concrete [13-16, 17, 18]. The test method is versatile since different configurations may be used to test different mechanical properties of concrete such as flexural strength (beams [13-15] and plates[16]), direct tensile strength [17] and fibre pull-out strength [18]. The data obtained from this test method can be interpreted by similar means as the drop-weight impact test method and also allows for the use of instrumentation [13-16, 17, 18]. The pendulum impact test offers significant benefits such as eliminating the rebound effect [13, 14, 16], providing easy instrumentation [13, 18] and allowing adjustments to the impact energy and sample geometry. Despite these advantages, the main limitation of the pendulum impact test method is to consider the influences of boundary conditions and inertial resistance of the test specimen as to not over-estimate the impact resistance [13, 17, 18]. A futher limitation is the energy absorbed by the test instrument caused by the difference in stiffness between the test instrument and test specimen [15, 19]. Bluhm [19] argued that the pendulum should be sufficiently stiff in order to reduce the elastic energy stored in the pendulum. Gopalaratnam et al. [15] further suggested that the adverse effects of test specimen inertia may be limited by ensuring a large difference in mass between the pendulum and test specimen in conjunction with a large difference in stiffness. These limitations, however, are applicable to all impact test methods and not only the pendulum impact test method.

Other impact test methods include the projectile impact test method [20] (of which the limiting factors are safety and the need of equipment able to achieve very high data sampling rates), impact testing by means of servo-hydraulic machines [6] (of which the main limiting factor is the cost of the machine), the SHPB impact test method (which has several limitations such as test specimen size [13], the lateral inertial confinement effect [21] and boundary conditions [22]) and the fibre pull-out test method, where no correlation between a single-fibre pull-out test and beams tested under impact loads could be found. This has been attributed to the fact that a single-fibre pull-out test does not consider fibre orientation, nor fibre-to-fibre interaction [4].

In summary, the main limitations that adversely affect all impact test methods are test setup stiffness and test specimen inertia. Other limitations are test repeatability and reliability, cost, safety and practical applicability. The main objective of this study is to propose a pendulum impact test method that has been purposely designed to take into account these limitations. A direct comparison has been made between the proposed pendulum impact test method and the drop-weight impact test method specified in ACI 544.2R-89. This is due to the gravity-driven nature of both the test methods and similarities in their application. Both test methods apply a similar range of kinetic energy at similar impact velocities. It is important to note that the strain rate experienced by a test specimen is directly proportional to the impact velocity. Therefore, it would be unfair to compare these two test methods to other test methods such as the projectile impact test method.

2. DESIGN AND SETUP OF THE PROPOSED PENDULUM IMPACT TEST DEVICE

The setup of the proposed pendulum impact device is shown in Figure 2. The overall setup of the device and position of the high-speed cameras are shown in Figure 2 (a). Figure 2 (b) shows the setup and alignment of the test specimen perpendicular to the pendulum impact hammer, whereas Figure 2 (c) indicates the position of the accelerometer on the back end of the impact hammer.The pendulum arm consists of a 2 m piece of IPE 100 that rotates about two pillow block bearings attached to a frame connected to a 500 mm thick reinforced concrete wall. Additional plates were added at the bottom of the pendulum arm so that the total mass of the arm equals 50 kg. The plates were configured such that the centre of mass of the pendulum arm is aligned with the tup. This is to avoid introducing additional moments to the test specimen during impact.

The test specimen is supported at the ends by adjustable brackets attached with thin wires to the overhead frame. This assembly has a mass of approximately 3 kg, resulting in a pendulum arm to test specimen ratio of 16.67. By performing modal analyses of the test specimen support assembly it was found that the natural frequency of the assembly was reduced by a factor of 2.14 due to the mass of the brackets at the ends of the test specimen and due to the test specimen hanging from wires when compared to a test specimen that is traditionally simply supported. From the dynamic calculations performed by Gopalaratnam et al. [15], a reduction of the natural frequency of the test specimen results in an increase in the ratio of stiffness between the pendulum and test specimen for a constant pendulum stiffness. From the calculations it can further be deduced that the stiffness ratio has a larger influence on the over-estimation of the impact resistance of the test specimen. Therefore, it is expected that more reliable results may be obtained during testing since the pendulum is expected to store less elastic energy and the test specimen is expected to give less inertial resistance.

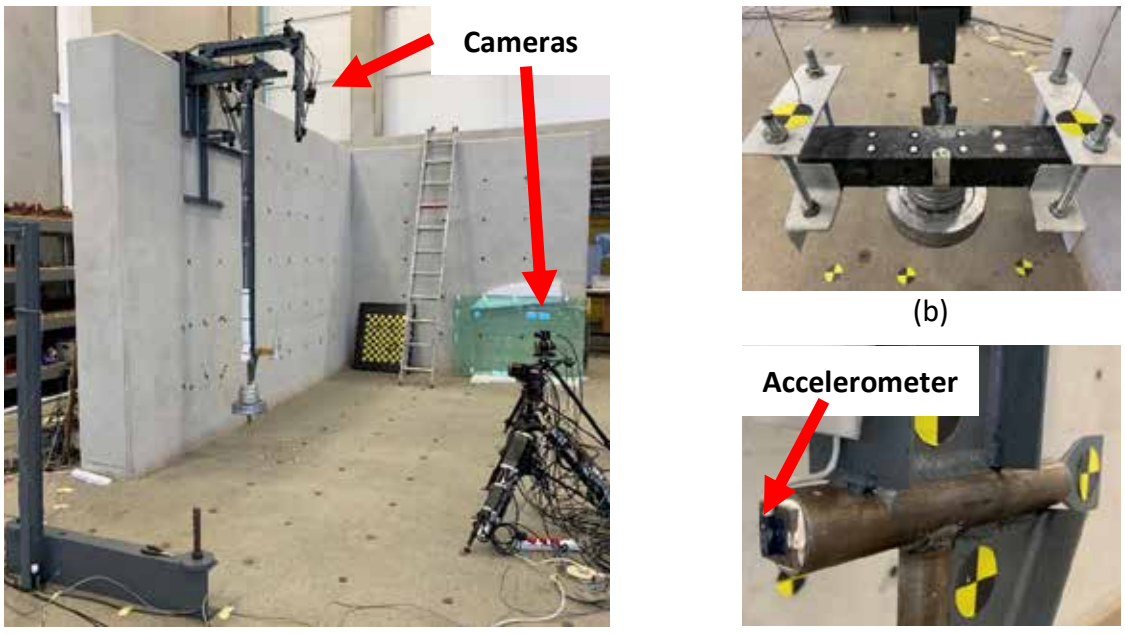

(a) (b) (c)

Figure 2: Setup of the proposed pendulum impact test device

3. EXPERIMENTAL PROGRAM AND TEST RESULTS

3.1 Mixture Design and Quasi-Static Mechanical Properties

The mixture of UHPFRC considered for the study is shown in Table 1. The table also displays the Relative Densities (RD) of the materials. The materials used were a CEM I 52.5R, undensified silica fume (USF), unclassified fly ash (FA), water, Dolomite stone (≤ 9.50 mm), Dolomite sand (≤ 4.75 mm), a superplasticiser and 2 % (by volume) hook-ended steel fibres. The steel fibres had a length of 30 mm and diameter of 0.50 mm and a tensile strength of 1 500 MPa. A total of ten 100 mm cubic test specimens were cast to determine the compressive strengths of the mixture in accordance with SANS 5863:2006. Three 200 mm x Ø100 mm cylindrical test specimens were cast to determine the modulus of elasticity and Poisson's ratio in accordance with ASTM C469. The cylindrical test specimens were cut in half in order to determine the splitting tensile strength in accordance with SANS 6253:2006. Lastly, three beams of 500 x 100 x 100 mm in dimension were cast to determine the modulus of rupture in accordance with SANS 5864:2006. The mean values of the quasi-static mechanical properties are shown in Table 2.

3.2 Proposed Pendulum Impact Test Method Results

Figure 3 displays the results of the impact tests performed at various fall heights. From the figure it can be seen that an exponential decrease in the number of blows were needed for the test specimen to reach failure with an increase in the fall height. A p-value test was performed on the pearson product-moment correlation coefficient between the fall height and the logarithm of the number of blows. A p-value of less than 0.05 was achieved and therefore the results were deemed to be statistically significant. Merely four test specimens were required per fall height (which resulted in 16 test specimens in total) required to obtain statistically significant data as opposed to the 55 test specimens required as proposed by Abid et al. [7]. Furthermore, it is clear from the figure that significantly less blows were needed for the test specimen to reach failure as opposed to that of the ACI 544.2R-89 drop-weight impact test. The proposed pendulum impact test method required a maximum of 30 blows for the test specimen to reach failure at the lowest fall height as opposed more than 1 000 blows required by the ACI 544.2R-89 drop-weight impact test. It can also be seen that with an increase in fall height, a decrease in dispersion of the results occurred.

Figure 4 shows an example of the acceleration time-history of an impact event obtained by the accelerometer placed on the proposed pendulum impact test device. The acceleration time-history of an impact event may be analysed by means of Fast-Fourier Transformation (FFT), Response Spectrum Analysis (RSA), or by generating an Euler characteristic curve followed by a Principal Component (PC) analysis in order to distinguish between different impact events or to determine the associated strain rates and energy absorbed by the test specimen.

Figure 5 displays the capabilities of using high-speed photography. Capturing images at 7 600 fps enables detailed observations to be performed as can be seen in Figure 5 (a). With the use of software such as TEMA [23] it is possible to perform motion analyses and Digital Image Correlation (DIC). From Figure 5 (a) it can be seen that the movement of the test

specimen during the impact event can be accurately tracked, which gives rise to a multitude of calculation possibilities such as calculating deflections, rate of change of deflection, rotation of the test specimen about it's supports, etc. This can further be extended with DIC which allows for the calculation of strains and therefore strain rate. From Figure 5 (b) it can be seen how the change in strain in the test specimen occurred during the impact event. The blue colour indicates a strain of approximately zero whereas the red indicates tension. As soon as the tup of the pendulum makes contact with the test specimen it can be seen that a tension zone develops at the opposite side of the test specimen.

Table 1: Mixture design

Material	**RD**	**Mixture [kg/m³]**
CEM I 52.5R	3.14	542
Undensified silica fume	2.45	146
Unclassified fly ash	2.22	146
Water	1.00	146
Dolomite stone ≤ 9.50 mm	2.85	251
Dolomite sand ≤ 4.75 mm	2.91	1 240
Superplasticiser	1.06	25.6
Hook-ended steel fibres	7.85	149
Theoretical density		2 646

Table 2: Quasi-static mechanical properties

Property	**No.**	**Mean**
Compressive strength [MPa]	10	167.8
Modulus of elasticity [GPa]	3	54.6
Poisson's ratio	3	0.146
Splitting tensile strength [MPa]	6	15.2
Modulus of rupture [MPa]	3	20.1

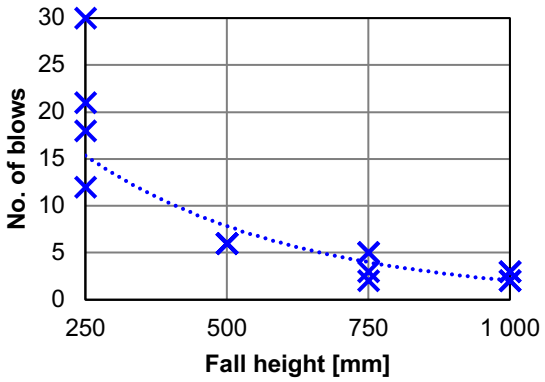

Figure 3: Number of blows required to reach failure at each fall height

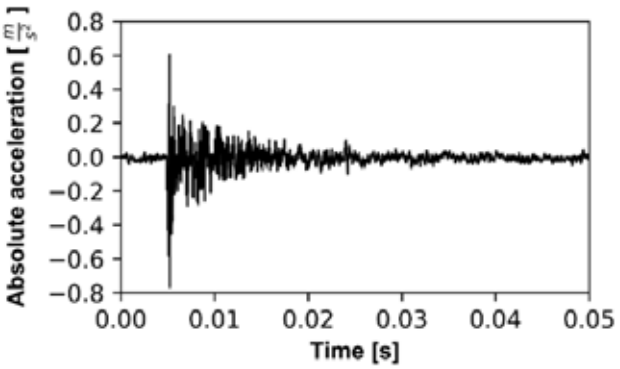

Figure 4: Acceleration time-history of an impact event

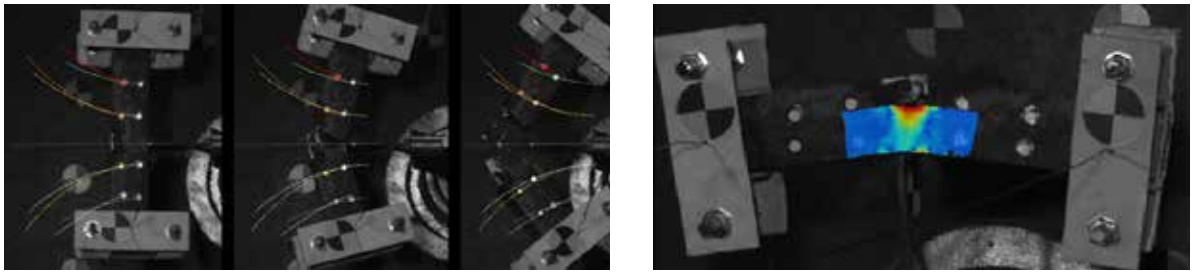

(a) (b)

Figure 5: Capabilities of high-speed photography

4. CONCLUSIONS AND RECOMMENDATIONS

From the test results it can be confirmed that the design and setup of the proposed pendulum impact test method has sufficiently addressed the following limitations:

- By changing the boundary conditions of the test specimen, the stiffness ratio between the pendulum and test specimen was increased, resulting in a decrease in inertial resistance of the test specimen and reducing the energy absorbed by the pendulum.
- Significantly less number of blows was needed for the test specimens to reach failure as opposed to the ACI 544.2R-89 drop-weight impact test.
- Significantly fewer test specimens need to be tested to obtain statistically significant test results as opposed to the ACI 544.2R-89 drop-weight impact test.
- The proposed pendulum impact test method does not suffer from the rebound effect.
- The proposed pendulum impact test method can easily be instrumented and adjusted or modified and is therefore more versatile than the ACI 544.2R-89 drop-weight impact test.

It is, however, recommended that tests should be conducted on UHPFRC mixtures that have different volumes of steel fibres in order to ensure that the proposed test method is able to differentiate between the mixtures. It is further recommended that the data obtained from the accelerometer and high-speed photography be properly analysed and compared to verify that they are able to produce reliable and reproduceable results that correspond with one another.

REFERENCES

[1] Othman, H., Marzouk, H. & Sherif, M., “Effects of variations in compressive strength and fibre content on dynamic properties of ultra-high performance fibre-reinforced concrete” *Construction and Building Materials* **195** (2019) 547-556.

[2] Banthia, N., “Enhancing impact and blast resistance of concrete with fiber reinforcement”, in “Resilience of Cities to Terrorists and Other Threats”, NATO Science for Peace and Security Series C: Environmental Security, North Atlantic Treaty Organisation, Moscow, 2008, 171-187.

[3] Pająk, M., “Dynamic response of SFRC under different strain rates – An overview of test results”, in “7th International Conference, Analytical models and new concepts in concrete and masonry structures”, AMCM2011, Kraków, 2011.

[4] Yoo, D-Y. & Banthia, N., “Impact resistance of fiber-reinforced concrete – A review”, *Cement and Concrete Composites* **104** (2019) 103389.

[5] Bindiganavile, V., "Dynamic Fracture Toughness of FRC", PhD Thesis, The University of British Columbia, Canada, 2003.
[6] Adendorff, J., "A constitutive model for the dynamic tensile behaviour of UHPFRC", Masters' Dissertation, University of Pretoria, South Africa, 2002.
[7] Abid, S., Hussein, M., Ali, S. & Kazem, A., "Suggested modified testing techniques to the ACI 544-R repeated drop-weight impact test", *Construction and Building Materials*, **244** (2020) 118321.
[8] American Concrete Institute, *ACI 544.2R-89, "*Measurement of Properties of Fiber Reinforced Concrete", ACI Committee 544, USA, 1999.
[9] Ramakrishnan, V., Coyle, W., Dahl, L. & Schrader, E., "A comparative evaluation of fiber shotcretes", *Concrete International*, **3** (1981) 59-69.
[10] Suaris, W. & Shah, S., "Inertial effects in the instrumented impact testing of cementitious composites" *Cement, Concrete, and Aggregates*, **3** (1982) 77-83.
[11] Banthia, N., Mindess, S. & Bentur, A., "Impact behaviour of concrete beams" *Materials and Structures*, **20** (1987) 293-302.
[12] Al-Abdalay, N., Zeini, H. & Kubba, H., "Effect of impact load on SIFCON" *Global Journal of Researches in Engineering*, **19** (2019) 17-27.
[13] Máca, P., Sovják, R. & Konvalinka, P., "Impact testing of concrete: the measurement device", in "International Conference on Advances in Civil, Structural and Mechanical Engineering – CSME 2014", Institute of Research, Engineers and Doctors, Hong Kong, 2014, 63-67.
[14] Li, P. & Yu, Q., "Responses and post-impact properties of ultra-high performance fibre reinforced concrete under pendulum impact" *Composite Structures*, **208** (2019) 806-815.
[15] Gopalaratnam, V., Shah, S. & John, R., "A modified instrumented charpy test for cement-based composites" *Experimental Mechanics*, **24** (1984) 102-111.
[16] Yu, R., van Beers, L., Spiesz, P. & Brouwers, H., "Impact resistance of a sustainable Ultra-High Performance Concrete (UHPC) under pendulum impact loadings" *Construction and Building Materials*, **107** (2016) 203-215.
[17] Banthia, N., Mindess, S. & Trottier, J-F., "Impact resistance of steel fiber reinforced concrete" *ACI Materials Journal*, **93** (1996) 472-479.
[18] Pacios, A., Ouyang, C. & Shah, S., "Rate effect on interfacial response between fibres and matrix" *Materials and Structures*, **28** (1995) 83-91.
[19] Bluhm, J., "The influence of pendulum flexibilities on impact energy measurements", in "STP 176-EB Symposium on Impact Testing", ASTM International, West Conshohocken, 1956, 84-93.
[20] Adendorff, J. & Kearsley, E., "The influence of fibre reinforcement on the ballistic resistance of concrete", in "Proceedings of the Young Concrete Researchers, Engineers & Technologist Symposium", Johannesburg, South Africa, 2021, 132-139.
[21] Lv, T., Chen, X. & Chen, G., "Analysis on the waveform features of the split Hopkinson pressure bar tests of plain concrete specimen" *International Journal of Impact Engineering*, **103** (2017) 107-123.
[22] Ren, L., Yu, X., Guo, Z. & Xiao, L., "Numerical investigation of the dynamic increase factor of ultra-high performance concrete based on SHPB technology", *Construction and Building Materials*, **325** (2022) 126756.
[23] *Tema Pro – advanced motion and deformation analysis: ISAB (2022) Image Systems – TEMA and TrackEye, motion analysis*. Available at: https://imagesystems.se/tema-pro/ (Accessed: 3 March, 2023).

YCRETS 2023
YOUNG CONCRETE RESEARCHERS, ENGINEERS & TECHNOLOGISTS SYMPOSIUM

CEMENT & CONCRETE SA

Geo-polymerization of mining tailing for use as a pavement construction material – a review

Gbenga Aderinto (1), Jacob Ikotun (1,2), and Valentine Katte (3)

(1) Department of Civil Engineering, Durban University of Technology, Pietermaritzburg, South Africa

(2) Department of Civil and Mining Engineering, University of Namibia, Namibia

Abstract

Pavement construction usually involves using large quantities of natural aggregate materials majorly extracted from quarries and, in many cases, with the use of conventional stabilizers such as Portland cement, lime, and bitumen. In many developing countries, the exploitation of quarries has been so massive that there exists a shortage of these aggregates. Hence, the use of conventional stabilizers is a common practice. However, the use of conventional stabilizers is a major source of environmental contamination for the environment. Therefore, alternative aggregate materials and stabilization techniques in pavement construction are highly sought after. Recently, some researchers have proposed a new approach as an alternative to using conventional binders via alkali activation called geo-polymerization to produce geopolymers. Some studies have shown that mine tailings (MT) can be used as a road base material through geopolymerization. Even though there are different types of tailings, specific interest is on copper, iron, and gold tailings, this is due to their dominance in mining areas of South Africa. This paper presents a review of the mechanical properties of geopolymerized tailings to enhance understanding of their potential application in sustainable infrastructures, such as pavements.

Keywords: Geopolymerization, pavement, mine tailings, mechanical strength, stabilization.

1. INTRODUCTION

Pavements are structures designed to withstand traffic loads and are composed of several layers made up of natural aggregate materials such as sand, cobblestones, and laterites. The functionality of the pavement is determined by the geotechnical properties of these aggregates and binding materials. Pavement construction requires a large quantity of natural aggregate materials, with an average of 20,000 tons of aggregate needed for every kilometre of the roadway [1]. Around 90% of the aggregates used in pavement construction are either virgin or sourced directly from quarries [1]. Developing nations are already experiencing a shortage of high-quality natural aggregate materials. This scarcity poses a significant challenge to the construction and

maintenance of pavements, which are vital to transportation infrastructure. In areas facing a shortage of natural construction materials, two options exist: finding new quarries or using conventional stabilizers like Portland cement (OPC) and lime to enhance the mechanical properties of low-grade materials like soils and mine tailings (MT). However, the use of these stabilizers has significant environmental consequences, including high energy consumption and emission of greenhouse gases [2].

Mine tailings are waste materials generated during the extraction, chemical, and physical treatment of mineral ores, and the mining industry produces vast amounts of them annually [3]. In South Africa, over 315 million tons of tailings are generated every year, with gold tailings accounting for 105 million tons [4], it was also stated that copper tailings in South Africa occupied a large surface area of land [5-6]. The properties of tailings vary depending on the type of mineral ore and the compounds they contain, such as silicon, aluminium, quartz, pyrite, lead, and uranium. Although tailings are considered useful for geopolymerization due to their fine particle sizes, high Silica (Si) and Aluminium (Al) content. However, they contain toxic elements/metals, in the form of chlorides or sulphate solutions [1, 5]. Due to the existence of hazardous materials in tailings, they cannot be utilized in civil construction projects. Therefore, tailings are required to be reprocessed into less hazardous waste before disposal or reuse for construction purposes [8]. Disposing of mine tailings is costly and can result in various environmental problems such as land use, air pollution, water bodies contamination, and tailings dam failures [9].

Geopolymerization of MT offers sustainable and eco-friendly solutions to environmental problems caused by mine tailing disposal. This process involves the chemical reaction of alumino-silicates materials in an alkaline solution, creating a geopolymer material. Geopolymers offer several advantages over conventional stabilizers, including rapid strength development, acid resistance, immobilization of toxic metals, reduced energy consumption, and greenhouse gas emissions [10-12]. As a result, geopolymer has been identified as a potential alternative construction material, with some researchers studying its potential use in road construction.

2. TYPES OF MT AND THEIR PROPERTIES

Tailings from various minerals have been used as substitutes for aggregate materials in road construction, with iron, copper, coal, tungsten, granite, and gold being the most used types [9]. These tailings are predominantly sand-sized ranging from 28% to 70%, and fall under the ML, SM, and SP categories of the Universal Soil Classification System (USCS), [13-16]. The geotechnical properties of tailings are determined by their mineral composition and collection location [9]. Tables 1 and 2 summarize the geotechnical and chemical properties of various types of tailings.

Table 1. Geotechnical properties of various types of MT

Types of MT	Specific gravity	Liquid limit (%)	Plastic limit (%)	Plasticity index (%)	Maximum Dry Density (KN/m^3)	Optimum Moisture Content (%)	Sand size (%)	Finer than micron (%)	USCS	Ref
Iron	3.08 - 3.74	28	19	9	_	_	_	_	_	[17] [18]
Copper	2.72 - 2.82	25.2 – 28	11.5 - 13	13.7 -15.	16.7 -16.9	13.3 -16.0	43-55	45 -57	SC	[15] ,
Gold	2.78 - 2.86	44.0	_	Non-plastic	15.7 -17.0	17 -22.5	17-28	72 -83	ML	[15] ,
Coal	2.03	_	_	Non-plastic	15.5	12.0	70	15	SM	[20]
Bauxite	3.00	37	33	4	_	_	3	30	ML	[21]

ML: Low plasticity silts
SM: Silty-sand mixtures
SP: Poorly- graded sands

Table 2. Chemical Composition of various types of MT

Types of MT	AlO_3	SiO_2	Na_2O	SO_3	K_2O	Fe_2O_3	MgO	CaO	MnO	Ref.
Iron	3.36 - 3.40	41.95 - 45.64	0.41	_	0.61	31.32-47.70	_	_	_	[22], [23]
Copper	13.96 - 14.10	55.90 - 71.52	3.02 - 4.12	2.22	1.82 - 3.89	3.07 - 3.64	0.49 - 1.78	0.16-2.27	0.06 - 0.07	[16], [24]
Gold	15.05	60.40	_	0.30	0.40	6.60	1.70	6.90	_	[24]
Bauxite	14.00	1.20	_	_	_	30.90	_	2.50	1.70	[25]
Tungsten	14 - 16.66	53 - 55.60	0.62	3 - 5.80	3.5 - 7.6	12.33 - 14.60	1.27	_	_	[26]

3. STABILIZATION OF MT THROUGH GEOPOLYMERIZATION

Previous studies have documented the use of conventional stabilizers to stabilize MT [15, 17-20]. However, these stabilizers have significant drawbacks such as high energy consumption and the emission of large amounts of carbon dioxide (CO_2) during manufacturing. In 2016, the production of OPC accounted for nearly 8% of global CO_2 emissions [21]. As a result, there is a pressing need for more environmentally sustainable MT stabilization methods.

Researchers have studied the stabilization of different MTs alone or in integration with other materials based on geopolymerization [9,22-25,28-36]. These indicate the possibility of

geopolymerized tailings being used in construction based on their mechanical strength: Unconfined Compressive Strength (UCS) in accordance with the aggregate material specifications for road construction in different countries. Table 3. summarizes the UCS required by the standards of several countries for cement-treated materials in road base and subbase layers. So far, only a few researchers have investigated the geopolymerization of MT as a road base construction material. Tables 4 and 5 show the stabilization of MT with conventional stabilizers and through geopolymerization MT.

Table 3. Requirements for cement-treated materials as road base/subbase in different countries.

Country	Stabilizer OPC content (%)	7-day UCS (MPa) – (base/subbase)
South Africa	1.5 – 3.0	1.5 – 3.0 (base)
United Kingdom (UK)	2 – 5.0	2.5 – 4.5 (base)
China	> 4 (road-mix method) > 5 (central-plant mixing)	> 2 (subbase), > 4 (base)
Spain	3.5 – 6.0	4.5 – 6.0 (base)
U.S.A	3 - 10	1.03 – 2 .75 (base) [26] 2.06 – 5.51 (base) [27]

Table 4. Stabilization of MT with conventional stabilizers.

No.	Waste material (wt.%)	Grain size	Stabilizer	Curing Condition	Test conducted	UCS (MPa)	Ref.
1	Copper MT (100%)	1.0 - 0.001 mm, 41% passing No. 200 sieve (0.0075 mm)	OPC (2-12%)	At ambient temperature: OPC: for 7, 28, and 90 days.	UCS, tensile, and shear strength	3.45 (8% OPC) – 7 days	[28]
2	Kimberlite MT	0.075- 0.020 mm	OPC (5%)	Cured in moisture sand for 7 and 28 days	CBR and UCS	1.33 (7 days), 2.05 (28 days)	[29]
3	Granite MT	97% < 4.75 mm	OPC (3-6%)	Ambient temperature for 7, 28, and 90 days	UCS, drying shrinkage	4.37, 6.39, and 7.17 (5% OPC), 7, 28, and 90 days	[30]
4	Iron MT (90- 99%)	85% < 0.075 mm	OPC (1-10%)	for 7 days;	UCS, CBR,	1.32 (5% OPC)	[31]
5	Gold MT (93- 97%	28% < 0.425, mm 71% < 0.075 mm	OPC (3-7%	Mixtures were placed in a humid room at 23 ±2˚C for 7 days	UCS, pulse velocity test	1.8 (7% OPC)	[32]
6	Iron MT (0- 10%)	< No. 200 sieve	OPC (1-4%)	7- and 28-day curing	UCS	-	[33]

Table 5. MT improved through geopolymerization.

No	Waste material (wt.%)	Grain size	Alkali activator	Curing condition	Test conducted	UCS (MPa)	Ref.
1	Copper MT (100%)	100%< 0.420 mm	NaOH (0, 3, 5, 7, and 11 M)	Oven at 35^0C for 7 days	UCS, SEM	5.32 (11 M (NaOH)	[9]
2	Copper MT (100%)	36%< 0.075 mm	NaOH (0- 6%)	Ambient temperature for 7 days	UCS, SEM	2.5 (2% NaOH)	[34]
3	Tungsten MT (100%)	100%< 2 mm	-	-	Los Angeles abrasion test and freeze-thaw resistance	-	[35]
4	Gold MT (100%)	74% < 0.075 mm	Na_2SiO_3	8, 14, 21, and 28 days at room temperature	UCS	30(8% of Na_2SiO_3)	[9]
5	Copper MT	100%< 0.420 mm	NaOH (5, 10, 15 M)	ambient temperature for 4 days	UCS	4.4(10 M)	[36]

4 DISCUSSION

The lack of quality natural construction materials and the disposal problem associated with MT prompted the interest of researchers in the field of transportation engineering to find an alternative solution. These reviews showed that geopolymerized MT as an alternative material for road construction has good mechanical properties compared to construction materials being stabilized with conventional stabilizers. The research on the unconfined compressive strength (UCS) of geopolymerized MT is the common variable stipulated by different standards. In terms of (UCS), the standards presented in Table 3 and the 7-day UCS values by the studies listed in Tables 4 and 5 are compared, it was observed that geopolymerized MT conforms to the specifications of various countries, indicating the feasibility of MT as a suitable aggregate material for road construction. As with any waste, the use of MT for pavement construction should incorporate environmental considerations such as leachate of toxic metals/elements and durability for long-term use. The standards related to the use of wastes as alternative aggregate materials in construction are limited.

5. CONCLUSIONS

As a result of systematic reviews on the use of geopolymerized MT as a material for road construction, the following conclusions have been derived:

• The most significant benefit of geopolymerization is the use of a variety of industrial by-products as the basic raw materials in their composition.

• Geopolymerized MT has good compressive strength suitable for road construction.

• Geopolymerized MT represents an important step towards sustainability since conventional stabilizers are characterized by high energy consumption levels and leave a large carbon footprint (the geopolymerized binder effuses 80% less CO_2 than Ordinary Portland cement) [37].

• In addition, the utilization of industrial by-products in the geopolymerization allows waste to be recycled and lowers the surface area of landfill space required while simultaneously supporting environmental conservation.

Despite the general acceptance of Ordinary Portland cement, geopolymerization has the potential to revolutionize cement production due to its advantages. However, insufficient information is evident in some areas of geopolymerization, which necessitates further research. Thus, more studies are needed to understand the compressive strength of geopolymerized tailings with multiple precursors and their behaviour under both laboratory and field conditions.

REFERENCES

[1] Sherwood, P.T., 1995. *Alternative materials in road construction*.

[2] Pacheco-Torgal, F., 2015. Introduction to handbook of alkali-activated cements, mortars, and concretes. In *Handbook of alkali-activated cements, mortars, and concretes* (pp. 1-16). Woodhead Publishing.

[3] Edraki, M., Baumgartl, T., Manlapig, E., Bradshaw, D., Franks, D.M. and Moran, C.J., 2014. Designing mine tailings for better environmental, social, and economic outcomes: a review of alternative approaches. *Journal of Cleaner Production*, *84*, pp.411-420.

[4] Grace, O.M., Simmonds, M.S., Smith, G.F. and van Wyk, A.E., 2009. Documented utility and biocultural value of Aloe L. (Asphodelaceae): a review. *Economic Botany*, *63*(2), pp.167-178.

[5] Mhlongo, S.E., Makatu, F.L., Malaza, N.K. and Ramalata, A.T., 2022. Evaluation of copper tailings from the abandoned Messina Mine for possible reuse in recreational projects, South Africa. *Journal of Degraded and Mining Lands Management*, *9*(2), pp.3359-3366.

[6] Gitari, W.M., Thobakgale, R. and Akinyemi, S.A., 2018. Mobility and attenuation dynamics of potentially toxic chemical species at an abandoned copper mine tailings dump. *Minerals*, *8*(2), p.64.

[7] Koch, J., Chakraborty, S., Li, B., Kucera, J.M., Van Deventer, P., Daniell, A., Faul, C., Man, T., Pearson, D., Duda, B. and Weindorf, C.A., 2017. Proximal sensor analysis of mine tailings in South Africa: An exploratory study. *Journal of Geochemical Exploration*, *181*, pp.45-57.

[8] Adiansyah, J.S., Rosano, M., Vink, S. and Keir, G., 2015. A framework for a sustainable approach to mine tailings management: disposal strategies. *Journal of cleaner production*, *108*, pp.1050-1062.

[9] Manjarrez, L. and Zhang, L., 2018. Utilization of copper mine tailings as road base construction material through geopolymerization. *J. Mater. Civ. Eng*, *30*(9), p.04018201.

[10] Li, Z., Ding, Z. and Zhang, Y., 2004, May. Development of sustainable cementitious materials. In *Proceedings of international workshop on sustainable development and concrete technology, Beijing, China* (pp. 55-76).

[11] Drechsler, M. and Graham, A., 2005, October. Geopolymers-an innovative materials technology bringing resource sustainability to construction and mining industries. In *Proceedings of the IQA Annual Conference* (pp. 12-15).

[12] Shi, C. and Fernández-Jiménez, A., 2006. Stabilization/solidification of hazardous and radioactive wastes with alkali-activated cements. *Journal of hazardous materials*, *137*(3), pp.1656-1663.

[13] Indraratna, B., Gasson, I. and Chowdhury, R.N., 1994. Utilization of compacted coal tailings as a structural fill. *Canadian Geotechnical Journal*, *31*(5), pp.614-623.

[14] Festugato, L. and Corte, M.B., 2018. Discussion of "Unconfined Compressive Strength of Synthetic and Natural Mine Tailings Amended with Fly Ash and Cement" by Mohammad H. Gorakhki and Christopher A. Bareither. *J. Geotech. Geoenviron. Eng*, *144*(5), p.07018009.
[15] Consoli, N.C., da Silva, A.P., Nierwinski, H.P. and Sosnoski, J., 2018. Durability, strength, and stiffness of compacted gold tailings–cement mixes. *Canadian Geotechnical Journal*, *55*(4), pp.486-494.
[16] Mahmood, A.A. and Mulligan, C.N., 2010, January. Investigation of the use of mine tailings for unpaved road base. In *Proceedings of the annual international conference on soils, sediments, water, and energy* (Vol. 12, No. 1, p. 11).
[17] Silva, I., Castro-Gomes, J.P. and Albuquerque, A., 2012. Effect of immersion in water partially alkali-activated materials obtained of tungsten mine waste mud. *Construction and Building Materials*, *35*, pp.117-124.
[18] Indraratna, B., Gasson, I. and Chowdhury, R.N., 1994. Utilization of compacted coal tailings as a structural fill. *Canadian Geotechnical Journal*, *31*(5), pp.614-623.
[19] Filho, J.N.S.A., Da Silva, S.N., Silva, G.C., Mendes, J.C. and Peixoto, R.A.F., 2017. Technical and environmental feasibility of interlocking concrete pavers with iron ore tailings from tailings dams. *Journal of Materials in Civil Engineering*, *29*(9), p.04017104.
[20] Zhang, M., Zhao, M., Zhang, G., Mann, D., Lumsden, K. and Tao, M., 2016. Durability of red mud-fly ash based geopolymer and leaching behaviour of heavy metals in sulfuric acid solutions and deionized water. *Construction and Building Materials*, *124*, pp.373-382.
[21] Ojuri, O.O., Adavi, A.A. and Oluwatuyi, O.E., 2017. Geotechnical and environmental evaluation of lime–cement stabilized soil–mine tailing mixtures for highway construction. *Transportation Geotechnics*, *10*, pp.1-12.
[22] Oluwasola, E.A., Hainin, M.R. and Aziz, M.M.A., 2016. Comparative evaluation of dense-graded and gap-graded asphalt mix incorporating electric arc furnace steel slag and copper mine tailings. *Journal of Cleaner Production*, *122*, pp.315-325.
[23] Janošević, N., Đorić-Veljković, S., Topličić-Ćurčić, G. and Karamarković, J., 2018. Properties of geopolymers. *Facta Universitatis. Series: Architecture and Civil Engineering*, *16*(1), pp.045-056.
[24] Hu, N., Bernsmeier, D., Grathoff, G.H. and Warr, L.N., 2017. The influence of alkali activator type, curing temperature, and gibbsite on the geopolymerization of an interstratified illite-smectite rich clay from Friedland. *Applied Clay Science*, *135*, pp.386-393.
[25] Pacheco-Torgal, F., Castro-Gomes, J. and Jalali, S., 2008. Alkali-activated binders: A review: Part 1. Historical background, terminology, reaction mechanisms and hydration products. *Construction and building Materials*, *22*(7), pp.1305-1314.
[27] Plan, R.T., 2005. Arizona Department of Transportation.
[28] Federal Highway Administration (FHWA), 2015. Highway Statistics Series Publications, Washington DC.
[29] Sultan, H.A., 1979. Stabilized copper mill tailings for highway construction. *Transportation research record*, (734).
[30] Swami, R.K., Pundhir, N.K.S. and Mathur, S., 2007. Kimberlite tailings: a road construction material. *Transportation research record*, *1989*(1), pp.131-134.
[31] Qian, G., Huang, T. and Bai, S., 2011. Use of cement-stabilized granite mill tailings as pavement subbase. *Journal of Materials in Civil Engineering*, *23*(11), pp.1575-1578.
[32] Güneyisi, E., Gesoğlu, M. and Mermerdaş, K., 2010. Strength deterioration of plain and metakaolin concretes in aggressive sulphate environments. *Journal of Materials in Civil Engineering*, *22*(4), pp.403-407.
[33] Consoli, N.C., da Silva, A.P., Nierwinski, H.P. and Sosnoski, J., 2018. Durability, strength, and stiffness of compacted gold tailings–cement mixes. *Canadian Geotechnical Journal*, *55*(4), pp.486-494.
[34] Osinubi, K.J., Yohanna, P. and Eberemu, A.O., 2015. Cement modification of tropical black clay using iron ore tailings as admixture. *Transportation Geotechnics*, *5*, pp.35-49.

[35] Méndez-Ortiz, B.A., Carrillo-Chávez, A. and Monroy-Fernández, M.G., 2007. Acid rock drainage and metal leaching from mine waste material (tailings) of a Pb-Zn-Ag skarn deposit: environmental assessment through static and kinetic laboratory tests. *Revista mexicana de ciencias geológicas*, *24*(2), pp.161-169.

[36] Sangiorgi, C., Lantieri, C., Tataranni, P., Castro-Gomes, J. and Gabriel, M., 2016. Reuse of mining waste into innovative alkali-activated-based materials for road pavement applications. In *Functional Pavement Design* (pp. 1735-1744). CRC Press.

[37] Giannopoulou, I.P. and Panias, D., 2006. Development of geopolymeric materials from industrial solid wastes. In *2nd International conference on advances in mineral resources management and environmental geotechnology, Greece*.

[38] Bruschi, G.J., dos Santos, C.P., Tonini de Araújo, M., Ferrazzo, S.T., Marques, S.F.V. and Consoli, N.C., 2021. Green stabilization of bauxite tailings: mechanical study on alkali-activated materials. *Journal of Materials in Civil Engineering*, *33*(11), p.06021007.

YCRETS 2023
YOUNG CONCRETE RESEARCHERS, ENGINEERS & TECHNOLOGISTS SYMPOSIUM
CEMENT & CONCRETE SA

Performance of slag-metakaolin-based geopolymer concrete (GPC) with recycled plastic eco-aggregate

Babatunde L. Ajayi, and Adewumi J. Babafemi

Department of Civil Engineering, Stellenbosch University

Abstract

The high demand for concrete in the construction industry leads to a high cement production rate, thereby increasing carbon emissions (CO_2), resulting in global warming and detrimental effects on human survival. One-part "just add water" geopolymer binder is a potential sustainable binder that could substitute ordinary Portland cement. Currently, there are limited studies on the mechanical properties of one-part slag-metakaolin-based GPC with plastic waste as a substitute for fine aggregate. This paper presents the performance of a one-part slag-metakaolin-based geopolymer using anhydrous sodium silicate, sodium hydroxide and calcium hydroxide as activators. Also, the influence of 5% and 10% replacement of natural sand with RESIN8 (recycled plastic waste containing Resins 1-7) is also reported on the composite's fresh properties. Furthermore, the effects of two curing methods on the mechanical properties (compressive and flexural strength) are presented. Adding plastic waste as fine aggregate in concrete improved the workability, but there was a reduction in the mechanical strength of GPC as the percentage of RESIN8 increased. However, the compressive strength of 28 days water cured (WC) GPC with 5% and 10% RESIN8 were 25.6 MPa and 23.4 MPa, respectively, and ambient cured (AC) GPC with 5% and 10% RESIN8 were 24.1 MPa and 21.7 MPa, respectively.

Keywords: geopolymer concrete, RESIN8, metakaolin, slag, mechanical properties.

1. INTRODUCTION

Over the past few decades, due to global warming, there has been a high demand for sustainable concrete binder development. The intensified demand for concrete in the construction industry has led to a high cement production rate and increased Carbon emissions (CO_2). The International Energy Agency [1] and Wan-En et al. [2] reported that 7% of the global CO_2 emission was generated by the cement industry and 0.83 kg of CO_2 per kg of ordinary Portland cement (OPC) [3]. According to Davidovits [4], the production of 1 tonne of cement generates an almost equivalent quantity of carbon emissions (0.99 tonne) during the calcination of limestone and combustion of carbon-based fuel. Furthermore, Andrew [5] reported that the global cement CO_2 emission in 2016 was 1.45±0.20 Gt out of the accumulated 39.3 Gt of CO_2 from 1900-2016, and South Africa emitted more than 6 Mt of CO_2 from 1950-2016. Hence the need for sustainable Portland cement (PC)-free binder.

Geopolymer is a new generation and PC-free binder for concrete production comprising aluminosilicate precursors and activators, with promising performance and capable of replacing

PC in concrete. There are various aluminosilicate precursors, such as fly ash, ladle slag, red mud, metakaolin (MK), ground granulated blast furnace slag (GGBS), etc. However, the abundant availability (over 5000 Mt) [6] and physicochemical stability properties of MK have made it more suitable and recognised for engineering applications [7]. MK is produced by de-hydroxylation of kaolin between 650 ℃ and 800 ℃ [8], constituting an excellent amount of about 55% of SiO_2 and Al_2O_3 but deficient in CaO. On the other hand, ground granulated corex slag (CS) is rich in CaO; hence, it has been used in this study to fill the gap. GGBS is obtained in the metallurgical process of pig iron ore or ignition of coke at a temperature of 1500 ℃ with an approximate annual production of 270-390 million tonnes [6], while CS is obtained from the production of iron steel through the smelting reduction process.

The first invention of geopolymer started from a two-part application which required a corrosive, viscous and hygroscopic liquid activator that limited its practicability in cast-in-situ and mass concrete production to precast concrete [9]. Hence, the need to develop a one-part geopolymer which is user-friendly. One-part, otherwise referred to as "just add water" geopolymer requires anhydrous activators, which makes its application similar to PC and eradicate the transportation of large quantity of corrosive liquid activators for construction purposes. The most widely used anhydrous activators in one-part geopolymer are Na_2SiO_3 and NaOH. However, producing Na_2SiO_3 from the direct fusion of sand and sodium carbonate is energy-intensive, requiring 850-1088 ℃ [9] and generating a significant amount of carbon emission but lower than PC [10]. Therefore, there is a need to reduce the demand on Na_2SiO_3 by partially or fully replacing it with other viable activators; hence, NaOH and $Ca(OH)_2$ were used to replace anhydrous sodium metasilicate pentahydrate ($Na_2SiO_3.5H_2O$) partially.

The activation of MK-GGBS at equal proportion leads to the formation of C-S-H gel, which produces more stability in the matrix by filling the pores. Still, the high content of GGBS in the mixture reduces the durability properties through shrinkage cracks [11]. Hence, in this study, CS:MK at a proportion of 70:30 was chosen from trial mixes due to its performance over others while incorporating PVA fibre to avoid plastic shrinkage cracks.

The use of recycled aggregate is inevitable in concrete production based on the high demand for natural aggregates (fine and coarse aggregates). According to Babafemi et al. [12], aggregates amount to 75-80% of the volume of the concrete, with fine aggregate constituting 35-45%. Hence, the incorporation of recycled aggregate in concrete production has become crucial for sustainable development in the construction industry and a solution to the shortage of natural sand. Geyer et al. [13] estimated the global plastic produced from 1950 to 2015 to be 8,300 Mt, of which 30% was in use as of 2015, while 9% was recycled, 12% incinerated and 60% discarded and ended up in landfill, oceans and rivers (see Figure 1). In addressing this challenge, researchers have investigated the performance of concrete using recycled aggregate [12,14]. Hence, incorporating recycled plastic waste in concrete to mitigate environmental pollution and develop sustainable and economical concrete holds potential [12].

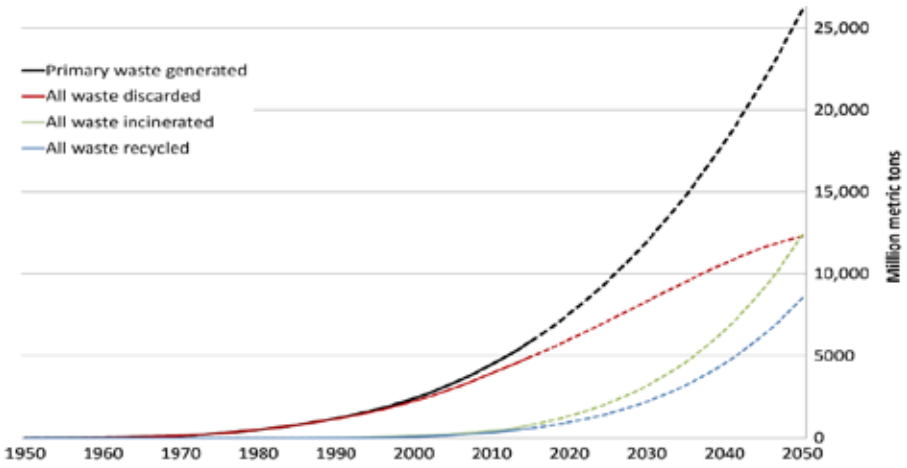

Figure 1: Global trend of plastic production and disposal in million metric tonnes from 1950-2015 and its projection to 2050 [13].

2. EXPERIMENTAL PROGRAMME

2.1 Materials

The materials used in this study are MK and CS (aluminosilicate precursors), locally sourced Malmesbury sand and 13 mm Greywacke stone, recycled plastic waste (sub2 mm), activators ($Na_2SiO_3.5H_2O$, NaOH, and Ca $(OH)_2$, water and admixtures. The MK was obtained from Kaolin Group, and the CS was produced by Arcelor Mittal Steel Plant and supplied by PPC Ltd, South Africa. The recycled plastic waste, patented as RESIN8, is a plastic aggregate that comprises all 7 types of plastics and has been modified to improve the performance of cement-based materials. It was supplied by Centre for Regenerative Design and Collaboration (CRDC), Cape Town. The chemical composition of the aluminosilicate precursors was determined by X-ray fluorescence (XRF) analysis, and the result is presented in Table 1. Figure 2(a-d) shows the precursors and aggregate used. The retarder (trisodium phosphate (NP)) and activators were purchased from Kimix Chemical Lab in Cape Town, South Africa. The specific gravities of MK, CS, sand and RESIN8 are 2.41, 2.90, 2.67 and 1.03, respectively. Polyvinyl alcohol (PVA) fibre having a specific gravity of 1.3 g/cm^3 was used to reduce the shrinkage of the mixes. The oxide molar ratio of the mix is 0.51, 4.45, 0.12, 0.76 and 21.38 for NaO_2/Al_2O_3, SiO_2/Al_2O_3, NaO_2/ SiO_2, $(Ca+Mg)O/SiO_2$ and H_2O/SiO_2, respectively, which are within the recommended molar ratio by Davidovit [15].

(a) (b) (c) (d)

Figure 2: Aluminosilicate precursors and fine aggregates (a) corex slag (b) MK (c) Resin8 (d) Malmesbury sand

Table 1: Chemical composition of aluminosilicate precursors

Compound	Al_2O_3	CaO	Fe_2O_3	K_2O	MgO	Na_2O	SiO_2	others
CS	14.49	38.46	1.35	0.6	11.92	0.16	32.96	0.55
MK	24.52	0.04	1.88	3.89	1.03	0.33	67.14	0.87

The moduli of sand, RESIN8 and Greywacke stone are 2.34, 2.53 and 6.75, respectively. Thorneycroft et al. [16] noted that the performance of plastic in concrete could be improved by matching the particle size distribution of plastic aggregates with the replaced sand. Hence, the plastic aggregate and sand used in this study were pre-treated to match the aggregate particle size distribution, which were both below 2 mm aggregate sizes, as shown in Figure 3.

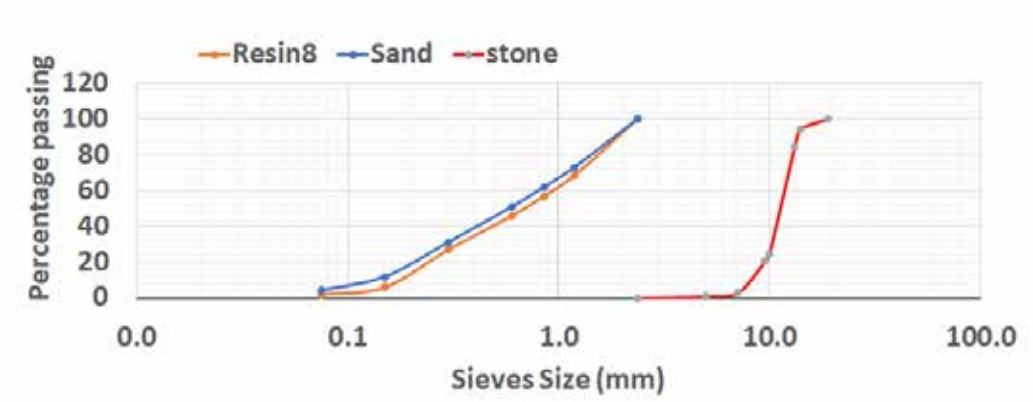

Figure 3: Particle size distribution curve of sand, RESIN8 and 13 mm Greywacke stone

2.2 Concrete Mix Proportion

The aggregate proportions and mix design were obtained by the packing density method [17], and the optimum proportion of the aluminosilicate precursors and activators was obtained through trial mixes using the Taguchi approach [18]. The proportion of CS to MK was 70:30, and 12% activator by weight of the binder was used. The optimum percentage combination of Na_2SiO_3: NaOH: $Ca(OH)_2$, hereafter referred to as SS:SH:CH, obtained from trial samples was 6:3.6:2.4 (% by weight of the binder). The admixtures used were 1.2% modified polycarboxylate superplasticiser and 1.5% PVA by wt. of the binder. The reference mix (0%) and RESIN8 mixes are presented in Table 2. The sand was replaced with RESIN8 by volume at 5% and 10%, which is denoted as R5% and R10%, respectively, and the targeted class of concrete for reference mix was C20/25 (strength of 20-25 MPa) with class S3 slump (100-150 mm).

Table 2: GPC mix design (kg/m^3)

Mark	MK	SL	SS	SH	CH	NP	CA	FA	RESIN8	PVA	water
0%	94	265	21.60	12.96	8.64	9	1167	778	0	2.6	221.7
R5%	94	265	21.60	12.96	8.64	9	1167	739	15	2.6	221.7
R10%	94	265	21.60	12.96	8.64	9	1167	700	30	2.6	221.7

3. EXPERIMENTAL TESTS

3.1 Fresh Properties

The workability and density of all the freshly mixed concrete samples were determined using a slump cone following BS EN 12350-2 [19].

3.2 Strength Tests

3.2.1 Concrete density and compressive strength

The concrete cube (100 mm) samples were cast and compacted using a vibration table in accordance with BS EN 12390-2 [20]. The concrete samples were cured for 7 and 28 days under ambient conditions and complete water immersion. The hardened concrete samples' densities were determined following BS EN 12390-7 [21], and compressive strength was determined following BS EN 12390-3 [22] using a KingTest Contest machine at a loading rate of 180 KN/min until the samples failed. The average failure loads of five samples were computed for each mix.

3.2.2 Flexural Strength

Three prismatic concrete replicates of 300 x 100 x 100 mm were cast per mix and cured for 7 and 28 days under ambient conditions as per BS EN 12390-1&2 [20, 23]. A four-point bending test was conducted on the specimens using a Zwick Z250 material testing machine at a load rate of 0.06 MPa/s according to BS EN 12390-5 [24].

4. RESULTS AND DISCUSSION

4.1 Workability of Mixes

The workability of the mixes increases with an increase in the percentage content of RESIN8, as shown in Figure 4a. The physical characterisation of the aggregates shows that sand has a high-water absorption (1.42%) than RESIN8 (0.68%) due to the hydrophobic nature of plastic, while sand is hydrophilic. Hence, the improved workability with the increase in RESIN8 [12, 25]. The fresh density of the mixes (Figure 4b) decreases with an increase in the percentage of RESIN8; this can be attributed to the light weight of plastic.

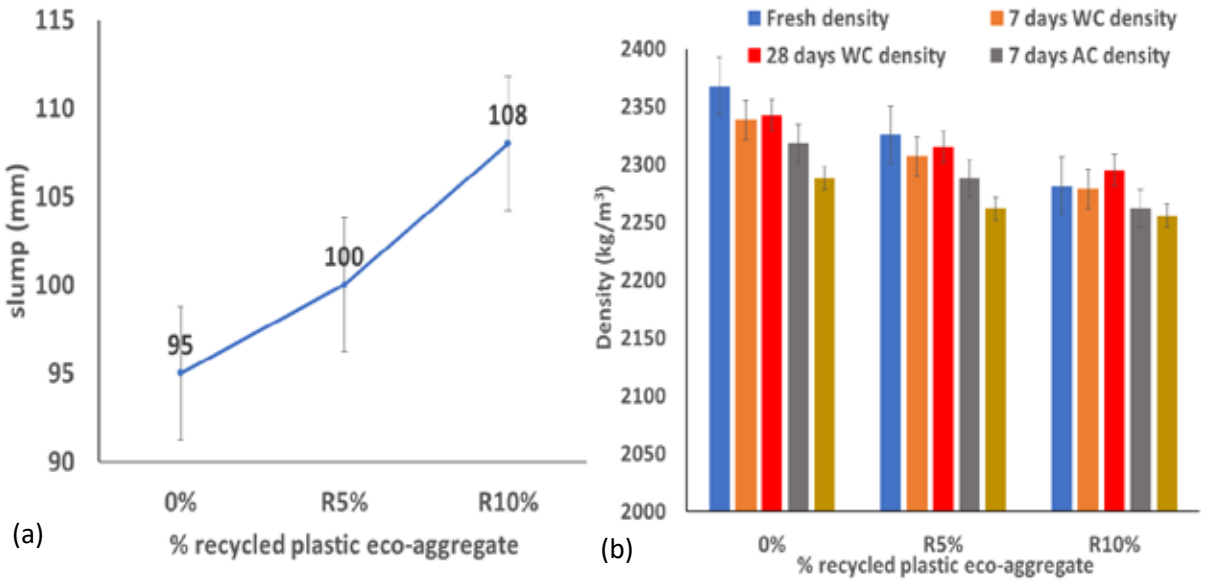

Figure 4. (a) Workability and (b) density of GPC with resin8.

4.2 Hardened Density

Similar to the fresh density, the hardened density of the samples reduced with an increase in the percentage content of RESIN8, and this is attributed to the lightweight characteristic of plastic with a specific gravity of 1.03, compared to sand with 2.67. The density of the concrete samples with 5% and 10% RESIN8 decreased by 1.14% and 1.4% for AC and 1.15% and 2% for WC, at 5% and 10%, respectively, compared to the control samples at 28 days. The density reduction with an increase in the percentage of plastic was also reported by [25, 26].

4.3 Compressive and Flexural Strength

The compressive and flexural strength of GPC are presented in Figure 5. From the 7- to 28-day, the compressive strength of the control samples increased by 6.9% and 9.4% for AC and WC samples, respectively. This implies an early age strength development in GPC. However, there is a 15.9%, 24.1%, and 14.7%, 22.2% decrease in the compressive strength of AC and WC samples containing R5% and R10%, respectively, compared to the control sample at 28 days. This is attributed to the weak interfacial bond around the plastic aggregates (interfacial transition zone, ITZ), increased porosity and lower stiffness of plastic compared to sand. In contrast, according to Thorneycroft et al. [16], the strength of a conventional concrete sample with plastic waste increased when the fine sand and plastic particle sizes were matched. The decrease in strength was also reported by [12, 25, 27, 28]. However, structural strength is achieved at a R5% content.

The flexural strength of the GPC samples decreased at R5% and increased at R10% at 7 days AC, but the strength at 28 days of AC samples decreased progressively with increased RESIN8 content. The flexural strength of the GPC samples at 28 days was 14.2%, 15.3%, and 14.1% of the compressive strength for control (0%), R5%, and R10%, respectively.

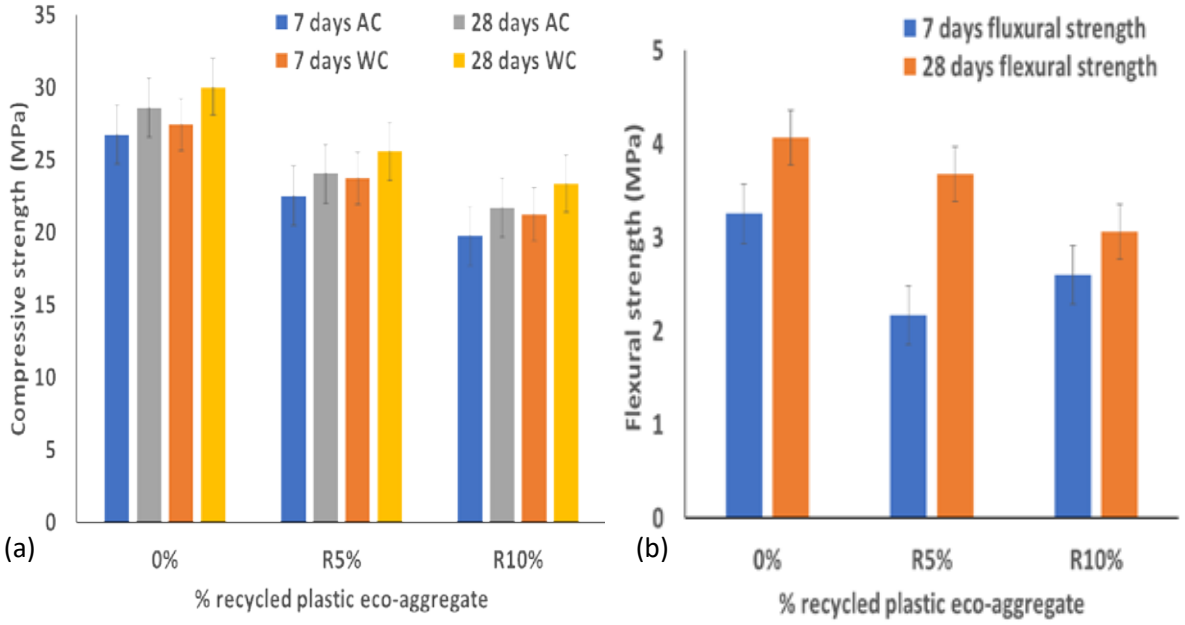

Figure 5. Mechanical properties of ambient and water-cured GPC (a) compressive strength (b) flexural strength (ambient cured).

5. CONCLUSIONS

This study investigated the effects of plastic waste (RESIN8) as a partial replacement of natural sand (5% and 10% by volume) on the fresh and hardened properties of slag-metakaolin- based geopolymer concrete. The workability, fresh and hardened density, and compressive and flexural strength were investigated. The following conclusions are summarised from the investigation.

1. The addition of RESIN8 increases the workability of slag-metakaolin-based geopolymer; however, it reduces the fresh density of the concrete mix.
2. Geopolymer can be effectively cured under ambient conditions and water curing methods. However, the concrete samples cured in the water exhibited higher compressive strength than those cured in ambient conditions.
3. The hardened density and the compressive strength of the geopolymer samples decreased with increased content of RESIN8 by 1.4% and 2% for density and 24.1% and 22.2% for compressive strength at R10% at 28 days AC and WC samples, respectively.
4. The flexural strength also decreased with an increase in the percentage content of RESIN8.

However, RESIN8 can substitute fine aggregates up to 10% by volume in slag (CS)-metakaolin-based non-structural geopolymer concrete and 5% in structural geopolymer concrete.

REFERENCES

[1] International Energy Agency, 'Cement technology roadmap plots path to cutting CO_2 emissions 24% by 2050', 2018, Accessed: May 08, 2023. [Online]. Available: https://www.iea.org/news/cement-technology-roadmap-plots-path-to-cutting-co2-emissions-24-by-2050

[2] Wan-En *et al.*, 'Towards greener one-part geopolymers through solid sodium activators modification', *J Clean Prod*, **378** (2022), doi: 10.1016/j.jclepro.2022.134370.

[3] Adesina, A., 'Performance and sustainability overview of sodium carbonate activated slag materials cured at ambient temperature', *Resources, Environment and Sustainability*, 3 (2021). doi: 10.1016/j.resenv.2021.100016.

[4] Davidovits, J., 'Global Warming Impact on the Cement and Aggregates Industries', *World Resource review* 6 (2) (1994) 263-278.

[5] Andrew, R. M., 'Global CO2 emissions from cement production', *Earth Syst Sci Data* 10 (1) (2018) 195–217. doi: 10.5194/essd-10-195-2018.

[6] Elzeadani, M., Bompa, D. v., and Elghazouli, A. Y., 'One part alkali activated materials: A state-of-the-art review', *Journal of Building Engineering*, 57 (2022). doi: 10.1016/j.jobe.2022.104871.

[7] Siddique, R. and Klaus, J., 'Influence of metakaolin on the properties of mortar and concrete: A review', *Applied Clay Science*, 43 (3-4) (2009) 392-400. doi: 10.1016/j.clay.2008.11.007.

[8] Cong, P. and Cheng, Y., 'Advances in geopolymer materials: A comprehensive review', *Journal of Traffic and Transportation Engineering*, 8 (3) (2021) 283-314. doi: 10.1016/j.jtte.2021.03.004.

[9] Luukkonen, T., Abdollahnejad, Z., Yliniemi, J., Kinnunen, P. and Illikainen, M., 'One-part alkali-activated materials: A review', *Cement and Concrete Research*, 103 (2018) 21-34. doi: 10.1016/j.cemconres.2017.10.001.

[10] Wang, Y. S., Alrefaei, Y. and Dai, J. G., 'Roles of hybrid activators in improving the early-age properties of one-part geopolymer pastes', *Constr Build Mater*, 306 (2021). doi: 10.1016/j.conbuildmat.2021.124880.

[11] Kuo, W., Wang, H. Y. and Shu, C. Y., 'Engineering properties of cementless concrete produced from GGBFS and recycled desulfurisation slag', *Constr Build Mater*, 63, (2014) 189-196. doi: 10.1016/j.conbuildmat.2014.04.017.

[12] Babafemi, A. J., Sirba, N., Paul, S. C. and Miah, M. J., 'Mechanical and Durability Assessment of Recycled Waste Plastic (Resin8 & PET) Eco-Aggregate Concrete', *Sustainability* 14 (9) (2022). doi: 10.3390/su14095725.

[13] Geyer, R., Jambeck, J. R. and Law, K. L., 'Production, use, and fate of all plastics ever made', (2017). [Online]. Available: https://www.science.org
[14] Babafemi, A. J., Šavija, B., Paul, S. C. and Anggraini, V., 'Engineering properties of concrete with waste recycled plastic: A review', *Sustainability*, 10 (11) (2018). doi: 10.3390/su10113875.
[15] Davidovit J., 'Mineral polymers and methods of making them', United State Patent, US4349386 (1982).
[16] Thorneycroft, J., Orr, J., Savoikar, P. and Ball, R. J., 'Performance of structural concrete with recycled plastic waste as a partial replacement for sand', *Constr Build Mater*, 161 (2018) 63-69. doi: 10.1016/j.conbuildmat.2017.11.127.
[17] Raj, N., Patil, S. G. and Bhattacharjee, B., 'Concrete Mix Design by Packing Density Method'. [Online]. Available: www.iosrjournals.org
[18] Cimbala, J. M., 'Taguchi Orthogonal Arrays', 2014.
[19] BS EN 12350-2, 'Testing Fresh Concrete-Slump test', London, UK, 2019.
[20] BS EN 12390-2, 'Testing Hardened Concrete Making and Curing Specimens for Strength Tests', London, UK, 2019.
[21] BS EN 12390-7, 'Testing Hardened Concrete Density', London, UK, 2019.
[22] BS EN 12390-3, 'Testing Hardened Concrete Compressive Strength of Test Specimens', London, Uk, 2019.
[23] BS EN 12390-1, 'Testing Hardened Concrete Shape, Dimensions and other Requirements for Specimens and Moulds', London, UK, 2021.
[24] BS EN 12390-5, 'Testing Hardened Concrete Flexural Strength of Test Specimens', London, UK, 2019.
[25] Ullah, K., Irshad Qureshi, M., Ahmad, A. and Ullah, Z., 'Substitution potential of plastic fine aggregate in concrete for sustainable production', *Structures*, 35 (2022) 622-637. doi: 10.1016/j.istruc.2021.11.003.
[26] Kunthawatwong, R., Wongsa, A., Ekprasert, J., Sukontasukkul, P., Sata, V. and Chindaprasirt, P., 'Performance of Geopolymer Mortar Containing PVC Plastic Waste from Bottle Labels at Normal and Elevated Temperatures', *Buildings*, 13 (4) (2023) 1031. doi: 10.3390/buildings13041031.
[27] Boucedra, A., Bederina, M. and Ghernouti, Y., 'Study of the acoustical and thermo-mechanical properties of dune and river sand concretes containing recycled plastic aggregates', *Constr Build Mater*, 256 (2020). doi: 10.1016/j.conbuildmat.2020.119447.
[28] Wongkvanklom *et al.*, 'Lightweight geopolymer concrete containing recycled plastic beads', in *Key Engineering Materials*, (Trans Tech Publications Ltd, 2019) 377–384. doi: 10.4028/www.scientific.net/KEM.801.377.

YCRETS 2023
YOUNG CONCRETE RESEARCHERS, ENGINEERS & TECHNOLOGISTS SYMPOSIUM
CEMENT & CONCRETE SA

Influence of nanobubble treated wastewater on concrete

Bianca M. Augustyn (1), Landon Olivier (1), Isobel Brink (1), and Riaan Combrinck (1)

(1) Department of Civil Engineering, Stellenbosch University, South Africa

Abstract

The large consumption of potable water in the construction industry is a rising issue, and along with the ever-increasing demand for fresh water, an alternative solution needs to be investigated, more specifically in concrete production. This study investigates the feasibility of using nanobubble-treated wastewater or contaminated water to produce concrete. The use of untreated, contaminated water in concrete can have positive or negative effects on its properties. Nanobubbles were incorporated with contaminants in the form of table salt (chlorides), sugar, detergents, and algae, respectively, to determine the ability of nanobubbles to mitigate the effects of these contaminants on concrete properties.

Concrete tests were conducted on samples that made use of untreated and treated concrete mixing water. The results were compared based on the chemical analysis of the water, the flowability of the concrete, the compressive strengths, and finally the absorption of the concrete. The chemical results show that the nanobubbles neutralise the water, while the compression strength results indicate that the nanobubbles reduce the negative or positive effects of the contaminants. From the results, it can be concluded that there is great potential for treating wastewater with nanobubbles for use in concrete.

Keywords: wastewater, nanobubbles, contaminants, treated, untreated, concrete

1. INTRODUCTION

In the last decade, research into nanobubbles has reached new heights. The potential of this recent technology is already so vast, with the promise of even greater problem-solving potential after further research [1, 2].

These nanobubbles present unique characteristics that prove to be beneficial for several applications within technological areas – these properties include the high surface area versus the volume of the bubbles, along with the significant stability and longevity of the bubbles. Nanobubble research related to pollutants or contaminants has shown enhanced removal of contaminants such as oils, colloidal soils, and organic or inorganic precipitates [3]. The research also revealed that nanobubbles behaved in a stable manner within the water and organic solutions; this stable behaviour was recorded for months without any significant changes in the nanobubble's size or concentration [4].

Furthermore, nanobubbles have the potential to remove toxins from various types of wastewater and the contaminants that are present in them, as recently demonstrated by their use in water treatment procedures [5]. This treatment is done by initiating chemical reactions that would not have occurred without the addition of nanobubbles, thus catalysing the wastewater treatment process and increasing its efficiency.

The general wastewater treatment process involving nanobubbles includes flotation, aeration, and disinfection. These processes are usually done to increase the efficiency of existing treatment methods, rather than acting as individual treatment methods [5].

Research on the influence of nanobubble waters on concrete has been conducted but remains limited. Research suggests that the nanobubble water used within the concrete mixture penetrates the microstructures of the cement paste, forming part of the cement hydration process due to increased zeta potential and surface tension of the mixing water. These increased characteristics catalyse the hydration reaction process and accelerate the pozzolanic reaction, increasing the concrete's water tightness and compressive capability [6].

Research using both microbubbles and nanobubbles within concrete yielded an improvement in the concrete's strength and a decrease in the concrete's workability. The compressive strength and tensile strength increased by 16% and 19%, respectively, and the setting temperature of the concrete was reduced. Other changes measured within the concrete made using microbubbles and nanobubbles relative to the mixture made using standard potable water were that the early-stage and later-stage setting times decreased, requiring the concrete to be cast within a shorter period [7].

Nanobubble technology in concrete is still in the initial stages of research, and more is needed to apply it to the wastewater treatment required for concrete use. This study used untreated and nanobubble-treated contaminated water in concrete to determine the effect of four common contaminants on the concrete's properties before and after treatment.

2. EXPERIMENTAL FRAMEWORK

2.1. Contaminants for Chemical and Concrete Tests

Chemical and concrete tests were conducted using untreated and nanobubble-treated contaminated water with four contaminants: chlorides, sugar, detergents, and algae. The concentration limits prescribed for use in concrete are discussed below.

Chlorides are often found in sea or brackish water, highly mineralised surfaces, or groundwater. One of the concentration limits for chlorides within concrete mixtures is 10 000 mg/l [8]. Chlorides were added to potable water in the form of sodium chloride or table salt, which has a 61.24 % composition of chlorides. This results in a concentration limit of 16 329 mg/l of sodium chloride to achieve the 10 000 mg/l of chlorides within each sample contaminated with chlorides.

Sugar is predominantly found in rivers and groundwater along the east coast of South Africa, near sugar cane plantations. The concentration limit for sugar within concrete mixtures is 1 500 mg/l [9], and normal food-grade white sugar was used.

Detergents are a significant contaminant present in residential greywater. While the concentration limit for detergents is not well defined in literature, it was determined for this study using the general mass of detergent (90 grams) for the average amount of water used in a single load of laundry (70 litres of water), resulting in a concentration limit of 1 286 mg/l.

Algae are found in several water sources and are especially present in dams and rivers. Algae water from a pond in the Botanical Gardens of Stellenbosch University was used as the source of algae water for this study. The concentration of this water was not tested, but it had a green-to-yellow appearance, indicating the presence of significant amounts of algae.

For the chemical tests, the concentration limits mentioned above were used. The chemical analysis for the contaminated water was tested at a nanobubble replacement level of 0% and 90%. For the concrete tests, five times the concentration limit was used: 10% of the water was contaminated with the respective contaminants, followed by the addition of 90% potable water for the untreated water and 90% nanobubble water for the treated water.

2.2. Concrete Mixtures

Conventional concrete was used as the basis for all mixtures. The cement used was a CEM II 52.5 Suretech Portland cement manufactured by PPC (Pretoria Portland Cement). Locally available natural quarry sand, known as Malmesbury sand, with a fineness modulus of 2.6 and a relative density of 2.6 was used as fine aggregate. The coarse aggregate used was a 13-mm Greywacke stone with a relative density of 2.8. The cement and aggregate remained constant throughout the experimental process, while the water used for mixing varied.

The reference mixture used municipal or potable water, as appropriate for conventional concrete. The other concrete mixtures contained untreated contaminated water and nanobubble-treated contaminated water, respectively. The concrete mixtures and their proportions are given in Table 1.

Table 1: Concrete mix proportions

	Reference Mixture (kg/m^3)	**Chloride Mixtures (kg/m^3)**	**Sugar Mixtures (kg/m^3)**	**Detergent Mixtures (kg/m^3)**	**Algae Mixtures (kg/m^3)**
Cement	348	348	348	348	348
Sand	901	901	901	901	901
Stone	900	900	900	900	900
Water	209	209	209	209	209
Pollutant	0	17.1	1.6	1.3	*

*The concentration of the pollutant is unknown due to the fact that the water is not dosed but collected.

2.3. Chemical and Concrete Tests

A chemical analysis was performed on both the untreated and treated water samples using a HACH Pocket Pro+ tester. The water samples were tested to get an indication of the pH and conductivity values before and after the samples were treated with the nanobubbles.

A slump test was performed on one concrete sample in accordance with the guidelines given by SANS 5862-1:2006. The compressive capability of a concrete mixture was determined on 100-mm concrete cubes according to the guidelines set out by SANS 5863:2006. Three cubes were tested for each concrete mixture at 3, or 5, 7, 14, 21, and 28 days (the algae mixtures were tested on 5 days while the other mixtures were tested on 3 days).

The ASTM C1585-13:2013 provided a procedure in which the water absorption of the various concrete mixtures was determined. For each concrete mixture, three samples were tested. This procedure involves measuring the weight of the specimen according to a specific

time scale and period while the cast concrete cube has one face exposed to water. This increase in mass is attributed to the capillary suction due to the capillary pores in the concrete.

3. EXPERIMENTAL RESULTS AND DISCUSSION

3.1. Influence of Chlorides

The pH readings of the water increased from 6.67 to 7.61 with the addition of sodium chloride at the concentration limit, caused by the sodium (Na^+) ions. This pH increase is, however, stabilised to that of municipal water once treated with nanobubbles. The conductivity results for the sodium chloride water were inconclusive due to tester limitations.

The slump test produced information on the flowability of the concrete mixes and showed that the slump increased from 36 mm to 105 mm with the addition of sodium chloride to the municipal water. The nanobubble-treated concrete mixture decreased the slump measurement slightly to 98 mm.

The results, shown in Figure 1, of the compression tests performed on the sodium chloride-contaminated concrete cubes indicated that the strength of the treated concrete yielded similar results to the reference mixture, while the untreated concrete strength was considerably higher than both the reference and the treated concrete mixtures. This increased strength can be attributed to the accelerated setting and hardening effect caused by the higher sodium chloride content [10]. It was observed that the strength of the nanobubble-treated concrete mixture followed a similar strength curve to that of the reference mixture, which is an indication that the treatment method cancelled out the influence of the sodium chloride on the compression strength.

Following the absorptivity test, it was found that the sodium chloride-contaminated samples had lower absorption than the reference mixture, which can be seen in Figure 2. The treated sample shows higher absorption compared to the untreated concrete samples but is still slightly lower than the reference mixture. This shows that the nanobubble treatment is effective in reducing the influence of sodium chloride contaminants on the concrete's compressive strength and absorptivity.

3.2. Influence of Sugar

The pH of the water samples increased slightly from 6.67 to 6.91 with the addition of sugar compared to the reference water. The pH decreased to 6.76, which is similar to that of the municipal water, after the addition of the nanobubbles. The conductivity of the treated water samples decreased from 45 mS to 39.6 mS.

The flowability of the concrete increased significantly to 186 mm with the addition of sugar to the mixing water, as expected due to sugar greatly influencing the setting and flowability of concrete [11]. Treating the water with nanobubbles slightly decreased the slump, resulting in a slump value of 175 mm.

The strength curve of the untreated sugar concrete in Figure 1 illustrates the expected effect of sugar on concrete, a delayed setting time, which can be seen by the low initial compressive strength. This compressive strength is much lower compared to the reference concrete mixture. The untreated mixture's overall strength also remained below that of the reference

mixture throughout the 28-day testing period, indicating a negative influence on the compressive capabilities of the concrete.

The treated mixture shows a significant increase in gradient at the early age strength compared to the untreated mixture; this shows that the treatment method has the potential to reduce the retardation effect that sugar has on concrete setting and strength gain.

Additionally, the compressive strength of the treated concrete is above the untreated sugar curve, which indicates an overall increase in compressive strength. The treated mixture had a higher compressive strength than the reference mixture between 12 and 21 days, after which it normalised to the reference mixture's strength. Treating sugary water with nanobubbles has the potential to eliminate the retardation effect on the concrete's setting time, which improves early-age strength development.

From Figure 2, the absorptivity tests showed that the sugar-contaminated water absorbed significantly less water (1.75 mm) compared to the reference (3.28 mm), indicating that the sugar makes concrete less susceptible to water ingress via capillary suction, which could potentially improve the concrete's durability. This can potentially be attributed to the influence sugar has on the setting and hardening time of concrete, which results in the formation of denser hydration products. With the addition of nanobubbles, the absorptivity depth decreased slightly to 1.60 mm compared to the untreated mixture.

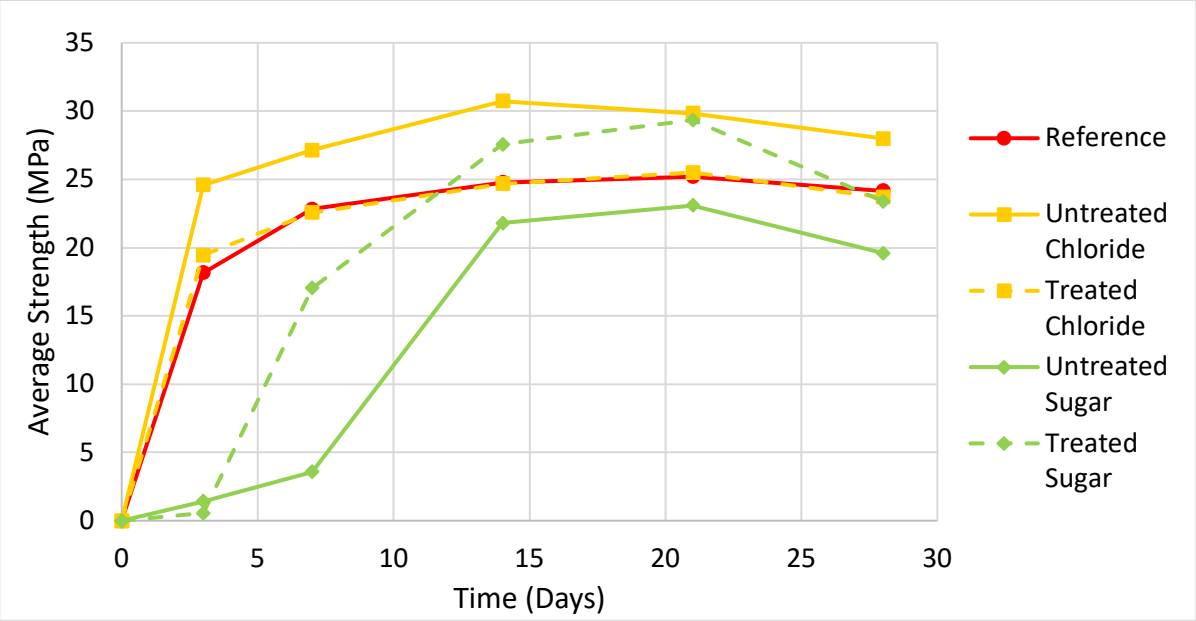

Figure 1 Chloride and sugar compression strength results

3.3. Influence of Detergent

The addition of detergents to water caused a significant increase from 6.67 to 10.13 in the pH compared to the reference water, changing the water into a basic solution. This indicates a greater possibility of alkali-aggregate reactions, which can negatively impact concrete durability. It was found that the addition of nanobubbles did not change the pH significantly.

The conductivity of the samples treated with nanobubbles decreased from 3105 mS to 1614 mS relative to the untreated sample.

The addition of detergents significantly increased the slump measurement to 134 mm compared to the 36 mm of the reference mixture. There was a negligible decrease of 4 mm in the slump measurements by treating water with nanobubbles.

The influence of the detergent decreased the compression strength significantly relative to the reference mixture, which can be seen in Figure 3. This is likely due to the significant increase in entrapped micro air bubbles caused by the detergent's visible foaming effect. The treatment using the nanobubbles showed a slight increase in the compressive strength of the concrete mixture compared to the untreated mixture, and the nanobubbles have the potential to decrease the negative influence of detergents on the concrete's compressive strength.

Analysing the results of the concrete cubes contaminated with the detergent mixing water, as shown in Figure 2, an absorption depth of 2.99 mm was recorded, which slightly decreased compared to the reference mixture. The treated detergent concrete showed similar absorption to the untreated concrete.

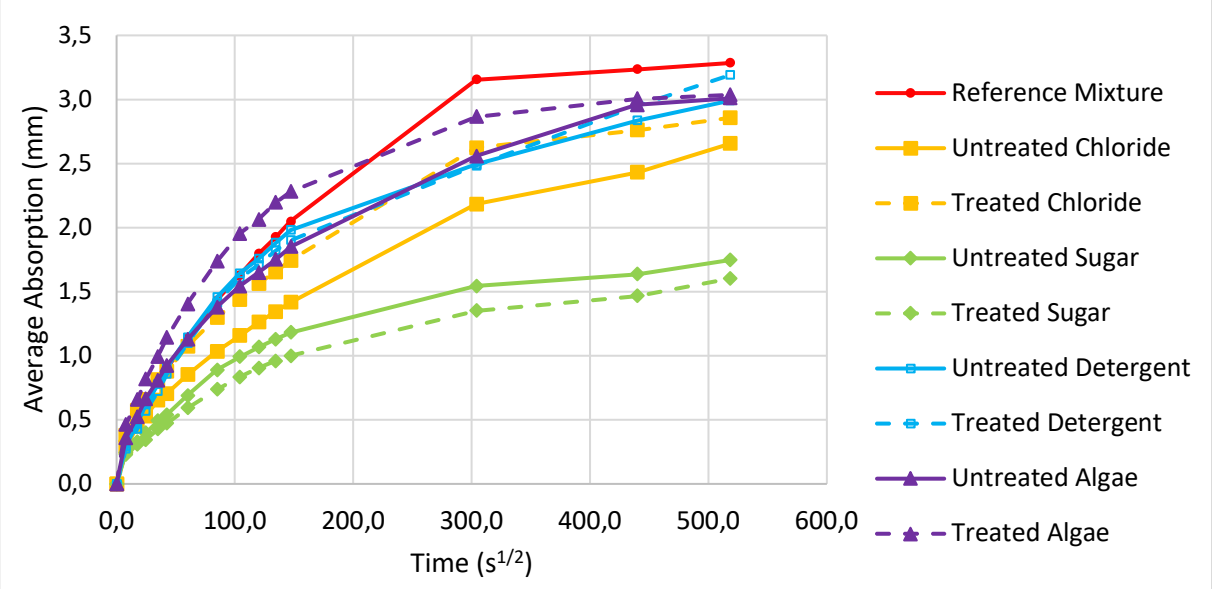

Figure 2 Absorptivity of all concrete mixtures

3.4. Influence of Algae

Treating the contaminated algae water with nanobubbles reduced the pH of the samples from 7.03 to 6.5, which is close to that of municipal water. The addition of nanobubbles caused a decrease in the water's conductivity capability from 277 mS to 250.75 mS.

The algae showed a negligible effect on the slump, both relative to the reference mixture as well as between the treated and untreated concrete mixtures.

From Figure 3, the algae-contaminated concrete mixtures resulted in slightly higher compressive strengths than the reference mixture. The reason for this increase is unclear and requires further investigation. Once the water was treated using nanobubbles, the concrete's

compressive strength tended towards the reference mixture, indicating that the treatment is useful in reducing the influence of the contaminants on the concrete's hardened properties.

As seen in Figure 2, the initial absorption for the treated algae concrete increased slightly in relation to the reference mixture but decreased after 200 seconds to a value just below that of the reference concrete. The untreated concrete abruption was, however, lower than both the reference and treated algae concrete.

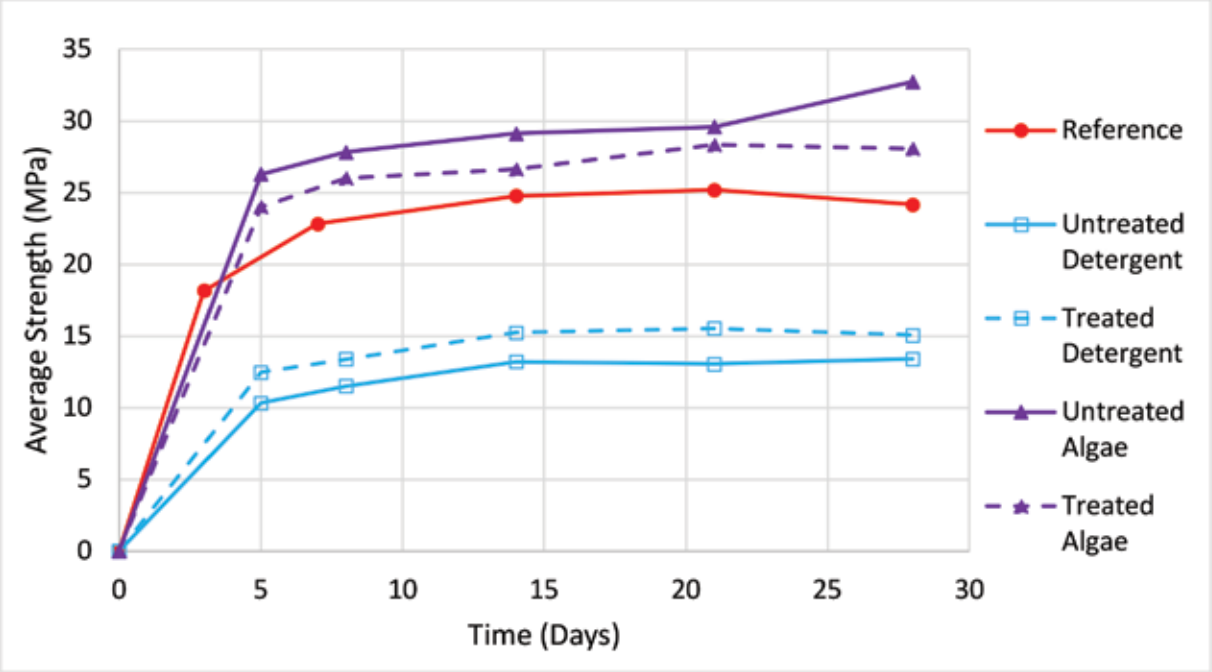

Figure 3 Detergent and algae compression results

4. SUMMARY AND CONCLUSIONS

The following significant conclusions can be drawn from this study.

- The results obtained from the chemical analysis show that the addition of nanobubbles had a neutralising effect on the pH values of chloride-, sugar-, and algae-contaminated water. This neutralising effect on the pH reduces the chances for alkali-silica reactions. The nanobubbles resulted in a slight decrease in the conductivity of the sugar- and algae-contaminated water. A big reduction was seen in the conductivity values for detergent water. This lower conductivity has the potential to lower the corrosion of steel, which is an electrochemical process due to the flow of ions and electrons.
- The untreated chloride and algae concrete yielded greater compression strengths than the reference mixture. The strength was reduced to near the reference mixture when the contaminated water was treated with nanobubbles. The addition of sugar had a negative effect on the compression strength of concrete due to its retardation effect on the setting time. However, treating the sugar-contaminated water with nanobubbles significantly reduced the retardation effect and increased the early-age strength of the concrete. The use of detergent-contaminated water significantly

lowered the compression strength of the concrete compared to the reference concrete. Treating the water with nanobubbles had a slight positive change in its strength characteristics.

- The treatment with nanobubbles slightly decreased the absorption of sugar-contaminated concrete, whereas it increased the absorption of the treated chloride, detergent, and algae concrete.
- All the results indicate that, in general, treating contaminated water with nanobubbles neutralises the effect that the contaminant has on the concrete's properties. This shows that treating contaminated water using nanobubble technology has the potential to allow the use of non-potable and contaminated waters within concrete.

ACKNOWLEDGEMENTS

The support of Fine Bubble Technologies (Pty) Ltd. is gratefully acknowledged.

REFERENCES

[1] Aggarwal, Y., and R. Siddique. 2014. "Microstructure and properties of concrete using bottom ash and waste foundry sand as partial replacement of fine aggregates." *Constr. Build. Mater.* 54: 210–223.

[2] Khoshroo, M., Javid, A. A. S., and Katebi ,A. 2018. "Effects of micro-Nano bubble water and binary mineral admixtures on the mechanical and durability properties of concrete." *Constr. Build. Mater.* 164 (Mar): 371–385.

[3] Azevedo, A., Oliveira, H. and Rubio, J. (2019) "Bulk Nanobubbles in the mineral and environmental areas: Updating research and applications," *Advances in Colloid and Interface Science*, 271.

[4] Takahashi, M., K. Chiba, and P. Li. 2007. "Free-radical generation from collapsing microbubbles in the absence of a dynamic stimulus." *J. Phys. Chem. B* 111 (6): 1343–1347.

[5] Temesgen, T., Bui, T., Han, M., Kim, T. and Park, H., 2017. Micro and Nanobubble technologies as a new horizon for water-treatment techniques: A review. Advances in Colloid and Interface Science, 246, pp.40-51.

[6] Kim, S., H. Kim, M. Han, and T. Kim. 2019. "Generation of sub-micron (Nano) bubbles and characterization of their fundamental properties." *Environ. Eng. Res.* 24 (3): 382–388.

[7] Arefi, A., Saghravani, S. F., and Mozaffari Naeeni, R. 2016. "Mechanical behavior of concrete made with micro-Nano air bubbles." *Civ. Eng. Infrastruct. J.* 49 (1): 139–147.

[8] Alexander, M. (2021). Fulton's Concrete Technology, 10th Edition, Cement and Concrete SA.

[9] Owens, G. (2009). Fulton's Concrete Technology, 9th Edition, Cement and Concrete Institute.

[10] Ojoawo, S.O., Oladejo, A.M. and Olaniyan, O.S. (2014) "Effect of chloride-contaminated water on the compressive strength of Plain Concrete," *IOSR Journal of Mechanical and Civil Engineering*, 11(3), pp. 99–108.

[11] Otunyo, A.W., Onwusiri, S.C. and Nwaiwu, N. (2015) "Effect of sugar cane juice on slump values, setting times and strength of concrete," *Nigerian Journal of Technology*, 34(2), p. 254.

YCRETS 2023
YOUNG CONCRETE RESEARCHERS, ENGINEERS & TECHNOLOGISTS SYMPOSIUM
CEMENT & CONCRETE SA

The design and analysis of anchor connections in lightweight concrete

Nikhiel Budhai

Technical Department, UPAT SA (PTY) LTD

Abstract

The recent development in environmental studies show lightweight concrete as a suitable building material which aligns with sustainable principles. In terms of anchor design, concrete is the most preferred base material and is well-suited for anchoring; although the frequent use of lightweight concrete in the construction sector suggests the performance of fixing systems in lightweight concrete should be explored.

Anchor connections are used in all facets of the building and construction sector – namely household, structural and industrial fixings. This study explores the concept of anchor design and discusses the contributing factors that affect the overall performance of a fixing system. Innovative designs and alternate building materials prompt new development in the fixings industry, therefore in order to adapt and develop new fixings, one must understand the basics of anchor design.

Keywords: sustainable principles, lightweight concrete, anchor design, fixing systems

1. INTRODUCTION

It is known that solid concrete is the most preferred base material for anchors [3]. However, the importance for lightweight concrete to be identified as suitable base material in terms of anchor technology has been gaining traction within the anchor technology industry [2].

This study explores the theory of anchor design and demonstrates significant concepts through a case study [2]. Base materials, load-bearing capacities, failure modes and installation criteria are introductory concepts used to explore anchor design theory [1]. To showcase the industry development of concrete, an experiment which focuses on the performance of anchor technology in lightweight concrete is conducted.

2. THEORETICAL BACKGROUND

Anchor connections are generally used in steel to concrete connections to transmit loads from one element to another via anchor bolts [3]. The anchor bolts are used to distribute load actions into its base material and are influenced by key parameters such as its base material, load bearing capacities and anchor failures of the most unfavorable anchor [3].

2.1. Base Materials

There are various types of base materials available for anchoring. The most common types are concrete (cracked and uncracked), masonry (composite material composed of hollow or solid brick), boards and panels [4]. Each base material varies in compressive strength which has an influence on the anchor connection [3].

2.2. Load Bearing Capacities

The load bearing capacity of anchors refers to the tensile and shear (and combined tensile and shear) loads applied to an anchor connection [4]. Load actions are transferred via anchor bolts which function on two basic principles: Expansion/Undercut theory or Bonding theory [3].

2.2.1. Expansion/Undercut theory

This principle uses mechanical interlock and friction to hold an anchor into its base material [3]. Mechanical interlock of anchors transfers the load to the base material by locking against the base material [3]. Expansion anchors work on the principle of friction to create a force between the anchor and its substrate [3].

2.2.2. Bonding theory

Chemical anchors rely on bonding between the chemical, anchor and substrate [3]. In this case, the load is transferred from the anchor to the base material via the bond created by the chemical components. A chemical reaction occurs between the epoxy mortars which produce different strengths of chemical bonds [5]. Each chemical mortar has unique chemical components that require curing and drying times [5].

2.3. Failure Modes

Anchor connections fail when the load applied to the anchor connection exceeds its ultimate working capacity [4]. Anchor design is based on understanding the failure modes and providing sufficient resistance within a connection to prevent failures. Failures are classified into four modes: (a) Steel failure, (b) Pull-out failure, (c) Concrete cone failure, (d) Splitting failure. A description of each failure mode is given below [3].

2.3.1. Steel failure

Steel failure is a direct failure of steel, which occurs when the tensile load causes the steel to snap, whilst the contact between stud and base material remains intact [3].

2.3.2. Pull-out, pull-through and pry-out failure

Pull-out failure occurs when the anchor is pulled out of its base material, whilst pull-through failure occurs when the anchor disassembles at the expansion point and pulls out [3]. Pry-out failure occurs when the anchor is removed with excessive shear [3].

2.3.3. Concrete cone

Concrete cone failure refers to when a conical section is developed around the anchor and breaks out from its base material in this shape [3]. The cone is approximated to be 1.5 times the effective depth, with the tip of the cone being the part of stud that's furthest into its base material [6].

2.3.4. Splitting failure

Splitting failure refers to the cracking (or splitting) of a base material due to the incorrect embedment depths [3]. This failure mode is influenced by the spacing and embedment depths of an anchor connection.

2.4. Installation Dimensions for Anchor Bolts

Anchorage depth, spacings, and edge distances have an influence on the load bearing capacity of an anchor connection [3]. Figure 1 illustrates an overall description of the influencing dimensions considered when installing fixing systems: diameter of anchor bolt (d_0), effective depth (h_2), fixture thickness (t), Installation torque (T_{inst}) [3].

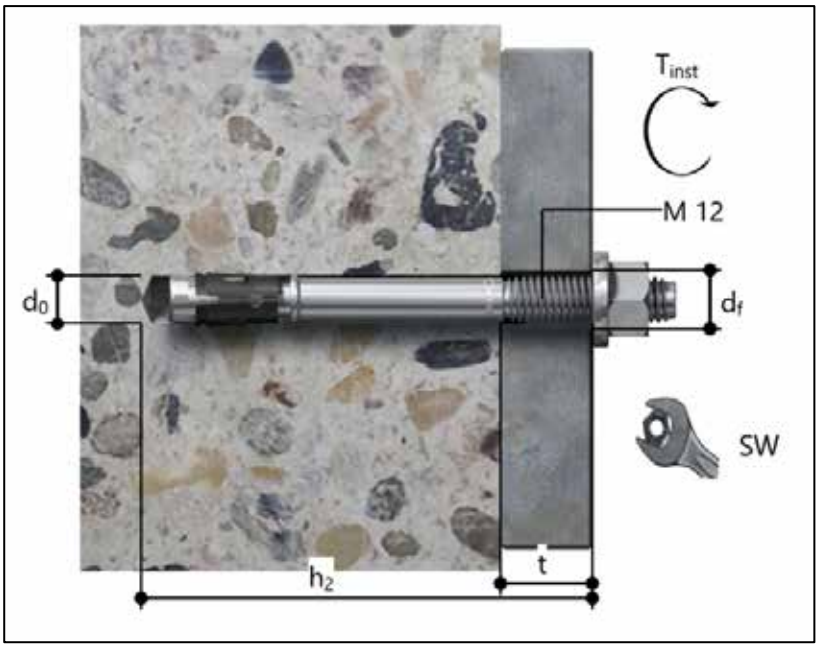

Figure 1: Influencing dimensions for typical anchor connection [3]

3. DESIGN OF ANCHORS

Anchor design involves applying engineering principles to determine safe-working conditions for anchor connections. This is calculated by using partial safety factors and the ultimate failure loads [4].

Partial safety factors are theoretical values which quantify the effect of the different parameters outlined above, on the overall anchor design. The equations shown in Table 1 are extracted from SANS: 51992 Part 4: Design of fastenings for use in concrete [5].

Table 1: Partial safety factors with correlating failure modes [5]

FAILURE MODES	PARTIAL SAFETY FACTORS Accidental design situations
STEEL FAILURE – Anchor fastenings	
1. Tension	$\gamma_{Ms} = 1.05 f_{uk}/f_{yk} \geq 1.25$
2. Shear	$\gamma_{Ms} = \frac{1.0 f_{uk}}{f_{yk}} \geq 1.25$ $when\ f_{uk} \leq 800 N/mm^2 and\ f_{yk}/f_{uk} \leq 0.8$
CONCRETE RELATED FAILURE	
3. Concrete cone failure	$\gamma_{Mc} = \gamma_c \cdot \gamma_{inst}$
4. Concrete edge failure	$\gamma_c = 1.2$
5. Concrete pry-out failure	$\gamma_{inst} = 1.0$ $for\ fasteners\ in\ tension\ and\ shear$
6. Concrete splitting failure	$\gamma_{Msp} = \gamma_{Mc}$
7. Pull-out failure	$\gamma_{Mp} = \gamma_{Mc}$

where,

- γ_{Ms} = partial safety factor for steel failure
- f_{uk} = nominal characteristic steel ultimate tensile strength
- f_{yk} = nominal characteristic steel yield strength
- γ_{Mc} = partial safety factor for concrete cone, concrete edge, concrete blowout and pry-out failure modes
- γ_c = partial safety factor for concrete edge failure
- γ_{inst} = factor accounting for the sensitivity to installation of post-installed fasteners
- γ_{Msp} = partial safety factor for concrete splitting failure
- γ_{Mp} = partial safety factor for concrete pull-out failure

4. CASE STUDY

In order to learn more about the role of lightweight concrete as a base material, a case study is conducted to explore the working capacities of a sample of fixing systems through a series of mechanical tensile loading tests.

A sample of fixing systems, containing four different types of systems are installed in lightweight concrete blocks. A tensile load is applied to each system, and the mode and load at failure is recorded. Each system is installed and tested four times and an average performance result is determined. Using design concepts outlined in the previous section, a design analysis is calculated to determine the safe-working capacities of the various systems.

4.1. Methodology

The information presented in Table 2 show critical data that describes the materials and equipment used for this case study.

Table 2: Test materials & Equipment

MATERIAL/EQUIPMENT	DESCRIPTION
1. Lightweight concrete block	1.1. Dimension: 700x340x120 mm 1.2. Density: 480 kg/m^3 1.3. Compressive strength: 2.58 MPa
2. Fixing systems	2.1. Duo Power Plug & Coach screw 2.2. SXRL 2.3. UX 2.4. Nylon Hammer fix (Green) 2.5. Nylon Hammerfix (Standard)
3. Power tools	3.1. Percussion drill with masonry drill bit. Bit size: 9 mm Bit size: 7 mm
4. Hydraulic tensile tester	4.1. Hydraulic tester with 10 kN calibrated gauge

4.2. Test Setup and Procedures

Figures 2 and 3 illustrates the samples of fixing systems installed and tested until failure. The results are tabulated and shown in Table 3.

The sample set of fixing systems are selected according to the size and length of the plug and screw. The dimensions of each system are chosen with similar characteristics to ensure that the testing and recorded results are fair and unbiased.

Table 3: Results obtained through tensile testing

FIXING SYSTEM		RESULTS	
Type	Dimensions	Failure Mode	Failure load
Duo Power (Duo Line)	ø size: 10 mm Length: 50 mm	1. Pull-out failure 2. Pull-out failure 3. Pull-out failure 4. Pull-out failure	0.2 kN 0.3 kN 0.2 kN 0.2 kN
Duo Power (Duo Line)	ø size: 10 mm Length: 80 mm	1. Pull-out failure 2. Pull-out failure 3. Pull-out failure 4. Pull-out failure	1.6 kN 1.6 kN 1.4 kN 1.4 kN
SXRL (Frame fixing)	ø size: 10 mm Length 80 mm	1. Pull-out failure 2. Pull-out failure 3. Pull-out failure 4. Pull-out failure	1.2 kN 1.4 kN 1.3 kN 1.0 kN
UX (Universal Plug)	ø size: 10 mm Length: 50 mm	1. Pull-out failure 2. Pull-out failure 3. Pull-out failure 4. Pull-out failure	0.8 kN 0.7 kN 0.8 kN 0.6 kN
Nylon Hammer fix (Standard)	ø size: 8 mm Length: 80 mm	1. Pull-out failure 2. Pull-out failure 3. Pull-out failure 4. Pull-out failure	0.1 kN 0.2 kN 0.2 kN 0.2 kN
Nylon Hammer fix (Green)	ø size: 8 mm Length: 80 mm	1. Pull-out failure 2. Pull-out failure 3. Pull-out failure 4. Pull-out failure	0.2 kN 0.2 kN 0.1 kN 0.2 kN

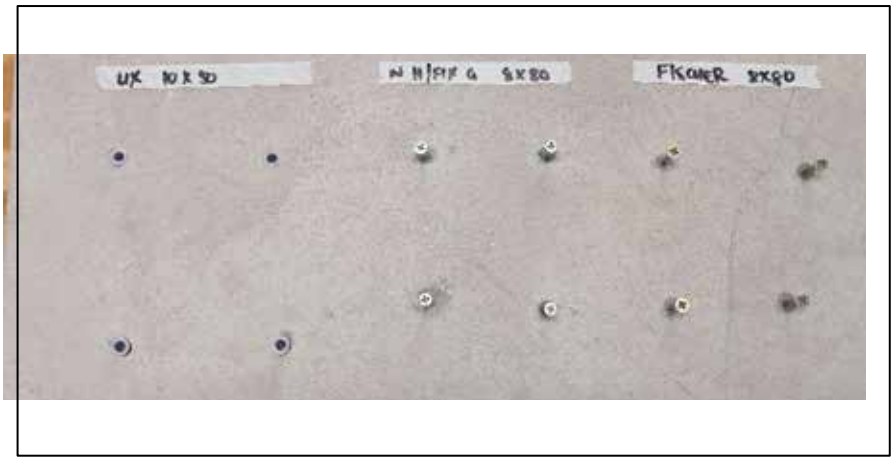

Figure 2: Fixing systems installed and tested: UX (10x80), N H/FIX G (8x80), N H/FIX S (8x80)

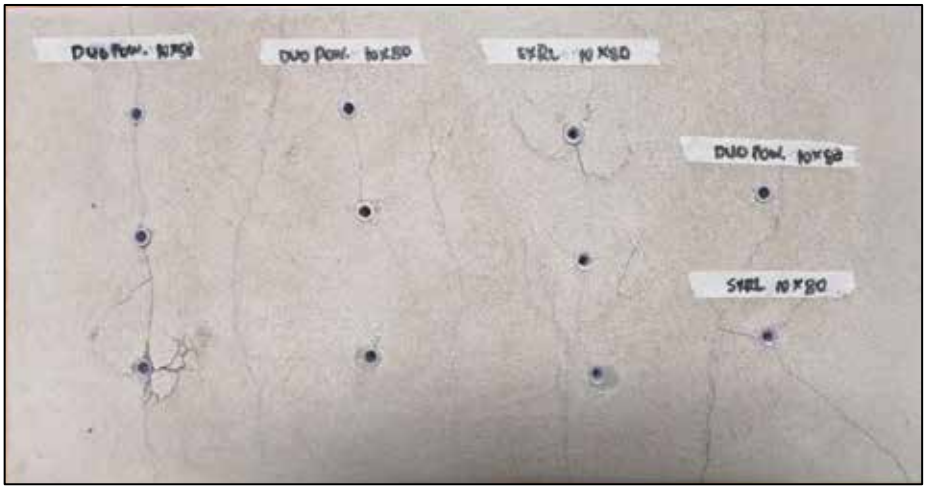

Figure 3: Fixing systems installed and tested: D/P (10x50), D/P (10x80), SXRL (10x80)

5. DISCUSSION OF RESULTS

Figures 2 and 3 illustrate the failure modes of the relevant fixing system. Minor cracks developed in the lightweight concrete block, which questions the structural integrity of lightweight concrete as a base material. Physical inspection of each fixing system indicates that pull-out failure can be identified as the ultimate failure mode.

Table 4: Determination of safe working loads

FIXING SYSTEM	AVERAGE ULTIMATE TENSILE FAILURE LOAD	PARTIAL SAFETY FACTOR	SAFE-WORKING LOAD
Duo Power 10x50	0.23 kN	4	0.06 kN
Duo Power 10x80	1.5 kN	4	0.38 kN
SXRL 10x80	1.23 kN	4	0.31 kN
UX 10x80	0.73 kN	4	0.18 kN
Nylon Hammerfix (Standard) 8x80	0.18 kN	4	0.04 kN
Nylon Hammerfix (Green) 8x80	0.18 kN	4	0.04 kN

Partial safety factors are used to factor the ultimate tensile failure load, as shown in Table 4. The partial safety factors used in the calculations are given by the manufacturer and are adhered to according to each product's technical guidelines for installation [6]. It can be noticed that the Duo Power (10x80) fixing system is able to withstand 1.5 kN (±150 kg) tensile load which yields a safe-working load of 0.38 kN (± 38kg). This type of plug and screw is deemed the best performer in comparison with the remaining plugs and screws in the test sample.

6. CONCLUSION

It is important to discuss and explore the design of fixing systems, since these systems are used in all facets of the building and construction sector. The benefits of lightweight concrete align with sustainability principles and call for innovative fixing systems that are able to perform in variable base materials with high load capacities. The results prove that each fixing system is unique in design and each physical property of the system can be considered as contributing factors to the overall working capacity.

To showcase the recent development with lightweight concrete, various fixing systems are tested, and their performance is studied under tensile loading. For the purpose of this study, the pricing of different fixings systems isn't considered, however, in reality, price has a major influence over the type of fixing system used. This study contributes towards the research and development of anchor technology in lightweight concrete for the building and construction sector.

ACKNOWLEDGEMENTS

The author expresses thanks to Green Crete, UPAT SA (PTY) LTD. and fischer for their contributions towards the completion of this study.

REFERENCES

[1] Michal Kuruc, et al., "Lightweight concrete from a perspective of sustainable reuse of waste byp *ruction and building materials,* vol. 319, p. 126061, 2022.

[2] P. Mahrenholtz, "Latest development in adhesive anchoring," *IOP Conference eries Materials Sc eering,* vol. 10, no. 1775, p. 1048, 2021.

[3] fischerwerke GmbH & Co. KG, Technical Handbook International, 08 ed., Germany: fischer, 2013.

[4] Australian Engineered Fasteners and Anchors Council, "Design Concepts for post-installed ar rs," *AEFAC Technical Note,* vol. 01, no. 2, p. 6, 2013.

[5] SANS:51992-4, "Design of fastenings". South Africa 2021.

[6] fischer, "fischer International," 1993. [Online]. Available: https://www.fischer-internationa ssed 30 April 2023].

[7] The Constructor Building Ideas, "What is green concrete?," 2013. [Online]. / //theconstructor.org/concrete/green-concrete/5566/. [Accessed 27 April 2023].

YCRETS 2023
YOUNG CONCRETE RESEARCHERS, ENGINEERS & TECHNOLOGISTS SYMPOSIUM
CEMENT & CONCRETE SA

The role of sustainability in target reliability assessment

Lloyd Chaitezvi (1), Christina H. McLeod (1)

(1) Department of Civil Engineering, University of KwaZulu-Natal

Abstract

Reliability is a measure of structural performance and is central to modern structural design. Current structural standards incorporate reliability to minimise risk and optimise the design of a structure using probabilistic methods, with target reliability as a measure of structural performance. However, the need to preserve the planet and combat climate change requires the design of structures to contribute to curbing harmful environmental effects. Most design standards mention the need for sustainability, but do not give comprehensive guidelines on its incorporation in the determination of reliability, which is the basis of structural design. This paper provides a framework for future research which aims to incorporate sustainability in the determination of target reliabilities. Structural deterioration models will be integrated with a sustainable framework design model. The sustainable design framework will be derived from a Life Cycle Analysis, which includes quantified and weighted sustainability indicators. Due to the vagueness of the term sustainability, the No Effect Level and Expert Panel methods are recommended for quantifying sustainability indicators. This will enable target reliabilities covering all aspects of sustainability to be determined and recommended.

Keywords: target reliability, serviceability, sustainability, framework

1. INTRODUCTION

This paper provides a framework for future research focussing on the role and effects of including sustainability factors in assessing and determining the target reliability of structures. Reliability is the basis of current structural design methods and is a measure of structural performance [1]. Structural design standards such as Eurocode (EN1990, 2002), (ISO 2394, 2015), SANS 2394, SANS 10160-1 (SANS 2018), ANSI ASCE 7-10 [2], and the *fib* Model Code 2010 [3] employ reliability methods in the design of new and the assessment of existing structures. Probabilistic methods are used to analyse risk and safety of the structure's occupants, maintenance workers and the public within the vicinity [4]. A structure's performance in relation to a minimum or acceptable required performance is governed by limit states. Consideration of limit states ensures optimal behaviour of the structure or structural component with focus on human safety, functionality, aesthetics, and comfort to users [2]. This must include sustainability aspects which consider economic, social, and environmental impacts during the life cycle of a structure.

The advent of climate change has prompted the world to move towards saving the planet by curbing greenhouse gas emissions, lessening resource usage, and reducing waste production. Structural designs are now required to contribute positively to climate change, as their construction has significant negative environmental impacts. Reinforced concrete infrastructure poses two major challenges in the attainment of global sustainability. The first challenge is the emissions from the manufacturing of construction materials such as Portland cement, which accounts for 5% of global CO_2 emissions. The second challenge is in the sustainability of transportation methods for construction materials and structural components [5]. Despite all these challenges, of which structural design is a major contributor, most design standards have received minor to no updates on considering sustainability in structural reliability analysis. The *fib* Model Code 2010 (MC 2010) outlined the basic principles and performance requirements of concrete, concrete elements, and structures in relation to the environment, the society, and the economy [3]. This is currently being updated so that the Model Code 2020 Draft includes the sustainability performance of a structure by combining economic, social and environmental aspects in the life cycle of a structure [6].

SANS, like most current design standards, have received minor updates with regards to sustainability and more so, the effects of sustainability on the target reliability of a structure. SANS 2394, adopted from ISO 2394, focusses on general principles on the reliability of structures, and highlights the fact that sustainability in relation to reliability is still a concept under development [7]. Structural design must include the sustainability concept in line with Sustainability Development Goals. Currently, SANS 10400-XA [8] outlines energy usage in buildings by considering thermal properties of materials, and water supply systems in different climatic conditions. It is imperative that structural design standards incorporate sustainability performance to complement structural performance in the life cycle of the structure.

2. STRUCTURAL PERFORMANCE AND RELIABILITY

Structural performance depicts the behaviour of a structure/structural component when it is subjected to an action or a combination of actions. MC 2010 [3] outlines three major categories namely structural safety, serviceability, and sustainability. These requirements stem from stakeholder demands which influence how the structure functions to meet their essential needs. Structural safety and sustainability cater for social needs while serviceability focusses on the requirements of clients and users. Durability and robustness are other critical aspects to structural performance. Durability refers to the ability of a structure to meet safety and serviceability targets throughout its life with crack width, carbonation depth and chloride content as performance indicators for concrete structures in particular. Robustness is a structural safety aspect, which is defined as the ability of a structure to withstand accidental or exceptional actions without being disproportionately damaged, or the ability of a structure to revert to its original function after undergoing repairs. Performance indicators for robustness consist of redundancy and the resistance of a damaged structure [1].

Limit States are conditions under which structural performance is below an acceptable level, whose exceedance of adverse conditions results in failure or impaired function of a structure. The state of material degradation is a measure of durability associated with limit states. However, limit states associated with durability should be clarified on whether they are applicable to either serviceability limit states or ultimate limit states [9]. This is important in reliability management to ensure that the performance requirements are satisfied in a well-balanced manner throughout the life cycle of the structure. The assurance of structural performance to an acceptable level of probability of failure corresponding to a reference period is known as target reliability [2].

2.1 Target Reliability

Target reliability is differentiated based on the use of the structure, type of structure and situations considered in the design [1]. The reliability index, β, is a standard of measure of reliability, which is related to the probability of failure through the following function:

$$\beta = -\Phi^{-1}(P_F) \quad (1)$$

where Φ( ) is the Gaussian distribution, and P_F is the probability of failure. Reliability indices are scattered as they are dependent on various factors such as the type of structural component, loading conditions and structural materials together with theoretical models used to describe the basic variables [10]. Target reliability values for generic structures in South Africa are well defined in SANS 10160-1 [11] and are generally dependent on the costs of increasing safety together with economic, societal, and environmental consequences of structural failure. Cost optimisation is the main factor in determining target reliability except where human safety is a higher risk in the event of failure. This requires additional constraints which determine minimum reliability levels to minimise risk from a societal perspective [12]. Target reliability through cost optimisation is represented by the following function:

$$Z(d) = C_0 + C_1.d + A(d) + D(d) \quad (2)$$

where C_0 are the initial construction costs without the decision parameter, C_1 are the costs related to changes in the decision parameter *d*, A(*d*) represents obsolescence costs, and D(*d*) represents the costs related to failure. Societal limits on target reliability are determined by considering individual and group risk requirements through the Life Quality Index (LQI). The determination of LQI constitutes mainly of the Gross Domestic Product per capita to reduce risk, ratio of work to leisure time, demography, societal willingness to pay, and the number of fatalities expected in the case of failure [12]. (ISO 2394, 2015) [7] specifies an acceptable fatality of 10^{-6} per year, with a corresponding annual Ultimate Limit State (ULS) reliability index of 4,7 [10]. Target reliability optimisation currently includes economic aspects with regards to structural and societal safety, with focus on the Ultimate Limit State. Way *et al,* 2022 [12, 13] indicated that the proper determination of target reliability with regards to the Serviceability Limit State (SLS) has not been considered in design standards. Current design standards also do not incorporate sustainability with the exception of including costs of environmental consequences from an economic perspective. There is a need for a sustainable design framework to be integrated with structural design models.

3. SUSTAINABILITY

Sustainability is defined as the ability to fulfil current needs of humankind with respect to nature, society, and humans without compromising the needs of future generations [6]. This concept was introduced with the intention of curbing climate change by stabilising the concentration of greenhouse gases in the atmosphere. Sustainability also applies to urban development, which relies on the construction of infrastructure, with concrete as the most widely used material [6]. Reinforced concrete structures pose a major sustainability challenge due to cement production. Regional, local and project specific frameworks have been devised to aid in making designs and infrastructure management more sustainable. These frameworks consist of three subsets which are knowledge based, rating based, and performance based. Knowledge based methods are defined by the criteria under which sustainability was defined and consists of manuals, guidelines, and design recommendations. Rating based frameworks consist of discrete allocation of conditions under which a structure is deemed sustainable. This includes design checklists and sustainability calculators. Performance based tools include continuous impact variables which consist of Life Cycle Assessment methods and the analysis of material flow. This includes simulation tools for assessing environmental impacts and can incorporate economic, social, and environmental aspects. The continuity of performance tools makes them preferrable to knowledge and rating methods as probabilistic analysis can be incorporated [5]. This allows the use of limit states to define the sustainability performance of a structure.

3.1 Sustainability Performance

Structural performance with regards to safety must be complemented by appropriate levels of sustainability [1]. This entails meeting stakeholder demands while striking a balance between economic efficiency, social responsibility, and improving environmental quality. The performance criteria of sustainability must be determined by skilled stakeholders to avoid conflict, ambiguity, and incompleteness of these criteria. The desired level of satisfaction must be achieved in compliance with statutory responsibilities and requirements [6].

3.1.1 Economic performance

The economic performance of a structure is normally conducted through a Life Cycle Cost Analysis (LCCA) to assess the financial feasibility of projects. This is based on discounted cash flow analysis which is tied to the net present value of a structure, and is useful when different economic alternatives of a project are required [6]. Economics highlight the interdependence between risk and cost of safety. There are two main categories in the economics of a project, which are direct and indirect costs. Direct costs are carried by the owner, and these are related to design and construction, overheads, operation and inspection, maintenance, and end of life costs. Indirect costs are those borne by society as a result of the project. To the user, these costs may be time lost due to maintenance and rehabilitation. Societal costs can be associated with the preservation of cultural values, heritage, beliefs, etc. However, these costs are not easy to quantify in monetary terms. Target reliabilities can be determined based on economic optimisation unless the structure poses a major risk to human life in the event of failure [2].

3.1.2 Social performance

Social performance focusses on stakeholder satisfaction during the structure's life cycle, forming a connection between structural engineering and the society. The first aspect outlines the impacts of how users perceive and behave in relation to a structure's function. The second aspect focusses on safety and security, which is based on risk analysis that includes threats, vulnerabilities, expected loss and potential impact, particularly on the environment [6]. Life-saving costs are generally applied when societal or individual risk is the basis for determining target reliability. This gives rise to consequence classes which outline the risks to human life. The Life Quality Index shows societal preference for life safety and is expressed in terms of the willingness to save one's life. LQI depends on GDP, leisure-work ratio and life expectancy [2].

3.1.3 Environmental performance

Environmental performance is based on either Life Cycle Assessment (LCA) or the evaluation of Environmental Impact. The Environmental Impact is further subdivided into the Life Cycle Concept [5]. The Life Cycle Concept considers the total environmental effect of a product, from the acquisition of raw materials through to disposal. The environmental impact of the entire structure can be expressed as a profile composed of values of different criteria, or as a single characteristic value impact. The Environmental Impact value can be expressed as an eco-cost or a normalised system of points [6]. It can also be depicted in terms of a limit state of sustainability, which relates the performance requirement and structural performance over the life cycle. However, this method has not been fully developed [5]. The impact related to a particular step of the life cycle incorporates all environmental damages which combine the weighting and the number of essential environmental criteria. The determination of weighting factors is complex and subjective due to different criteria with a variety of characteristic features. It is a sensitive approach which requires a decision based on a panel of experts on local, regional, and national levels. Three weighting approaches are currently available. The first approach entails Environmental Priority Strategies which constitute of the price to be paid by society to prevent harmful environmental impact. The second approach entails the Panel Method, which is an expert-based determination of weighting factors. The third approach is the No Effect Level (NEL), which provides the relation between zero effect and the current level of a particular environmental aspect. The difference between the zero effect and environmental impact is called a sustainability indicator. A combined Panel-NEL method is also feasible, where experts determine the impact/weighting of a sustainability indicator. Either basic costs or an Environmental Impact evaluation should be an assessment condition for the entire structure or structural elements where the performance of a structure, deterioration, extent and future degradation are determined [6].

4. ASSESSMENT OF THE EFFECTS OF SUSTAINABILITY ON TARGET RELIABILITY

The methodology to determine the effects of sustainability on target reliability will entail the integration of a structural deterioration model with a sustainable design framework. A representative structure, whose performance failure is governed by serviceability, will be chosen to determine the associated risks and consequences. The structural model will be analysed iteratively until it fails to meet the minimum performance criteria. Annual target reliabilities to restore performance to acceptable levels will be determined from the economic, social, and environmental perspectives. Cost optimisation will be conducted to determine the target reliability from an economic perspective, while the Life Quality Index will be used to calculate the target reliability from a social perspective, considering the requirements on human safety and individual risk. This is a combination of human safety and economic aspects.

Target reliability from an environmental perspective will be determined by quantifying the anticipated environmental impacts. This will entail the derivation of environmental indicators in line with the work to be carried out. Some of the indicators outlined in the *fib* Model Code 2010 include CO_2, SO_x, and NO_x emissions, non-renewable resource usage and waste production [3]. However, more precise sustainability indicators will be derived to quantify the environmental impacts, from design to construction [6]. The significance of the indicators will be determined by weighting factors. Two methods, which are the Panel Method and the No Effect Level Method, will be assessed and compared. The impact due to the indicators will be normalised into costs of reducing environmental damage to determine target reliability. The target reliabilities obtained from the economic, social, and environmental aspects will be compared to determine the final target reliability. The target reliabilities will also be assessed to determine their suitability, upon which a decision can be made to either demolish the structure or conduct the necessary construction/repair methods. The methodological approach is shown in Fig 1.

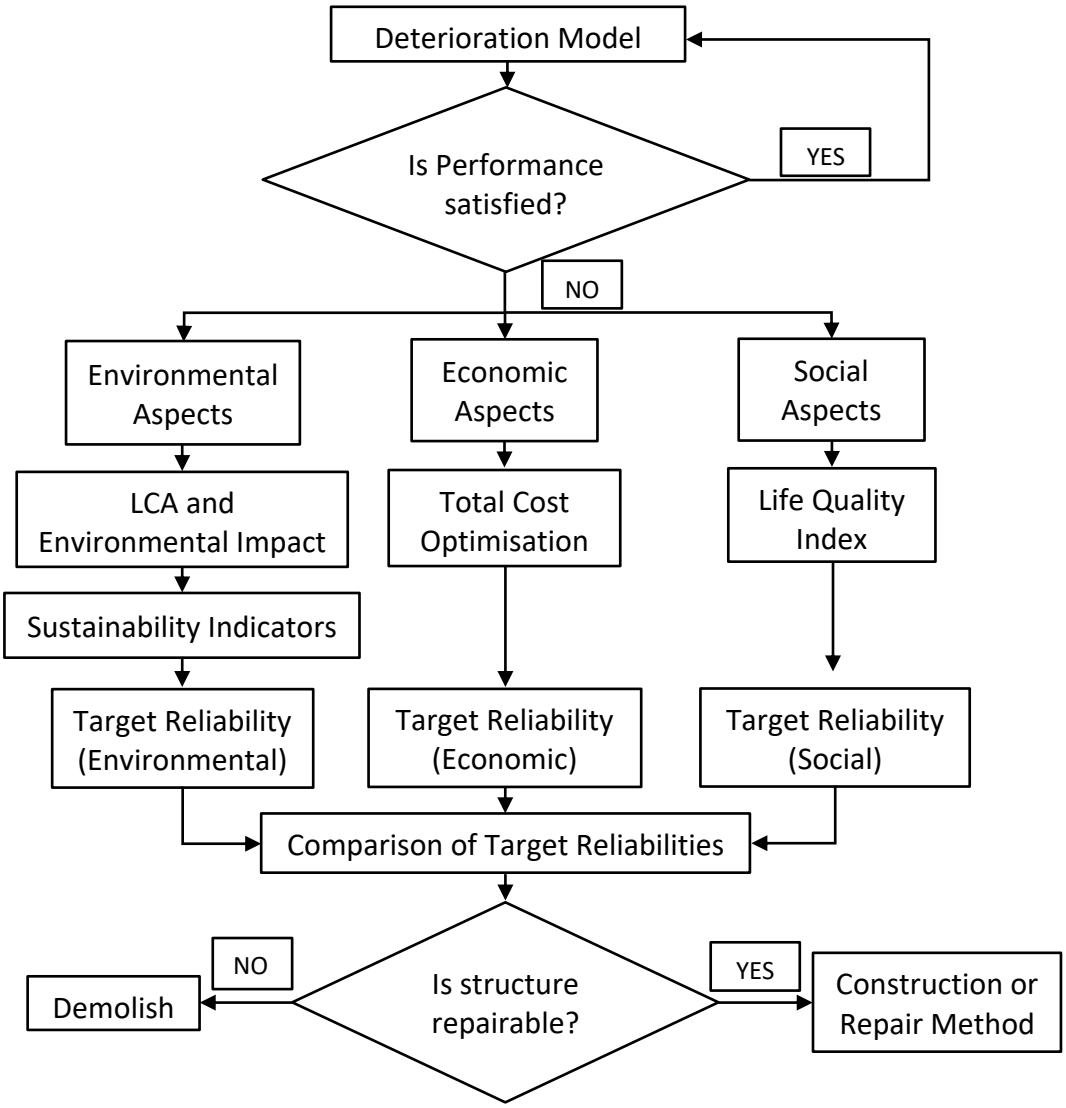

Figure 1. Flowchart of Methodological Approach

5. EXPECTED RESULTS & DISCUSSION

Expected results will entail an integrated structural deterioration model which incorporates sustainability aspects in the assessment and determination of annual target reliability. The model will help to evaluate the impact of environmental factors on target reliability. Inclusion of all aspects means that overall sustainability performance can be determined during the life cycle of the structure. Comparison of target reliabilities allows the consideration of alternative and environmentally friendly methods in construction activities. However, the concept of sustainability needs to be clearly defined in line with structural design standards. The vagueness of the current definition complicates the derivation and quantification of indicators. Currently, the Model Code 2020 [6] recommends using a panel of experts to

determine the weighting of sustainability indicators. This is still a subjective and complex undertaking, therefore a clear definition is needed beforehand. The inclusion of quantified environmental indicators would define a sustainability limit state, which is lacking in structural design standards. Environmental impact assessment allows alternative methods of repair and maintenance in place of conventional methods. Uncertainties in the environmental model will result from variations in material quantities used, different types of construction processes and waste generated.

6. CONCLUSION

Target reliability is a major aspect of structural design. It is well defined by design standards considering the Ultimate Limit State. This paper highlights the need for target reliability to be derived from a serviceability perspective while including sustainability. The research is expected to determine a link between sustainability and structural design using reliability as a basis. This will ensure that a sustainability evaluation is conducted from the design to the construction of a structure. Sustainability will first be considered from an SLS perspective, and any evaluations will be on an existing structure. Further research will enable the incorporation of sustainable factors in the assessment of existing structures also considering the Ultimate Limit State.

7. REFERENCES

[1] Bigaj-van Vliet, A. and Vrouwenvelder, T., 'Reliability in the performance-based concept of fib Model Code 2010', *Structural Concrete*, **14** (4) (2013) 309-319.

[2] Sykora, M., Diamantidis, D., Holicky, M., and Jung, K., 'Target reliability for existing structures considering economic and societal aspects', *Structure and Infrastructure Engineering.* **13**, (1) (2016) 181-194.

[3] fib, 'fib Model Code for Concrete Structures 2010', (Lussane, Switzerland, 2013).

[4] Schneider, J., Vrouwenvelder, T., 'Introduction to Safety and Reliability of Structures', (International Association for Bridge and Structural Engineering) 3rd Edn (Zurich, 2017).

[5] Lepech, M.D., Geiker, M., and Stang, H., 'Probabilistic design and management of environmentally sustainable repair and rehabilitation of reinforced concrete structures', *Cement and Concrete Composites*. **47** (2014) 19-31.

[6] fib, '2nd Draft Model Code 2020', (2022).

[7] ISO, 'General principles on reliability for structures' , 4th Edn (2014).

[8] SABS Standards Division, 'SANS 10400-XA: The application of the National Building Regulations', 1st Edn (Pretoria, 2011).

[9] JCSS, 'Probabilistic Model Code Part 1 - The Basis of Design', 12th Draft (2001).

[10] Holicky, M., 'Reliability Analysis for Structural Design', 1st Edn (Stellenbosch, 2009).

[11] Retief, J.V., and Dunaiski, P.E., 'Background to SANS 10160', 1st Edn (Stellenbosch, 2009).

[12] Way, A.C., de Koker, N., and Viljoen, C.: 'Target reliability for new road bridges in South Africa', *Journal of the South African Institution of Civil Engineering*. **64**, (3) (2022) 10-19.

[13] Way, A.C., McLeod, C.H., and Viljoen, C., 'Basis of serviceability limit state target reliability: Fact or Fiction', Proceedings of the 14th International Conference, Dublin, Ireland, 2023 (Applications of Statistics and Probability in Civil Engineering).

YCRETS 2023
YOUNG CONCRETE RESEARCHERS, ENGINEERS & TECHNOLOGISTS SYMPOSIUM

CEMENT & CONCRETE SA

Use of different industrial and agricultural by – products in formulation of one – part geopolymer binder

Damund de Klerk (1, 2), Abdolhossein Naghizadeh (1), Stephen O. Ekolu (2)

(1) Department of Engineering Sciences, University of the Free State

(2) Department of Civil Engineering, Nelson Mandela University

Abstract

A one – part geopolymer binder is produced by combining solid aluminosilicate materials with solid alkali activators, which can be activated with water, akin to ordinary Portland cement. The current study investigated the potential use of different silica – rich industrial or agricultural by – products to formulate a one – part fly ash – based geopolymer binder. For this purpose, aluminosilicate by – products comprising fly ash, silica fume, rice husk ash or glass waste, were each blended with sodium hydroxide at a ratio of 1.8, then fused at temperatures of 600, 650, 700, 750 and 800 °C for 1 hour to obtain the fused material. In each case, the one – part geopolymer binder was prepared by mixing the fused material and fly ash as geopolymer precursors. The geopolymer binder was mixed with fine aggregate and water to prepare mortar mixtures, which were subjected to workability measurements as well as compressive strength testing. Cubes of 50 mm size were cast and cured at 80 °C in an oven for 24 hours, then they were stored at ambient temperature for six days until compressive strength testing. Results show that regardless of the fusion material type, an increase in the ratio of silicate source to sodium hydroxide in fusion material led to strength loss along with increases in workability. Overall, the glass waste fusion material fused at 600°C, resulted in the best 7 – day compressive strength of 33.6 MPa along with a flow workability of 185 mm.

Keywords: one – part geopolymer, fusion, silica source, compressive strength, fly ash

1. INTRODUCTION

Portland cement – based concrete is extensively employed in global construction practice, owing to its cost – effectiveness and engineering properties in comparison to other building materials. However, there are some disadvantages of ordinary Portland cement (OPC) that mainly relate to its adverse effects on the environment. Intensive carbon emissions and energy consumption resulting from the manufacture of OPC cement, are among the most negative aspects of utilising the binder. Cement production uses 4.7 million British thermal units (BTUs), equivalent to approximately 180 kilograms of coal, and produces almost a ton of

CO_2 for every ton of cement produced [1]. The resulting CO_2 emissions significantly contribute to global warming.

The geopolymer binder presents a potential alternative to OPC and offers a more environmentally sustainable binder option by comparison. A wide range of aluminosilicate materials can be used to produce geopolymer binders through their activation by strong alkali – activators. In order to produce geopolymer binders, aluminosilicate resources used are typically either natural pozzolans, such as volcanic ash, laterite soil, kaolin clay, zeolite or industrial by – products including fly ash (FA), ground granulated blast – furnace slag (GGBS), rice husk ash (RHA), metakaolin, silica fume (SF), etc. [2-7]. Dissolution of aluminosilicate raw materials in alkali activator solution generates Al and Si monomers in the aqueous environment, which subsequently form a polymeric structure with Si, Al, and O components through a polycondensation process. The final geopolymer microstructure contains alkalis, such as sodium (Na) and potassium (K), to maintain the charge balance [8].

The vast majority of research conducted on geopolymer binders has been done using binary alkali – activator solutions consisting of sodium/potassium silicate and sodium/potassium hydroxide. Although the use of concentrated alkali – activator solution results in the production of a hardened geopolymer binder system with appropriate properties, the practical application of strong alkali solution poses a risk due to their high pH values, which can be harmful to human health. As such, the incorporation of highly concentrated alkali solutions into geopolymer binder mixtures may potentially elicit some resistance from industry stakeholders with regard to replacing conventional cement with these alkali – activated materials [8].

The formulation of a one – part geopolymer binder system is a means of eliminating alkali – activator solutions from among the ingredients of geopolymer mixtures. The one – part geopolymer binder system is activated by only adding water, which is more advantageous for commercial use [10,11].

Similar to OPC, the one – part geopolymer binder is prepared by mixing solid aluminosilicate (silica source) materials with solid alkali activators that can be activated by only adding water [10,12]. Any substance that provides alkali cations, raises the mixture's pH, and stimulates the dispersion of silica and alumina within the system can be used as an activating agent in a one – part geopolymer binder [13]. Various studies have been reported in the literature, on the formulation of one – part geopolymer binders using various starting materials.

Yang [14] utilized a sodium silicate powder combined with FA or GGBS as the raw materials to formulate a one – part geopolymer binder cured at ambient temperature. It was reported that the highest 7 – day compressive strength results of the FA – based and GGBS geopolymer mortars, were 3.2 MPa and 48.46 MPa, respectively. Nematollahi [10] reported 7 – day compressive strengths of 33.9 MPa and 37.3 MPa for the combined 75% FA / 25% GGBS geopolymer binder cured at ambient temperature and 60 °C in the oven, respectively.

The present study investigated the effects of various fused materials made using different silica – rich materials and solid sodium hydroxide (NaOH), on the properties of fresh and hardened geopolymer mortars. Silica – rich materials comprising glass waste (GW), FA, RHA and SF, were employed in the experiment. This study also investigated the effect of different fusing temperatures on the flow workability and compression strength of geopolymer mortar samples. The benefits of employing this fusion approach are threefold: firstly, it generates a powder product instead of a liquid solution; secondly, it significantly reduces the production costs associated with activator synthesis, thereby lowering the price of alkali – activated concrete; and thirdly, the utilization of a low – temperature fusion methodology results in a reduced carbon footprint [15].

2. EXPERIMENTS

2.1 Materials and Methods

The silica – rich materials used for fusion were FA, RHA, SF and GW. The low calcium (Class F) FA obtained from Lethabo power station of Eskom SOC Ltd in South Africa, was used as the aluminosilicate raw material, which was fused with the silica – rich materials at 600 to 800 °C. SF was obtained from Mapei South Africa (Pty) Ltd, while GW was supplied by Consol Glass (Pty) Ltd. The coarse GW particles were crushed to powder and sieved through a 150 µm sieve, to obtain fine material for fusing with NaOH. RHA was burned in a laboratory electric furnace at a temperature of 400 °C for 1 hour at a rate of 3 °C per minute, in order to reduce the unburned carbon content of its composition. The chemical compositions of GW, SF, FA and RHA are given in Table 1. Kiran Global (pty) Ltd, supplied the industrial grade NaOH flakes used in the study. The silica sand of sizes 0.8 to 1.4 mm was used as fine aggregate for the preparation of mortar mixtures. The silica sand was supplied by Sallies Silica (Pty) Ltd.

Table 1: Chemical compositions of glass waste, silica fume, fly ash and rice husk ash.

Oxides	Glass waste (%)	Silica Fume (%)	Fly Ash (%)	Rice Husk Ash (%)
SiO_2	83.21	97.56	56.46	89.20
CaO	10.73	1.04	3.14	0.73
Al_2O_3	3.72	0.28	34.93	0.37
Na_2O	3.52	0.23	0.07	0.10
Fe_2O_3	1.97	0.12	3.24	0.60
MgO	1.09	0.29	1.87	1.53
K_2O	0.22	0.48	0.31	1.71
TiO_2	0.20	-	0.83	0.03
P_2O_5	0.06	-	0.48	1.08
SO_3	0.05	-	0.34	3.88
Mn_2O_3	0.04	-	0.02	0.14
Loss of ignition	4.55	-	0.71	3.88

The fusion process consisted of mixing each of the silica sources with NaOH flakes at a ratio of 1.8. The constant aluminosilicate/alkali ratio used in the experiment was based on optimum Na_2O and SiO_2 rates in FA geopolymer mixes adapted from previous studies [6,16,17]. The peak fusion temperature was varied at 600, 650, 700, 750 and 800 °C, while the heating rate and

peak durations were kept constant at 3 °C per minute and one hour, respectively. The temperature variation range, and peak duration of 60 minutes used were adapted from other studies [18,19]. Afterwards, the fused material was finely ground using a laboratory ball – mill, for a duration of 1 hour to obtain powder. The fused materials were stored in sealed containers, to avoid possible carbonation.

To prepare mortar mixtures, the fused materials were mixed with FA and sand using a laboratory mortar mixer. The dry materials were mixed for two minutes, then water was added, while the mixer was running, and mixing continued for an additional two minutes. The ratios of sand to FA, fused material to FA and water to FA, were kept constant at 2.25, 0.25, and 0.4, respectively. In the control sample, only NaOH was used without any additional silica – rich material. Table 2 provides the mix proportions used.

Table 2: Mix proportions of one – part geopolymer mortars prepared using the different silica source / NaOH fused materials and fly ash (FA).

Mix ID	Fusing Temp (°C)	Silica Source in Fused Mat	Fused Mat/ FA	Sand/ FA	Water/ FA	Solid NaOH (g)	Fused Mat (g)	FA (g)	Sand (g)	Water (g)
Control	-	-	0	2.25	0.4	63	0	450	1013	180
GW600	600	Glass Waste	0.25	2.25	0.4	-	113	450	1013	180
GW650	650	Glass Waste	0.25	2.25	0.4	-	113	450	1013	180
GW700	700	Glass Waste	0.25	2.25	0.4	-	113	450	1013	180
GW750	750	Glass Waste	0.25	2.25	0.4	-	113	450	1013	180
GW800	800	Glass Waste	0.25	2.25	0.4	-	113	450	1013	180
FA600	600	Fly Ash	0.25	2.25	0.4	-	113	450	1013	180
FA650	650	Fly Ash	0.25	2.25	0.4	-	113	450	1013	180
FA700	700	Fly Ash	0.25	2.25	0.4	-	113	450	1013	180
FA750	750	Fly Ash	0.25	2.25	0.4	-	113	450	1013	180
FA800	800	Fly Ash	0.25	2.25	0.4	-	113	450	1013	180
RHA600	600	Rice Husk Ash	0.25	2.25	0.4	-	113	450	1013	180
RHA650	650	Rice Husk Ash	0.25	2.25	0.4	-	113	450	1013	180
RHA700	700	Rice Husk Ash	0.25	2.25	0.4	-	113	450	1013	180
RHA750	750	Rice Husk Ash	0.25	2.25	0.4	-	113	450	1013	180
RHA800	800	Rice Husk Ash	0.25	2.25	0.4	-	113	450	1013	180
SF600	600	Silica Fume	0.25	2.25	0.4	-	113	450	1013	180
SF650	650	Silica Fume	0.25	2.25	0.4	-	113	450	1013	180
SF700	700	Silica Fume	0.25	2.25	0.4	-	113	450	1013	180
SF750	750	Silica Fume	0.25	2.25	0.4	-	113	450	1013	180
SF800	800	Silica Fume	0.25	2.25	0.4	-	113	450	1013	180

* GW600, FA600, RHA600 and SF600 stands for glass waste, fly ash, rice husk ash and silica fume, mixed with alkali of Silica Source / NaOH ratio of 1.8 and fused at 600 °C.

After mixing, the fresh mortars were subjected to flow table testing to measure the flow workability, in accordance with ASTM C230 [20]. For compressive strength testing, 50 mm mortar cubes were cast, according to ASTM C109 [21]. To prevent the mixture's liquid components from evaporating, plastic sheets were used to enclose the fresh mortar cubes, which were then oven – cured at 80 °C for 24 hours. They were removed from the oven, then demoulded once having cooled down to room temperature. After demoulding the cubes were

sealed again, then stored for ambient curing at room temperature. The cube samples were tested for compressive strength at the age of 7 days.

3. RESULTS AND DISCUSSIONS

3.1 Flow Workability

Figure 1 shows the effect of fusion temperature on flow workability of the fresh mortar mixtures made using different silica – rich based fused materials. The flow for mortars made using GW, increased with an increase in fusion temperature from 600 to 800 °C. The highest flow workability of 247 mm was given by the mixture made using the GW that had been fused at 800 °C. At the lower fusion temperature of 600 °C, the flow workability of GW mortar were also lower giving 185 mm. This observation can be attributed to the higher conversion of GW to solid sodium silicate at 600 °C, whereas an increase in fusing temperature to 800 °C reduces the conversion rate [19]. The presence of higher sodium silicate content in the fused material, gives higher dissolved Si which leads to an increase in viscosity of the fresh mixture upon introduction of water, in turn reducing flow workability. While the lower conversion rate of GW in relatively higher fusing temperatures, results in a higher content of non – soluble phase responsible for improving workability.

In the mixtures made using fused materials based on FA, RHA or SF, there was no observed significant relationship between fusion temperature and flow workability. This observation can be attributed to the less effectiveness of the fusion process to enhance reactivity at the employed fusion temperatures, as similarly observed for the compressive strength results; discussed later in section 3.2.

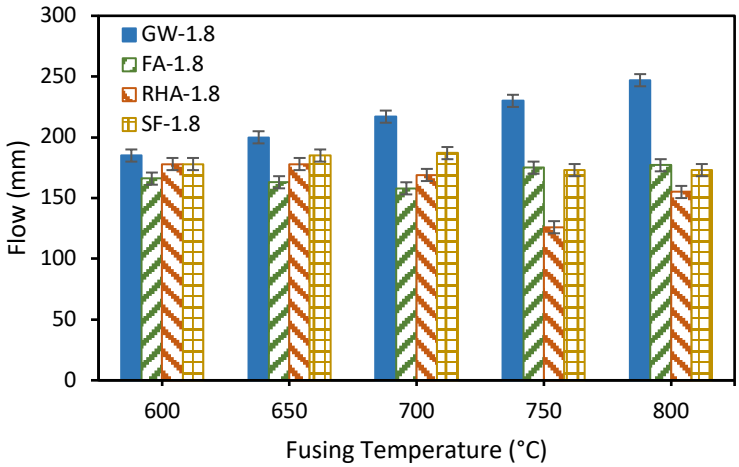

Figure 1: Effects of fusion temperature on flow workability results of one – part fly ash geopolymer mortars made with the different silica source / NaOH fused materials.

3.2 Compressive Strength

Figure 2 depicts the impact of fusion temperature on the 7 – day compressive strength results of mixtures containing a range of fused materials derived from different sources of silica. The curing conditions for all the mixes consisted of one day of storage in the oven at

80 °C, followed by 6 days of ambient curing. The mixture exhibiting the highest compressive strength of 33.6 MPa was the fused material derived from GW as the silica source, and subjected to a fusion temperature of 600°C. Furthermore, a reduction in compressive strength is evident upon elevating the fusion temperature in mixtures utilizing GW as the silica source in the fused material. This can be explained by the higher conversion rate of GW particles to sodium silicate and higher solubility of the fused material in water, when produced at the optimum fusion temperature of 600 °C [19]. The less soluble the fused material is in water, the lower the compressive strength of the sample. All the other mixes made with the other different silica sources in the fused materials, gave very low compressive strengths compared to the results of the GW material. Mortars prepared using GW/NaOH materials, fused at 600 to 700 °C, gave compressive strengths higher than the 16 MPa of the control mixture prepared using NaOH without any silica source in the activator. The significant difference between compressive strengths of the control mixture and the results of the mortars prepared using GW – based fused material, confirms the effectiveness of the employed fusion method.

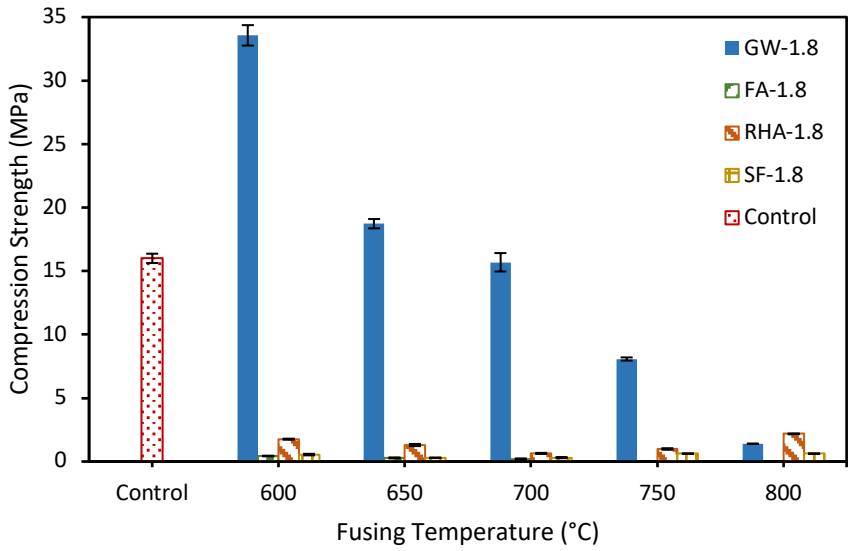

Figure 2: Effects of fusion temperature on compression strength results of one – part fly ash geopolymer mortars made with the different silica source / NaOH fused materials

4. CONCLUSIONS

The current study focussed on use of the different silica – rich industrial or agricultural by – products to formulate a one – part fly ash – based geopolymer binder. The silica – rich materials that were used in the present study were fly ash, rice husk ash, glass waste and silica fume. These silica – rich materials were combined with alkali at a silica source to NaOH ratio of 1.8 and fused at temperatures of 600, 650, 700, 750 and 800 °C. The study evaluated the effects of different fusion temperatures on flow workability and compressive strengths of mortars containing each of the silica rich fused materials. The conclusions drawn from findings of the present study are as follows:

- The flow workability of mortar mixtures containing glass waste fused material, increased with an increase in fusion temperature.
- Changes in the fusion temperature showed no significant changes on flow workability results of the mixtures containing fused materials based on silica fume, rice husk ash or fly ash.
- The compressive strengths of mortar mixtures containing glass waste fused material, decreased with an increase in fusion temperature.
- The compressive strengths of mortar mixtures containing fused materials based on silica fume, rice husk ash and fly ash, were very low and remained constant with an increase in fusion temperature.
- The fusion temperatures of 600 to 650 °C, gave the highest compressive strength results of one – part fly ash based geopolymer mortars made using glass waste – based fused material.

REFERENCES

[1] Petrillo, A., Cioffi, R., De Felice, F., Colangelo, F., & Borrelli, C. (2016). An environmental evaluation: a comparison between geopolymer and OPC concrete paving blocks manufacturing process in Italy. *Environmental Progress & Sustainable Energy*, 35(6), 1699-1708.

[2] Ekolu, S. O., Hooton, R. D., & Thomas, M. D. A. (2006). Studies on Ugandan volcanic ash and tuff. In *Proceedings from the International Conference on Advances in Eng. & Technology,* pp. 75-83.

[3] Okoye, F. N., Durgaprasad, J., & Singh, N. B. (2016). Effect of silica fume on the mechanical properties of fly ash based-geopolymer concrete. *Ceramics International*, 42(2), 3000-3006.

[4] Tchadjie, L. N., & Ekolu, S. O. (2017). Enhancing the reactivity of aluminosilicate materials toward geopolymer synthesis. *Journal of materials science*, 53(7), 4709-4733.

[5] Naghizadeh, A., & Ekolu, S. O. (2017). Pozzolanic materials and waste products for formulation of geopolymer cements in developing countries: a review. *Concr. Beton*, 151, 22-33.

[6] Naghizadeh, A., & Ekolu, S. O. (2019). Method for comprehensive mix design of fly ash geopolymer mortars. *Construction and Building Materials*, 202, 704-717.

[7] Sinngu, F., Ekolu, S.O., Naghizadeh, A. and Quainoo, H.A. (2022). Experimental study and classification of natural zeolite pozzolan for cement in South Africa. *Journal of The South African Institution of Civil Engineering*, 64(4), pp.1–14.

[8] Naghizadeh, A., & Ekolu, S. O. (2022a). Activator-related effects of sodium hydroxide storage solution in standard testing of fly ash geopolymer mortars for alkali–silica reaction. *Materials and Structures*, 55(1), 22.

[9] Naghizadeh, A., Ekolu, S.O. and Solomon, F. (2022b). Challenges and Problems of Geopolymer Brick Masonry: A Review. *Key Engineering Materials*, 916, pp.136–144.

[10] Nematollahi, B., Sanjayan, J. and Shaikh, F.U.A. (2015). Synthesis of heat & ambient cured one-part geopolymer mixes with different grades of silicate. *Ceramics Intern.*, 41(4), pp.5696–5704.

[11] Hajimohammadi, A. and van Deventer, J.S.J. (2016). Characterisation of One-Part Geopolymer Binders Made from Fly Ash. *Waste and Biomass Valorization*, 8(1), pp.225–233. doi:

[12] Ye, N., Yang, J., Liang, S., Hu, Y., Hu, J., Xiao, B. and Huang, Q. (2016). Synthesis and strength optimization of one-part geopolymer based on red mud. *Cons.& Building Mats*, 111, pp.317–325.

[13] Provis, J.L. (2018). Alkali-activated materials. *Cement and Conc Research*, [online] 114, pp.40–48.

[14] Yang, K.-H., Song, J.-K., Ashour, A.F. and Lee, E.-T. (2008). Properties of cementless mortars activated by sodium silicate. *Construction and Building Materials*, 22(9), pp.1981–1989.

[15] Vinai, R., & Soutsos, M. (2019). Production of sodium silicate powder from waste glass cullet for alkali activation of alternative binders. *Cement and Concrete Research*, 116, pp. 45-56.
[16] Naghizadeh, A. and Ekolu, S.O. (2020). Effects of Compositional and Physico – Chemical Mix Design Parameters on Properties of Fly Ash Geopolymer Mortars. *Silicon*, 13(12), pp.4669–4680.
[17] Naghizadeh, A., S.O. Ekolu, Leonel Tchadjié Noumbissié and Solomon, F. (2023). Long-term strength development and durability index quality of ambient-cured fly ash geopolymer concretes. *Construction and Building Materials*, 374, pp.130899–130899.
[18] Naghsh, M., & Shams, K. (2017). Synthesis of a kaolin-based geopolymer using a novel fusion method and its application in effective water softening. *Applied Clay Science*, 146, pp. 238-245.
[19] Keawthun, M., S. Krachodnok, and A. Chaisena. (2014). Conversion of waste glasses into sodium silicate solutions. *Int. J. Chem. Sci* 12, no., pp. 83-91.
[20] Astm, C230. (2002). Standard specification for flow table for use in tests of hydraulic cement. *West Conshohocken*, PA: ASTM International.
[21] ASTM, C109. (2008). Standard test method for compressive strength of hydraulic cement mortars. *West Conshohocken*, PA: ASTM International.

YCRETS 2023
YOUNG CONCRETE RESEARCHERS, ENGINEERS & TECHNOLOGISTS SYMPOSIUM
CEMENT & CONCRETE SA

Experimental study to evaluate the performance of a natural carbonation prediction (NCP) model

Billy E. Edamu (1), Stephen O. Ekolu (2), Fitsum Solomon (2), and Harry Quainoo (1)

(1) Department of Civil Engineering Science, University of Johannesburg, South Africa

(2) Department of Civil Engineering, Nelson Mandela University, Gqeberha, South Africa

*Corresponding author: billyekolu@gmail.com

Abstract

This paper presents an evaluation of a recently developed natural carbonation prediction (NCP) model. In the present study, the NCP model was evaluated using data from an experimental investigation conducted using concrete mixtures of 0.5 water - cementitious (w/cm) ratios, and of various concrete strengths. CEM I 52.5N ordinary Portland cement was used in the mixtures, with or without 10% silica fume, 30% fly ash and 50% slag. Concrete cubes of 100 mm size were cast and cured in water for 7 days then exposed outdoors to undergo carbonation under the natural environment in Johannesburg, South Africa. The cube samples were stored at an urban outdoor site. After 6 years of outdoor exposure of the samples, carbonation measurements were done to generate data sets used to evaluate the model. Results show that the model's predictions were in agreement with actual carbonation measurements. Findings of this study confirm the model's accuracy, and also imply that the NCP model can potentially be used under different environments for various concrete structures.

Keywords: natural carbonation; prediction model; service life; reinforced concrete; corrosion

1. INTRODUCTION

With ongoing worldwide climate change associated with rise in carbon-dioxide (CO_2) concentration in the atmosphere along with rise in global temperature, it can be expected that long-term durability aspects of concrete structures, are being adversely affected. As such, there is a crucial need for practical carbonation prediction models, that can be employed to define specifications for use to build future climate resilient structures, as old and current standards are quickly becoming inadequate under the changing global climate conditions.

Assessment of carbonation-induced damage upon service life, whether for new or existing reinforced concrete, involves consideration of two stages: (1) initiation period during which the carbonation front under CO_2 diffusion, penetrates the cover concrete such that the loss of alkalinity causes de-passivation of reinforcing steel. (2) propagation period in which,

depending upon the local moisture conditions, the de-passivated steel corrodes. The corrosion products then cause expansive stresses that crack the cover concrete. Further corrosion then progressively leads to spalling, delamination and loss of steel area thereby causing structural damage.

Service life is the total time duration comprising the sum of initiation and propagation periods. It is known that propagation period is very short being about 2 to 5 years in concrete structures that may have an initiation period of typically more than 30 to 50 years. On this basis, it can be reasonable to neglect propagation time while giving consideration specifically to initiation period as the basis for determining service life. This approach is evident in the literatures, with most researches focussing upon development of carbonation prediction models without much emphasis on propagation models.

A closer look into the various factors influencing the mechanism, highlights the complexity of carbonation modelling, more so with ongoing climate change. Since 2015, the natural CO_2 concentration in the atmosphere has exceeded 400 ppm, however, it fluctuates seasonally over the year, as well as locally within the exposure site as influenced by industrial activities, traffic, wind factors and ventilation. Also, relative humidity (RH) is of absolute importance to carbonation. Maximum carbonation intensity occurs at 50 to 70% RH. At low RH, there isn't sufficient presence of moisture to support carbonation reactions, while at RH > 80%, the saturated concrete hinders CO_2 penetration into concrete [1, 2]. RH varies widely with seasonal changes in the tropical regions, and may range from 40% RH in dry season to 80% RH during wet season [3]. Indoor and outdoor exposure conditions are known to differently influence concrete carbonation, with the former giving generally higher carbonation ingress.

Nearly all the carbonation models proposed in the literatures are experimental techniques that have not been evaluated against real – life behaviour of concrete structures, with very few exceptions such as the fib-Model Code [4] and the natural carbonation prediction (NCP) model [5]. Comparison done in Ekolu 2018 [5] showed that the NCP and fib-Model Code models exhibit a similar level of prediction accuracy. In Ekolu 2020a [6], the NCP model was employed to predict carbonation in 69 existing concrete structures located worldwide in the urban settings of Johannesburg (South Africa), Bhopal (India), Brasilia (Brazil), Blenio (Switzerland), Tallin (Estonia), Seoul (South Korea), Taipei (Taiwan) and Turin (Italy). It was found that the NCP model made realistic predictions of actual ongoing carbonation in the existing concrete structures. Independent researches have also shown that the NCP model outperforms most other models [7, 8].

In this study, experimental investigation was conducted using concrete mixtures of 0.5 water - cementitious (w/cm) ratios, and of various concrete strengths. CEM I 52.5N ordinary Portland cement was used in the mixtures, with or without 10% silica fume, 30% fly ash and 50% slag. Concrete cubes of 100 mm size were cast and cured in water for 7 days then exposed outdoors to undergo carbonation under the natural environment in Johannesburg, South Africa. Data of this study were used to evaluate a recently developed NCP model [5]. After 6 years of outdoor exposure of the samples, carbonation depth measurements were done, then the results were compared with the model's predictions.

2. EXPERIMENTAL DETAILS

2.1 Test Samples

The cement types, w/cm ratios and supplementary cementitious materials (SCM) employed, are given in Table 1. After casting, the hardened concrete samples were cured for 7 days in water at 23 °C and subsequently, four contiguous surfaces of cube samples were coated with epoxy. The remaining non-coated opposite cube sides were exposed to natural carbonation under sheltered or unsheltered outdoor conditions until the testing date. Also, the four concrete mixtures were tested for compressive strength at the age of 28 days, giving the results presented in Table 1.

Table 1: Cement types, w/cm ratios and SCMs used.

Mix	Type of SCM	Cement type	%SCM	w/cm	28-day strength (MPa)
PC5	Ordinary Portland cement	CEM I	0	0.50	38.2
FA5	Fly ash	CEM IIB-V	30	0.50	27.2
SG5	Slag	CEM IIIA	50	0.50	22.8
SF5	Silica fume	CEM IIA-D	10	0.50	30.0

2.2 NCP Model

The NCP model [5] is given in Eqns (1) to (7). The mathematical equations represent various relationships which once combined, estimate carbonation depth in concrete at any given age. The three major components of the model are: (1) concrete strength, (2) the type of cementitious material, and (3) environmental factors comprising RH, CO_2 concentration, and sheltering from rain.

$$d_{f,t} = e_h.e_s.e_c.cem(F_{c,t})^g.\sqrt{t} \quad (1)$$

where e_h, e_s, e_c are environmental correction factors for RH /temperature, shelter effect and CO_2 concentration, respectively. $F_{(c,t)}$ is the function for strength growth with time (t), which in turn is converted into carbonation progression using the scalar quantity, *cem*, coupled with exponent, *g*, both factors being dependent on the type of cement.

Environmental factors for relative humidity (RH) and shelter:

$$e_h = 16\left(\frac{RH-35}{100}\right)\left(1-\frac{RH}{100}\right)^{1.5} \text{ for } 50\% \le RH \le 80\% \quad (2)$$

This factor is applicable under tropical annual ambient temperatures of 10 to 30°C.

$$e_s = \begin{cases} 1.0 \text{ for sheltered outdoor exposure} \\ f_c^{-0.2} \text{ for unsheltered outdoor exposure; } f_c \text{ is 28-day strength} \end{cases} \quad (3)$$

Environmental factors for varied CO_2 concentrations:

$$e_c = \begin{cases} \alpha f_c^r \text{ for } 20 < f_c < 60 \text{ MPa} \\ 1.0 \text{ for } f_c \geq 60 \text{ MPa} \end{cases} \quad (4)$$

where α and r, are correction factors for natural carbonation under varied CO_2 concentrations:

28 - day strength (MPa)	Correction factor		CO_2 concentration level (ppm)				
			200	300	500	1000	2000
$20 < f_c < 60$	$e_c = \alpha f_c^r$	α	1.4	1.0	2.5	4.5	14.0
		r	-1/4	0	-1/4	-2/5	-2/3
$f_c \geq 60$	$e_c = 1.0$						

Time-dependent strength growth function ($F_{c,t}$):

$F_{c,t} = \frac{t}{a+bt}.f_c$, where $f_c = f_{c28}$ or f_{cbn}

(a) Using 28-day strength (f_{c28})

(i) Short-term ages, t < 6 years (5a)

$$a = 0.35, b = 0.6 - {}^{t^{0.5}}/_{50}$$

(ii) Long-term ages, t ≥ 6 years (5b)

$$a = 0.15t, b = 0.5 - {}^{t^{0.5}}/_{50}$$

(b) Using long-term insitu strength (f_{cbn})

(i) Short-term ages, t < 15 years (6a)

$$a = 0.35, b = 1.15 - {}^{t^{0.6}}/_{50}$$

(ii) Long-term ages, t ≥ 15 years (6b)

$$a = 0.15t, b = 0.95 - {}^{t^{0.6}}/_{50}$$

Cement factors for carbonation conductance: (7a)

SCM	Cement types	Scalar, *cem*	Conductance factor, *g*
20% any	CEM I, CEM II/A	1000	-1.5
30% fly ash	CEM II/B, CEM IV/A	1000	-1.4
50% slag	CEM III/A, CEM IV/B	1000	-1.4

*SCM – supplementary cementitious material

Alternatively, *g*, may be determined using the equation

$$g = \frac{\%SCM}{500} - 1.5 \quad (7b)$$

Footnote: Cube strength (f_c) is related to core or cylinder strength (f_{cyl}) through the conversion, $f_c = 1.25\ f_{cyl}$. The cube strength values used in the model's equations must be $\geq$ 20 MPa.

2.3 Carbonation Measurement

After exposure of samples outdoors for 6 years, they were split then the fresh surfaces were sprayed with phenolphthalein indicator solution. The depth of carbonation was recorded 24 h after spraying the indicator solution, as recommended by RILEM CPC-18 [9]. For each split surface, the measurements for depth of carbonation were performed at 11 points along each opposite end of the surface, and the 22 values thus obtained were averaged.

3. RESULTS AND DISCUSSION

The 28-day strength results of the concrete cubes, are given in Table 1. The carbonation depths were measured 6 years after initial casting of the concrete cubes. The model employs RH, 28-day concrete strength, cement type, CO_2 concentration and time, as its input data (Section 2.2). The comparison of results can be seen in Figures 1 and 2.

An average annual relative humidity of 60 % was used in the model, along with an average CO_2 level of 400 ppm. These values of the environmental factors were based on air quality readings recorded at the outdoor exposure site. The age for each sample was taken as the precise duration from the date of casting to the date of testing for carbonation depth.

The measured results were compared against carbonation depth values predicted by the model. In Figure 1, the predicted values and measured values of carbonation depths show a strong agreement with points lying along the line of equality. Evidently, the model's predictions are realistic for concretes subjected to natural carbonation under both *sheltered* and *unsheltered* outdoor exposure conditions.

It is notable that values of carbonation depths greater than 10 mm exhibited significant dispersion, with predicted values tending to be relatively higher than measured results. A close look at the data shows that this tendency was associated with mixtures that had lower strength. For example the mix SG5 that had 22 MPa strength, gave the measured carbonation of 11.82 mm which was lower than the predicted 18.4 mm depth. Similarly, the mix FA5 which had concrete strength of 27.2 MPa, gave 8.5 mm carbonation depth while the predicted value was 14.1 mm. The mixtures PC5 and SF5 that had concrete strengths of 38.2 MPa and 30 MPa, gave values of measured and predicted values that were generally in agreement, falling close to the line of equality (Figure 1). The foregoing observation underscores the necessity of the condition given in the footnote of Eqn (8), requiring that cube strength must be greater than 20 MPa, as lower strength values invariably alter predictions of the model to give disproportionately high values.

Prediction accuracy of the model was evaluated using statistical error parameters comprising the root mean square of error (RMSE) and coefficient of variation of error (CVE), calculated as given in Eqns (8) and (9).

$$\text{RMSE} = \sqrt{\sum_{1}^{n} \frac{(\text{Residual})^2}{n}} \quad (8)$$

$$\text{CVE}\ (\%) = \frac{\text{RMSE}}{\bar{X}_{mv}}.100 \quad (9)$$

where *residual* is the difference between the predicted and corresponding measured value, n is total number of paired data points, and $\bar{X}_{mv}$ is the mean of measured values.

The CVE and RMSE values obtained were 36.9% and 2.87, indicating that the model's predictions were accurate and consistent with those reported in the earlier associated studies [5, 6, 10, 11]. The prediction accuracy of the NCP model is also similar to those of code-type models which give typical CVE values of 20 to 50% [6].

The residuals seen in Figure 2 show more dispersion with increase in carbonation depth, due to lower quality concretes which tend to carbonate faster. This observed pattern is consistent with similar findings reported in the previous studies [5, 11]. It may be recalled that lower quality concretes are typically those of lower strength, which in turn exhibit correspondingly higher variability, which explains the observed fanning out heteroscedasticity seen in Figure 2.

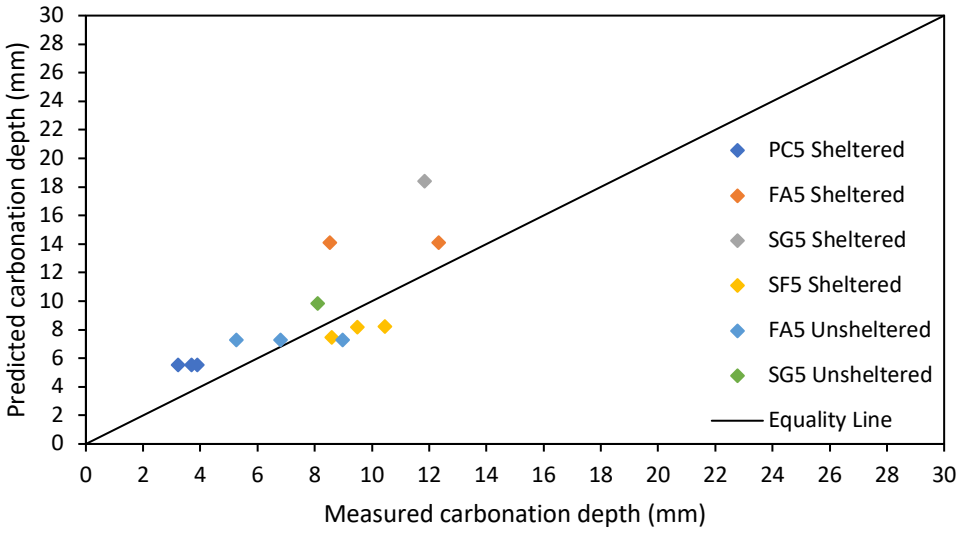

Figure 1: Plot of predicted carbonation depths against measured carbonation depths.

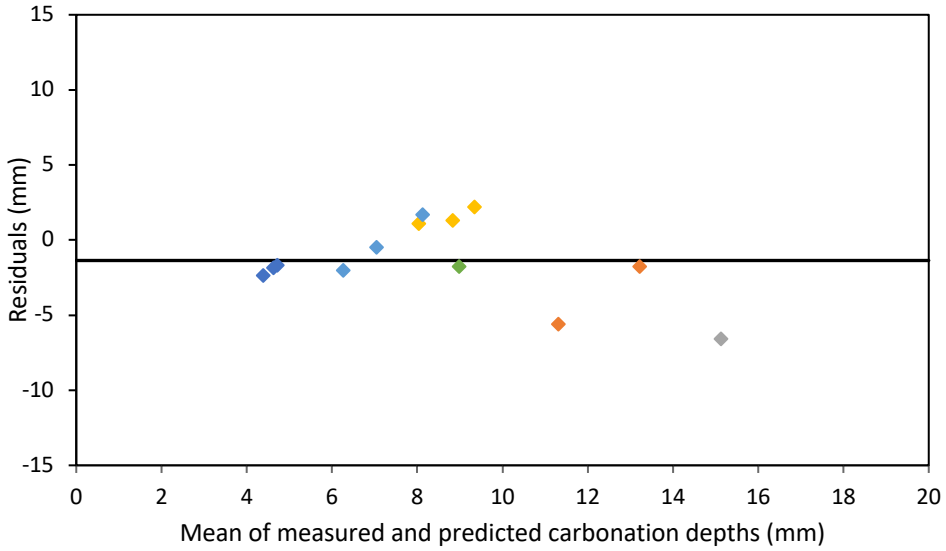

Figure 2: Plot of residuals against mean of measured and predicted carbonation depths.

4. CONCLUSIONS

In this study, an outdoor experiment of 6 years was carried out to obtain data used to evaluate the NCP model. The experiment involved exposure of concrete cubes outdoors for natural carbonation to occur under *sheltered* and *unsheltered* exposure conditions in Johannesburg, South Africa. The measured carbonation depths were compared with values predicted by the model.

Comparison of predicted carbonation depth values versus actual measured values, showed strong agreement which depicts the potential of the NCP model for use under different environmental exposure conditions.

Findings of the present study also confirm that the NCP model is applicable to various concretes including those containing supplementary cementitious materials such as fly ash, slag and silica fume, amongst others. The prediction accuracy of the NCP model was shown to be similar to those of code-type models, typically giving 20 to 50% coefficient of variation of error.

REFERENCES

[1] Parrot, L.J., 'A review of carbonation in reinforced concrete', *Cement and Concrete Association.* BRE, (1987), 42p.

[2] Quillin, K., 'Modelling degradation processes affecting concrete', BRE Centre of concrete construction, CRC Ltd, 151 Rosebery Avenue, London, ECIR 4GB, (2001) ISBN 1860815316.

[3] Eludoyin, O.M., Adelekan, I.O. and Webster R., 'Air temperature, relative humidity, climate regionalization and thermal comfort of Nigeria', *International Journal of Climatology,* Publ. online at Wiley Online Library (wileyonlinelibrary.com), (2013) DOI: 10.1002/joc.3817

[4] *fib* Model Code 2010, 'Model code 2010 final draft', vol. 1 & 2, fib bulletin N. 65 & 66', Lausanne, 2012.

[5] Ekolu, S.O., 'Model for practical prediction of natural carbonation in reinforced concrete: Part 1-formulation', *Cement and Concrete Composites*, 86 (2018) 40-56.

[6] Ekolu, S.O., 'Model for natural carbonation prediction (NCP): practical application worldwide to real life functioning concrete structures', *Engineering Structures*, 224, (2020a), https://doi.org/10.1016/j.engstruct.2020.111126

[7] Gopal, R. and Sangoju, B., 'Carbonation-induced corrosion: a brief review on prediction models', *Journal of the Institution of Engineers*, India, (2020), DOI: 10.1007/s40030-020-00434-8

[8] Costa, R., Franchetto, A., Gouveia, A., Ziegler, F., Pessoa, K. and Garcez, M., 'Service life prediction for concrete structures based on carbonation front depth models', *Revista ALCONPAT* 12 (1), 47 – 60, (2022), DOI: https://doi.org/10.21041/ra.v12i1.558

[9] RILEM CPC-18M. 'Measurement of hardened concrete carbonation depth', *Materials and structures* 17 (12) (1988) 453-455.

[10] Ekolu, S.O., 'Implications of global CO_2 emissions on natural carbonation and service lifespan of concrete infrastructures – reliability analysis', *Cement and Concrete Composites* (2020b), https://doi.org/10.1016/j.cemconcomp.2020.103744

[11] Ekolu, S.O. and Solomon, F., 'A case study on practical prediction of natural carbonation for concretes containing supplementary cementitious materials', *KSCE Journal of Civil Engineering* 26(3), (2021) 1163-1176.

YCRETS 2023
YOUNG CONCRETE RESEARCHERS, ENGINEERS & TECHNOLOGISTS SYMPOSIUM
CEMENT & CONCRETE SA

Hardened properties of 3D-printed limestone calcined clay cement concrete

Kamoru A. Ibrahim*, Mustapha B. Jaji, Gideon P.A.G. van Zijl, and Adewumi J. Babafemi*

Department of Civil Engineering, Stellenbosch University

*Corresponding author. E-mail address: kaibrahim@sun.ac.za & ajbabafemi@sun.ac.za

Abstract

The emergence of a highly productive construction technology named 3D printed concrete (3DPC) is a breakthrough in the construction industry due to its ability to conserve natural resources, reduce waste, and minimise time and costs associated with the construction of concrete infrastructure. This study investigates the performance of fibre-reinforced 3DPC made with limestone calcined clay cement (LC^3) to minimise the detrimental environmental footprint of ordinary Portland cement. LC^3 has been a promising supplementary cementitious material showing better performance in terms of strength development, compared to Portland cement and other blended cements. The mechanical response of LC^3 3DPC reinforced with micro synthetic polypropylene fibre under compression and splitting tensile loading including the modulus of elasticity is examined. The test results reveal that the anisotropic phenomenon was pronounced in mechanical characterisation of the 3D-printed specimens when subjected to loading conditions in different orientations. The peak load values of cylindrical specimens is lesser than that of cubic specimens, having mean strength ratios of 73% and 88% for compression and splitting tension, respectively. Finally, the relationship between the mechanical strength of both the cast and printed specimens cured for 28-day in a climate-controlled room at 23°C (± 2°C) and 65% (± 5%) relative humidity is presented.

Keywords: 3DPC, LC^3, compression, modulus of elasticity, splitting tensile

1. INTRODUCTION

The property of extrusion-based 3D printed concrete (3DPC) is investigated on both the micro- and macro-scales. The macro-scale: compressive strengths (cubes; f_{cu} and cylinders with slenderness equal to two; f_c geometries) are key material parameters in the analysis of concrete structures, which are conventionally utilised as a quality control parameter of concrete and to evaluate the structural application class. Other parameters such as modulus of elasticity (*E),* tensile strength (f_t), and flexural capacity ($f_{flex.}$) are related to compressive strength and cannot be neglected when determining the ultimate load-carrying capacity of concrete elements. A multi-directional mechanical performance is studied in 3DPC, due to its anisotropic properties, i.e., a 3DPC element has different orthotropic mechanical capacities depending on the testing direction. This makes it different from monolithic conventional

concrete structures where the structural integrity tests are normally done in one direction [1, 2].

Unlike the conventional construction method of cast-in-place concrete, 3D concrete printing (3DCP) is an emerging technique for digital fabrication that produced free-form structures and structures of complex geometries without moulds/formwork and other special tools [3]. This promotes architectural expression, where the production costs become independent of the produced structural components' quantity, shape, and complexity [4]. However, high cement content is required for the extrusion process of 3DPC and its sustainability benefits in terms of free forms and materials efficient design might be affected. Hence, the addition of limestone and calcined kaolinitic clay (naturally available supplementary cementitious materials) sufficiently reduced the clinker content of digital concrete; saving embodied carbon footprints, energy consumption, and cement/concrete production cost [5–7].

Many studies have attempted to utilise a combination of limestone powder and calcined kaolinitic clay to develop printable cementitious materials [8–10]. Their findings showed comparable mechanical properties to those of ordinary Portland cement (OPC) and Portland pozzolanic cement (PPC), and the improvement of some durability aspects. Limestone calcined clay cement (LC^3) is an intrinsic rheology modifier and pozzolanic material, which releases carbo-aluminate hydrate when calcite reacts with tricalcium alumina in the pore solution. Due to these actions, the capillary pores are filled, thereby reducing the porosity of cement-based materials and enhancing the mechanical performance at later ages [7, 8, 11].

In this study, the influence of limestone calcined clay (LC^2) on the mechanical properties of fibre-reinforced 3DPC (FR-3DPC) tested in a compressive setup was investigated by measuring the compressive strength, the splitting tensile strength, and the elastic modulus. Seven (7) concrete cubes (mould-cast) and thirty (30) cylindrical (10 mould-cast and 20 printed (10 D1 and 10 D3)) specimens were prepared and tested in the laboratory in this investigation.

2. EXPERIMENTAL FRAMEWORK

2.1. Experimental Materials

Pretoria Portland cement (PPC) Suretech clinker (CEM I 52.5 N) conforming to SANS 50197-1 [12], LC^2, and gypsum were used as raw materials for this study. Natural Malmesbury sand with fineness modulus of 2.12 and 4.75 mm nominal maximum size was utilised to improve the self-supporting behaviour of the material through mechanical occlusion. The particle size distribution curve of the sand and binders, as obtained from sieve analysis and laser diffractometry (Mastersizer 2000 and Hydro 2000SM), respectively, is shown in Fig. 1 with the mean particle size (D_{50}) of 307.28 μm, 19.36 μm, 18.81 μm, and 234.53 μm for sand, CEM I 52.5 N, LC^2, and gypsum, respectively. LC^2 has a relatively finer-grained structure than CEM I. Normal-modulus polypropylene (PP) fibre with its properties illustrated in Table 1 was incorporated in the 3DPC to control plastic shrinkage cracking and minimises brittleness [13]. The mixing water was added to the dry mixture, with a liquid Chryso Quad 20 viscosity modifying admixture (VMA) and high-efficiency Chryso Premia 310 superplasticiser (SP) for

tailoring and optimising the rheological properties of ternary blended concrete to meet the 3DPC performance requirements. The chemical properties of the clinker (Portland cement) and other raw materials were obtained by X-ray fluorescence spectrometry (XRF) and are presented in Table 2, and the mix design of LC^3 FR-3DPC is shown in Table 3.

Table 1: Properties of the micro-synthetic fibre

Description	Young's modulus	Yield stress	Diameter	Length	Aspect ratio
PP	3 GPa	300 MPa	30 μm	6 mm	200

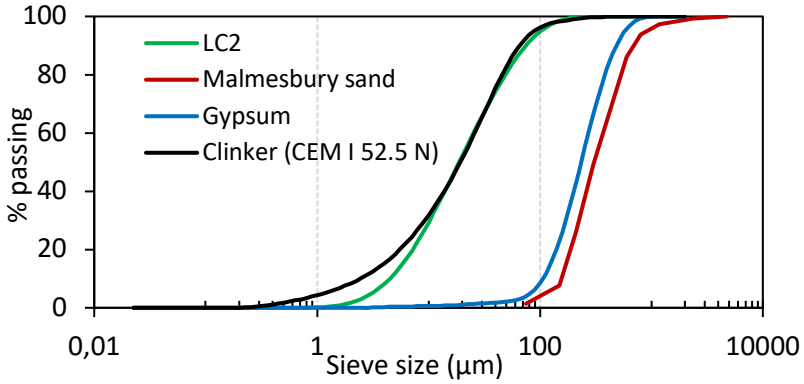

Fig. 1. Particle size distribution of LC^2, Malmesbury sand, Gypsum, and CEM I 52.5 N

Table 2: Chemical composition of cement and other raw materials

% Weight	Al_2O_3	CaO	Fe_2O_3	K_2O	MgO	Na_2O	SiO_2	TiO_2	LOI	Other
Clinker	4.08	62.92	3.16	0.57	1.00	0.18	19.90	0.23	5.08	2.88
LC^2	13.32	17.90	1.24	2.03	0.77	0.24	49.64	0.56	14.57	0.05
Gypsum	0.21	13.17	0.05	0.06	0.14	0.06	57.95	0.03	11.24	17.09

Table 3: Materials mix constituent proportioning (kg/m^3)

Mixture	Clinker	LC^2	Gypsum	Sand	Water	SP	VMA	PP
LC^3 FR-3DPC	381.9	343.7	38.2	1229	343.7	7.637	2.291	9

2.2. Experimental Methods

The 3D concrete mix design approach developed at the Structures and Building Materials Laboratory of Stellenbosch University (S&BML-SU) was modified for LC^2 inclusion. Mixing was done mechanically in a Hobart concrete mixer in the following order: dry mixing of aggregate and binders, mixing water addition, then the addition of admixtures (SP and VMA), and lastly, PP. Specimens for hardened properties were cast and compacted using an electro-mechanically driven vibration table, taken to the climate control room, and stripped after 24 hours. The printing technique adopted is extrusion-based using a gantry-type 3D printer, which operates in three translational degrees of freedom with a build volume of roughly one cubic metre (1 m^3) coupled with a concrete pump and circular nozzle of 25 mm diameter. The

printing parameters selected, and the procedures followed to attain it were aligned with those reported by Ibrahim et al. [14]. The printing (rectangular solid object which is schematically represented in Fig. 2 with geometry) and curing for the cast and printed samples were made in a climate-controlled room at a temperature of 23°C (± 2°C) and 65% (± 5%) relative humidity.

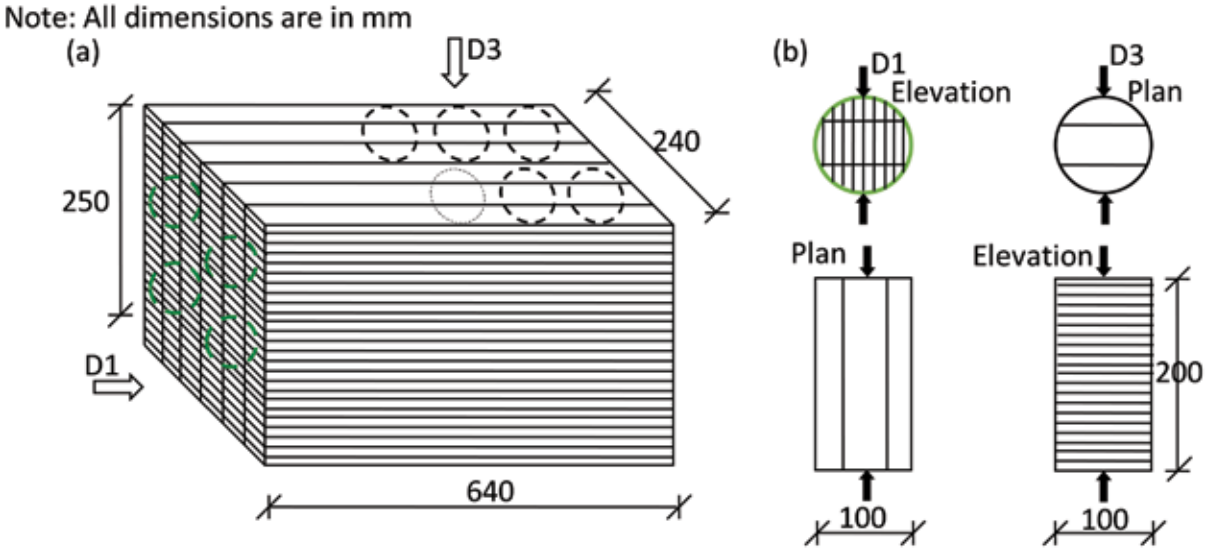

Fig. 2. The schematic representations of printed (a) object and (b) specimens: D1 & D3

2.3. Experimental Testing

Compressive strength test: The strength evolution characterisation for compressive (f_{cu}, cube & f_c, cylinder) strengths on the cast and printed (cored) specimens were executed after 28 days of curing using a 2 MN King Test Contest press machine at loading rates of 180 kN/min and 90 kN/min for cubes and cylindrical specimens, respectively, until failure adhering to BS EN 12390-3 [15] and ASTM C39 [16]. The test specimens were 100 mm cubes (cast) and 100 mm diameter × 200 mm long cylinders (cast and printed). Printed specimens were cored in two directions: D1 and D3 (see Fig. 2) in longitudinal and perpendicular to the printing direction, respectively.

Splitting tensile strength test: The splitting tensile test (f_{st}, cube & f_{sti}, cylinder) was performed on 100 mm cubes and 100 mm diameter x 200 mm height cylindrical specimens after 28 days of curing. The specimens were tested in a Zwick Z250 material testing machine at loading rates of 1.0 mm/min and 0.75 mm/min for cubes and cylinders, respectively, in accordance with BS EN 12390-6 [17].

Modulus of elasticity: Young's modulus (E) characterisation was conducted on 100 mm diameter x 200 mm height cylinders (cast and printed specimens) after 28 days of curing as per ASTM C469/C469M-14 [18]. Three linear variable differential transducers (LVDTs) with a 70 mm gauge length are circumferentially arranged at 120° intervals. Then, the testing was conducted using a 2 MN King Test Contest press machine at a loading rate of 90 kN/min with

a 2 MN loadcell, loaded uniaxially up to 40% of their ultimate compressive capacity, and measurements were taken through an HBM Spider8 data acquisition system.

3. RESULTS AND DISCUSSION

3.1. Compressive Strength

The results of the compressive strength tests (f_{cu} & f_c) of LC^3 FR-3DPC specimens are depicted in Fig. 3. The mould-cast cylindrical specimens had an average strength of 73% of the cube's strength. In comparison to the printed specimens, the percentage decrease in strength are 3% and 9% for D1 and D3, respectively. This aligns with the anisotropic mechanical behaviour of 3DPC reported by van den Heever [19]. The increase in strength of the cast specimens is attributed to the restraining of the crack expansion, which reduced the stress concentration at the crack tip due to the presence of fibres. Several micro-cracks and the fibres bridge across the micro-cracks are observed in the concrete volume, making the failure mode change from fragile/brittle to ductile. Table 4 summarises the mechanical properties of the LC^3 FR-3DPC obtained from compressive strength, splitting tensile strength, and modulus of elasticity tests, with a minimum of three specimens tested for the observation. There is insignificant variation in the strength results of all specimens tested, showing the coefficient of variation (CoV) for all the results obtained to be less than 10%, indicating reasonable repeatability, consistency, and accuracy [14].

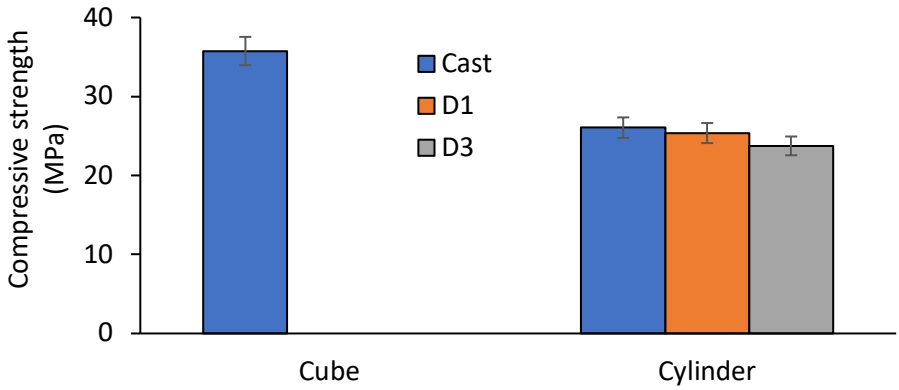

Fig. 3. Compressive strength development of LC^3 FR-3DPC specimens after 28 days curing

Table 4: Average mechanical properties of LC^3 FR-3DPC at 28 days curing age with CoV and number of specimens tested in brackets.

Specimen type	f_{cu} (MPa)	f_c (MPa)	f_{st} (MPa)	f_{sti} (MPa)	E (GPa)
Cast	35.76 (0.031; 4)	26.05 (0.030; 4)	3.27 (0.101; 3)	2.86 (0.048; 3)	21.43 (0.011; 3)
D1	–	25.37 (0.052; 4)	–	1.70 (0.050; 3)	18.77 (0.028; 3)
D3	–	23.75 (0.032; 4)	–	2.64 (0.028; 3)	16.09 (0.036;3)

3.2. Splitting Tensile Strength

Fig. 4 depicts the results of the splitting tensile strength for LC^3 FR-3DPC mixture with the specimens undergo pure tensile stress when subjected to a compressive force applied to a narrow region along its length at 28 days testing. The mean strength of 88% of the cube's strength is achieved for cylindrical cast specimens, indicating higher strength values recorded for cubic specimens when compared with cylindrical specimens, which is conformed to BS EN 12390-6 [17]. Also, the percentage decrease between the cast and D1 orientation is relatively large compared with D3, showing a significant difference between the specimens with 41% and 8% for D1 and D3, respectively. The presence of fibres influences the failure mode in cast and D3 specimens with the avoidance of sudden failure due to fibre bridging effect.

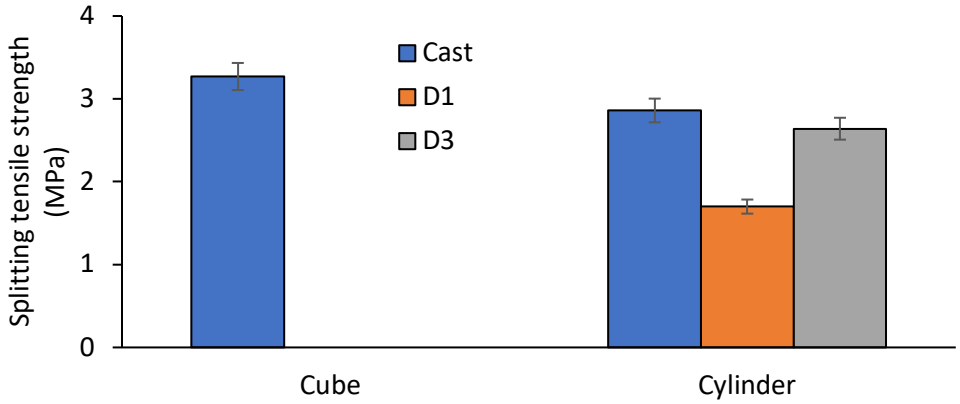

Fig. 4. Splitting tensile strength results and failure patterns for LC^3 FR-3DPC specimens at 28 days of curing

3.3. Modulus of Elasticity

The modulus of elasticity results of LC^3 FR-3DPC mix are presented in Fig. 5 and summarised in Table 4. It is evident that a higher value was recorded for the mould-cast specimens. In comparison, the percentage decrease between cast and printed specimens is 12% for D1 and 25% for D3. This significant difference might be due to the presence of air voids (increased porosity) between the deposited filament layers. Modulus of elasticity is one of the crucial material parameters for structural analysis, which is influenced by various factors such as the nature and compatibility between the matrix and filler, the filler distribution in the matrix, and interfacial structure and morphology [20].

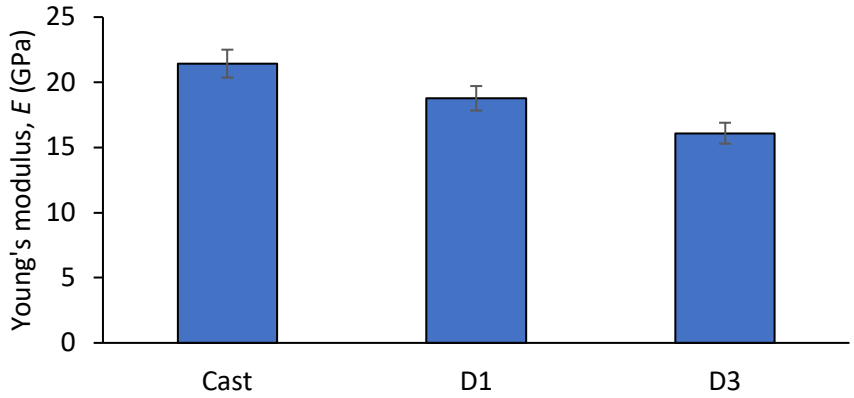

Fig. 5. Young's modulus results for LC^3 FR-3DPC specimens at 28 days of curing

4. CONCLUSIONS

The present study examined the effect of LC^3 on mechanical properties of FR-3DPC using cubes and cylindrical specimens. Based on the experimental observations, the following conclusions are drawn:

- The mean compressive strength of cylindrical specimens is 73% of the mean compressive strength of cubic specimens. This is ascribed to the difference in aspect ratio of specimen height to width of 2 for cylinders and 1 for cubes, and associated confinement in the cubes. The mean splitting tensile strength of cylindrical specimens was 88% of that of cubic specimens.
- Highest strength (compression and tension) and stiffness (Young's Modulus) were exhibited by mould-cast specimens. This could be ascribed to lower porosity and smaller pore size of cast specimens, compared with specimens extracted from 3D printed concrete.
- Fibres influence the post-peak mechanical behaviour of LC^3- based 3D printed concrete. This is ascribed to the fibre crack bridging effect. D3 splitting tensile specimens remained intact after registering their peak resistance.
- Anisotropic mechanical behaviour of LC^3 FR-3DPC was demonstrated for printed specimens in compression, splitting tension, and Young's modulus with the highest strength values recorded in D1 and D3 orientations for compression and Young's modulus, and splitting tension, respectively.

ACKNOWLEDGEMENTS

The first and second authors express their gratitude to the Tertiary Education Trust Fund (TETFund) under the Federal Ministry of Education, Nigeria for their financial support. The authors also thank Kaolin Group (Pty) Ltd, South Africa for providing the LC^2. Constituent materials were supplied in-kind by SAPY Corehfil Polypropylene fibres, PPC, and Chryso Cape Town, South Africa.

REFERENCES

[1] Cho, S., *"Rheo-mechanics and Foam Stability of 3D Printable Foamed Concrete with Nanoparticle Incorporation",* PhD Dissertation in Engineering, Stellenbosch University, South Africa, (2021) 134pp.

[2] Panda, B., Paul, S.C. & Tan, M.J., Anisotropic mechanical performance of 3D printed fiber reinforced sustainable construction material. Mater. Lett., 209: (2017) 146–149.

[3] Weger, D. Lowke, D. and Gehlen, C., 3D printing of concrete structures using the selective binding method – Effect of concrete technology on contour precision and compressive strength, 11th fib International PhD Symposium in Civil Engineering, The University of Tokyo, Tokyo, Japan, (2016) 8 pp.

[4] Nematollahi, B. Xia, M. and Sanjayan, J., Current progress of 3D concrete printing technologies, in: Proceedings of 34th International Symposium on Automation and Robotics in Construction, Taiwan, (2017) 260–267.

[5] Ruan Y, Jamil T, Hu C, Gautam BP, Yu J., Microstructure and mechanical properties of sustainable cementitious materials with ultra-high substitution level of calcined clay and limestone powder, Construction and Building Materials, 22: 314, 125416, (2022) 8 pp.
[6] Mohan MK, Rahul AV, Van Tittelboom K, De Schutter G., Rheological and pumping behaviour of 3D printable cementitious materials with varying aggregate content, Cem. Concr. Res. 2021; 139, 106258, https://doi.org/ 10.1016/j.cemconres.2020.106258.
[7] Scrivener K, Martirena F, Bishnoi S, Maity S., Calcined clay limestone cements (LC^3), Cem. Concr. Res. 2018; 114: 49 – 56, https://doi.org/10.1016/j.cemconres. 2017.08.017.
[8] Chen, Y. Figueiredo, S.C. Li, Z. Chang, Z. Jansen, K. Copuroglu, 0. Schlangen, E., Improving printability of limestone-calcined clay based cementitious materials by using viscosity modifying admixture. Cem Concr Res.; 132: 106040. (2020) 18 pp.
[9] Beigh, M.A.B. Nerella, V.N. Schröfl, C. Mechtcherine, V., Studying the Rheological Behavior of Limestone Calcined Clay Cement (LC^3) Mixtures in the Context of Extrusion-Based 3D-Printing. In: Bishnoi, S. (eds) Calcined Clays for Sustainable Concrete. RILEM Bookseries, vol 25. Springer, Singapore, 2020; https://doi.org/10.1007/978-981-15-2806-4_26.
[10] Reißig, S. Nerella, V.N. Mechtcherine, V., Material Design and Rheological Behavior of Sustainable Cement-Based Materials in the Context of 3D Printing. In: Buswell, R., Blanco, A., Cavalaro, S., Kinnell, P. (eds) Third RILEM International Conference on Concrete and Digital Fabrication. DC 2022. RILEM Bookseries, vol 37. Springer, Cham. 2022; https://doi.org/10.1007/978-3-031-06116-5_65.
[11] Gunnelius, K.R. Lundin, T.C. Rosenholm, J.B. Peltonen, J., Rheological characterization of cement pastes with functional filler particles, Cem. Concr. Res. 65, (2014) 1–7.
[12] SANS 50197–1; South African National Standard; Cement - Part 1: Composition, specifications, and conformity criteria for common cements, 2013.
[13] Van Zijl, G.P.A.G., Kruger, P.J., Cho, S., Zeranka, S., 3D printing polymer fibre concrete. In: Proceedings of the International Inorganic-Bonded Fiber composites Conference. 23–26 Oct 2018, Cape Town, South Africa, (2018) 5–14.
[14] Ibrahim K.A, van Zijl G.P.A.G. Babafemi A.J., Influence of Limestone Calcined Clay Cement on Properties of 3D Printed Concrete for Sustainable Construction, Journal of Building Engineering, (2023), 34 pp, doi: https://doi.org/10.1016/j.jobe.2023.106186.
[15] BS EN 12390-3; Testing Hardened Concrete Compressive Strength of Test Specimens. The British Standards Institution: London, UK, 2019.
[16] ASTM C39/C39M-18; Standard Test Method for Compressive Strength of Cylindrical Concrete Specimens; ASTM International: West Conshohocken, PA, USA, 2018.
[17] BS EN 12390-6; Testing Hardened Concrete Tensile Splitting Strength of Test Specimens. The British Standards Institution: London, UK, 2009.
[18] ASTM International- ASTM C469/C469M-14; Standard Test Method for Static Modulus of Elasticity and Poisson's Ratio of Concrete in Compression. 04 (2014) 1–5.
[19] Van den Heever, M., "Experimental and Computational Mechanics for the Constitutive Modelling of Extrusion-based 3D Concrete Printing", PhD Dissertation in Engineering, Stellenbosch University, South Africa, (2021) 232 pp. https://scholar.sun.ac.za.
[20] Liang, J-Z., Predictions of Young's Modulus of Short Inorganic Fiber Reinforced Polymer Composites, Composites: Part B (2012), doi: 10.1016/j.compositesb.2012.01.010.

YCRETS 2023
YOUNG CONCRETE RESEARCHERS, ENGINEERS & TECHNOLOGISTS SYMPOSIUM
CEMENT & CONCRETE SA

Misconceptions around compressive strength of cementitious repair materials for structural repair

Nicholas Jarratt (1) and Hans Beushausen (1)

(1) Department of Civil Engineering, University of Cape Town

Abstract

Compressive strength is a critical parameter in the design and construction of reinforced concrete elements. It is a quick and cost-effective test, making it an attractive feature for quality control during construction. While higher strength classes indicate higher structural capacity, compressive strengths higher than that required at the ultimate limit state have no structural benefit and may even reduce sustainability, increase costs and lead to cracking. This paper summarizes research on compressive strength and its influence on concrete repair conducted by the Concrete Materials and Structural Integrity Research Unit at the University of Cape Town. The studies showed that a higher compressive strength has a higher tendency to crack under restrained shrinkage, and high-strength mortars do not structurally contribute to repaired members subjected to axial compressive loads in the long term. The paper concludes by recommending that upper limits on compressive strength be placed in repair standards and specifications and that greater attention be paid to parameters that influence crack sensitivity, particularly shrinkage, to achieve more durable repairs.

Keywords: Keywords: Concrete Compressive Strength, Structural Repair Materials, Structural Design, Quality Control, Durability.

1. INTRODUCTION

Compressive strength is arguably the most important property of concrete due to its use as the main parameter for structural design and for quality control and conformity assessment of concrete during construction. Concrete is typically graded into various strength classes. A higher strength class indicates a higher structural capacity, i.e., the ability to withstand higher stress when loaded. This higher load-bearing capacity is often mistaken to be a sign of higher quality, with many structural engineers and contractors assuming that a higher-strength concrete yields superior structural performance or durability. A particular example is the structural repair of damaged concrete members, where the aim is to restore the load-carrying capacity of a damaged concrete member to or beyond its original state [1]. European standards on the performance characteristics of repair materials for structural repairs list compressive strength as one of the top requirements. However, these requirements are no more than arbitrary lower-bound limits that have led to the production of commercial

products with incredibly high strengths that far exceed these lower limits [2]. Datasheets on these high-strength repair materials sometimes describe them as “high-performance” but only focus on compressive strength and give little information on other characteristics.

This paper discusses the role of compressive strength in the load-bearing behaviour of reinforced concrete (RC) members, highlighting its importance in the structural design process. Subsequently, the rationale for using compressive strength as a parameter for quality control and conformity assessment is laid out, which helps to explain how compressive strength has developed into a general quality label for concrete. A summary of research on compressive strength and its influence on concrete repair conducted by the Concrete Materials and Structural Integrity Research Unit at the University of Cape Town is then presented, which shows that a higher compressive strength in repair mortars not only provides no additional benefit but reduces the repairs’ performance. Practical measures aimed at attaining more durable repairs are also presented.

2. COMPRESSIVE STRENGTH IN STRUCTURAL DESIGN AND QUALITY CONTROL

In the structural design of RC elements, concrete compressive strength is required to model and analyse the structure’s load-bearing capacity at the ultimate limit state (ULS). At ULS, structural optimisation of a RC cross-section aims at the reinforcing steel yielding as the concrete fails under compression, resulting in optimum use of material resources. Notably, from a structural engineering point of view, the concrete compressive strength is only needed for this imaginary moment in the lifetime of a structure, i.e. structural failure under a theoretical maximum load. In practice, conservative assumptions for selecting ultimate loads coupled with a range of material and structural safety factors should prevent the concrete from ever being exposed to stresses remotely close to the ultimate strength. For the expected everyday loads, which in structural design are considered for the Serviceability Limit State (SLS) and include the self-weight of the structure and conservatively assumed live loads, the concrete is expected to experience compressive stress levels around 30% of its compressive strength. Therefore, the ultimate compressive strength is irrelevant to the load-bearing capacity of a structure subjected to realistic everyday loads. The only practical effect of increased compressive strength is the associated increase in the concrete’s elastic modulus and reduction in creep, both of which may assist in reducing load-induced deformations, such as deflections in suspended beams or slabs. However, a desired reduction in deformation can more effectively be attained by other means, like an increase in the cross-sectional dimensions. Therefore, specifying and constructing concrete structures with a higher concrete strength than that used in the structural design for the ULS has no real added benefit for the load-bearing behaviour of the structure.

Concrete mix designs and specifications are typically based on achieving the required characteristic design strength, with the associated quality control measure being compressive strength testing at 28 days. Thus, while compressive strength is a necessary structural parameter for ULS design, it also serves as a quality control parameter due to its ease and cost-effectiveness of measurement. The assumption that higher strength equates to superior

quality can be misleading, though, as concrete with a higher strength than that required for ULS design provides no structural benefit and may increase costs and reduce sustainability due to the need for a higher cement content. Higher strength can also result in lower workability, reduced bleeding, increased hydration heat development, increased brittleness, and increased risks of Alkali Aggregate Reaction and drying shrinkage cracking. The effects of higher concrete strength on the overall increased risk of cracking are significant, as cracking of the concrete cover depth, which protects the embedded steel reinforcement from corrosive agents, can significantly reduce the durability of concrete structures.

3. THE CORRELATION BETWEEN CRACKING AND COMPRESSIVE STRENGTH IN REPAIR MATERIALS

One of the main aspects impairing the performance of cementitious repair materials is cracking due to restrained shrinkage, which may result in reduced bond strength between the repair material and substrate and reduced durability due to the increased ingress of deleterious agents into the repaired structure.

The relationship between compressive strength and shrinkage cracking tendency was investigated for a total of 40 different concrete repair mortars with strengths ranging from around 10 – 60 MPa [3]. The mortars were manufactured with different cementitious binder types and contents, water/binder ratios, chemical admixtures, mineral additives, water contents, aggregate combinations, and curing conditions. The tendency to crack was investigated with the ring test according to AASHTO and ASTM, which provides a comparative evaluation of the sensitivity of the cementitious material to crack under the effect of restrained shrinkage and is a helpful tool for the optimization of material performance concerning selected specimen parameters, compressive strength in this case. Figure 1 shows the compressive strength and age at cracking for the 40 different mortars tested[1].

It can be observed in the figure that, while there is a scatter in results, an inverse relationship exists between the age at cracking and compressive strength, with a higher compressive strength generally increasing the tendency to crack. This phenomenon was also reported earlier by Dittmer and Beushausen [4]. Furthermore, it was observed that increasing the compressive strength at 28 days beyond approximately 35 MPa did not significantly change the age at cracking, pinpointing this strength as the “cracking threshold” in this research project. The results were owed to the correlation between stress and strain as expressed through Hooke’s Law. Increasing strength is generally accompanied by a corresponding increase in elastic modulus and a decrease in tensile creep and relaxation. With other characteristics constant, an increase in elastic modulus and a reduction in tensile creep and relaxation generate higher stresses when shrinkage deformations are restrained, consequently increasing the susceptibility of the cementitious material to cracking.

[1]Note that three specimens were tested for compressive strength and restrained shrinkage per a mix, respectively.

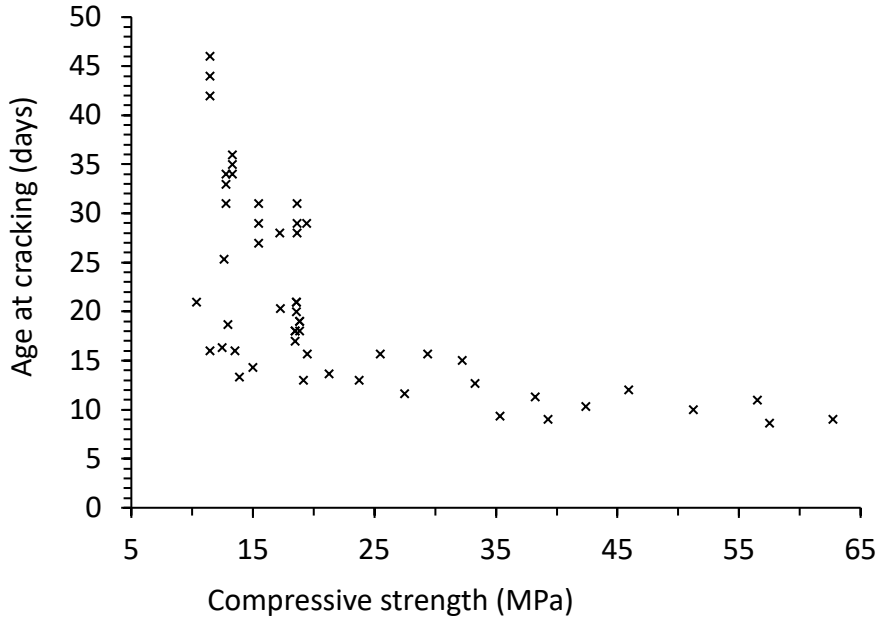

Figure 1: Age at cracking versus compressive strength at 28 days across test specimens [3].

4. STRUCTURAL EFFECTS OF COMPRESSIVE STRENGTH IN REPAIR MATERIALS

The notion for cementitious repair materials to have a high compressive strength is the perception that these materials can structurally contribute to the load-bearing capacity of repaired reinforced concrete members. While various studies have considered the ultimate contribution of repair materials to members under axial load states, few studies have focused on their long-term performance.

The long-term effects of high-strength cement-based repair materials on repaired members under compressive loads were investigated using an analytical model developed using Hooke's law and Euler-Bernoulli beam theory [5, 6]. The model makes various assumptions relating to uniform strain, load eccentricities, and the transfer of stresses between the concrete substrate and repair material. Externally applied loads and characteristics of the concrete substrate and repair material serve as inputs to the model. These characteristics are compressive strength, elastic modulus, drying shrinkage, and specific creep, which are time-dependent. However, since concrete repairs are typically conducted on aged concrete structures, the concrete substrate's drying shrinkage and creep characteristics would be negligible and thus were not considered. One-day time step increments were used to monitor the influence of the repair material properties on the repaired member over time.

The analytical problem considered an unreinforced concrete square column repaired with high-strength cement-based concrete. The square column had a 500 × 500 mm cross-section, with the repair spanning the columns' entire width and going to a depth of 100 mm, making up 20% of the columns' cross-sectional area (see Figure 2). Damage was assumed to be

concentrated to where the repairs were conducted, an example of which could be poor workmanship (e.g. honeycombing) not detected during construction. The repair material selected was a high-strength cement-based concrete made of a SikaGrout-212 grout and 9.5 mm Greywacke stone aggregate. The dry-mix content of the SikaGrout-212 grout was 1645 kg/m^3, while the stone content was 461 kg/m^3. A water/binder ratio of 0.14 was used (as per the material datasheet) to yield a water content of 230 kg/m^3. It was assumed that all loads were removed before the repair and that the only form of strain recovery in the substrate over the repair period was elastic. One day after the repair, an axial compressive load of 25 MPa was applied and maintained.

Compressive strength, elastic modulus, shrinkage, and creep tests were conducted on the repair material at various ages, while the concrete substrate was chosen to have an elastic modulus of 25 GPa and compressive strength of 50 MPa. The high-strength cement-based concrete had compressive strengths of 42 and 77 MPa and an elastic modulus of 25.5 and 28.5 GPa at 1 and 28 days of age, respectively. Its drying shrinkage and creep were tested at 1 day of age and exposed to a temperature and relative humidity of 22 ± 1°C and 55 ± 5%, respectively. After 90 days, the drying shrinkage strain and specific creep of the high-strength concrete were 340 μ-ε and 120 μ-ε/MPa, respectively, with 89% of the drying shrinkage strain measured after 13 days. The model results in Figure B showed that while the stress in the repair was equivalent to the concrete substrate when loaded, it dropped significantly in the following days, with only 20% of its original stress remaining in the repair after eight days. Conversely, due to this drop in stress, the stress in the substrate increased by 20% in the first eight days. After 14 days of loading, the stress in the repair was below 2.5 MPa, while the stress in the substrate concrete was slightly above 30 MPa.

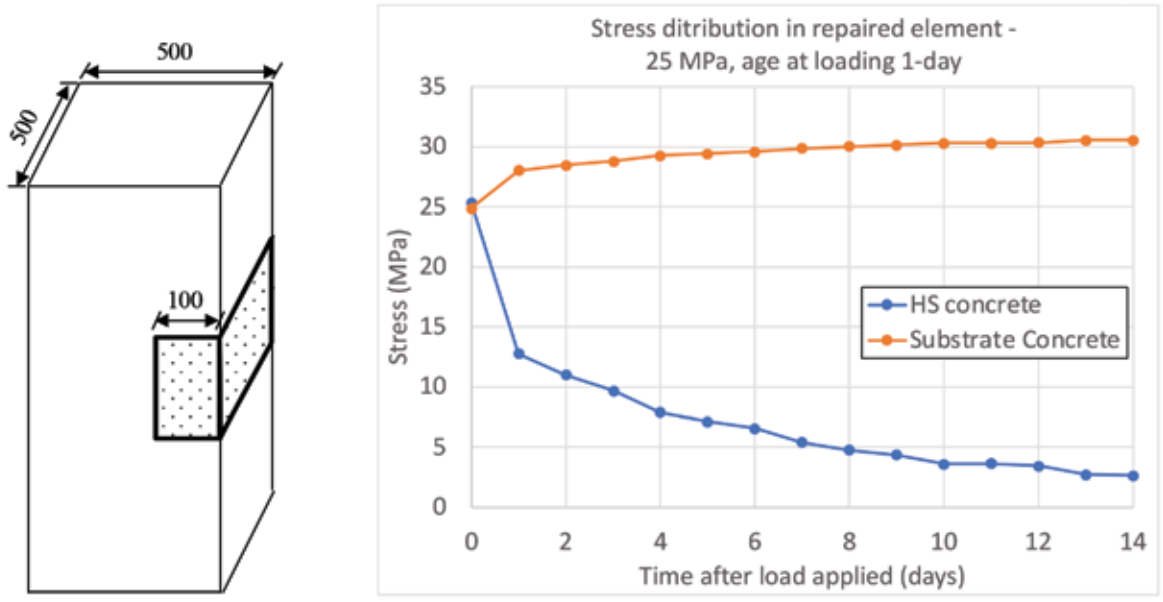

Figure 2: Repair geometry and stress outputs from analytical model over time [5].

The equivalences in stress distribution between the repair and substrate on the day of loading (one day after repair) were owed to the similarities in the elastic moduli. However, as shrinkage and creep develop in the repair material, the repair stress reduces and is transferred to the concrete substrate. This stress reduction results in the repairs' contribution to resisting the externally applied loads reducing over time, leaving the substrate concrete to withstand these surplus loads. The repair is effectively then no longer contributing to the load-bearing capacity of the column after 14 days, despite the high strength values of the repair material.

5. MORE FOCUS ON DURABILITY THAN COMPRESSIVE STRENGTH IN REPAIR MATERIALS

The studies above illustrate that the common belief that high strength is a sign of high quality in concrete repair materials is misleading. Not only do these high strengths increase the susceptibility of a cementitious material to crack, but they offer no benefit in contributing to the load-bearing capacity of a repaired member under axial compressive loads. Instead, more focus should be placed on improving the durability of repairs by limiting the repair materials' susceptibility to cracking. Such remarks have been echoed by Tilly [7] and Vaysburd et al. [8], who noted an undue emphasis on strength and not enough on durability.

A simple measure is to put upper bound limits to compressive strength values in standards and specifications for materials used in repair, where an acceptable range is defined based on the requirements of the repair. Such an approach would reduce the use of excessively high-strength repair materials, which have been shown to be highly susceptible to cracking.

Material properties that influence crack sensitivity should also be considered. An example of this is given in Table 1, which shows how influential a parameter is towards crack sensitivity. One parameter listed as a major factor that has been raised in the studies above is shrinkage. Despite its importance, very little attention is given to this property. Vaysburd et al. [8] found that of the 120 North American repair projects reviewed, not a single specification gave a limitation on shrinkage. Commercial products have also had an influence, often labelling themselves as "non-shrinking" or "shrinkage-compensating". However, research at times has shown this not to be the case and that some of these materials could be more classified as low shrinkage than anything else [9, 10].

Greater emphasis on shrinkage must thus be placed if repairs are to be more durable. Specifying strain limits and, more importantly, the age and exposure conditions are critical steps in this regard. However, further steps towards evaluating the repair material's sensitivity to cracking must also be considered. A combination of free and restrained shrinkage tests, such as the ring test [11], are considered suitable for evaluating repair mortars. The free shrinkage test observes the amount of shrinkage a repair mortar undergoes for a given exposure condition, while the restrained shrinkage test evaluates its tendency to crack when this shrinkage is restrained.

Table 1: Material properties that influence the repair materials sensitivity to cracking [12].

Parameter	Effect		
	Major	Moderate	Minor
Drying shrinkage	x		
Modulus of elasticity	x		
Creep		x	
Compressive strength	x		
Early strength	x		
Paste content	x		
Cement content and type	x		
Aggregate content, type and size	x		
Coefficient of thermal expansion			x
Water to cementitious materials ratio			x
Accelerating admixtures	x		
Plasticizers		x	
Silica fume	x		
Fly ash		x	
Slag		x	
Water content	x		
Slump (within typical ranges)			x

6. CONCLUDING REMARKS

This paper presented a summary of research conducted by the Concrete Materials and Structural Integrity Research Unit at the University of Cape Town on compressive strength and its influence on concrete repair. The studies showed that repair mortars with a higher compressive strength generally have a significantly higher tendency to crack under the effects of restrained shrinkage. Furthermore, in cases where repairs are expected to structurally contribute, the developed analytical model revealed that the contribution of high-strength repair mortars rapidly declines in the first days of loading. More emphasis should thus be placed on the repair materials' durability and limiting its susceptibility to cracking than its compressive strength. Placing upper limits to the compressive strength in repair standards and specifications, while placing greater emphasis on shrinkage and crack sensitivity of repair

materials are seen as simple measures to reduce the use of excessively high-strength repair materials and attain more durable repairs.

REFERENCES

[1] ACI Committee 364 (2018) Physical properties and characteristics affecting the sensitivity to cracking of cementitious repair materials (ACI 364.16 TechNote). Farmington Hills, MI.

[2] Wood, J. (2009) 'Structural repair of defects and deterioration to extend service life', Concrete Solutions: Proceedings of the International Conference on Concrete Solutions, Padua, Italy, pp. 329–335. doi: 10.1201/9780203864005.ch57.

[3] Beushausen, H. and Arito, P. (2018). The influence of mix composition, w/b ratio and curing on restrained shrinkage cracking of cementitious mortars. *Construction and Building Materials*, 174, pp.38-46.

[4] Dittmer, T., Beushausen, H. (2014). The effect of coarse aggregate content and size on the age at cracking of bonded concrete overlays subjected to restrained deformation, *Construction and Building Materials*, Vol 69, October 2014, pp. 73-82.

[5] Naraghi, V., Jarratt, N. and Beushausen, H. (2022). Investigating the structural contribution of patch repairs to reinforced concrete elements. In MATEC Web of Conferences (Vol. 361, p. 03002). EDP Sciences.

[6] Naraghi, V. (2022). Effectiveness of high strength repair mortars in structural patch repairs of concrete members under axial compression. University of Cape Town.

[7] Tilly, G. (2011) 'Durability of concrete repairs', in Grantham, M. G. (ed.) Concrete Repair: A Practical Guide. 1st edn. Oxfordshire: Routledge, pp. 231–247. doi: 10.1201/b12433-15.

[8] Vaysburd, A., Bissonnette, B., Garbacz, A. and Courard, L. (2016) 'Specifying Concrete Repair Materials', *Materiały Budowlane*, 1(3), pp. 44–47. doi: 10.15199/33.2016.03.13.

[9] Beushausen, H. and Alexander, M.G. (2006). Failure mechanisms and tensile relaxation of bonded concrete overlays subjected to differential shrinkage. *Cement and concrete research*. Vol. 36, p. 1908-1914.

[10] Emmons, P.H. and Vaysburd, A.M. (1995). Performance criteria for concrete repair material. Phase I. Vicksburg, US Army Corps of Engineers. (Technical report; REMR-CS-47).

[11] ASTM C1581 (2018). Standard Test Method for Determining Age at Cracking and Induced Tensile Stress Characteristics of Mortar and Concrete under Restrained Shrinkage. West Conshohocken, PA: American Society for Testing and Materials.

[12] Vaysburd, A. M., Bissonnette, B. and Fay, K. F. von (2015) Compatibility Issues in Design and Implementation of Concrete Repairs and Overlays. US Bureau of Reclamation. (Report No. MERL-2014-87).

YCRETS 2023
YOUNG CONCRETE RESEARCHERS, ENGINEERS & TECHNOLOGISTS SYMPOSIUM
CEMENT & CONCRETE SA

The effect of nanobubble water on the fresh properties of conventional concrete and 3d printing concrete

Simba S. Kanyenze (1), Dawid J. Joubert (1) and Riaan Combrinck (1)

(1) Department of Civil Engineering, Stellenbosch University

Abstract

Micro-nanobubble- and nanobubble-infused mixing water has shown potential in improving the hardened properties of conventional concrete. However, there is no extensive reporting on the effects of pure nanobubble water on the fresh properties of traditional concrete. Good fresh properties allow for good placing and curing of concrete, affecting a concrete structure's durability. No publicly available literature exists on using micro-nanobubbles or nanobubbles in 3D concrete printing (3DCP). This study addressed the previously mentioned research gaps by carefully studying the fresh properties of both types of concrete. This study concluded that air nanobubble water slightly increases the flowability of conventional concrete. They also slightly enhance the thixotropy of 3D printing concrete.

Keywords: fresh properties, nanobubbles, 3D printing concrete, concrete

1 INTRODUCTION

Micro-nanobubble- and nanobubble-enriched water have been added to conventional concrete to alter its fresh and hardened properties. Micro-nanobubbles are gaseous bodies with a diameter size distribution of 100 µm or smaller that are evenly distributed within a liquid medium. On the other hand, nanobubbles are gaseous bodies with a diameter of less than 1 µm. However, in most industries where nanobubbles are applied, nanobubble diameters range between 100 nm and 200 nm [1].

There is a crucial difference between micro-nanobubble water and nanobubble water. Micro-nanobubble water is less stable than pure nanobubble water. Microbubbles with a diameter range between 1 µm and 100 µm are more buoyant than the smaller nanobubbles [1, 2]. As a result, microbubbles in the liquid medium gradually reduce in size before collapsing onto themselves [2]. Lower buoyancy nanobubbles, on the other hand, have longer stagnation times and move in the liquid medium in a Brownian motion [2]. Several studies have shown that temperature, pH, salt concentration in the water, and gas type all influence nanobubble stability [2-4].

Literature shows that micro-nanobubbles and nanobubbles decrease the flowability of conventional concrete, increase mechanical properties, and increase durability. This is due to nanobubbles' unique properties, which include large specific surface area, long stagnation times, long-term stability, and a high gas-liquid mass transfer rate [4-6]. In concrete, the probability of the nanobubbles colliding with cement particles is high because of the significant difference in size between the two entities. Equation 1 illustrates the collision

probability between micro-nanobubbles and cement particles where P_c is the probability of collision between a bubble and another particle, Re is the Reynolds number, D_p is the particle diameter [m], and D_b is the bubble diameter [m] [7].

$$P_c = \left(\frac{3}{2} + \frac{4Re^{0.72}}{15}\right)\left(\frac{D_p}{D_b}\right)^2 \quad (1)$$

As a result, nanobubbles effectively disperse cement particles throughout the concrete matrix, allowing them to hydrate more easily. The hydration reaction is accelerated, resulting in decreased setting time and reduced flowability in conventional concrete [7]. Consequently, the homogeneity of the concrete mixture improves, resulting in improved mechanical and durability properties. Zeta potential measurements have also shown that nanobubbles have a negative charge, making them more effective in dispersing cement particles [2, 3, 8]. According to other researchers, the increase in hydration temperature observed using micro-nanobubble water in the concrete is caused by the bubble's localised collapse [9]. Some hypotheses propose that the bubbles function as nucleation points for the precipitation of calcium silicate hydrate (CSH) gel and calcium hydroxide (CH) crystals [9, 10].

Micro-nanobubbles have been used in shotcrete [10] and self-compacting concrete [11] to improve early-age strength, flowability, and durability. Arefi, Saghravani and Naeeni [12] conducted the first use of micro-nanobubble water in concrete at the University of Iran, where they observed a decrease in the workability of the concrete with micro-nanobubble water. A study by Khoshroo, Shirzadi Javid and Katebi [8] utilised air micro-nanobubbles with zeolite and chekneh pozzolan to investigate conventional concrete's fresh and hardened properties. The investigation showed a decrease in the slump of the concrete (due in part to the addition of pozzolans), a marked increase in the mechanical properties of concrete, and an increase in concrete durability.

No literature could be found on using nanobubble and micro-nanobubble water in 3D concrete printing. This significant gap in literature creates an opportunity to contribute to the global body of knowledge in this aspect of nanobubble application. In the last ten years, 3D concrete printing (3DCP) has received significant global research attention [13]. This is due to the method of construction's low labour requirement, which allows for significant cost savings. Besides significantly decreasing labour, 3D concrete printing is safer than conventional construction methods [14]. 3D printing concrete has also shown a lower carbon footprint than other construction methods [15].

Several materials, including fibres and various nanomaterials, have been used in 3DCP to change the fresh and hardened properties [16-18]. A 3D printing concrete mix begins to flow when the pressure applied to the mix during pumping exceeds the static yield stress. The dynamic yield stress needs to be maintained to keep the mix flowing. However, if the dynamic yield stress is too low, the 3D printing mix could segregate [17]. If the dynamic yield stress is too high, the concrete is difficult to pump.

Thixotropy is a key fresh property determining whether a 3D printing concrete mix is printable. Thixotropy depends on the re-flocculation of particles within the concrete matrix and the irreversible chemical reactions that bring about strength build-up after deposition. The re-flocculation rate (R_{thix}) quantifies the flocculation process or the static yield stress build-

up rate after the concrete has been deposited. Therefore, the re-flocculation time (t_{rf}) is when a 3D printing concrete mix fully regains its static yield stress after agitation. The structuration rate (A_{thix}) quantifies irreversible chemical reactions, such as hydration, which occur thousands of seconds after deposition, resulting in a yield stress increase greater than the static yield stress. However, the A_{thix} is affected by other environmental factors, making R_{thix} a better measure of the thixotropy of a 3D printing concrete mix [17].

There has not been extensive research on using pure nanobubble water in conventional concrete, and there are no publicly available studies on using nanobubbles in 3D concrete printing. This study aims to use pure nanobubble water, that is, water with bubbles smaller than 1 µm, in conventional concrete and 3D printing concrete. The objective of the study is to investigate the effect of air nanobubble water on the fresh properties of conventional and 3D printing concrete.

2 EXPERIMENTS

2.1 Nanobubble Water Generation

An MK1 nanobubble generation machine, supplied by Fine Bubble Technologies (Pty) Ltd [19], was used to generate air nanobubbles at atmospheric pressure. The nanobubbles were generated in a 200-litre water tank for one hour. The water was collected 30 minutes after turning the machine off into 10-litre polyethene water containers and stored in a temperature-controlled room (maintained at 23 °C) for at least 24 hours. Malvern Panalytical's Nanosight NS300 was used to measure the nanobubble concentration, mean, and mode bubble diameters using nanoparticle tracking analysis [20]. At 30 minutes after generation, the average nanobubble concentration was 1.58 x 10^8 bubbles/ml, with a mean diameter of 137.8 nm (mode 103.1 nm, standard deviation 61.5 nm). The air nanobubble water results are shown in Figure 1. These results are consistent with results obtained by N. Kalogerakis, G.C. Kalogerakis and Botha [21], who also used the same nanobubble generation machine.

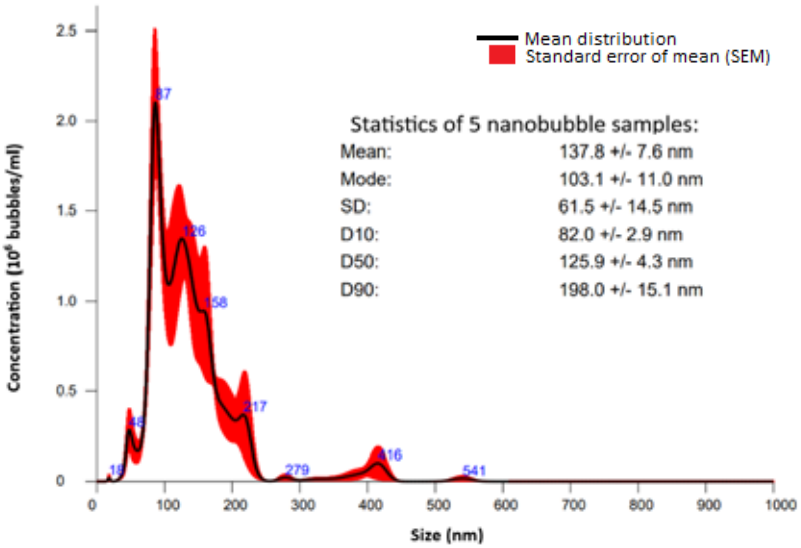

Figure 1: Nanoparticle tracking analysis results performed on 5 samples of air nanobubble water.

2.2 Mix Design and Mix Procedure

This study included two reference mixtures, one conventional concrete reference mix (REF-CONV) and a standard Stellenbosch University 3D printing concrete mix (REF-3D) [17]. One air nanobubble conventional concrete mix was used (ANBC-23). The mix contained air nanobubble water which was stored for 24 hours at 23 °C in a temperature-controlled room One 3D printing concrete mix which contained air nanobubble water stored at 23 °C for 24 hours in a temperature-controlled room was used in this experiment (ANB3DC-23). The normal tap water used in the reference mixes was also stored in the temperature-controlled room at 23 °C for 24 hours before mixing. The mix designs of the concrete mixtures are shown in Table 1. Before mixing, the dry constituents for each mix were weighed into containers, sealed, and stored in the same temperature-controlled room (at 23 °C) as their respective water types for the same amount of time (24 hours).

A CEM II/A-L 52.5 N cement from Pretoria Portland Cement (PPC) was used for all the mixes [22]. The conventional concrete mixes contained a natural pit sand, known locally as Malmesbury sand, and 13 mm Greywacke stone as coarse aggregate. The relative density (RD) of the Malmesbury sand was 2.6, the fineness modulus (FM) was 1.35, and the dust content (< µm 75) was 2.6%. In the 3D printing concrete mixes, a mixture of Malmesbury sand and dune sand, known locally as Phillipe sand, was used. The resulting sand mixture's FM, RD, and dust content were 0.81, 2.64, and 3.2%, respectively. DuraPozz fly ash class F, CHRYSO silica fumes and CHRYSO Premia 310 superplasticiser was used in the 3D printing concrete mixes.

Table 1: Conventional and 3D printing concrete mixtures.

	Mix names			
Constituents [kg/m^3]	REF-CONV	ANBC-23	REF-3D	ANB3DC-23
Normal tap water	209	-	261	-
Air nanobubble water	-	209	-	261
Cement	348	348	579	579
Malmesbury sand	901	901	-	-
Coarse aggregate	900	900	-	-
Malmesbury & Phillipi sand mix	-	-	1169	1169
Fly ash	-	-	165	165
Silica fumes	-	-	83	83
CHRSYO Premia 310	-	-	7	7

2.3 Slump and Flow Table Test

Slump and flow table measurements were conducted just before the rheological characterisation of the conventional and 3D printing concrete mixes was performed, respectively. The slump test [23] was used to measure conventional concrete mixtures' consistency (or flowability). The flow table test [24] was used to assess the flowability of the 3D printing concrete mixes. At least three measurements of slump and flow diameter were conducted, respectively.

2.4 Rheological Characterisation and Buildability Test

An ICAR rheometer [25] was used for the rheological characterisation of the conventional and 3D printing concrete mixes. One stress growth test was used to obtain the conventional concrete mixes' initial static and dynamic yield stress. Using a series of stress growth tests as explained in a study by Kruger, Zeranka and van Zijl [17], the R_{thix}, A_{thix} and t_{rf} of the 3D printing concrete mixes were obtained. Three rheological characterisation measurements were conducted for each mix. The buildability of the 3D printing concrete mixes was evaluated to validate the effect of nanobubbles in 3D printing concrete [17]. A circular hollow column with an outer diameter of 250 mm is printed at a rate of 60 mm/s until failure. Each layer was approximately 10 mm tall and had a maximum width of 35 mm. Only one buildability test was conducted.

3 CONVENTIONAL CONCRETE RESULTS

Figure 2 shows the yield stress and slump results for the two conventional concrete mixes. The coefficient of variation (CoV) for all of the results ranged from 4% to 21%. ANBC-23 has a higher initial static and dynamic yield stress than REF-CONV by 10.7% and 4.9%, respectively. However, the yield stress results do not agree with the slightly (4.6%) higher slump result obtained for ANBC-23 compared to REF-CONV. The higher static yield stress for ANBC-23 compared to REF-CONV can be expected to translate to a lower slump. This is not the case, however, given the larger variation in slump results for ANBC-23 compared to REF-CONV as well as the still rather small variation in slump results, the slump results of these two mixes can be considered very similar. Apart from the static yield stress, the rest of the results for ANBC-23 and REF-CONV have differences of less than 5%. This shows that nanobubbles generated by the MK1 nanobubble machine do not change the fresh properties of conventional concrete significantly. The slump results shown in Figure 2 contradict the slump results in the study conducted by Arefi, Saghravani and Naeeni [12], where a significant decrease in flowability (or consistency) was observed. The difference in results can be attributed to the use of micro-nanobubble water as opposed to pure nanobubble water in this experiment, which resulted in different water properties and the subsequent effects on concrete.

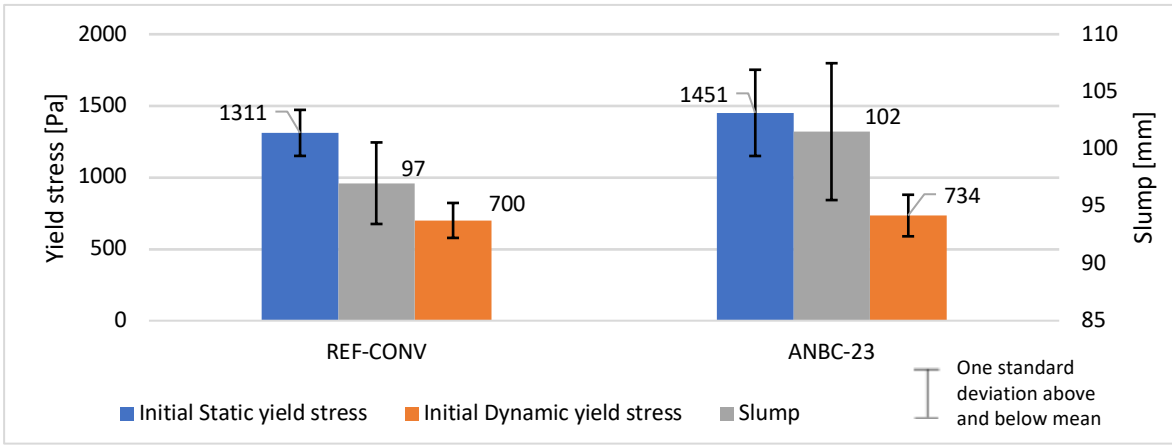

Figure 2: Slump, static and dynamic test results for REF-CONV and ANBC-23.

4 3D PRINTING CONCRETE RESULTS

Figure 3 depicts the flow diameter, static yield stress, and dynamic yield stress results for the two 3D printing concrete mixes. The coefficient of variation (CoV) for all of the results ranged from 0.2% to 20%. ANB3DC-23 has a higher initial static and dynamic yield stress compared to REF-CONV by 4.4% and 7.9%, respectively. The flow diameter results are similar with only a 1.2% decrease in the flow diameter from REF-3D to ANB3DC-23. These results mean that slightly more energy is needed to initiate and maintain the flow of ANB3DC-23. The R_{thix}, A_{thix} and t_{rf} for REF-3D and ANB3DC-23 were also comparable, as shown in Table 2. The R_{thix} of ANB3DC-23 was slightly higher than that of REF-3D. Therefore, the t_{rf} of ANB3DC-23 was shorter than that of REF-3D. The A_{thix} of ANB3DC-23 was marginally lower than that of REF-3D.

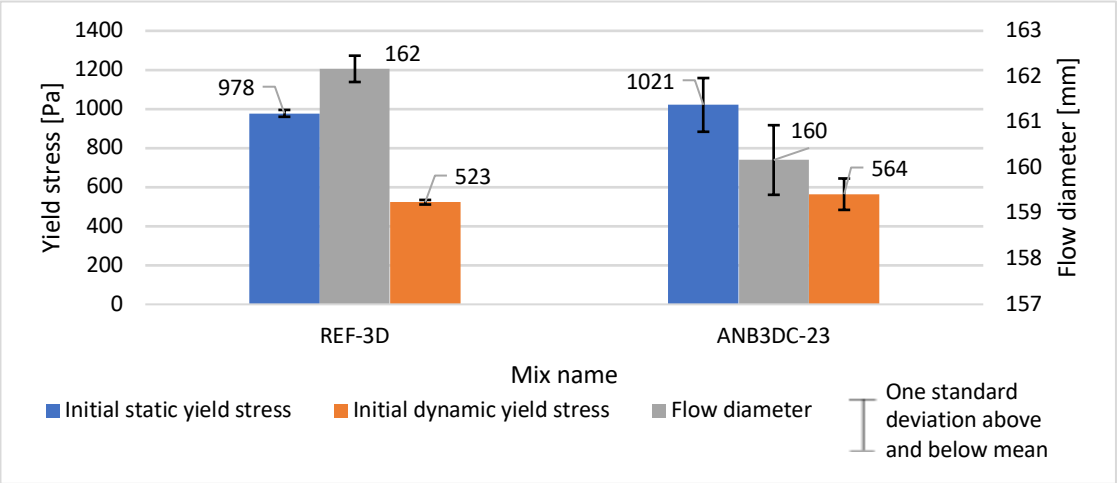

Figure 3: Flow diameter, static and dynamic yield stress results for REF-3D and ANB3DC-23.

Table 2 depicts the buildability test results. These results are comparable and correlate with the R_{thix} and A_{thix} results. The slightly higher A_{thix} result of REF-3D explains why more layers were obtained. After deposition, there was slightly faster structuration in REF-3D than in ANB3DC-23. However, as explained in the introduction several factors other than hydration influence A_{thix}; therefore, R_{thix} is a better measure of the thixotropy of a 3D printing concrete mix. From the results, it can be concluded that ANB3DC-23 is slightly more thixotropic than REF-3D.

Table 2: R_{thix}, A_{thix}, t_{rf} and buildability results for the two 3D printing concrete mixes.

Mix name	R_{thix} [Pa/s]	A_{thix} [Pa/s]	t_{rf} [s]	Buildability [layers]
REF-3D	2.91	0.363	156.2	21
ANB3DC-23	2.95	0.355	154.8	19

The results for the 3D printing concrete mixes are similar. They demonstrate that the pure nanobubble water produced by the MK1 nanobubbler does not significantly affect the fresh properties of 3D printing concrete. This means gases such as carbon dioxide could potentially be incorporated in the nanobubbles as a form of carbon capture and the gases could

participate in the hydration reaction without significantly changing the thixotropy of the 3D printing concrete mix. Because the MK1 is lightweight and compact, and requires routine maintenance every three months, transportation and maintenance costs can be kept to a minimum [19]. As long as the cost of delivering regular water to a construction site is low, the overall cost of producing nanobubble water is insignificant in comparison to other construction costs.

5 CONCLUSIONS

Air nanobubbles seem to slightly increase the flowability of conventional concrete. The air nanobubbles also increase the static and dynamic yield stress of conventional concrete. However, the change in the fresh properties of conventional concrete is not significant. Air nanobubbles slightly increase the initial static and dynamic yield stress of 3D printing concrete. Hence, the thixotropy of the 3D printing concrete is slightly enhanced. Because conventional concrete and 3D printing concrete are such different materials, the technology that works for conventional concrete may not work for 3D printing concrete. This fact also explains why the fresh properties differ when air nanobubble water is added. Hardened and durability property tests on conventional or 3D printing concrete containing air nanobubble water had not been performed at the time of writing this paper. As a result, the authors are unable to make a valid comment on the long-term properties of concrete containing nanobubble water at this time.

6 ACKNOWLEDGEMENTS

The support of Fine Bubble Technologies (Pty) Ltd is gratefully acknowledged.

REFERENCES

[1] ISO 20480-1:2017, “Fine bubble technology - General principles for usage and measurement of fine bubbles - Part 1: Terminology,” 2017.

[2] P. Khan, W. Zhu, F. Huang, W. Gao, and N. A. Khan, “Micro-nanobubble technology and water-related application,” *Water Sci Technol Water Supply*, vol. 20, no. 6, pp. 2021–2035, 2020, doi: 10.2166/ws.2020.121.

[3] W. Jia, S. Ren, and B. Hu, “Effect of water chemistry on zeta potential of air bubbles,” *Int J Electrochem Sci*, vol. 8, no. 4, pp. 5828–5837, 2013.

[4] J. N. Meegoda, S. Aluthgun Hewage, and J. H. Batagoda, “Stability of nanobubbles,” *Environ Eng Sci*, vol. 35, no. 11, pp. 1216–1227, 2018, doi: 10.1089/ees.2018.0203.

[5] H. Sharma and N. Nirmalkar, “Enhanced gas-liquid mass transfer coefficient by bulk nanobubbles in water,” *Mater Today Proc*, vol. 57, pp. 1838–1841, 2022, doi: 10.1016/j.matpr.2022.01.029.

[6] J. Villadsen, J. Nielsen, and G. Lidén, “Gas–Liquid Mass Transfer,” in *Bioreaction Engineering Principles*, Boston, MA: Springer US, 2011, pp. 459–496. doi: 10.1007/978-1-4419-9688-6_10.

[7] P. Mohsen Zadeh, S. F. Saghravani, and G. Asadollahfardi, “Mechanical and durability properties of concrete containing zeolite mixed with meta-kaolin and micro-nano bubbles of water,” *Structural Concrete*, vol. 20, no. 2, pp. 786–797, 2019, doi: 10.1002/suco.201800030.

[8] M. Khoshroo, A. A. Shirzadi Javid, and A. Katebi, “Effects of micro-nano bubble water and binary mineral admixtures on the mechanical and durability properties of concrete,” *Constr Build Mater*, vol. 164, pp. 371–385, 2018, doi: 10.1016/j.conbuildmat.2017.12.225.

[9] Z. Wan, T. He, X. Ma, K. Zhang, and Y. Hu, “Research on the synergy of micro-nano bubble water and alkali-free liquid accelerator to improve the early strength and hydration rate of cement,” *Journal of Building Engineering*, vol. 57, no. July, p. 104909, 2022, doi: 10.1016/j.jobe.2022.104909.
[10] H. Liu, Z. Tian, X. Sun, J. Xiang, and X. Jiao, “Study on the multiscale properties of cement-based materials containing nano-bubble water,” *Constr Build Mater*, vol. 360, no. 1, p. 129595, 2022, doi: 10.1016/j.conbuildmat.2022.129595.
[11] B. Yahyaei, G. Asadollahfardi, and A. M. Salehi, “Study of using micro-nano bubble to improve workability and durability of self-compact concrete,” *Structural Concrete*, vol. 23, no. 1, pp. 579–592, Feb. 2022, doi: 10.1002/suco.202000208.
[12] A. Arefi, S. F. Saghravani, and R. M. Naeeni, “Mechanical Behavior of Concrete, Made with Micro-Nano Air Bubbles,” *Civil Engineering Infrastructures Journal*, vol. 49, no. 1, pp. 139–147, 2016, doi: 10.7508/ceij.2016.01.010.
[13] A. J. Babafemi, J. T. Kolawole, M. J. Miah, S. C. Paul, and B. Panda, “A concise review on interlayer bond strength in 3D concrete printing,” *Sustainability (Switzerland)*, vol. 13, no. 13, 2021, doi: 10.3390/su13137137.
[14] M. Batikha, R. Jotangia, M. Y. Baaj, and I. Mousleh, “3D concrete printing for sustainable and economical construction: A comparative study,” *Autom Constr*, vol. 134, no. November 2021, p. 104087, 2022, doi: 10.1016/j.autcon.2021.104087.
[15] H. Alhumayani, M. Gomaa, V. Soebarto, and W. Jabi, “Environmental assessment of large-scale 3D printing in construction: A comparative study between cob and concrete,” *J Clean Prod*, vol. 270, p. 122463, Oct. 2020, doi: 10.1016/j.jclepro.2020.122463.
[16] J. Sun, F. Aslani, J. Lu, L. Wang, Y. Huang, and G. Ma, “Fibre-reinforced lightweight engineered cementitious composites for 3D concrete printing,” *Ceram Int*, vol. 47, no. 19, pp. 27107–27121, 2021, doi: 10.1016/j.ceramint.2021.06.124.
[17] J. Kruger, S. Zeranka, and G. van Zijl, “An ab initio approach for thixotropy characterisation of (nanoparticle-infused) 3D printable concrete,” *Constr Build Mater*, vol. 224, pp. 372–386, Nov. 2019, doi: 10.1016/J.CONBUILDMAT.2019.07.078.
[18] H. Yang, Y. Che, and M. Shi, “Influences of calcium carbonate nanoparticles on the workability and strength of 3D printing cementitious materials containing limestone powder,” *Journal of Building Engineering*, vol. 44, no. January, p. 102976, 2021, doi: 10.1016/j.jobe.2021.102976.
[19] Fine Bubble Technologies, “MK1 Nanobubbler Operation and Maintenance Manual,” 2018. www.finebubbletechnologies.com (accessed Feb. 09, 2022).
[20] Malvern Panalytical, “Nanosight NS300 User Guide,” Worcestershire, 2019.
[21] N. Kalogerakis, G. C. Kalogerakis, and Q. P. Botha, “Environmental applications of nanobubble technology: Field testing at industrial scale,” *Canadian Journal of Chemical Engineering*, vol. 99, no. 11, pp. 2345–2354, 2021, doi: 10.1002/cjce.24211.
[22] PPC Limited, “PPC Limited,” *PPC Limited*, 2023. https://www.ppc.africa/ (accessed Feb. 09, 2023).
[23] SANS 5862-1, “Concrete tests - Consistence of freshly mixed concrete - Slump test,” *SABS Standards Division*, 2006.
[24] ASTM C1437, “Standard Test Method for Flow of Hydraulic Cement Mortar: C1437-01,” *Standard*, pp. 7–8, 2001.
[25] Germann Instruments, “ICAR Rheometer,” *Product Specifications*, 2010. https://www.germanninstruments.com/concrete-rheometer-icar-plus/ (accessed Feb. 09, 2022).

YCRETS 2023
YOUNG CONCRETE RESEARCHERS, ENGINEERS & TECHNOLOGISTS SYMPOSIUM
CEMENT & CONCRETE SA

Comparison of permeability-reducing admixture and supplementary cementitious material for improved durability of concrete

Amé Kleynhans (1), Elsabe P. Kearsley (1)

(1) Department of Civil Engineering, University of Pretoria, Pretoria, 0028, South Africa

Abstract

As the focus of industry becomes increasingly concentrated on minimising life-cycle cost and environmental impacts, longevity of concrete structures becomes more important. Durability of concrete is a crucial factor in its performance over its expected lifespan. This study compares the effectiveness of a permeability-reducing admixture for hydrostatic conditions (PRAH) and fly ash as a supplementary cementitious material and filler, on the durability of concrete. The compressive strength, self-healing capabilities and various tests assessing durability were completed. The effect of curing conditions on PRAH and fly ash mixes were also evaluated. Concrete mixes incorporating fly ash performed better than Portland cement mixes in self-healing capability, oxygen permeability, and chloride conductivity. Some beneficial durability results were obtained from the combination of fly ash and PRAH. The inclusion of PRAH marginally reduced the depth of penetration of water under pressure for air-cured Portland cement mixes. Water-cured samples exhibited superior performance across all tests associated with durability.

Keywords: Permeability-reducing admixture (PRAH), Supplementary cementitious materials (SCM), Durability

1. INTRODUCTION

Society's insatiable appetite for concrete makes it the most widely employed construction material by volume [1]. To minimise the well documented environmental impact, consumption of energy and raw materials of concrete, it is crucial to maximise the lifespans of concrete structures. Long lasting structures are also more economic, especially if maintenance requirements are reduced. The durability of a material is associated with the resistance to deterioration over the required service life of the structure it forms part of. Concrete durability is therefore an important factor to ensure long lasting structures. Consequently, durability and sustainability are interdependent.

The deterioration mechanisms of concrete are related to its penetrability. Penetrability is defined as the degree to which concrete permits gases, liquids or ionic species to move through its pore structure [2]. Therefore, the intended application and exposure environment of concrete is important when evaluating concrete durability.

2. BACKGROUND

There are two main schools of thought on methods to achieve improved durability within concrete without lowering the water/cement ratio of a concrete mix design. The first, is a commonly used method to include supplementary cementitious materials (SCMs) such as fly ash. Due to the pozzolanic activity and improved packing density (filling effect) provided by SCMs the mechanical properties and durability of concrete are improved [3, 2]. The second method is the use of more recently developed permeability-reducing admixtures. Theoretically, permeability-reducing admixtures react with water and other concrete hydration products to form insoluble crystals which fill the pores and voids throughout the concrete matrix, thereby reducing permeability and so improving durability. In the absence of moisture, the active ingredients remain dormant. The curing conditions for concrete containing such admixtures can therefore not be ignored. However, literature reveals contradictory results and conclusions for 'permeability-reducing admixture for hydrostatic conditions' (PRAH). De Souza Oliveria et al. [4] reported a reduction in permeability with the use of PRAH. In 2021, Gojević et al. [3] concluded that permeability results were dependent on water-cement ratio, while Pazderka and Hájková [5] concluded that the effect of waterproofing admixture is negligible. With varying test methods, curing conditions and cement types, there is no definitive consensus on the reliability of waterproofing admixtures. There is also a lack of research into the use of PRAH along with SCM [6].

The purpose of this study was to compare the effectiveness of a commercially available PRAH and fly ash as a fine filler and pozzolanic material on the mechanical and durability properties of concrete. The effect of curing conditions on the aforementioned properties was also evaluated.

3. EXPERIMENTAL SETUP

3.1 Mix Design

A total of eight concrete mixes were cast to compare the effect of a PRAH and fly ash as a cement extender (SCM) and fine filler material, as well as curing conditions on the hardened properties of concrete. A water content of 220l/m³ was used to achieve adequate workability characterized by a 40mm slump measurement for the crushed aggregate used, as prescribed by Soutsos and Domone [7]. A CEM I 52.5R Portland cement (PC) reference mix with water-cement (w/c) ratio of 0.5 and a fly ash reference mix with a water-binder (w/b) ratio of 0.5 were considered. The w/c and w/b ratios of 0.5 were selected based on ratios given by the United States Bureau of Reclamation [8], for durability class concrete subject to exposure of extreme severity. The fly ash mix resembled the PC mix but with 25% of the cement and 50% of the fine aggregate portions replaced with unclassified fly ash (FA). The cement replacement yields a CEM II-B for the fly ash mixes (SANS 50197-1:2013) [9]. As per manufacturer recommendation, 1% by mass of cement PRAH was added to each reference mix to produce the applicable admixture samples. Each mix was placed either in a 25°C water bath or wrapped in plastic after casting and demoulding, to achieve water- and air-cured conditions. Locally available materials were used and a single source of cement, aggregate and unclassified fly ash were considered. Table 1 contains the dry materials and curing conditions of each mix.

Table 1 Dry material compositions [kg/m³] and curing conditions

Mix		Cement	FA SCM	PRAH	Fine Aggregate	FA Fine Aggregate	Coarse Aggregate	Curing Condition
PC	BW	440	-	-	907	-	911	Water
	BA	440	-	-	907	-	911	Air
	BPW	440	-	4.4	904	-	911	Water
	BPA	440	-	4.4	904	-	911	Air
FA	FW	330	110	-	434	332	911	Water
	FA	330	110	-	434	332	911	Air
	FPW	330	110	4.4	432	332	911	Water
	FPA	330	110	4.4	432	332	911	Air

3.2 Test Methods

Various tests were performed to evaluate the hardened properties of the mixes. Table 2 contains the properties tested, applicable standard followed and specimen dimensions.

Table 2 Testing procedures

Property	Standard	Specimen description
Compressive strength	SANS 5863:2006[10]	100 mm cubes
Self-healing effect	-	100 mm cubes
Hydration of matrix	-	100 mm cubes
Oxygen permeability	SANS 3001-CO3-2:2022[11]	70 mm disks described in SANS 3001-CO3-1:2015[12]
Water sorptivity	SANS 516-3:2009[13]	
Chloride conductivity	SANS 3001-CO3-3:2021[14]	
Depth of penetration of water under pressure	EN 12390-8:2019[15]	150 mm cubes

Coppola et al. [16] described self-healing as the ability of the material to restore mechanical characteristics and self-sealing as merely the ability to seal surface cracks. The seal-healing capacity of concrete can be considered as part of its durability. Retesting the compressive strength of the material is therefore a good measure of mechanical properties restored and an indicator of self-healing capability as opposed to measuring crack widths which only provide an indication of self-sealing on the surface of the material. As such, to assess the self-healing of each of the concrete mixes, the specimen which were tested for compressive strength at 7, 28 and 56 days were placed in water and retested 28 days after initial compressive strength testing.

The hydration of the concrete matrix was evaluated through mass gain/loss cycles. The mass gain/loss was determined by first leaving the samples in their allocated curing condition for a week, and then cycling the samples between a 50°C oven and 25°C water bath each week for 16 weeks. The samples were weighed between cycles and the mass gain/loss calculated as a percentage of initial mass after demoulding.

4. RESULTS AND DISCUSSION

4.1 Compressive Strength

The compressive strength of each mix was tested at 7, 28 and 56 days respectively. The results showed PRAH was inconsequential to compressive strength and the largest difference in strength was because of curing conditions. The air-cured samples were 13-20% weaker than water-cured samples at 28 days. The PC mixes' strength plateaued after 28 days, for both curing conditions. In contrast, the FA mixes showed continued strength increase over the testing period. This can be attributed to the spherically shaped fly ash particles which provided improved packing density of the concrete. This filler effect, along with fly ash's potential for pozzolanic reaction provided additional strength, which was noticeable when comparing the PC and FA mixes at as early as 28 days.

4.2 Self-healing Effect

The results of retesting the compressive strength of the samples originally tested at 7, 28 and 56 days are shown in Figure 1. The percentage of initial strength of the retested samples is also shown numerically on each bar.PRAH had no noticeable effect on the self-healing of the specimen. The fly ash mixes showed greater self-healing capacity than the PC mixes particularly at early age initial testing. The fly ash samples originally tested on 7 days all produced greater retested strengths. However, it should be noted that these specimens had the weakest initial strength and therefore present high percentages of initial strength on retesting. Nevertheless, the fly ash mixes performed at least 10% better, regardless of age and PRAH, when compared to the PC mixes. These results can be explained by the presence of microcracks in the samples after initial testing, which allowed water ingress while the samples were in the water bath. Hence, the unhydrated cement within the matrix had access to additional water to hydrate. These hydration products strengthen the matrix and simultaneously contribute to the pozzolanic reaction of the fly ash, further increasing strength.

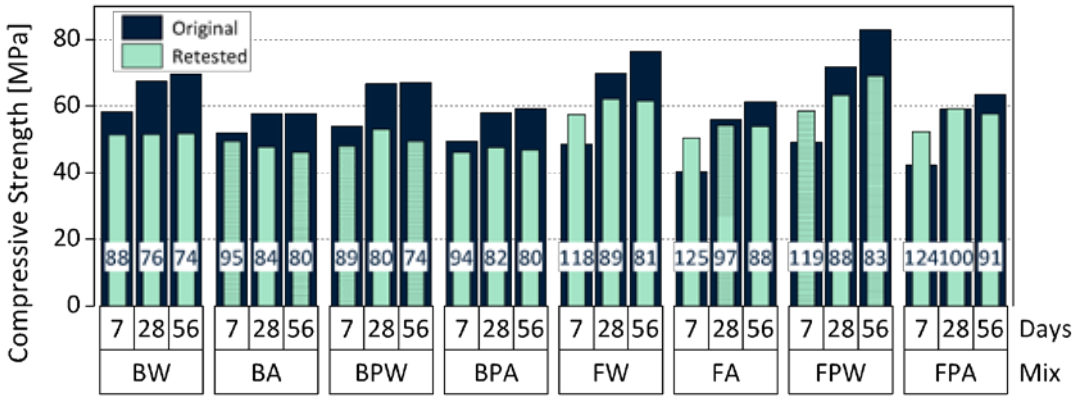

Figure 1 Self-healing effects in terms of compressive strength

4.3 Hydration of Concrete Matrix

The purpose of the mass gain/loss testing was to evaluate the continued development of hydration products or crystal growth within the concrete matrix over time. The results over the 16-week testing period are shown in Figure 2.The different mixes experienced similar mass gain/loss for the first 28 days after which distinction between the fly ash and PC mixes become

increasingly evident. The mass lost with each drying cycle significantly decreased after the 4th week for the fly ash mixes. This corresponded to the generally accepted principle that the pozzolanic reaction of fly ash only starts after a few weeks and therefore the concrete matrix would contain more hydration products [17]. There was no clear indication of increasing mass because of crystal growth resulting from the addition of PRAH. The PC mixes showed marginal increase in mass because of further hydration of the cement but were much closer to plateau than the FA mixes. This is because CEM I cement hydrates and gains strength faster than CEM II-B, cement but the reaction slows down sooner as a result. This trend correlated to the results presented for compressive strength and self-healing effects in terms of cement hydration and pozzolanic reaction.

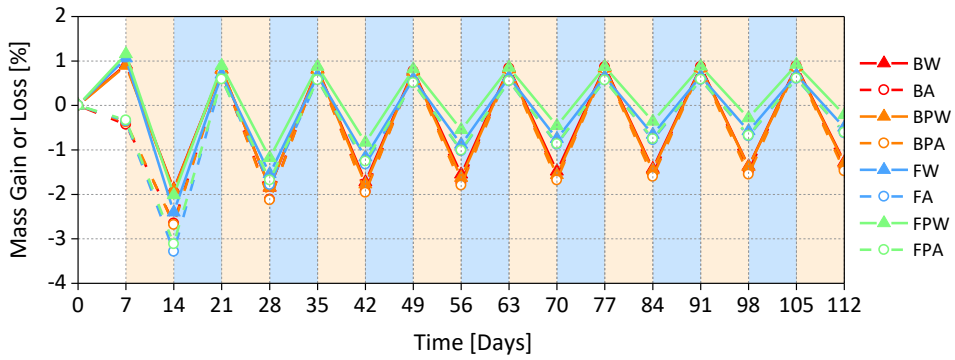

Figure 2 Mass gain/loss with water and oven cycling

4.4 Durability According to SANS3001-CO3

The results of the oxygen permeability and chloride conductivity are presented in Figure 3 and Figure 4. The durability class ranges according to Alexander et al.[18] are shown on the right side of each graph.

The oxygen permeability test is an assessment of the gas permeability of concrete which is generally accepted as a durability-related property of concrete. The overall micro and macro-structure of the concrete is evaluated through this test and it is useful to assess the interconnectedness of the pore structure [2]. The oxygen permeability index (OPI) calculated by this test method is plotted on a log scale and small differences are therefore significant. Torrent and Fernández Luco [19] stated that OPI detected the difference between binder types as well as curing conditions. All the tested samples can be rated as 'Excellent' according to the durability classifications suggested by Alexander et al. [18]. The difference between curing conditions is evident as all water-cured samples performed better than their air-cured counterparts. The fly ash samples yielded higher OPI values than the PC samples, a result also found by Heiyantuduwa [20]. Gas permeability is not commonly used to assess PRAH and therefore literature on their performance is lacking. According to Figure 3, the effect of PRAH can be marginally beneficial when combined with fly ash.

The South African chloride conductivity test is an accelerated diffusion test related to chloride ingress into concrete. The penetration of chloride provides favourable conditions for the corrosion of reinforcement bars. Therefore, chloride ion penetration is recognised as the main cause of long-term deterioration of reinforced concrete structures [21]. From Figure 4 it is apparent that the fly ash samples produced much lower chloride conductivity than the PC samples, a finding supported by multiple authors [2, 20, 22]. Air-cured samples showed an

increase in conductivity compared to water-cured samples. The effect of PRAH was slightly advantageous when used along with fly ash. The water sorptivity test is a measure of rate of absorption of the concrete. The results found in this study were variable with no clear trend regarding binder or inclusion of PRAH. Results from literature on absorption of PRAH mixes also vary and are contradictory [3, 4, 21, 23].

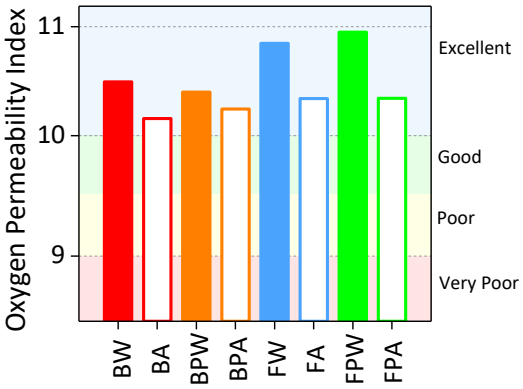

Figure 3 Oxygen permeability index

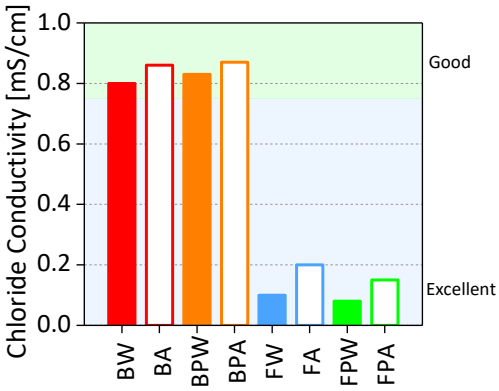

Figure 4 Chloride conductivity index

4.5 Water Depth Penetration

Water depth penetration under pressure is another test method associated with durability. The average depth of penetration was determined for each mix based on EN 12390-8:2019[15], however the test was conducted on mature samples - older than 80 days. This was to permit sufficient time for any crystal growth due to inclusion of PRAH and comparatively further cement hydration or pozzolanic reaction of the reference samples, to occur. A similar approach was adopted by García Calvo et al. [24]. Figure 5 presents the average depth of penetration for each mix. The most notable difference in penetration depth derives from the different curing conditions as all air-cured samples showed significantly larger penetration depths compared to their water-cured counterparts. It should be noted that for reinforced concrete structures with cover of 30 mm or less, the results for air cured samples are detrimental. The performance of the water-cured samples underlines the necessity of implementing adequate curing conditions for concrete. The inclusion of PRAH had no significant effect on the penetration depths of the water-cured samples but reduced the penetration depths of the PC air-cured samples to a small extent. The inclusion of fly ash produced improved results for the air-cured samples, regardless of the presence of PRAH. Literature reports various findings for depth of penetration for concrete with PRAH. Coppola et al. [16] reported improved watertightness with PRAH but stated that the effects were more prominent in poor quality concretes (w/c=0.6) and also concluded that the effectiveness of the admixture in water-cured samples was reduced. Gojević et al. [3] also reported reduced water penetration with PRAH but for high w/c ratios. Conversely, Cappellesso et al. [23] found PRAH increased water penetration. In this study the inclusion of PRAH marginally reduced the depth of water penetration for PC air-cured samples, but the incorporation of fly ash reduced depth of penetration to a greater extent. Neither fly ash nor admixture equalled results obtained from water curing.

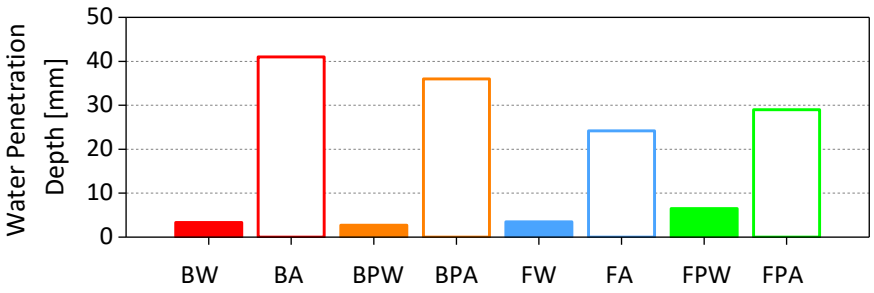

Figure 5 Average depth of water penetration

5. CONCLUSION

The conclusions of this study are as follows:

1) The pozzolanic reactions and filler effect supplied by the fly ash in concrete had more advantageous effects on the compressive strength, self-healing, hydration products within the concrete matrix, oxygen permeability and chloride conductivity when compared to concrete containing PRAH.
2) The inclusion of fly ash was more effective in reducing depth of water penetration of concrete when compared to PRAH for air-cured samples.
3) The effects of curing conditions were clearly seen in strength and durability testing. Water-curing produced superior results compared to air-curing.

The conclusions of this study indicated that improved durability for gaseous and ionic environments can be achieved through the inclusion of fly ash as SCM and fine filler. However, the best durability results derive from adequate water curing.

REFERENCES

[1] Damtoft, J.S., Lukasik, J., Herfort, D., Sorrentino, D. and Gartner, E.M. (2008). Sustainable development and climate change initiatives. *Cement and Concrete Research*. Vol.38(2).

[2] Alexander, M.G. (2021). *Fulton's concrete technology* Tenth Edition. Midrand, South Africa: Cement & Concrete SA.

[3] Gojević, A., Ducman, V., Netinger Grubeša, I., Baričević, A., Banjad Pečur, I. (2021). The Effect of Crystalline Waterproofing Admixtures on the Self-Healing and Permeability of Concrete. *Materials* 14, no. 8: 1860

[4] de Souza Oliveria, A., da Fonseca Martines Gomes, O., Ferrara, L., de Moraes Rego Faibairn, E. & Toles Filho, R.A. (2021). An overview of a twofold effect of crystalline admixtures in cement-based materials: from permeability-reducers to self-healing stimulators. *Journal of Building Engineering.* Vol. 41.

[5] Pazderka, J. & Hájková, E. (2016) Crystalline Admixtures and their effect on selected properties of concrete. *Acta Polytechnica.* Vol.56, No. 4.

[6] Tibbetts, C.M., Riding K.A. & Ferraro, C.C. (2021). A critical review of the testing and benefits of permeability-reducing admixtures for use in concrete. *Cement.* Vol. 6.

[7] Soutsos, M. and Domone, P.L.J. (2018). Construction materials: Their nature and behaviour. Boca Raton: CRC Press.

[8] United States. Bureau of Reclamation (1987). Design of small dams. Third ed. U.S. Dept. of the Interior, Bureau of Reclamation.

[9] South African National Standard. *SANS 50197-1:2013 Cement: Part 1: Composition, specifications and conformity criteria for common cements (2013).* Pretoria: South African Bureau of Standards.
[10] South African National Standard. *SANS 5863:2006 Concrete tests: Compressive strength of hardened concrete* (2006). Pretoria: South African Bureau of Standards.
[11] South African National Standard. *SANS-3001-CO3-2:2022. Civil engineering test methods: Part CO3-2: Concrete durability index testing -Oxygen permeability test* (2022). Pretoria: SABS.
[12] South African National Standard. *SANS-3001-CO3-1:2015 Civil engineering test methods: Part CO3-1: Concrete durability index testing – Preparation of test specimens* (2015). Pretoria: South African Bureau of Standards.
[13] South African National Standard. *SANS 516-3:2009 Concrete durability index testing: Part 3: Water sorptivity test* (2009). Pretoria: South African Bureau of Standards.
[14] South African National Standard. *SANS-3001-CO3-3:2021. Civil engineering test methods: Part CO3-3: Concrete durability index testing -Chloride conductivity test* (2021). Pretoria: South African Bureau of Standards.
[15] European Standard *EN 12390-8:2019 – Testing hardened concrete- Part8: Depth of penetration of water under pressure* (2019) Brussels
[16] Coppola, L., Coffetti, D. & Crotti, E. (2018). Innovative carboxylic acid waterproofing admixture for self-sealing watertight concretes. *Construction and Building Materials.* Vol 171.
[17] Fraay, A.L.A., Bijen, J.M., de Haan, Y.M. (1989). The reaction of fly ash in concrete a critical examination. *Cement and Concrete Research*. Vol. 19(2), pp. 235–246.
[18] Alexander, M.G., Mackechnie, J.R., Ballim, Y. (1999) Guide to the use of durability indexes for achieving durability in concrete structures. *Achieving durable and economic concrete in the South African context.* Research monograph No. 2.
[19] Torrent, R. Fernández Luco, L. (eds.). (2007). Non-destructive evaluation of the penetrability and thickness of the concrete cover - *State-of-the-art report of RILEM Technical Committee 189-NEC.* Bagneux: RILEM.
[20] Heiyantuduwa, R. (2018). *Chloride ingress in concrete structures exposed to South African marine environments.* PhD thesis. University of Cape Town
[21] Amran, M., Debbarma, S., Ozbakkaloglu, T. (2021). Fly ash-based eco-friendly geopolymer concrete: A critical review of the long-term durability properties. *Construction and Building Materials* Vol. 270.
[22] Simčič, T. Pejovnik, S., De Schutter, G., Bosiljkov, V.B. (2015). Chloride ion penetration into fly ash modified concrete during wetting–drying cycles. *Construction and Building Materials* Vol. 93, pp. 1216-1223.
[23] Cappellesso, V.G., dos Santos Petry, N., Dal Molin, D.C.C. & Masuearo, A.B. (2016). Use of crystalline waterproofing to reduce capillary porosity in concrete. *Journal of Building Pathology and Rehabilitation* 1:9.
[24] García Calvo, J.L., Sánchez Moreno, M., Carballosa, P., Pedrosa, F., Tavares, F., (2019). Improvement of the Concrete Permeability by Using Hydrophilic Blended Additive. *Materials* 12, 2384.

YCRETS 2023
YOUNG CONCRETE RESEARCHERS, ENGINEERS & TECHNOLOGISTS SYMPOSIUM

CEMENT & CONCRETE SA

Assessing the mechanical and durability properties of concrete incorporating recycled clay masonry rubble bricks as fine aggregates

Thilivhali M. Malima, Olatokunbo E. Omisakin, and Janina P. Kanjee

School of Civil and Environmental Engineering, University of the Witwatersrand

Abstract

Construction and demolition waste is a significant environmental problem worldwide, with 58% of the 4.48 million tons of such waste ending up in landfills as reported by SAWIC in 2017. To mitigate this issue, this project aims to investigate the feasibility of incorporating 50% recycled clay masonry rubble bricks (CMRB) in place of natural fine aggregate in concrete, thereby reducing the environmental impact of construction waste. The study encompassed casting 84 100mm cubes utilising natural fine Andesite aggregate and 84 100mm cubes, replacing 50% of the fine aggregate with recycled CMRB. The cubes were cast using 14mm Andesite coarse aggregates and a water-to-binder ratio of 0.6. The compressive strength and durability properties (with respect to oxygen permeability, water sorptivity and chloride conductivity) were assessed at three ages, 28, 56 and 90 days. The results revealed that the incorporation of CMRB as fine aggregates in concrete reduced workability, but positively influenced the mechanical and durability properties of the 50% CMRB concrete mix. The improved properties can primarily be attributed to the calcinated clay present in the crushed recycled clay masonry rubble bricks, which exhibits pozzolanic behaviour. These findings suggest that using recycled clay masonry rubble bricks as a replacement for natural fine aggregate in concrete can lead to a reduction in environmental impact while also improving concrete properties.

Keywords: recycled clay masonry rubble bricks (CMRB); fine aggregates; compressive strength; durability.

1. INTRODUCTION

Construction and Demolition (C&D) waste refers to waste generated from the construction, remodelling, repair, and demolition of structures. C&D waste is a major contributor to environmental degradation and pollution, as well as occupying landfill space due to its non-biodegradable nature [1]. To address these issues, there is increasing pressure to find sustainable solutions, such as recycling C&D waste as fine aggregate in concrete [2]. Previous research has shown that incorporating recycled masonry rubble in concrete can enhance its

compressive strength and durability in the short term, up to 28 days [3]. This study aimed to evaluate the mechanical and durability properties of finely recycled masonry clay rubble bricks as a replacement for natural fine aggregate in concrete, over a longer period of time. The objective was to reduce waste generation and the demand for natural fine aggregate while also determining the long-term performance of concrete with recycled clay masonry rubble bricks as fine aggregates.

2. MATERIALS AND TEST METHODS

2.1. CMRB as Fine Aggregates Replacement

The CMRB aggregates used in this study were obtained from clay masonry bricks collected from a construction site located at The University of the Witwatersrand. Unfortunately, the composition and age of the brickwork remain unknown. Prior to crushing the bricks, excess mortar and paint (physical impurities) were removed from the CMRB using a hammer and chisel. The CMRB were then mechanically crushed to produce particle size and grading characteristics that closely matched those of the control fine Andesite aggregates utilized in this study. A grading profile, depicted in Figure 1, was used to determine the amount of masonry rubble aggregate required to achieve a grading profile that was comparable to the one produced using natural fine Andesite aggregate, as described in SANS 1083 [4], in terms of fraction size and mass.

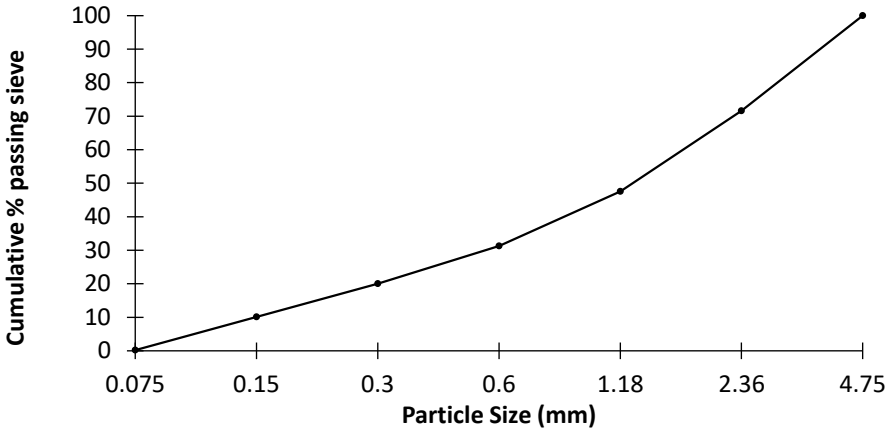

Figure 1: Grading profile for natural fine Andesite aggregate

2.2. Concrete Mix Design

Two concrete mixes were designed with a w/b ratio of 0.6, with one mix having 0% CMRB aggregate replacement and the other having 50% CMRB aggregate replacement. Table 1 provides a summary of the details of these mix designs.

Table 1: Concrete proportions in kg/m³

Constituents	0% CMRB	50% CMRB
PC (CEM I 52.5 R)	251	251
Fly Ash (FA)	107	107
Andesite stone content	761	761
Andesite sand content	1077	538.5
CMRB sand content	0	538.5
Water	215	215
Admixture (Superplasticiser)	0	1.25

2.3. Testing Approach

i. Slump tests

To measure the workability of fresh concrete, slump tests were conducted in line with SANS 5862-1:2006 [5].

ii. Compressive strength tests

100 mm concrete cubes samples were prepared, water cured and tested in accordance with SANS:5863[6]. The cubes were loaded using a cube machine which had a maximum loading capacity of 2 000 KN. The compressive strength of the concretes was determined at 28, 56 and 90 days after casting.

iii. Durability test

Three durability index (DI) tests namely the oxygen permeability, water sorptivity and chloride conductivity tests were performed. These tests measure the resistance of the cover concrete to the transportation of ions and fluids through the concrete thus affecting deterioration. The tests produce reliable indices for the characterization of concretes.

The DI test specimens were prepared in accordance with SANS 3001: CO3-1 [7]. The oxygen permeability index (OPI) test was conducted according to SANS:3001-CO3-2 [8]. The water sorptivity test was conducted in accordance with the Durability Index Manual [9]. The chloride conductivity test was conducted according to SANS:3001-CO3-3[10].

3. RESULTS AND DISCUSSION

The investigation into the mechanical and durability properties of concrete made using CMRB as fine aggregates was conducted over a period of three months. The results are outlined and further discussed below.

3.1. Slump Test

The slump tests results in Figure. 2, showed that the use of CMBR resulted in a decrease in the workability of the concrete.

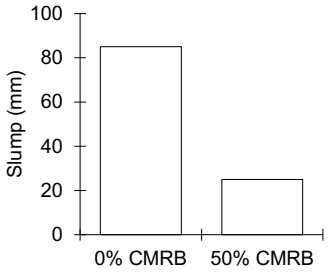

Figure 2: Slump results for concrete made using 0, 50% CMRB as fine aggregate.

The slump results for 0% and 50% CMRB were 85 mm and 25 mm respectively, as shown in the figure above. The high porosity of the rubble can be attributed to the absorption of some of the mixing water leading to the decrease in the workability, hence a decrease in slump [11].

3.2. Compression Strength

In general, the compressive strength is observed to increase with the incorporation of fine CMRB aggregates, for all three testing ages as seen in Figure 3.

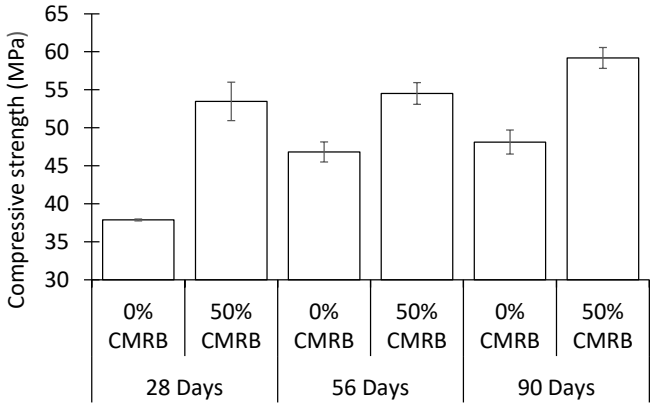

Figure 3: Compressive strength of concrete made using 0, 50% CMRB as fine aggregates at 28, 56 and 90 days.

At ages 28, 56, and 90 days, the compressive strengths of 50% CMRB were 53.5, 54.5, and 59.2 MPa respectively. In comparison, the compressive strengths of 0% CMRB at the same ages were 37.9, 46.8, and 48.1 MPa respectively. After 28 days, the average compressive strength of the replacement mix was found to be 41.2% higher than that of the control mix. This difference was further observed to be 16.5% and 23% at ages 56 and 90 days, respectively. The findings indicate that the 50% CMRB mix, which is a blend of 50% recycled CMRB and 50% fine Andesite aggregates, exhibited higher compressive strength compared to the control mix consisting of 100% fine Andesite aggregates.

The observed increase in strength can be primarily attributed to the calcinated clay present in the crushed recycled clay masonry rubble bricks, which exhibit pozzolanic behaviour [12].

3.3. Durability Index Testing

The durability of concrete can be measured by the oxygen permeability index, water sorptivity and porosity, and chloride conductivity tests. All three durability indices were obtained to determine the overall durability of concrete incorporating fine CMRB aggregates.

3.3.1. Oxygen permeability index

The Oxygen Permeability Index (OPI) is indirectly proportional to permeability. The value of OPI indicates the resistance of a given concrete to the ingress of gases. A high value of the OPI corresponds to a high resistance to gaseous ingress.

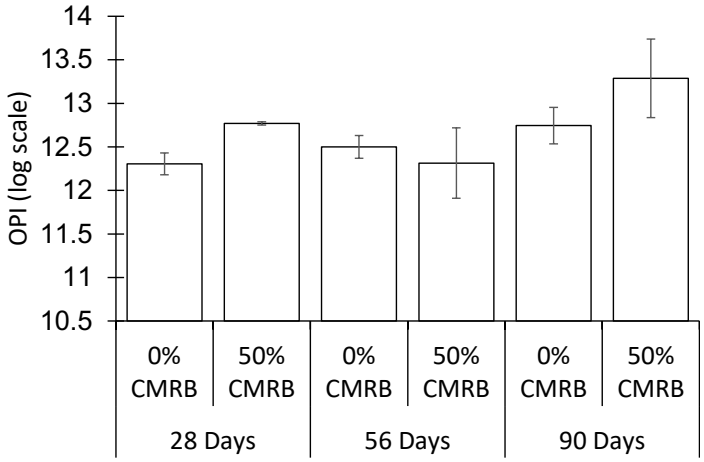

Figure 4: OPI for concrete made using 0 and 50 % CMRB as fine aggregates at 28, 56 and 90 days.

At ages 28, 56, and 90 days, the OPI for 50% CMRB were 12.8, 12.3, and 13.3 respectively. In comparison, the OPI for 0% CMRB at the same ages were 12.3, 12.5, and 12.7 respectively. Figure 4 displays a general trend where the OPI value increases with the incorporation of fine CMBR aggregates at 28 and 90 days. However, at 56 days, the replacement mix showed a lower OPI value compared to the control mix, which can be regarded as an outlier. The increase in permeability can be attributed to the pozzolanic reactivity of the crushed recycled clay masonry rubble bricks, resulting in the formation of cementitious hydration products [13].

3.3.2. Water sorptivity index

Ingress of moisture in concrete by capillary suction is obtained using this index. A higher value of WSI implies a decreased resistance to the ingress of liquids in a given concrete specimen.

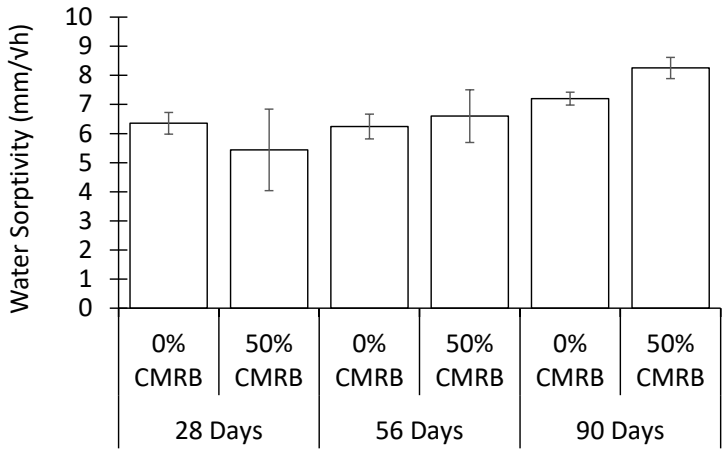

Figure 5: Water sorptivity for concrete made using 0 and 50 % CMRB as fine aggregates at 28, 56 and 90 days.

At ages 28, 56, and 90 days, the WSI for 50% CMRB were 5.4, 6.6, and 8.3$mm/\sqrt{h}$ respectively. In comparison, the WSI for 0% CMRB at the same ages were 6.4, 6.2, and 7.23$mm/\sqrt{h}$ respectively. Figure 5 indicates that the 50% CMBR mix exhibited a higher WSI value at 56 and 90 days compared to the control mix. This can be attributed to the porous nature of the fine CMBR aggregates, resulting in a higher absorption of moisture.

3.3.3. Chloride conductivity index

Chloride Conductivity Index (CCI) indicates the resistance of concrete to the ingress of chloride. A higher CCI value suggests a decreased resistance to chloride ingress.

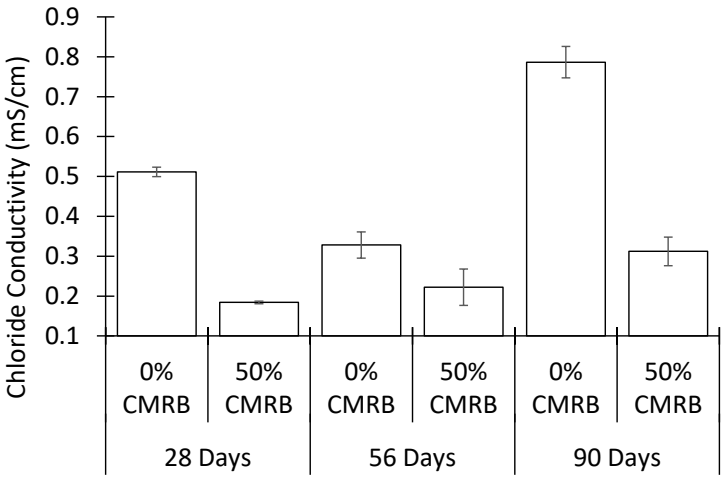

Figure 6: Chloride Conductivity for concrete made using 0 and 50 % CMRB as fine aggregates at 28, 56 and 90 days.

At ages 28, 56, and 90 days, the CCI for 50% CMRB were 0.18, 0.22, and 0.31mS/cm respectively. In comparison, the CCI for 0% CMRB at the same ages were 0.51, 0.33, and

0.79mS/cm respectively. The results of the chloride conductivity tests showed that the replacement mix exhibited greater resistance to chloride penetration than the control mix at 28, 56, and 90-day ages. At 28 days, the replacement mix was approximately 65% better than the control mix, whereas at 56 and 90 days, the percentage difference was found to be 33% and 61%, respectively. This result may be attributed to the presence of a clay mineral, such as kaolinite, in the masonry bricks used during production. This mineral is known to bind with chloride ions, forming stable compounds that effectively reduce the amount of chloride ions that can penetrate the concrete [14].

4. CONCLUSION

The effects of replacing fine Andesite aggregate with fine CMRB aggregate on the mechanical and durability properties of concrete was assessed in this study. Two concrete mixes were investigated: 0% CMRB (the control mix) and 50% CMRB (the replacement mix). The properties tested include workability, compressive strength, and South African durability index of each concrete mix produced. The results are summarised below:

- The slump test results obtained indicate that the incorporation of fine CMRB aggregates in the concrete mixture reduced its workability. The high porosity of the rubble can be attributed to the absorption of some of the mixing water leading to the decrease in the workability.
- The compressive strength is observed to increase with the incorporation of fine CMRB aggregates, for all three testing ages. This result is attributed to the calcinated clay present in the crushed recycled clay masonry rubble bricks, which exhibit pozzolanic behaviour.
- For both the 0 and 50 % CMRB mixes, three durability indices were assessed. OPI results revealed a general trend where the OPI value increases with the incorporation of fine CMBR aggregates at 28 and 90 days. The increase in permeability can be attributed to the pozzolanic reactivity of the crushed recycled clay masonry rubble bricks, resulting in the formation of additional cementitious hydration products.
- WSI indicates that the 50% CMBR mix exhibited a higher WSI value at 56 and 90 days compared to the control mix. This can be attributed to the porous nature of the fine CMBR aggregates, resulting in a higher absorption of moisture.
- The CCI tests yielded conclusive results in which the 50% CMBR had the lower CCI values at all three testing ages compared to the control mix. These results may be attributed to the presence of a clay mineral, which is known to bind with chloride ions, forming stable compounds that effectively reduce the amount of chloride ions that can penetrate the concrete.

In summary, the results suggest that recycled CMBR has the potential to be used as a substitute for natural fine Andesite aggregates in concrete. However, further testing is necessary to assess the long-term mechanical properties of the concrete incorporating 50% CMBR, such as shrinkage and creep.

REFERENCES

[1] Blengini, G.A., 2009. Life cycle of buildings, demolition and recycling potential: A case study in Turin, Italy. Building and environment, 44(2), pp.319-330.

[2] Olubambi, A., Aigbavboa, C., Thwala, D.T., and Samuel, S. (2020). Determining the Impact of Construction and Demolition Waste Reduction practices on Green Building Projects. Proceedings of the International Conference on Industrial Engineering and Operations Management, Dubai, UAE, March 10-12, 2020.

[3] Maleka L. and Mohlatlole, K, (2020). Investigating the effect of using masonry rubble as fine aggregate on concrete compressive strength and durability. Honours Thesis, University of the Witerwatersrand.

[4] SANS 1083:2006., 2006. Aggregate from natural sources. Aggregates for concrete, Pretoria: South African Bureau of Standards.

[5] SANS 5862-1:2006, 2006. Concrete tests – Consistence of freshly mixed concrete - Slump test. Pretoria: South African Bureau of Standards.

[6] SANS 5863:2006., 2006. Concrete tests – compressive strength of hardened concrete, Pretoria: South African Bureau of Standards

[7] SANS 3001-CO3-1:2015., 2015. Civil engineering test methods Part CO3-1 Concrete durability index testing - Preparation of test specimens. Pretoria: South African Bureau of Standards.

[8] SANS:3001-CO3-2, Part CO3-2: Concrete durability index testing - Oxygen permeability test, Pretoria, Gauteng: South African Bureau of Standards, 2015.

[9] Durability Index Manual, University of Cape Town, 2017.

[10] SANS:3001-CO3-3, Part CO3-3: Concrete durability index testing - Chloride conductivity test, Pretoria, Gauteng: South African Bureau of Standards, 2015.

[11] Kim, Y.Y., Lee, K.M., Bang, J.W. and Kwon, S.J. (2014). Effect of W/C Ratio on Durability and Porosity in Cement Mortar with Constant Cement Amount. Advances in Materials Science and Engineering, [online] 2014, pp.1–11. doi:https://doi.org/10.1155/2014/273460.

[12] Bektas, F., Wang, K., and Ceylan, H. (2008) Use of Ground Clay Brick as a Pozzolanic Material in Concrete. Journal of ASTM International 5(10) DOI:10.1520/JAI101681

[13] Tremiño, R.M., Real-Herraiz, T., Letelier, V. and Ortega, J.M. (2021). Four-years influence of waste brick powder addition in the pore structure and several durability-related parameters of cement-based mortars. Construction and Building Materials, 306, p.124839. doi:https://doi.org/10.1016/j.conbuildmat.2021.124839.

[14] Kijjanon, A., Sumranwanich, T., Saengsoy, W. and Tangtermsirikul, S. (2023). Chloride Penetration Resistance, Electrical Resistivity, and Compressive Strength of Concrete with Calcined Kaolinite Clay, Fly Ash, and Limestone Powder. Journal of Materials in Civil Engineering, [online] 35(3). doi:https://doi.org/10.1061/(asce)mt.1943-5533.0004643.

YCRETS 2023
YOUNG CONCRETE RESEARCHERS, ENGINEERS & TECHNOLOGISTS SYMPOSIUM
CEMENT & CONCRETE SA

Experimental investigation of the effect of alkaline activator and mix constituents on foam stability of foamed alkali-activated materials

Khanya Mazolwana (1), Humaira Fataar (1) and Algurnon S. van Rooyen (1)

(1) Department of Civil Engineering, Stellenbosch University

Abstract

Stable foamed concrete (FC) is formed by mixing pre-formed foam into a mortar base mix. For foam stability in normal FC, Kearsley and Mostert [1] indicated, using a modified hydraulic turntable test, that the base mix of normal FC requires a spreadability between 220 – 250 mm. Cho et al. [2], with the aim of 3D printing FC, showed that with the inclusion of nano-silica (nS) and calcium aluminate cement (CSA) a smaller base mix spreadability (<180mm) can be utilised. In this paper, foam stability in foamed alkali-activated material (F-AAM) with a target spreadability in the range of 220 – 235 mm is investigated. AAM is produced using cement-less binder, filler, and alkaline activator (AA). The effect of activator concentration is evaluated by producing mixes with varying AA concentrations. AAM spreadability is assessed using a modified hydraulic turntable test [1,2]. Foam stability is tested gravimetrically by filling a standard 100 mm cube mould and determining the density ratio.

Study results indicate that higher spreadability is associated with increased AA solution and less sand content. Based on isolated cases of material attaining stability, it can be concluded that stability does exist for the material for certain density ratios, despite a scattered data set.

Keywords: Foam concrete, Alkali-Activated Materials, Foam Stability, Spreadability

1. INTRODUCTION

One of the goals of sustainable development is climate action which has been threatened by the high levels of carbon dioxide (CO_2) emissions generated on the planet. The construction industry is one of the main contributors to CO_2 emissions, as CO_2 is a by-product of cement production [3]. This pitfall in construction has paved the way for environmentally friendly concrete such as geopolymer concrete. This type of cementitious material has provided the construction industry with a sustainable alternative to cement-containing concrete. Geopolymer concrete typically uses binders such as Fly Ash (FA), Ground Granulated Corex Slag (GGCS) and silica fume (SF) to eliminate the use of Ordinary Portland cement (OPC) [4,5]. Since AAMs are by-products of existing industrial processes, geopolymer concrete production forms part of the circular economy of construction.

The binders utilised in geopolymers are termed alkali-activated materials (AAMs) as they start chemically reacting once the binder encounters an alkali activator (AA), therefore geopolymerisation occurs. Common AA includes sodium hydroxide (SH), sodium silicate (SS) and calcium hydroxide (CH) [5]. Geopolymers are often distinguished between one-part and two-part geopolymers. The latter is the more conventional geopolymer type with superior mechanical properties [6, 7]. Two-part geopolymers are produced in a mix where the AA is in

solution form and mixed with a solid AAM. While in one-part geopolymers, a solid form of AA and AAM are mixed with just water to activate the mix. One-part geopolymers have been recognized by researchers for their applicability to much larger-scale production and potential in-situ casting [8].

Foamed concrete (FC) is a lightweight concrete (LWC) that can be designed to use high volumes of FA. The material is made by adding preformed foam to a mortar base mix, designed in a specific range of water content and consistency, that does not cause the foam to degrade. Kearsley and Mostert [1] determined that for FC with high FA replacement, a spreadability between 220 – 250 mm was the optimal range for mixed water content and subsequently, foam stability. In their study into 3D printable foam concrete, Cho [2] investigated a spread range of 180 – 220 mm and found stability at a spreadability of 180 mm. Researchers agree on FC's viability as a construction material, especially in non-structural applications and can be designed for densities between 400 and 1600 kg/m^3 [9].

This study aims to develop stable F-AAM by investigating foam stability in AAM with spreadability ranging from 220 - 235 mm. Literature indicates that F-AAM's vulnerability to collapse lies in its foam stability, which is affected by different factors [10, 11]. Factors include base mix composition and consistency which are assessed as spreadability using a hydraulic turntable test. This study investigates the effect of an SH and SS as an AA on the stability of a two-part F-AAM.

2. MIX DESIGN AND EXPERIMENTAL TESTING

2.1 Materials and Mix Design Methodology

In its basic form, F-AAM is composed of three components: binder material, alkali-activated solution, and foam. The binder material used in this investigation consists of locally sourced low calcium Class-F FA and GGCS with relative density 2.37 and 2.65, respectively. Their chemical compositions are shown in Table 1.

Graded fine silica sand with a maximum particle size of 0.6 mm and relative density of 2.65 was utilised to investigate the effect of sand on plain F-AAM. Additionally, 6 mm polypropylene (PP) fibres with a relative density of 0.91 were used as fibre reinforcement for F-AAM.

Table 1: Percentage of the chemical composition of FA and GGCS [12]

	SiO_2	Al_2O_3	Fe_2O_3	CaO	MgO	K_2O	Na_2O	Ti_2O
Fly Ash	54.1	31.8	3.2	4.9	1.2	0.8	0.4	1.7
GGCS	31.8	14.5	1.3	36.5	11.7	0.6	0.1	0.5

AA solution comprising of a SS solution and SH pellets is utilised. The SS has a molar ratio of 2 and a relative density of 2.34. The SH is of 99% purity and has a relative density of 1.15. A hydrolysed protein-based foaming agent, FoamTech, was used to produce the pre-formed foam, with a relative density of 0.075 ± 0.005, by diluting it with water and ferrous sulphate at 1:40 and 1:80 ratios, respectively.

The mix design of F-AAM is formulated using mass and volume balance. The approach is adapted from McCormick [13] and Kearsley and Mostert [1] where the total mass (m_{tot}) of the mix constituents is equated to the design target density (ρ_m) and expressing the mix constituents as a ratio to the main binder. The volume of the total (V_{tot}) mix is then set to 1000 litres. In this investigation, FA is used as the unknown parameter, x, and all other constituents are determined as a ratio of FA, see equations (1) and (2).

$$m_{tot} = \rho_m = x\left[1 + \sum_{i=0}^{n}(a+b)_i\right] + sh + ss + RD_f V_f \quad (1)$$

$$V_{tot} = 1000 = x\left[\frac{1}{RD_x} + \sum_{i=0}^{n}(b+k)_i\right] + \frac{sh}{RD_{sh}} + \frac{ss}{RD_{ss}} + Vf \quad (2)$$

Where:

$$\sum_{i=0}^{n} b_i = (\mathrm{w}/s)\left(1 + \sum_{i=0}^{n} a_i\right)$$

$$sh = \left(x * \sum_{i=0}^{n} b_i * M * Mr\right)/(1000 * 99\%)$$

$$\sum_{i=0}^{n} k_i = \frac{a_0}{q_0} + \cdots + \frac{a_n}{q_n}$$

a_i represents the mass ratio of a mix constituent to fly ash and in the case of n=2, a_0, a_1 and a_2 refers to the GGCS, sand and fibre mass ratio, respectively. q_i is the relative density of each mix constituent, thus making k_i the volume of each constituent. 'sh' and RD_{sh} refer to the mass and relative density of SH, respectively. 'ss' and RD_{ss} refer to the mass and relative density of SS, respectively. M and Mr refer to the molarity and molar mass of SH, respectively. RD_f and V_f refer to the relative density and volume of foam in the mix.

2.2 Mix Design Methodology

In this investigation, 18 F-AAM mixes were designed using Equations (1) and (2) and are presented in Tables 2 and 3. For each mix design, AA was prepared by dissolving the required mass of SH in potable tap water and mixed with the aqueous SS solution. Thereafter the solution was left to cool down in a climate-controlled room for 24 hours. For each AA solution, an alkaline ratio (AR) of 1.5, 2.0 or 2.5 was chosen in combination with an SH molarity of 8M, 10M or 12M. For mixing, the dry materials were weighed off and added to a 25 L pan mixer, typically in the order of fly ash, slag, sand, and fibres, and mixed until uniform. For the mixes with sand, the sand was added at a ratio to the total binder, either 1, 1.25 parts or 1.5 parts to 1 part binder. Fibres were added as a percentage of the total volume of the mix (VF = 0.3%, 0.5% and 1%). The activator solution was then added to form the base mix (geopolymer) and mixed until homogeneous. The spreadability of the base mix was then determined using the modified hydraulic turntable test, described in Section 2.2, and accepted if a spread in the range of 220 – 235 mm was obtained. The water content of the base mix with a spread value

outside the optimum range was adjusted accordingly – by adding water if the spread was under 220 mm. The pre-formed foam was generated using a foaming agent, ferrous sulphate, and water in the foam generator shown in Figure 1 was added to accepted mixes and mixed for a further 5 minutes.

Figure 1: Foam generator

Table 2: F-AAM Mix design [kg/m^3] - Binder-only mixes investigating the effects and SH molarity, grouped by alkaline ratios.

	AR=1.5			**AR=2.0**			**AR=2.5**		
	8M	**10M**	**12M**	**8M**	**10M**	**12M**	**8M**	**10M**	**12M**
FA	639	487	607	609	497	512	539	557	622
GGCS	426	325	406	406	332	341	360	372	414
Water	172	285	164	184	251	216	225	187	126
SH	55	115	79	59	100	104	73	75	60
SS	83	172	118	118	201	207	182	188	151
Foam	24	17	24	24	19	20	21	23	26

Table 3: F-AAM Mix design [kg/m^3] - Mixes investigating the effects of sand and fibre.

	AR=2.0			**AR=2.5**			**AR=2.5**		
	s/b			**s/b**			**VF**		
	1	**1.25**	**1.5**	**1**	**1.25**	**1.5**	**0.3%**	**0.5%**	**1%**
FA	223	197	178	310	277	249	197	197	167
GGCS	148	132	119	208	185	166	131	131	112
Sand	371	412	444	518	575	621	492	491	420
Fibres	0	0	0	0	0	0	3	5	9
Water	260	259	260	126	126	125	207	207	251
SH	126	126	126	60	60	60	100	100	121
SS	252	251	252	151	151	151	250	250	301
Foam	18	18	18	27	27	27	21	21	18

2.3 Experimental Testing

As suggested by Kearsley and Mostert [1], the hydraulic turntable test evaluates the spread diameter using a Flow table test for hydraulic cement. An experiment was conducted using a mini-slump cone filled with fresh mortar. The spread diameter was taken as the average measured diameter in two directions perpendicular to each other. As prescribed by ASTM C-1437 Standard test method for flow of hydraulic cement mortar, the diameter measurements were taken after the cone was filled with the fresh geopolymer base mix and dropped 15 times from a height of 12.7 mm.

In addition to completing the hydraulic turntable tests on the AAM, the measured fresh density of the mix was calculated as in equation (3), with the density ratio then computed using equation (4). The density ratio is considered stable in the range of 0.98 - 1.02.

$$\text{Fresh density} = \text{M/V} = (\text{mass of fresh concrete})/0.001 \quad (3)$$

$$\text{Density Ratio} = (\text{Fresh Density})/(\text{Target Density}) \quad (4)$$

3. RESULTS AND DISCUSSION

To quantify stability, various mix design types were investigated as listed in Tables 2 and 3. Since density is not under investigation, a target density of 1400 kg/m^3 was kept constant throughout.

3.1 Effect of Mix Constituents on the Water Demand

Figure 3 shows the influence of mix constituents on water demand on the mixes. The water demand (adjusted w/s) is determined as a sum of the design w/s and additional water added to mixes with a spread less than 220 mm.

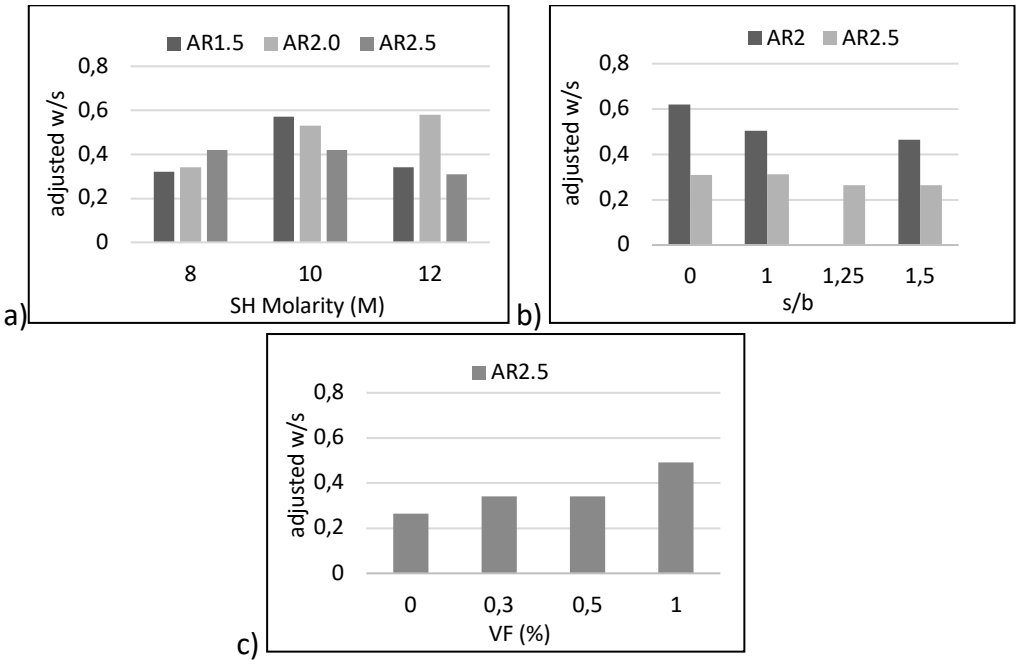

Figure 3: Effect on the water to solids ratio by a) SH molarity, b) Sand c) Fibre

According to Figure 3(a), an increase in AR results in an increase in the water demand of a mix. Increasing AR results in a decrease in water demand in 10M mixes, while there is no trend in 12M samples. A comparison of AR1.5 and AR2.5 across molarities does not show a linear relationship; however, for AR2, there is an increase in water demand for an increase in molarity. By the mix design equations, the activator content is proportional to the water demand of the mix. Therefore, an increase in activator content (AR) or activator concentration (molarity) will increase water demand.

The influence of sand content on the water demand of the mixes shows that water demand decreases with an increase in the sand. AR2.5 uses much less water in its mixes than AR2. Furthermore, fibre content affects water demand proportionally: an increase in fibre content causes an increase in water demand. The increase in solids, either fibres or sand, will decrease water demand, based on mix design derivation. This trend does not apply to the fibres. This could be due to the fibre nature but requires more research.

3.2 Effect of Activator Properties on Stability

The spreadability and fresh density ratio results are shown in Figure 4 (a) and (b). Table 2 shows that these mixes consist of binder material, activator, and foam only.

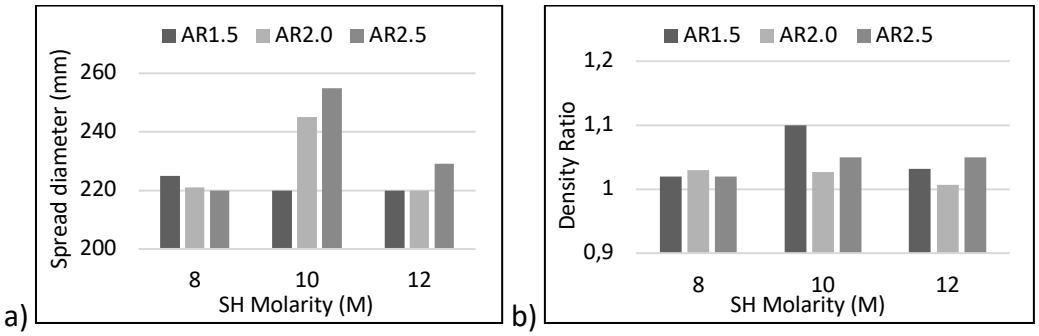

Figure 4: Graphs showing a) Spreadability - and b) Density Ratio with molarity.

Figure 4(a) shows that for an SH molarity of 8M, an increase in the AR results in a slight decrease in spread diameter. Conversely, for 10M and 12M, an increase in the AR results in an increase in spread diameter. Therefore, a mix with higher SH, and an increase in AR results in more consistency and spread. The spread diameter was expected to increase with AA concentration, to result in a much more flowable fresh mix, agreeing with the 10M and 12M mix trends.

For the density ratio, Figure 4(b), there is no trend between molarity and density ratio. For 8M mixes, AR1.5 and AR2 were within the suitable range. The 10 M mixes highly exceeded the upper limit of the suitable density ratio range but that was expected as the spreadability was out of the desired range. There is no trend for the 12M mixes. Thus, more research is required to determine the exact relationship between molarity and stability.

3.3 Effect of Sand on Stability

Figure 5 highlights the effect of sand to binder ratio (s/b) on foam stability. Only mixes with AR of 2.0 and 2.5 were selected to include sand as shown in Table 3.

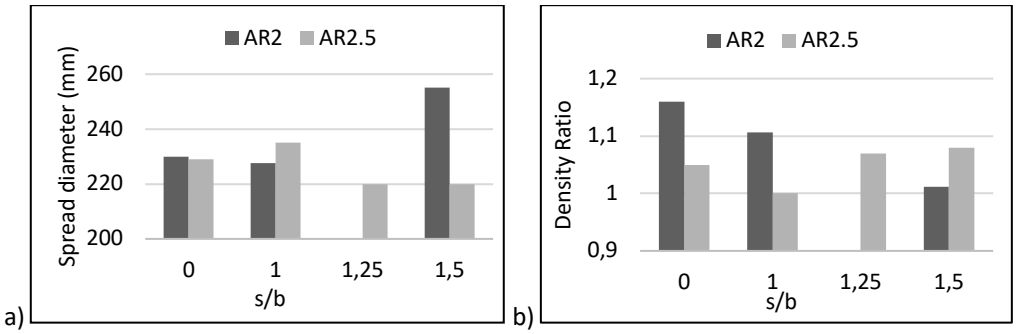

Figure 5: Effect of sand on stability parameters

In Figure 5(a), the AR2.5 mixes were in the required spreadability range, whereas the AR2 mix with an s/b of 1.5 had a spread above 250 mm. Based on Figure 3(b), an increase in sand content decreases the water demand, thus decreasing spreadability. From Figure 5(b) it is observed that AR2.5 mixes have density ratios close to 1, showing stability. However, for AR2 more frequent instability is noted. A contrasting relationship regarding density ratio and sand addition between mixes with an AR of 2 and 2.5 exists. In mixes with AR2, an increase in sand content results in improved stability whereas, in mixes with AR2.5 results in more instability.

3.4 Effect of Fibre Inclusion on Stability

Figure 6 shows the effect of fibre volume (VF) on spread diameter and density ratio.

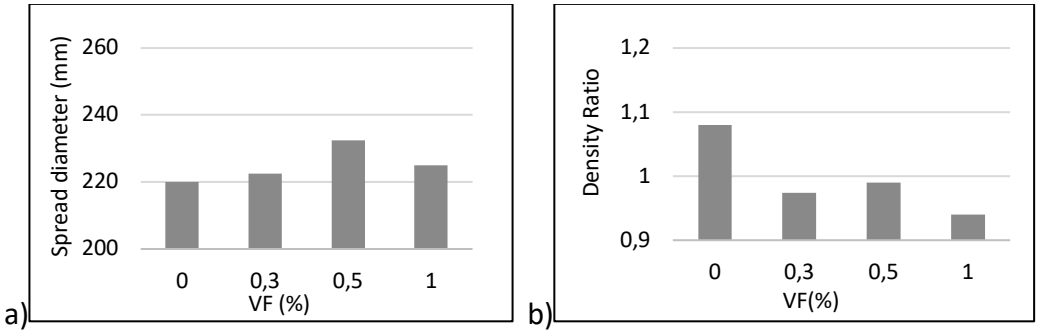

Figure 6: Effect of fibres on stability parameters

In Figure 6 (a), there is an increase in spreadability with an increase in VF between plain F-AAM and up to 0.5% fibre-reinforced F-AAM. Between 0.5% and 1% fibre-reinforced F-AAM, spreadability decreases. Typically, increasing fibre content would stiffen the fresh mix, thus decreasing the spread diameter. Thus, spreadability decreasing with an increase in dry materials is plausible.

The increase in spreadability with fibre could be attributed to the fibre property, but more research is encouraged to ascertain the true effect of fibre addition in the F-AAM fresh state. Figure 6 (b) shows that fibre inclusion increases the instability in the F-AAM mixes by decreasing the density ratio. Density ratios below 1 are recorded for VF. No trend between fibre volume inclusion and stability is observed.

4. CONCLUSION

The effect of varying AA solutions on foam stability in F-AAM mixes designed with low calcium FA, GGCS, sand, and fibres with spreadability values ranging from 220-250 mm was evaluated using modified hydraulic turntable and gravimetric stability tests. The purpose of this study was to correlate spreadability with stability by comparing mixes with spreadability of 220-235 mm with density ratios of 0.98 - 1.02. Based on the results the following conclusions can be drawn:

i. An increase in AAs and sand content decreases the water demand and spreadability. Further research is needed to determine the effects of fibre content.

ii. An increase in molarity results in improved stability in AR2.5 mixes, in contrast to AR2, where it leads to instability.

REFERENCES

[1] Kearsley, E.P. and Mostert, H.F., (2005). Designing mix composition of foamed concrete with high fly ash contents. In Use of Foamed Concrete in Construction: Proceedings of the International Conference held at the University of Dundee, Scotland, UK on 5 July 2005 (pp. 29-36). Thomas Telford Publishing.

[2] Cho, S., van Rooyen, A., Kearsley, E., and van Zijl, G., (2022). Foam stability of 3D printable foamed concrete. Journal of Building Engineering, 47, p.103884.

[3] Andrew, R.M., (2018). Global CO_2 emissions from cement production. Earth System Science Data, 10(1), pp.195-217.

[4] Abdollahnejad, Z., Pacheco-Torgal, F., Félix, T., Tahri, W. & Barroso Aguiar, J. (2015), "Mix design, properties and cost analysis of fly ash-based geopolymer foam", Construction and Building Materials, Elsevier Ltd, Vol. 80 No. May 2010, pp. 18–30.

[5] Dhasindrakrishna, K., Pasupathy, K., Ramakrishnan, S. & Sanjayan, J. (2020), "Effect of yield stress development on the foam-stability of aerated geopolymer concrete", Cement and Concrete Research, Elsevier, Vol. 138, p. 106233.

[6] Adesanya, E., Ohenoja, K., Luukkonen, T., Kinnunen, P. and Illikainen, M., (2018). One-part geopolymer cement from slag and pretreated paper sludge. Journal of Cleaner Production, 185, pp.168-175.

[7] Ren, J., Sun, H., Li, Q., Li, Z., Ling, L., Zhang, X., Wang, Y. and Xing, F., (2021). Experimental comparisons between one-part and normal (two-part) alkali-activated slag binders. Construction and Building Materials, 309, p.125177.

[8] Provis, J.L., Palomo, A. and Shi, C., (2015). Advances in understanding alkali-activated materials. Cement and Concrete Research, 78, pp.110-125.

[9] Yang, K.H., Lee, K.H., Song, J.K. and Gong, M.H., (2014). Properties and sustainability of alkali-activated slag foamed concrete. Journal of Cleaner Production, 68, pp.226-233.

[10] Dhasindrakrishna, K., Ramakrishnan, S., Pasupathy, K. and Sanjayan, J. (2021), "Collapse of fresh foam concrete: Mechanisms and influencing parameters", Cement and Concrete Composites, Elsevier Ltd, Vol. 122 No. March, p. 104151.

[11] Kunhanandan Nambiar, E.K. and Ramamurthy, K. (2008), "Fresh State Characteristics of Foam Concrete", Journal of Materials in Civil Engineering, Vol. 20 No. 2, pp. 111–117.

[12] Barnard, R., (2014). Mechanical properties of fly ash/slag based geopolymer concrete with the addition of macro fibres. *M. Eng. Thesis, Stellenbosch Un., South Africa*.

[13] McCormick, F.C., (1967). Rational proportioning of preformed foam cellular concrete. American Concrete Institution Journal, 64(2), pp.104-110.

YCRETS 2023
YOUNG CONCRETE RESEARCHERS, ENGINEERS & TECHNOLOGISTS SYMPOSIUM

CEMENT & CONCRETE SA

Conceptualising the behaviour of 3D printed concrete structures in fire

Selicia Pillay (1), Richard S. Walls (1) and Johann E. van der Merwe (2)

(1) Department of Civil Engineering, Stellenbosch University

(2) Department of Civil Engineering, University of Pretoria

Abstract

Three-dimensional printed concrete (3DPC) is becoming a growing alternative to traditional construction practices. In recent years this novel technique has been developed into practical construction applications, including structures such as façade panels, bridges, houses, and office buildings. Despite the considerable endeavours of academia and industry towards the advancement of 3DPC practices, existing knowledge on the structural behaviour of 3DPC in fire is limited. The structural performance of non-loadbearing 3DPC cavity walls were reported in this paper using appropriate numerical uncoupled thermo-mechanical models. The aim of this work is to conceptualise both thermal performance and thermally induced stresses in 3DPC walls exposed to elevated temperatures. Using free-body diagrams of typical 3DPC walls to evaluate numerical results, it is shown that significant internal stresses can develop, which are likely to cause extensive cracking with vertical cracking (perpendicular to printed concrete layers) being dominant rather than horizontal cracking, as may be expected.

Keywords: 3D-printed concrete; finite element modelling; fire performance; structural damage; standard fire.

1. INTRODUCTION

In comparison to other global industries, the construction sector has been slower to adopt new technologies [1]. Faced with skill scarcity, an expanding number of projects, and the need to limit its environmental impact, the construction industry is progressing to automation to improve productivity, cost efficiency, and reduce material waste. Automation revolutions, such as 3D printing, can transform the construction industry. Due to the novelty of 3DPC, limited research has been compiled regarding the structural behaviour of 3DPC in a fire. Therefore, this paper intends to develop an understanding of the behaviour in common wall configurations of 3DPC in a fire. The study serves as an important first step in guiding future research and identifying potential modes of failure that must be investigated through full-scale furnace testing and will potentially need design solutions developed for them.

2. THERMAL AND MECHANICAL PROPERTIES OF 3DPC

Thermal finite element analysis of 3DPC elements is reliant on the key influencing characteristics of the material's temperature-dependent thermal properties [2]. The thermal conductivity, specific heat, and relative density variations with elevated temperature govern the thermal behaviour of a material. The Eurocode for the design of concrete in fire, EN 1992-1-2 [3], provides the thermal properties at elevated temperatures for traditional concrete materials. Suntharalingam et al [4] showed an almost equivalent relationship between the proposed thermal properties of 3DPC and EN-1992-1-2 properties at elevated temperatures, which was used in this study to develop the finite element model. It is beneficial that preliminary research indicates that new thermal models for 3DPC materials do not need to be developed, although details regarding mechanical resistance require further research.

The mechanical properties of 3DPC samples (compressive, and flexural tensile strength) are significantly influenced by the bonding behaviour at the interlayers of the 3DPC [5]. A comparative study of various authors [6-10] was conducted in to consider a range of mechanical properties to consider for this study. The peak compressive stress assumed in this study is 40 MPa with a maximum flexural strength of 4 MPa. The density of the 3DPC at ambient temperature is assumed to be 2300 kg/m^3. The study considered isotropic material to allow a preliminary investigation of the behaviour. However, 3DPC anisotropic should be included in future work, as it will influence the maximum stresses than can be achieved in each direction, especially between layers. Despite this limitation, the study clearly highlights the susceptibility of fire-induced damage to inner layers of 3DPC wall panels.

3. DEVELOPMENT OF THE FINITE ELEMENT MODEL

In this work, a 3D finite element numerical model was developed in Abaqus [11] to evaluate the structural response of 3DPC wall panels with various cross-sectional patterns. The study considered non-load bearing 3DPC wall configurations and performed a decoupled heat transfer and mechanical analysis. The numerically investigated thermo-mechanical behaviour of the advanced wall configurations was based on the currently available geometries of 3DPC walls in the construction industry and the cavity provisions proposed by Wang et al (2012) [12] (Figure 1). All wall configurations are 1 000 mm high and 200 mm thick with the exposed and unexposed panels (external strip width) kept the same width (35 mm).

A heat transfer time step with a time of 3600 seconds (60 minutes) was created for the evaluation period, with an ISO 834 standard time-temperature used to define the exposed face gas temperature. This duration was considered adequate to illustrate the objectives of this work and is sufficient for the majority of buildings (such as offices, residential and institutional buildings) , except high-rise buildings. Figure 2 shows the detailed input of the heat transfer mechanisms that take place within a typical cross-section configuration. The external and internal predefined temperature was set at 20°C (ambient temperature). The time-temperature profile measured from the heat transfer analysis of all the cross-sections are applied as predefined fields to the perspective cross-sections over a normalized time

period in the mechanical analysis. Parameters for convection, cavity radiation and the general configuration for heat flow are also indicated on Figure 2.

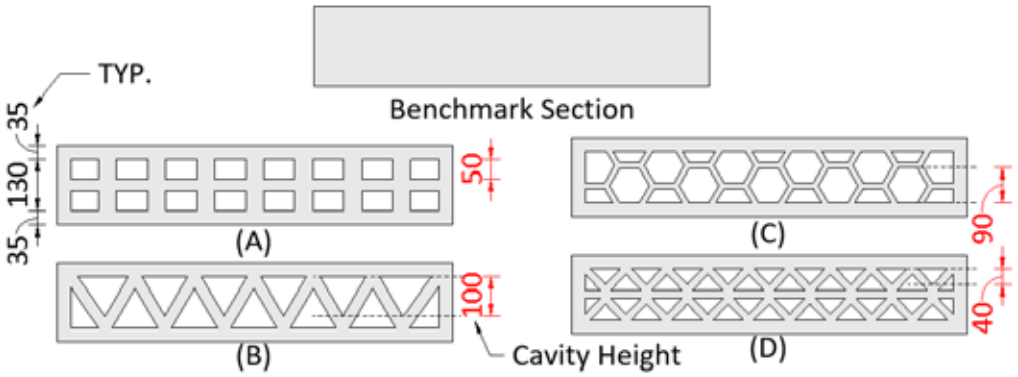

Figure 1: Wall configurations used in this study: (Top) Benchmark Section, (A) Cross-section A - lattice, (B) Cross-section B - truss, (C) Cross-section C - cellular, and (D) Cross-section D - triangular (unit: mm). Dimensions shown in red indicate cavity depths.

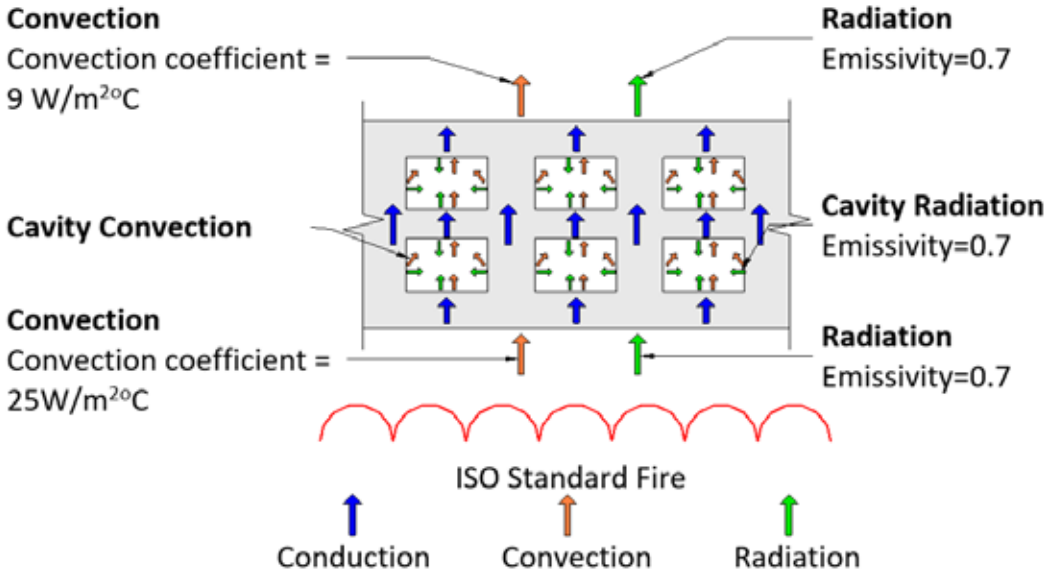

Figure 2: Heat transfer assumptions for the Abaqus [11] models.

4. THERMAL BEHAVIOUR OF 3DPC CAVITIES

4.1. Consideration of Fire Resistance

The fire performance of a structure or element is its ability to perform its design purpose in the event of a fire over a specific duration. The requirements for fire resistance are stability, integrity, and insulation. The insulation behaviour for similar wall configurations has been thoroughly investigated by Suntharalingam et al [4], who used the unexposed panel

temperature to investigate the insulation behaviour according to EN 1992-1-2 [3]. To satisfy the insulation criterion the unexposed panel should not exceed an average of 140°C and 200°C at any point on the unexposed surface.

4.2. Wall Panel Temperatures

Figure 3 depicts a comparison of the exposed surface temperatures of each cross-section with respect to time after 60 minutes of fire exposure. A higher front surface face temperature indicates a sample with a lower rate of heat transfer through it, i.e., it is a better insulator. This may be either positive or negative. Samples with lower temperature gradients (i.e., that let the heat through more rapidly) will fail fire test insulation requirements more quickly (140°C above ambient). However, higher temperature gradients lead to higher levels of induced thermal stresses, as the degree of thermal expansion between the front and back face differ more greatly.

As expected, a maximum temperature of 919°C is observed in Cross-section C (cellular) (i.e., close to the standard fire curve temperature of 945°C). This cellular configuration results in lowest resultant effective conductivity, with the mechanics discussed further below. The minimum exposed face temperature was observed in the cast solid section with a temperature of 895°C at 60 minutes. Figure 4 depicts the unexposed surface panel of the various wall cross-sections. It appears that the temperature curves follow an approximately exponential trend for all cross-sections. Cross-section B (truss) produced the maximum temperature on the unexposed surface of 43°C. All cross-sectional overall widths were kept the same to ensure consistency and not be a governing factor in the fire performance of the wall.

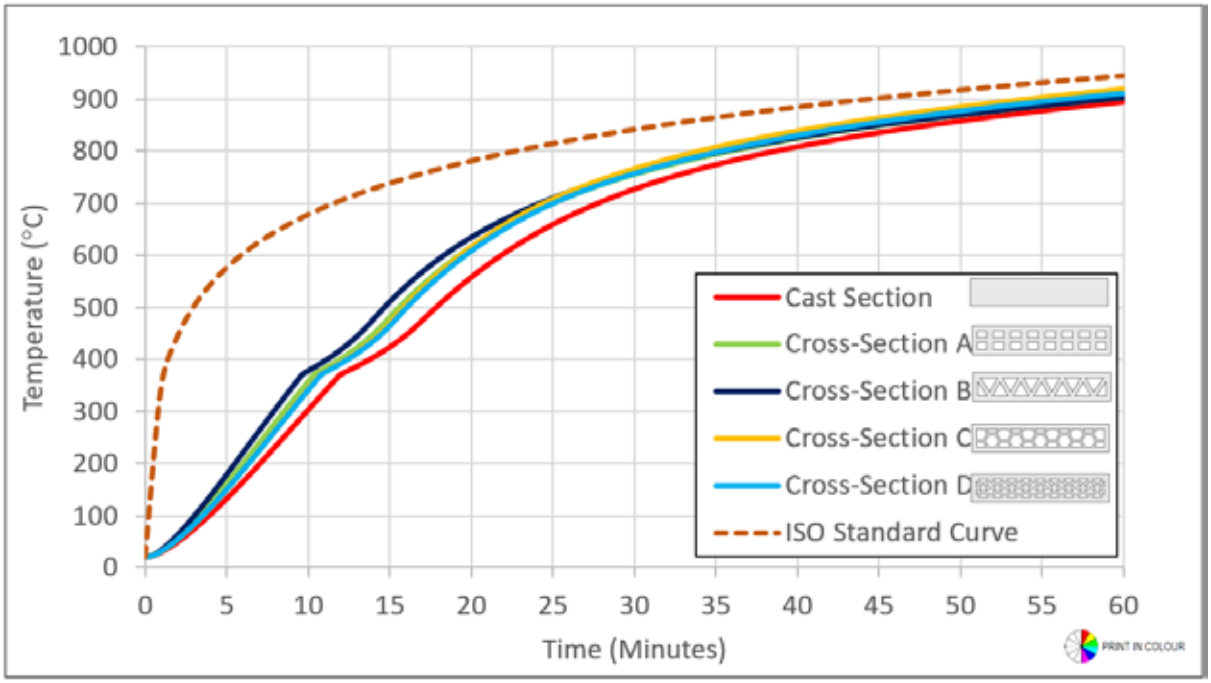

Figure 3: Exposed surface temperature for each wall configuration. No substantial differences noted between various cross-section geometry.

Heat transfer is based on the rate at which energy can flow through the system. Since energy can either be transferred by conduction (in solid sections) or convection and radiation (in cavities) the relative rate of heat transfer will vary. Cavity radiation is instantaneous in that as soon as the fire-exposed side of a cavity heats up it leads to energy transfer to the far side. However, the rate of transfer may be lower than conduction, depending on the distance covered. For deep cavities, cavity radiation results in more rapid transfer. When there are multiple layers of material the heat transfer mechanism sequence can be (1) conduction, (2) cavity radiation, (3) conduction, (4) cavity radiation, and (5) conduction. However, each intermediate layer will radiate back and transfer heat back to the fire-exposed side, leading to reduced energy transfer through the section. Hence, there is a complex, non-linear interaction of these factors depending on the geometry and heat transfer mechanisms, leading to some cross-sectional shapes heating faster than others.

Cross-section B (truss) showed the lowest performance in terms of insulation due to producing the highest temperature on the unexposed surface. This occurs as there is effectively one line of cavities to cross (albeit the cavities change in width). Cross-section C (Cellular) and Cross-section D (double layer triangular) displayed increased insulation performance due to producing a relatively low temperature on the unexposed surface. It is observed that Cross-section A (double layer lattice), Cross-section C (cellular) and Cross-section D (double layer triangular) had lower unexposed surface temperatures than the solid section, and this can be attributed to the air within the cavity reducing the heat transmission along with the thermal radiant feedback from multiple concrete lamina.

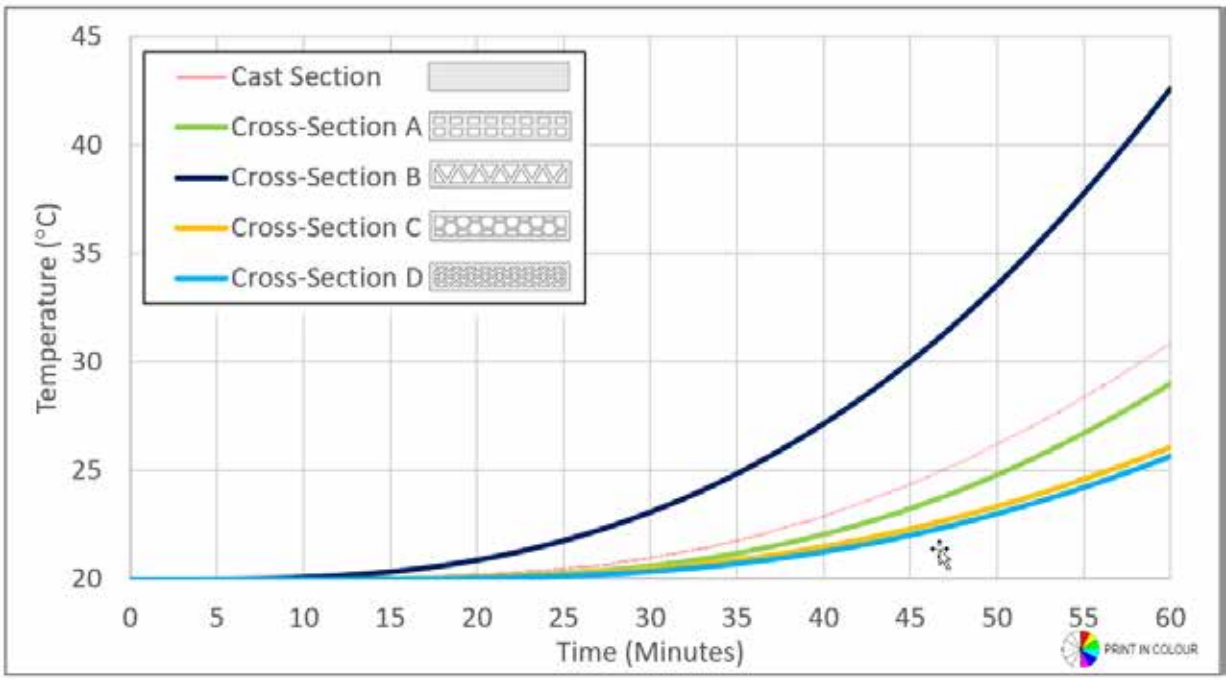

Figure 4: Unexposed surface temperature for each wall configuration.

All the cross-sections investigated pass the fire resistance insulation criterion of the unexposed face, with the highest temperature (43°C = 23°C above ambient) still being significantly below the requirement of around 140°C above ambient. Hence, from a thermal perspective a two-hour fire rating could potentially be attained by these samples. However, of great concern is the very high thermal gradients encountered, with changes in temperature of almost 900°C across sections which will lead to extensive internal stresses, as will now be discussed.

4.3. Stress-Strain Relationship of 3DPC Cavities

Due to the complex nature of the wall's configuration geometry, the behaviour of the stresses in 3PDC has not been extensively researched. As a first step this work proposes a simple free-body diagram, based on fundamental mechanics, for outlining the magnitude of stresses that might be expected during fire. Figure 5 illustrates the fundamental structural mechanics that occurs in a typical cavity cross-section which drives cracking.

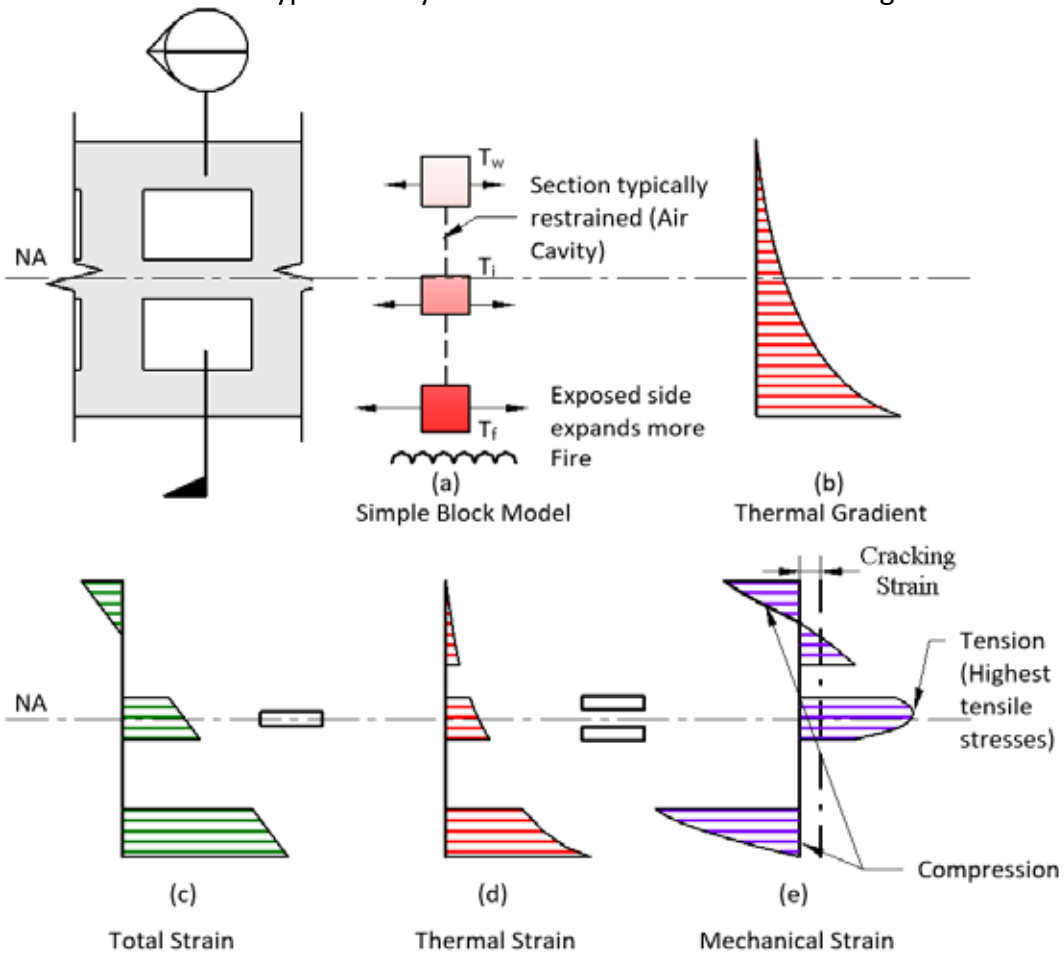

Figure 5: Type C Cross-section, showing (a) the simple block model, (b) the temperature profile, (c) the total strain is (d) subtracted from thermal strain and (e) indicates the complex mechanical strain profile.

The upper portion of the diagram indicates the cross-section (left), temperature profile (b) (right) and how the cross-section has been simplified into three layers (a). Assuming simple Euler-Bernoulli behaviour holds, the total strain in a cross-section will be as shown in (c). Considering that thermal strain is approximately proportional to the temperature, the thermal strain profile is as given in (d). The mechanical strain is the difference between the total and thermal strains. Depending on the temperature, and material model adopted, the mechanical stress (i.e., stress that results in structural elongations and cracking) will be approximately as shown in diagram (e).

From this diagram we see the first onset of cracking occurring in the internal middle layer, as depicted in Figure 5(e). Based on finite element models the time to onset of cracking ranged from 3 minutes for Cross-section A and D to 15 minutes for Cross-section B. This was influenced by the geometric distance from the exposed panel, resulting in the different onset of cracking times. It is of significant concern that simple models, and a free-body diagram based on fundamental structural mechanics, indicate that vertical cracking is likely to occur very quickly in sections. Also, it appears that cracking will start within the sample, rather than at the sample face, due to the thermal gradients and section geometries.

5. CONCLUSION

The work presented in this paper highlights a fundamental issue with the use of 3DPC and the thermal behaviour associated with it. The structural mechanics occurring within the 3DPC cavity walls are presented to illustrate the complex stress-strain relationship at elevated temperatures. The simplified illustrations of the internal stress and strain profiles are important for understanding why internal cracking may occur, and the predicted stress profiles, can be applied to various cross-sections in future work to identify the onset cracking. This is fundamentally important for post-fire damage assessment and consideration in the design process of the structure. Further investigations and research should be conducted into the thermal and associated mechanical behaviour of 3DPC walls. With 3DPC walls typically having low tensile strength (i.e. no reinforcement) this aspect should be investigated to consider whether 3DPC structures are as robust in fire as might be expected.

6. REFERENCES

[1] World Economic Forum, “Shaping the Future of Construction: A Breakthrough in Mindset and Technology,” World Economic Forum, Geneva, 2016.

[2] Y. Weng, M. Li, Z. Liu, W. Lao, B. Lu, D. Zhang and M. Tan , “Printability and fire performance of a developed 3D printable fibre reinforced cementitious composites under elevated temperatures,” *Virtual and Physical Prototyping,* vol. 14, no. 3, pp. 284-292, 2019.

[3] CEN, Design of concrete structures-Part 1-2: General rules-Structural fire design, 1 ed., Brussels: European Committee for Standardization, 2004.

[4] T. Suntharalingam, P. Gatheeshgar, I. Upasiri, K. Poologanathan and B. Nag, “Fire performance of innovative 3D printed concrete composite wall panels – A Numerical Study,” *Case Studies in Construction Materials,* vol. 25, no. 2, pp. 705-716, 2021.

[5] T. Bui, “Buildability and Mechanical Properties of 3D Printed Concrete,” *Materials,* vol. 13, no. 21, pp. 1-24, 2020.

[6] D. Heras, M. Moneeb and M. R. Taha, “Examining the significance of infill printing pattern on the anisotropy of 3D printed concrete,” *Construction and Building Materials,* vol. 262, no. 1, p. 120559, 2020.

[7] T. T. Le, S. Austin, S. Lim, R. Buswell, R. Law, A. Gibb and T. Thorpe, “Hardened properties of high-performance printing concrete,” *Cement and Concrete Research,* vol. 42, no. 3, pp. 558 - 566, 2012.

[8] V. N. Nerella, M. Krause, M. Näther and V. Mechtcherine, “Studying printability of fresh concrete for formwork free Concrete on-site 3D Printing technology (CONPrint3D),” Regensburg, 2016.

[9] B. Panda, S. C. Paul, N. A. Noor and Y. D. Tay, “Measurement of tensile bond strength of 3D printed geopolymer mortar,” *Measurement,* vol. 113, no. 2018, pp. 108-116, 2018.

[10] Y. Zhang, Y. Zhang, L. Yang, G. Liu, Y. Chen, S. Yu and H. Du, “Hardened properties and durability of large-scale 3D printed cement-based materials,” *Materials and Structures,* vol. 54, no. 45, pp. 1-114, 2021.

[11] Dassault Systèmes, *Abaqus Unified FEA (Abaqus 2021),* Providence, RI: Dassault Systèmes, 2021.

[12] Y. Wang, I. Burgess, F. Wald and M. Gillie, Performance-based fire engineering of structures, 1st ed., New York: Spon Press, 2012.

YCRETS 2023
YOUNG CONCRETE RESEARCHERS, ENGINEERS & TECHNOLOGISTS SYMPOSIUM
CEMENT & CONCRETE SA

Lightweight aggregate manufacturing for use in structural concrete

Richart G. Ross (1), Elsabe P. Kearsley (1)

(1) Department of Civil Engineering, University of Pretoria

Abstract

In this paper the manufacturing process of lightweight aggregate for the use in structural concrete is discussed. A reference mixture was cast in this pilot study to give a preliminary indication of the possibility of an ultra-lightweight structural concrete mixture. This paper outlines the materials and procedures used to create lightweight aggregate from local waste materials. This paper aims to indicate whether lightweight aggregates made from waste streams can be used in structural concrete. Although the initial results from this pilot study is promising, further research is needed to refine the properties of the lightweight aggregate.

Keywords: lightweight aggregate, lightweight concrete, manufactured aggregate, waste recycling

1. INTRODUCTION

The environmental impact of the construction industry is large. The construction industry was responsible for 39% of the total global yearly energy-related CO_2 emissions in 2018 [1]. Every effort should be made to ensure that the environmental impact of the construction industry is reduced. Lightweight concrete can be used to reduce the environmental impact of concrete. If the own weight of the structure is reduced the total load that the structure needs to support is reduced, therefore elements with smaller cross sections can be used. This will reduce the total volume of concrete used during construction and subsequently reduce the CO_2 emissions during construction.

In South-Africa 32.7% of the fly ash produced by the coal-fired power stations is recycled [2]. Although there is an increase in recycling of glass in South-Africa only 44% of glass was recycled in 2020 [3]. These two waste materials were used as the main components of the lightweight aggregate proposed in this paper. The aim of this paper is to prove that these two waste streams can be utilised to manufacture lightweight aggregates for use in structural concrete.

2. LITERATURE REVIEW

Lightweight aggregates can be manufactured from various materials. Tuan et al. [4] used wet sewage sludge and waste glass powder to manufacture lightweight aggregates. The effect of sintering temperatures between 830°C and 1100°C were also analysed during the study. It was found that an increase in sintering temperature led to an increase in bulk density of the lightweight aggregate.

Liu et al. [5] manufactured lightweight aggregates from waste glass and engineering muck. Lightweight aggregate with an apparent density of 1.461 g/cm^3 and a single-particle crushing strength of 20.81 MPa was manufactured. The improved mechanical properties were attributed to the formation of diopside in the aggregates. They found that an increase in glass content in the aggregate mixture led to an increase in diopside formation.

Li et al. [6] studied the influence of sintering temperature and dwelling time on the characteristics of lightweight aggregates produced from sewage sludge and waste glass powder. An increase in sintering temperature decreased the water absorption, density and compressive strength of the particles.

Fly ash has been used as the main component of manufactured aggregates in studies performed by various authors [7, 8].

Table 1 is a summary of different lightweight concrete mixtures made with glass aggregates.

Table 1: Summary of different glass aggregate concrete mixtures

Reference	Strength (MPa)	Density (kg/m^3)
Tuan et al. [4]	49.46	1947
Yousefi et al. [9]	8.20	987
Yousefi et al. [9]	26.25	1769
Rumsys et al. [10]	35.1	1590

The aim of this study was to determine a suitable mixture composition for producing lightweight aggregate from local streams of waste that can be used to manufacture structural concrete.

3. EXPERIMENTAL SETUP

The lightweight aggregate was manufactured by combining fly ash, dolomite, waste glass, kaolin clay, water and sodium metasilicate pentahydrate ($Na_2SiO_3{\cdot}5H_2O$) in different proportions. The fly ash and waste glass are local waste materials included in the aggregate mixture for strength purposes. The kaolin clay (also a local waste material from the Taaifontein kaolin deposit) was included to aid with the formation of the aggregate balls. The dolomite and $Na_2SiO_3{\cdot}5H_2O$ were included in the aggregate mixture to assist with the formation of voids in the aggregate once the heating cycle commenced. Water was used during the manufacturing process to form the aggregate balls and for all aggregate mixtures 20% by mass was used.

Firstly, the optimal proportion of fly ash, waste glass and dolomite were determined. This was done with a design of experiments setup to vary all three variables simultaneously. The mass ratio of glass and fly ash to kaolin clay and dolomite was kept constant at 80:20. The dolomite % was varied between 0% and 10% of the total weight of the lightweight aggregate.

Within the glass and fly ash portion, the ratio of glass to fly ash was varied from 0:100 to 100:0. This method yielded aggregate mixtures named Mix 1 to Mix 9 as shown in Figure 1.

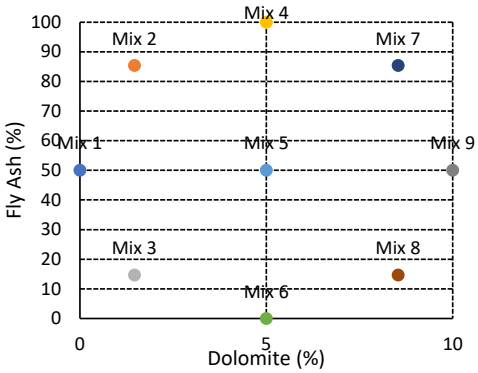

Figure 1*:* Design of experiments

The results from the initial design were analysed and it was determined that the optimal ratio of glass to fly ash is 85.36:14.64, but that the optimal dolomite percentage was not reached. For Mix 10 to Mix 12 this optimal glass to fly ash ratio was used and the percentage dolomite was increased with the same amount as for Mix 3 and Mix 8. Subsequently the percentage kaolin clay used was decreased. For Mix 11 and Mix 12 the percentage of kaolin clay used could not be decreased further. The same amount of kaolin clay as in Mix 10 was used for these two mixes and the mass ratios of glass and fly ash to kaolin clay and dolomite were changed to 72.93:27.07 and 65.86:34.14 respectively. The results from Mix 10 to Mix 12 were analysed and Mix 10 had the optimal percentage dolomite. Mix 10 was then used as the basis for the design of Mix 13 to Mix 17. In these mixes up to 15% in weight of $Na_2SiO_3{\cdot}5H_2O$ was added in steps of 3%. $Na_2SiO_3{\cdot}5H_2O$ was used as glass replacement.

3.1 Lightweight Aggregate Manufacturing Process

All the mixtures were manufactured using the same procedure. The waste glass, $Na_2SiO_3{\cdot}5H_2O$ and dolomite was milled in a ball mill whereafter it was sieved through a 150 µm sieve. All the dry constituents of the mixtures were pre-mixed in a disc granulator for a period of two minutes to ensure homogeneity. The disc granulator was set to rotate at 50 rotations per minute and was placed at an angle of 35° with respect to the horizontal. Water was added using a spray bottle. All mixtures were heated to 100°C for 2 hours whereafter it was heated to 850°C at a heating rate of 999°C/hr and kept there of 1 hour. The vents of the oven were then opened to allow the oven to gradually cool down. The lightweight aggregates were removed from the oven the following day once the oven had cooled to room temperature.

3.2 Lightweight Aggregate Testing Procedure

All mixtures were subjected to the same tests. Grading analysis, aggregate impact value (AIV), moisture absorption (MA) and relative density (RD) tests were performed on all the mixtures. AIV was chosen as the metric to determine the relative strength of the lightweight aggregate mixtures since it requires a smaller sample size than the regularly used 10% FACT and Aggregate Crushing Value tests. Since these lightweight aggregates are in the prototype

phase the smaller sample size used for AIV testing is beneficial for rapid testing and iterations [11].

The AIV tests [12], MA tests [13] and grading analyses [14] were conducted. Various RD test methods were used. For Mix 1 to Mix 12 the wax coating method was used. For Mix 13 to Mix 17 the wax method could not be used. For these mixes the water displacement method was used. The lightweight aggregates were weighed dry, then placed in water under 80 kPa of pressure for 4 hours whereafter the aggregates were fully saturated and therefore they sank.

3.3 Concrete Testing

To determine the strength of concrete containing manufactured lightweight aggregates, Mix 13 to Mix 17 were cast into respective concrete mixtures. A control concrete mix with dolomite aggregate was cast. The lightweight aggregate was used as coarse aggregate replacement due to the sizes that was manufactured and therefore all mixes contained dolomite sand as the fine aggregate. Only compressive strength, saturated and dry density of the mixtures were determined as this study only aimed to provide a proof of concept.

Three cubes were cast for 7-day strength testing and two for the dry density calculation. All 5 cubes were cured in water at 25°C. After seven days of curing two cubes were placed in an oven at 60°C for a week to dry whereafter the dry density of the concrete mix was determined. The lightweight aggregate was placed in water 24 hours before casting to ensure that they were saturated. The concrete mixtures are shown in Table 3. The coarse aggregate is shown in l/m3 since the mass of the coarse aggregate varied. A water cement ratio of 0.5 and a coarse aggregate to fine aggregate ratio of 60:40 were used.

Table 2: Concrete mix design

Mix	Control	Mix 13	Mix 14	Mix 15	Mix 16	Mix 17
Water (kg/m^3)	230	230	230	230	230	230
Cement (kg/m^3)	460	460	460	460	460	460
Fine aggregate (kg/m^3)	713	713	713	713	713	713
Coarse aggregate (l/m^3)	374	374	374	374	374	374
Coarse aggregate (kg/m^3)	1070	370	302	252	269	307
Absorbed water (kg/m^3)	0	113	101	104	113	107
Casting density (kg/m^3)	2473	1886	1806	1759	1785	1817

4. RESULTS AND DISCUSSION

4.1 Aggregate Testing

The aggregates that were manufactured were coarse and not suitable for fine aggregate replacement. For fine aggregate replacement the size of the manufactured aggregates must be reduced. The mean aggregate size of each aggregate mixture was 6.7 mm – 9.5 mm. The AIV, RD and MA test results are shown in Figure 2a, b and c respectively. The AIV and MA increased as the percentage fly ash increased and the dolomite content did not have a considerable influence on the AIV and MA. The RD of the lightweight aggregates decreased as the percentage fly ash and dolomite increased. As the percentage dolomite increased the RD

of the lightweight aggregate became less dependent on the percentage fly ash. Based on these results the dolomite content was increased as the optimal percentage dolomite was not yet reached in the initial design. Due to the high strength of aggregates with low fly ash compositions and the decreasing effect of the fly ash percentage on the RD as the percentage dolomite increases, a low fly ash percentage was used for the next aggregate designs.

The AIV results of mixtures 3,8,10,11 and 12 are shown in Figure 3. There is a slight increase in AIV as the dolomite percentage increased, but all these values are low. For comparison, the AIV of dolomite was 13 when it was tested. The 15.62% dolomite mixture has the smallest RD. This mixture was used as the base mixture for the mixtures where $Na_2SiO_3 \cdot 5H_2O$ was added since this mixture was the lightest.

Figure 4a shows the AIV results of the mixtures containing $Na_2SiO_3 \cdot 5H_2O$ (Mix 13 – Mix 17). There is a substantial increase in AIV as the percentage $Na_2SiO_3 \cdot 5H_2O$ increased. There is a clear peak at 9% whereafter the AIV reduced as the percentage $Na_2SiO_3 \cdot 5H_2O$ increased. In Figure 4b the RD and MA of these mixtures are shown. The same trend in the AIV results can be seen in the MA results. This trend coincides with the initial decrease and subsequent increase in RD as the percentage $Na_2SiO_3 \cdot 5H_2O$ increased. The RD increasing at higher percentages of $Na_2SiO_3 \cdot 5H_2O$ can be due to the heat cycle being suboptimal.

The MA of the aggregates is highly dependent on the surface of the aggregate. Since the aggregate is porous on the inside it absorbs significantly more water if the surface of the aggregate is also porous. The surface porosity of the aggregates should be reduced in future to decrease the MA of the aggregates.

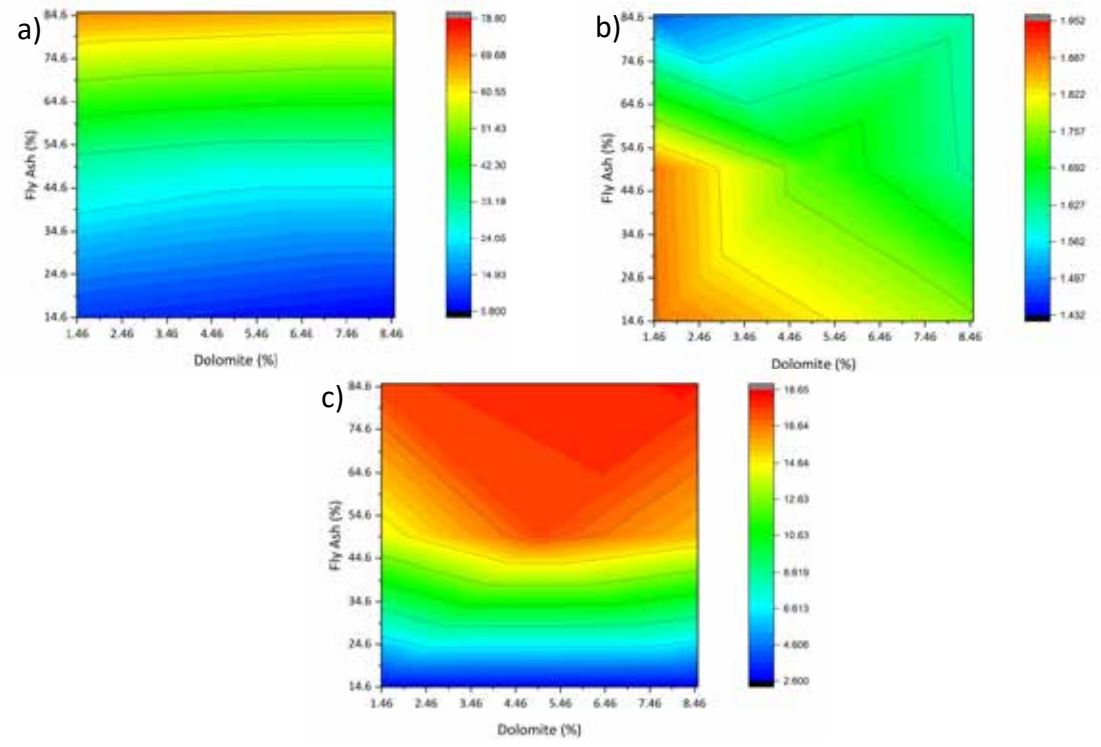

Figure 2: Design of experiments aggregate results a) AIV (%) b) RD and c) MA (%)

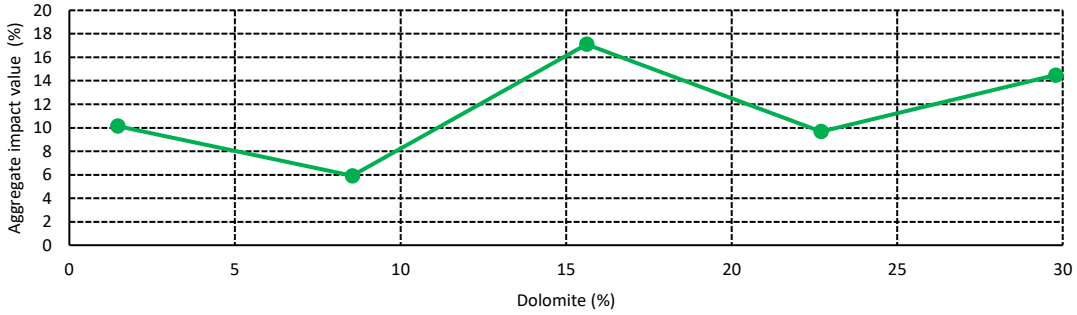

Figure 3: AIV results of the dolomite optimisation mixtures

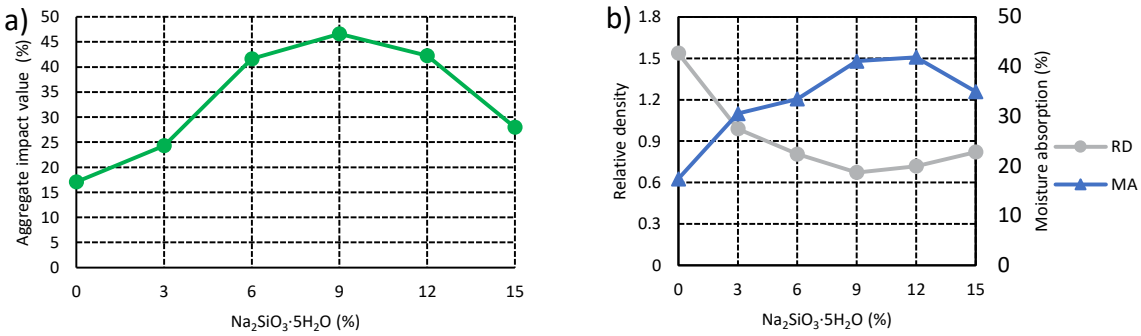

Figure 4: AIV, RD and MA results of the $Na_2SiO_3 \cdot H_2O$ mixtures

4.2 Concrete Testing

Figure 5a indicates that the strength of the concrete decreased as the saturated density of the concrete decreased. The same trend is observed if the dry density is used as shown in Figure 5b. In both instances there is a steep decline in strength for a marginal reduction in density among the lightweight aggregate concrete mixtures. Figure 6 illustrates that the lightweight aggregates with the highest AIV has the lowest strength. This supports the trend seen in Figure 5a and b. In Figure 6 the relationship between the lightweight aggregate AIV and concrete strength is linear. Therefore, this can be used to estimate the strength of the concrete cast with a lightweight aggregate based on the AIV of the lightweight aggregate.

In Figure 7 the strength of the concrete initially decreased as the percentage $Na_2SiO_3 \cdot 5H_2O$ increased, but at higher percentages $Na_2SiO_3 \cdot 5H_2O$ the strength of the concrete increased. This trend coincides with the saturated density reduction and increase. This also coincides with the trend of the AIV with increasing percentages of $Na_2SiO_3 \cdot 5H_2O$ seen in Figure 4a. In Figure 8 it is shown that the strength of the concrete increased as the RD of the lightweight aggregates increased. This is to be expected since the lightweight aggregate is the reason for the reduction of the concrete density and therefore it will match the trends in Figure 5a and b. In Figure 8 there is no relationship between the RD of the lightweight aggregates and the air entrapped in the concrete mixture. Figure 9 illustrates the difference between the dry- and saturated densities of the concrete mixtures. The dry densities of the concrete falls in the range of structural lightweight concrete [15]. The lightweight aggregate concrete cubes failed through the aggregates and therefore the reduction in aggregate strength caused a significant reduction in concrete strength. The strength of the paste of the lightweight aggregate

concrete can be reduced since the lightweight aggregate is governing the strength of the concrete.

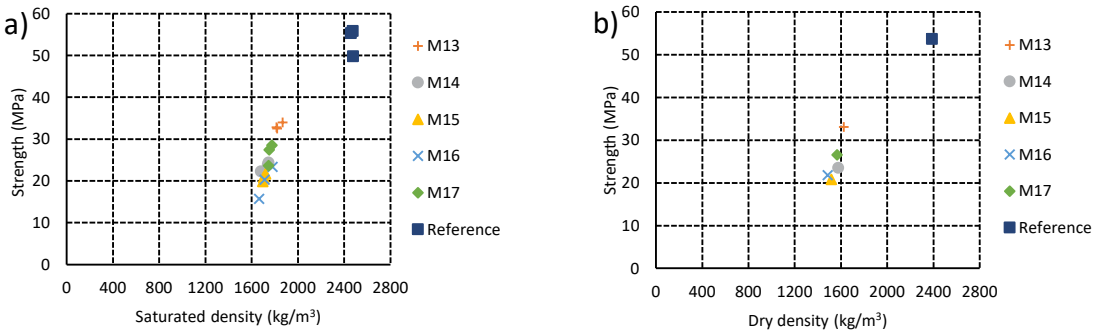

Figure 5: Strength of the concrete mixtures as a function of saturated and dry density

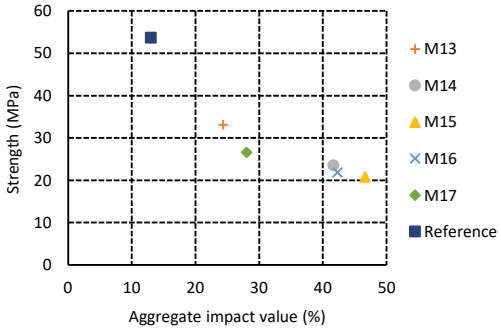

Figure 6: Strength of the concrete mixtures as a function of AIV

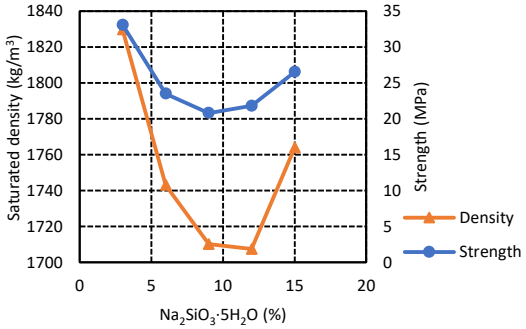

Figure 7: Density and strength of the concrete mixtures as a function of $Na_2SiO_3 \cdot 5H_2O$ content

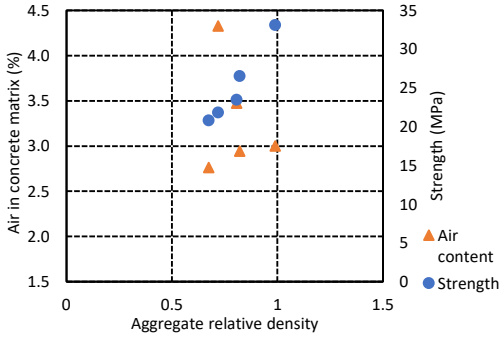

Figure 8: Air content and strength of the concrete mixtures as a function of the RD of the lightweight aggregates

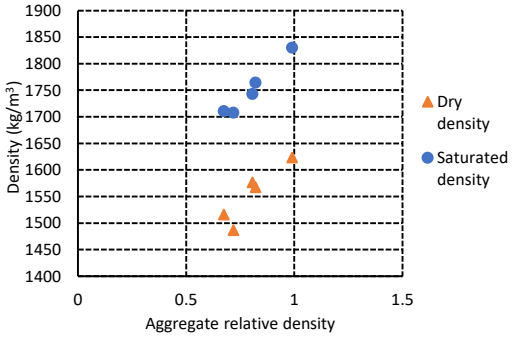

Figure 9: Dry and saturated density of the concrete mixtures as a function of the RD of the lightweight aggregates

5. CONCLUSIONS AND RECOMMENDATIONS

It is possible to produce lightweight aggregates that contain 67.8% South-African waste materials that can be used in structural concrete. A high mass ratio of glass improved the strength of the lightweight aggregates and the addition of $Na_2SiO_3 \cdot 5H_2O$ greatly reduced the

RD of the lightweight aggregate. Further investigation into the concrete properties should be done to determine if the concrete adheres to all the requirements of the structural concrete design code. Factors influencing size of aggregates produced should be analysed. The surface porosity of aggregates should be reduced. The concrete mixture should be optimised before structural concrete tests are performed on the concrete. A complete cost comparison to natural aggregates should also be done to ensure that the lightweight aggregates are affordable. This might require further optimisation of the lightweight aggregate mixture.

6. REFERENCES

[1] Abergel, T. Dulac, J. Hamilton, I. Jordan, M. and Pradeep, A. 'Global Status Report for Buildings and construction: Towards a zero-emission, efficient and resilient buildings and construction sector', in 'Global Alliance for Building and Construction, International Energy Agency and the United Nations'. ISBN no: 978-92-807-3768-4, (2019).

[2] Eskom Holdings Ltd. 'Eskom Integrated Report: 31 March 2021'. *https://www.eskom.co.za/wp-content/uploads/2021/08/2021IntegratedReport.pdf,* (2021).

[3] The Glass Recycling Company. *https://theglassrecyclingcompany.co.za/118363-2/*, (2021).

[4] Tuan, B.L.A. Hwang, C.L. Lin, K.L. Chen, Y.Y. and Young, M.P. 'Development of lightweight aggregate from sewage sludge and waste glass powder for concrete' in 'Construction and Building Materials'. **47** (2013) 334-339.

[5] Lui, Y. Wan, W. Yang, F. Hu, C. Lui, Z. and Wang, F. 'Performance of glass-ceramic-based lightweight aggregates manufactured from waste glass and muck' in 'Ceramics International'. **48** (2022) 23468-23480.

[6] Li, X. He, C. Lv, Y. Jian, S. Jiang, W. Jiang, D. Wu, K. and Dan, J. 'Effect of sintering temperature and dwelling time on the characteristic strength of lightweight aggregate produced from sewage sludge and waste glass powder' in 'Ceramics International'. **47** (2021) 33435-33443.

[7] Terzić, A. Pezo, L. Mitić, V. and Radojević, Z. 'Artificial fly ash based aggregates properties influence on lightweight concrete performances' in 'Ceramics International'. **41** (2) (March, 2015) 2714-2726.

[8] Kourti, I. and Cheesman, C.R. 'Properties and microstructure of lightweight aggregate produced from lignite coal fly ash and recycled glass' in 'Resources, Conservation and Recycling'. **54** (11) (September, 2010) 769-775.

[9] Yousefi, A. Tang, W. Khavarian, M. Fang, C. and Wang, S. 'Thermal and mechanical properties of cement mortar composite containing recycled expanded glass aggregate and nano titanium dioxide' in 'Applied Sciences'. **10** (7) (March,2020).

[10] Rumsys, D. Spudulis, E. Bacinska, D. and Kaklauskas, G. 'Compressive strength and durability properties of structural lightweight concrete with fine expanded glass and/or clay aggregates' in 'Materials'. **11** (12) (November,2018).

[11] Gomathi, P. and Sivakumar, A. 'Accelerated curing effects on the mechanical performance of cold bonded and sintered fly ash aggregate concrete' in 'Construction and Building Materials'. **77** (2015) 276-287.

[12] Indian Standard. 'Methods of Test for Aggregates for Concrete'. IS: 2386 Part IV – 1963.

[13] South African National Standard. 'Civil engineering test methods'. SANS 3001-AG20:2014.

[14] South African National Standard. 'Sieve analysis, fines content and dust content of aggregates'. SANS 201:2008.

[15] Eurocode, C.E.N. '2: Design of concrete structures – part 1-1: General rules for buildings'. EN 1992-1-1: 2004 (Comité Européen de Normalisation, Brussels).

YCRETS 2023
YOUNG CONCRETE RESEARCHERS, ENGINEERS & TECHNOLOGISTS SYMPOSIUM
CEMENT & CONCRETE SA

Evaluation and rectification of concrete defects in hydraulic structures during DLP-case of Isimba Hydro Power Plant (183mw) in Uganda

Godfrey Rwakafunjo (1), Chad S. Akita (2) Muzafalu Kayondo (3)

(1) Civil Engineer, Uganda Electricity Generation Company Limited (UEGCL)
(2) Project Manager, Isimba Hydro Power Project (UEGCL)
(3) Head Research and Business Development (UEGCL)

Abstract
The dam and concrete structures of Isimba Hydropower Plant were designed with 100-year service life with focus on structural reliability and operational integrity. Isimba Hydropower Plant (183MW) a run off river plant located in East Africa, Uganda was commissioned in March 2019 with a total defects liability period (DLP) of 4 years and has since been in operation for 3.5 Years. During the last 3.5 years of operation, numerous concrete defects manifested within the structure and these included; seepage through concrete in the galleries, leaking joints, washout and abrasion damage in the water ways, exposed reinforcement in water ways, and spalling. As a result, these defects were rectified by the Contractor in accordance with the contract as part of his obligation during DLP. The paper therefore, evaluates the genesis of the different categories of defects experienced within the hydraulic structures of Isimba HPP, the methodology used in rectification, challenges faced, the lessons learnt and recommendation for minimizing similar defects in new hydropower plants. The paper further discusses the roles of different professionals and stakeholders during DLP in ensuring delivery of a fit for purpose structure that is in line with the 100-year design service life.

Keywords: Isimba HPP, concrete, defects, DLP, rectification, hydraulic

1. INTRODUCTION

Hydraulic structures are structures that are fully or partially submerged in water. The essence of building hydraulic structures is to either divert, disrupt, store, or completely stop the natural flow of water bodies. Based on the work they are designed to perform on streamflow, hydraulic structures are categorized as water retaining structures (dams and barrages), water-conveying structures (artificial channels), and special-purpose structures (structures for hydropower generation or inland waterways) [1].

Like any other hydraulic structure, hydropower dams are susceptible to concrete defects given the harsh environment they are subjected to, while in operation. The sources include; hydrostatic pressure, abrasion, chemical attack, imposed loads, age-related deterioration and carbonation. Neglecting to perform periodic maintenance and repairs to concrete structures as they occur could result in failure [1]. Unlike conventional concrete for example in structures

that only carry loads, concrete in hydropower dams is normally under extreme hydrostatic and hydrodynamic pressure. This pressure forms part of the critical load to withstand [2].

About Isimba HPP

Isimba Hydropower Plant (HPP) is located in East Africa, Southern part of Uganda, on the Nile River (Longest River in the world) 50km downstream of its source; Lake Victoria. With four Kaplan turbines, the installed Capacity is 183.2MW (Figure 1). The complex constructed and commissioned in March 2019 consists mainly of the water-retaining dam, spillway, power-house, and the switchyard. The dam includes an earth rock fill dam on the left bank (LED), two gravity dams (GD1 and GD2) and an earth rock fill dam on the right bank[3]. The total volume of concrete cast was 357,020m^3.

Figure 1. Arial view of Isimba HPP

2. DEFECTS LIABILITY PERIOD

According to FIDIC [4], the Defects Lability Period (DLP) is the period which commences at works completion or a stage signified by issue of a takeover certificate or equivalent by the contract administrator in accordance with the construction contract and continues for the period specified in the contract. Ficken [5] acknowledges that the contractor is required to perform construction fully in accordance with the contract documents, usually consisting of at least plans, specifications and the building code within required time.

According to the Isimba HPP contract, during the DLP any defect found in the design, engineering, materials and workmanship of the plant supplied or of the work executed by the contractor was the contractor's obligation to be corrected to meet the specification.

During Isimba HPP's first year of Operation and Maintenance (O&M) several concrete defects were identified by the client (UEGCL), notified to the Owner's Engineer (OE) and consequently addressed by the Engineering Procurement and Construction (EPC) Contractor as part of his obligation during DLP. Therefore, this paper shall comprehensively evaluate the concrete defects encountered and rectification during the DLP of Isimba HPP.

3. CONCRETE DEFECTS AT ISIMBA HPP

Isimba Dam structures experienced numerous concrete related defects right from impoundment in November 2018 and they continued to manifest even after commissioning (March 2019). According to Obiora [6] concrete defects can either manifest at the beginning

of the early stages following loading, or later during the service life of the structure. Concrete defects affect over 65% of all structures globally according to recent statistics [6]. These defect normally result from poor handling methods, placing, insufficient curing, poor workmanship and poor materials. The defects included the following;

3.1 Seepage Through Walls

The seepage was through the walls, floor and joints that were more evident in lower galleries that included EL1017 (drainage gallery) EL1024masl (grouting gallery) EL1025masl (spiral case floor) EL 1030masl (cooling water floor) and EL1037masl (turbine pit floor).

With the dam crest at EL 1057masl a hydrostatic pressure head of 20-40meters largely influenced the magnitude of the leakages in the galleries (see Figure 2).

Figure 2: Concrete leakages along staircase from EL1025 and at EL1017

3.2 Damp Spot and Leakages Along Lift Joints

These were distributed across all the elevations more evident in the lower galleries (Figure 3).

Figure 3: Damp spots and leakage along lift joints at EL1024 and EL1017

3.3 Cracks

Cracks are the most commonly seen kind of defects observed in concrete structures, and may be due to various causes, including; overloading, drying shrinkage, and thermal stress. Cracks are widely regarded as a long-term durability and maintenance problem because they increase the permeability of the concrete [7]. Hairline cracks manifested in areas especially the ones previously grouted using a wrong methodology. Cracks at EL1030 and EL1037 were hidden since these floors were plastered and painted.

3.4 Concrete Defects in Waterways (draft tube and spiral case)

These were the most critical concrete defects experienced at Isimba HPP having been observed just after 2 years of commercial operation. They included; severe washout (Figure 4) and abrasion damage, exposed reinforcement, concrete spalling, long transverse concrete cracks, concrete pop outs at some sections of the ceiling slab, joint leakages and damp spots along the spiral case wall, leakage through crack seals and cavities in 2nd stage concrete.

Figure 4: Severe abrasion in Unit 3 draft tube (left) and abrasion in Unit 3 spiral case(right)

3.5 Shrinkage Cracks on the Intake and Tailrace Platform

Concrete defects on tailrace and Intake platforms manifested in the form of alligator cracks that ran horizontally and transverse across the entire platform. These cracks were categorised as shrinkage cracks with no structural effects attributed to rapid evaporation due to insufficient curing of the slab.

The cracks were also partly attributed to poor design due to insufficient expansion joints provided within the slabs whose dimensions were spanning over 95metres in length and 5-8metres wide.

4. ROOT CAUSE ANALYSIS OF THE CONCRETE DEFECTS

Laboratory tests on porosity of the cored as-built concrete sample showed a variability in porosity values with a wide range (6.1%-17.1%) which indicated problems with quality control during construction and possible presence of numerous pores within the structure.

Soft water attack was suspected after the first inspection of the spiral case owing to the uniform abrasion on the walls. Whereas during the preliminary stage soft water attack was ruled out by calculating Lingerie index, the recent developed Basson Index carried out in September 2022 confirmed the soft water attack of River Nile water on concrete. All the total calculated corrosion values from the samples obtained were greater than 1100 indicating a very high aggressiveness of the water [8].

5. RECTIFICATION METHODOLOGY FOR CONCRETE DEFECTS

According to Kurt [9], the first step to increase the likelihood of a successful repair, is to use a consistent, systematic approach to concrete repair. The recommended concrete repair and maintenance system consists of seven basic steps:

i. Determine the cause(s) of damage
ii. Evaluate the extent of damage
iii. Evaluate the need to repair
iv. Select the repair method and material
v. Prepare the existing concrete for repair
vi. Apply the repair method
vii. Cure the repair properly

Therefore, the above criteria laid out in [9] was used as a guiding tool while addressing the different categories of defects.

5.1 Methodology for Leakages, Damp Spots and Wet Cracks

The methodology was onsite based, with different defects having different methodology. Leakages along construction joints were injected with Sika 201 (polyurethane based material) at a spacing of 300mm, 400mm depth with pressure in the pump at 8-10MPa and holes drilled at an angle of 45^0 to the wall.

5.1.1 Calculation of grouting pressure

The grouting pressure (P_{max}) was calculated using the as-built concrete class in the powerhouse galleries. The design concrete strength for Isimba was C20/25 for the galleries therefore, laboratory test results were reviewed to qualitatively obtain the strength to avoid damage that could possibly emanate from injecting the material at high pressure.

$$P_{max} = \frac{\text{Concrete Strength X10}}{3} = \frac{25X10}{3} = \boxed{83\ \text{Bar}} \quad (1)$$

Therefore, 80Bar was adopted as the grouting pressure for all the Isimba structures.

5.1.2 Spacing of packers and depth

Along a dry or wet crack, packers were installed at an offset of 300mm from crack- packer and packer- packer which was equivalent to $^1/_2\,D$ as shown in Figure 5 where *D* is the thickness of the structure. A depth of 400mm was adopted which was within the acceptable range (200-600mm). The alternating pattern was used to ensure that the crack was intercepted, since the location of the crack underneath the surface is usually unknown.

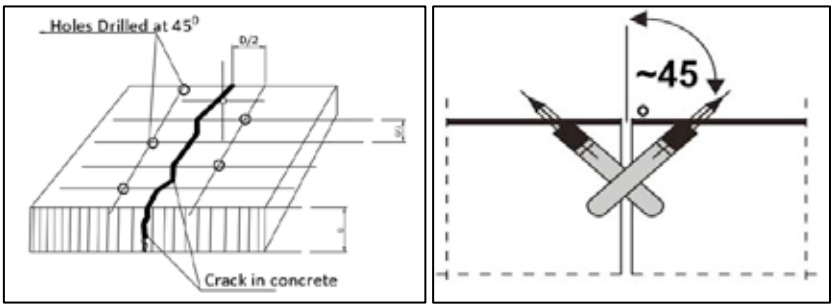

Figure 5: Schematic diagram showing spacing of grouting packers

5.1.3 Selection of polyurethane material

According to [9] cracks to be injected with polyurethane resin should not be less than 0.127mm. Sika Injection -201 CE an elastic polyurethane-based resin for permanent water tight sealing was used throughout the grouting process, Sika injection 101Rc for temporary water stoppage was used in few occasions in areas with high water flow. Hydrophilic based polyurethane resin (Sika201 and 101) were specifically selected due to their rapid reaction with water to form a permanent flexible foam that stops flow of water. This was necessary since over 95% of the defects at Isimba HPP had damp spots.

In other areas under hydrostatic pressure with numerous leaking points, curtain grouting was recommended that involved use of Sika 201 Injection while drilling grouting holes perpendicular to the wall at a spacing of 300mm from each other as shown in Figure 6.

Figure 6: Curtain grouting at EL1037 and stairs to EL1017

5.2 Methodology for Areas Under Intense Hydrostatic Pressure

These were areas in which grouting was first used however, intense leakages resurfaced within a very short time. It should be noted that polyurethane material is effective along thin lines of water passage. In such areas channels were instead adopted to act as pressure relief and the residue water directed to the nearby drainage channel. Since the leaking water normally contains calcium salt deposits, regular inspection and cleaning has been included in the maintenance routines to keep the leakage water flowing and prevent blockage.

5.3 Methodology for Concrete Defects in Units' Spiral Cases

Concrete repair for damaged surfaces, and lift joints in unit #1 #2, #3, and #4 spiral cases was undertaken using;

i. Sika Monotop 412S; a fiber reinforced low shrinkage repair mortar, then
ii. Sikagard 720 Epocem; an epoxy modified mortar to act as a moisture barrier and
iii. Sikagard PW; an epoxy coating with outstanding mechanical and chemical properties as a final sealing protective coating.

These products were applied independently or combined depending on the concrete defect as guided by the Sika technical personnel. Therefore, the coatings applied were designed to provide an improved concrete surface, for increased resistance or performance against specific external influences both mechanically and chemically. With only defective areas repaired instead of the whole area (Figure 7). Recommendations have been made to line the

entire spiral case walls with the same material in future. The same defects were observed in the draft tubes hence a similar procedure shall be adopted before expiry of the DLP.

Figure 7: Final coating of Sikagard PW in Unit 3 spiral case

5.4 Leaking Expansion and Construction Joints

Leakages were observed on several expansion joints right after commissioning with water through sides of the joint tapes. Old dilapidated joint tapes were removed and replaced with Sikadur - combiflex a high performance joint sealing system that allows variable and high levels of movement. This was bonded with sikadur epoxy to maintain the water tightness properties.

5.5 Methodology for Shrinkage Cracks on the Intake and Tailrace Platforms

A top concrete layer of 80mm depth was removed by hacking and re-works undertaken using Y-6 reinforcement mesh, fiber reinforced concrete of C40 grade cast and sufficiently cured for 14 days. The additional of cellulose fiber was intended to minimize possible shrinkage cracks. Expansion joints were also introduced at an interval of 3metres to eliminate possible cracks due to expansion and contraction.

6. ROLES OF EXPERTS AND INDEPENDENT CONSULTANTS

In countries where the Hydropower Dam Construction has not attained sufficient experience, there is need not to only rely of written experience in manuals, it was thus recommended to involve a panel of experts (PoE) with rich experience in dam construction and operation. For the case of Isimba HPP in April 2016 PoE comprised of 7 members with combined total professional experience of 300 years in dam engineering was instituted by the client (UEGCL) to ensure international best practices on dam engineering was applied from design to construction, operation and maintenance.

Other independent specialists included; NDT specialists independent laboratories (determining properties of the as-built concrete properties), MIRA image experts Level 2 experts and researchers. The contribution of all the above specialists/experts in additional to PoE was key in aiding the facility owner to make informed decisions.

7. CHALLENGES FACED AND LESSONS LEARNT

i. Re-occurrence of defects in treated areas. Whereas chemical grouting is acceptable, continuous grouting in the same area using polyurethane material could weaken the concrete structure and impact on its service life.
ii. With the right methodology employed by trained professionals in concrete grouting and repair techniques it is possible to eliminate most of the leakages.
iii. Most of the concrete related defects at Isimba emanated from deficiency in either design or construction procedures or methodologies. This could have been eliminated by in-depth peer review of the designs as well as following the right procedures during the entire construction phase by all teams. For example determining aggressiveness of water using Basson index instead of Langelier Saturation index.
iv. Periodic reviews and inspection by experts, should be maintained even during DLP to enable comprehensive assessment of the as-built structures and provide technical guidance to ensure delivery of a fit for purpose facility.

8. CONCLUSION

Concrete defects in a sophisticated construction like for Isimba hydro power plant can be effectively minimised right from the design stage, following proper construction procedures and practices, robust quality control system and use of proper methodologies for repairs throughout the construction phase to commissioning. In practice, whereas minor damp spots are acceptable in any hydraulic structure given concrete is not 100% water tight, it is critical that continuous evaluation of the defects' status is periodically ascertained to mitigate culmination into structural deficiency and consequently failure.

Therefore, developing a long-term monitoring system for hydraulic structures that is able to provide information for evaluating structural integrity, durability and reliability throughout the plant's life cycle is the most critical activity of any maintenance team to ensure optimal maintenance planning and timely intervention.

9. REFERENCES

[1] Chen S. Hydraulic Structures, First edit. London: Springer; 2015
[2] P.Novak, A.I.B. Moffat , C.Nalluri and R.Narayana : Hydraulic Structures 4th Edition; 2007
[3] Fichtner & Norplan. Tender Design Report for Isimba, 2012
[4] FIDIC., Conditions of Contract for Plant and Design –Build Contract 1999
[5] Ficken. B. W. 2006. Legal Consideration and Dispute Resolution
[6] Obiora, C.O., Ezeokoli, F.O., Belonwu, C.C. & Okeke, F.N. 2022. Defects in Concrete Elements: A Study of Residential Buildings of 30 Years and above in Onitsha Metropolis
[7] Aggelis, D. & Shiotani, 2007. Repair evaluation of concrete cracks
[8] M Alexander, M Otieno 2022. Final report on concrete durability assessment at the Isimba hydro power plant, based on extracted concrete cores
[9] Kurt F. von Fay et al, 2015. Guide to concrete repair second Edition, US Bureau of Reclamation
[10] Sika Services, 2019. "Sika Solutions for dams and hydropower plants". https://www.sika.com/ content /dam/dms/corporate/2/glo-sika-solutions-dams-hydropower-plants.pdf

YCRETS 2023
YOUNG CONCRETE RESEARCHERS, ENGINEERS & TECHNOLOGISTS SYMPOSIUM

CEMENT & CONCRETE SA

Review of monitoring methods for chloride-induced reinforcement corrosion on reinforced concrete bridges

Jaziitha Simon (1), Hans Beushausen (1) and Mike Otieno (2)

(1) University of Cape Town, Cape Town, South Africa

(2) University of the Witwatersrand, Johannesburg, South Africa

Abstract

Reinforcement corrosion is a serious durability problem that has been overlooked in the management of structures, as most Bridge Management Systems (BMS) primarily rely on visual inspection to determine the condition of bridges. The study aimed to identify monitoring methods for Reinforced Concrete (RC) bridges affected by chloride-induced reinforcement corrosion that can be included in the overall assessment jointly with visual inspections in the Struman BMS. The reviewed monitoring methods were categorised into visual inspections, Non-Destructive Testing (NDT), and remote monitoring. Monitoring technologies have the potential to allow for the early diagnosis of problems, resulting in better maintenance and damage prevention. They could also improve the speed and scope of condition assessments, offer reliable and comprehensive data, and eliminate traffic disruptions while taking measurements.

Keywords: chloride-induced reinforcement corrosion, Bridge Management System, Reinforced Concrete bridges, monitoring methods, condition assessment

1. INTRODUCTION

Reinforcement corrosion is a major cause of deterioration in Reinforced Concrete (RC) bridges, mainly caused by the ingress of chloride ions. This problem leads to a loss of structural capacity, concrete degradation, and increased maintenance costs. To manage and optimize allocated financial resources for bridge maintenance, repair, and rehabilitation, Bridge Management Systems (BMS) have been developed and implemented in different countries [1]. However, visual inspection remains the predominant method used in BMS to assess and monitor the condition of structures, despite the serious impact of corrosion.

2. CURRENT CORROSION MONITORING IN SOUTH AFRICA

The Struman BMS is commonly used in Southern African Development Community (SADC) countries. It was developed in South Africa to manage the maintenance of deteriorating bridges with limited budgets. The system uses visual inspections to rate defects on a scale of 1 to 4, based on their Degree, Extent, Relevance, and Urgency (DERU) [2]. The DERU rating data is used to prioritize bridges for repair and maintenance, and assessments are done every

five years. However, there is a need for the use of appropriate monitoring systems, particularly for reinforcement corrosion, which is a significant cause of deterioration in RC structures.

3. MONITORING OF REINFORCEMENT CORROSION

Chloride-induced reinforcement corrosion happens in three stages namely: initiation, propagation, and acceleration. Detecting corrosion at early stages through monitoring methods is important to prevent severe damage and reduce repair costs. Research on technologies for the early detection of corrosion has been increasing since the 1990s, with most publications on corrosion monitoring published in the last decade. The review focused on visual inspection, Non-Destructive Testing (NDT), and remote corrosion monitoring methods to evaluate reinforcement corrosion damage in RC structures, particularly bridges.

3.1 Visual Inspection

Visual inspection is a common and cost-effective method to identify corrosion on RC bridges, but it has limitations when it comes to assessing reinforcement corrosion. This is because defects only manifest on the surface of concrete when significant damage has already occurred. Visual inspections do not quantify the damage or identify the effect, making it difficult to establish effective maintenance practices to prevent advanced corrosion damage. Additionally, visual inspections are subjective, relying on the experience and judgement of the inspector [3]. While visual inspections still provide useful information about the condition of bridges, they need to be complemented by other methods to address their shortcomings.

3.2 Non-destructive Corrosion Monitoring

NDT methods assess the degree, extent, and severity of deterioration in a structure without affecting its integrity. Several types of NDT methods include electrochemical, elastic wave, electromagnetic, and thermal methods.

3.2.1 Electrochemical methods

Electrochemical methods measure parameters such as corrosion potential, concrete resistivity, and polarization resistance. These parameters can be measured periodically using surface electrodes or sensors or continuously using embedded sensors. By monitoring these parameters, the extent and severity of corrosion can be assessed, and appropriate interventions can be taken to prevent further damage.

Half-Cell Potential (HCP) measurement involves measuring the potential difference between two half-cells, usually a metal in its solution, and an external Reference Electrode (RE). HCP measurements are done using surface or embedded REs, and new methods involving climbing robots and flying drones have also been developed [4]. HCP measurements can identify high corrosion risk before visible damage appears on the surface of the structure, allowing for appropriate interventions to be taken at the right time. However, HCP measurements are affected by factors, such as the availability of oxygen, cover depth, and the composition of the pore solution, which should be considered during interpretation [4].

Electrical Resistivity (ER) affects the flow of ions and the rate of corrosion in the concrete. ER measurements have been used to indirectly assess the quality of the concrete, chloride ion

diffusion and degree of saturation. The Wenner Four probe is the most used device for measuring ER [5]. ER measurements can identify high corrosion risk areas but must be used in conjunction with other parameters such as HCP. However, ER measurements are influenced by various factors such as moisture content, temperature, concrete composition, curing conditions, cover depth, and probe contact during testing [4, 6]. Even though this method is fast, non-intrusive, and does not require connection to embedded steel, it does not indicate whether corrosion has occurred or to what extent active corrosion has occurred.

Linear Polarization Resistance (LPR) is a technique used to measure the corrosion rate of steel by monitoring corrosion activity over time. It works by correlating the HCP of corroding steel to the externally applied current. New technologies such as Gecor 8^{TM} and CorroMap simplify the measurement process by automatically evaluating and displaying data [7, 8]. These technologies are considered non-intrusive as they only require a connection to the reinforcement without damaging the structure. The Giatec iCOR is a wireless device that can measure corrosion rate, corrosion potential, and electrical resistivity without needing a connection to the steel in concrete [9]. Using one device for all three parameters saves time and reduces costs. This device also allows easy reporting, exporting, and sharing of results, enabling fast and efficient condition assessment. However, temperature, concrete resistivity, and relative humidity can affect the accuracy of measurements and should be considered.

3.2.2 Elastic wave methods

Elastic wave methods are used to estimate the mechanical properties and heterogeneous characteristics of concrete. They can detect damages caused by reinforcement corrosion, such as internal cracks, voids, delamination, and corrosion products. Examples of these methods include Impact Echo (IE), Ultrasonic Pulse Velocity (UPV), and Acoustic Emission (AE).

The IE method is based on the propagation and reflection of elastic waves in concrete. It works by inducing a low-frequency stress wave using a mechanical impact into the concrete, which reflects off internal cracks, voids, or changes in material characteristics. The resulting displacement-time curves are analysed in the frequency domain to detect anomalies. IE has been used in several studies to detect flaws such as internal cracks, voids, and delamination, as well as to determine the thickness of concrete elements and measure crack depth [10, 11].

The UPV method measures the propagation time of an ultrasonic pulse through concrete to determine its properties and detect internal flaws such as cracks, voids, and delamination caused by reinforcement corrosion [12]. Laboratory-based studies have attempted to relate UPV measurements to reinforcement corrosion. Amplitude attenuations correlate well with corrosion damages, while internal cracking results in wave attenuations and a decrease in UPV. UPV measured by the first wave peak describes the reinforcement corrosion process from the formation of corrosion products to the visibility of corrosion damage indicators on the concrete surface [13]. Even though UPV is less reliable in detecting shallow defects, it can estimate concrete strength, determine member thickness, and measure crack depth. Its results are influenced by pulse attenuation, concrete composition, and aggregate sizes.

The AE method is a technique that detects elastic waves generated from localised sources in concrete, such as internal crack growth and corrosion product generation [5]. The emitted elastic waves are detected using AE sensors. Detecting active cracks at an early stage makes it

suitable for long-term monitoring. AE analysis can also identify different stages of corrosion, including corrosion onset and nucleation of corrosion-induced cracking [13, 14]. However, there are currently no critical standards for its procedures, installation, or interpretation of results in terms of corrosion, and it has mainly been used in laboratory settings.

3.2.3 Electromagnetic methods

The cover meter and Ground-Penetrating Radar (GPR) are electromagnetic methods used to locate reinforcement and cover thickness. They are used to mark out the measurement grid which is essential to other monitoring methods such as ER, HCP, and LPR. Cover meters have been used for cover measurements because they are portable, lightweight, and easy to use. They are also established and standardised. The ACI 357 specifies a minimal cover of at least 50 mm for RC members subjected to seawater, which applies to submerged and atmospheric-exposed structural elements. SANS 10100-2, however, recommends a cover of 65 mm for members in contact with seawater [15].

GPR works by emitting and receiving high-frequency electromagnetic waves that can penetrate concrete and reflect when they encounter changes in material properties. GPR is also used to detect other subsurface features, such as voids and delamination, which can provide additional information about the condition of the structure [16]. This method is usually preferred because it can cover large areas of measurement in a short time. However, it can only be used on horizontal structural elements such as decks and slabs. Its use in corrosion evaluation is still in progress. GPR was found useful in providing bridge condition ratings in the BMS [16]. It can detect early reinforcement corrosion during the propagation period; larger wave transit times and lower amplitude zones were associated with increased chloride content and the presence of corrosion products [17, 18]. The GPR signal can thus be associated with changes within the concrete during the corrosion process, particularly from the formation of corrosion products to internal crack formation and propagation.

3.2.4 Thermal methods

Infrared Thermography (IRT) is a method used to detect radiation emitted from materials, including concrete. IRT can be passive or active. Passive IRT is commonly used, where specimens are artificially heated before testing to induce temperature differences. Defects disrupt heat transfer, causing localised differences in surface temperature [19]. IRT is preferred for bridge inspection and evaluation due to its high speed, reliability, accuracy, and cost-effectiveness [20]. It can detect sub-surface defects without requiring direct access to the element being inspected, which eliminates the need for traffic disruption and lane closures. Its application in detecting early reinforcement corrosion is still in the development stage. IRT has been used to detect reinforcement corrosion and delamination in RC bridges, but surface-related and environmental factors can affect the test results [16, 21].

3.3 Remote Monitoring

Remote monitoring systems for bridges use sensors connected to a data acquisition system and can be installed in new or existing structures. They are particularly useful for bridges that are difficult to access for regular inspections. These systems provide data that can help with planning and implementing required interventions to prevent premature deterioration. Six

different remote monitoring systems are discussed, including their application, principle, and parameters measured, as shown in Table 1.

Table 1: Summarized comparison of the remote monitoring systems

System characteristics	ALS*	ERS*	MRE*	CW*	CR*	ISE* sensors
Application						
Used in new structures	X	-	X	X	-	-
Used in existing structures	-	X	X	-	X	X
Principle						
Anodes placed at various depths in the	X	X	X	X	X	-
HCP technique (measurement of anode vs cathode)	X	X	-	X	-	X
Measured corrosion parameters						
Potential voltage (V)	X	X	-	X	X	X
Electrical current (μA)	X	X	-	X	X	-
Concrete resistance (kΩ)	X	X	X	-	-	-
Temperature (◦C)	X	X	-	-	-	-
Moisture content	-	-	X	-	-	-
Chloride concentrations	-	-	-	-	-	X

*ALS – Anode Ladder System ERS – Expansion Ring System
MRE – Multi-ring Electrode CW – CorroWatch
CR – CorroRisk ISE sensors –Ion Selective Electrode sensor

3.3.1 Time to corrosion monitoring systems

Time to corrosion monitoring systems measures the time to corrosion initiation by monitoring the ingress of aggressive agents, such as chlorides. These systems use a macrocell reinforcement corrosion approach and involve the measurement of current flow between separate anode and cathode areas [22]. Several anodes are placed at different depths within the concrete cover to determine the time to corrosion initiation continuously. The anodes are the same composition as the reinforcing steel to ensure they corrode at the same time. The onset of corrosion of the anodes is determined at any time, provided the cover to reinforcement is known. The depassivation of the anodes is related to an increase in electrical current and a decrease in potential using the specified thresholds [23]. Four methods (Anode-Ladder System, Expansion-Ring System, CorroWatch, and CorroRisk) use this principle.

The Anode-Ladder System (ALS) is used for long-term chloride-induced corrosion monitoring, typically embedded in new RC structures between the reinforcement cage and the concrete surface. The ALS determines the critical depth of chloride content when the six steel anodes that form up the anode ladder depassivates sequentially. The system has been used successfully in various countries to monitor corrosion in new structures [24, 25] The ALS is durable and typically designed for a service life of more than 100 years [23]. However, it

cannot be used in submerged structures because it needs to be installed near the concrete surface where sufficient oxygen is available.

The Expansion Ring System (ERS) developed by Sensortec [26] is used in existing structures before corrosion initiation. In structures where the propagation period has begun (when the critical depth of chloride content is reached), the corrosion potential and resistance indicate corrosion risk. The ERS comprises an expansion-ring anode (with six circular steel anodes), a titanium oxide cathode bar and a temperature sensor drilled into the concrete. This system has been tested in the laboratory and on-site, and it was found unsuitable for submerged elements [27].

CorroWatch (CW) and Corrorisk (CR) sensors were developed by Force Technology to provide early warning on corrosion initiation in RC structures. CW sensors are used in new structures, while CR sensors are installed in existing structures that are exposed to aggressive environments or are inaccessible for inspection. Measurements of potential and current in these systems are carried out continuously using a remote monitoring modem or automatic data logger attached to the system. Though these systems have been used in some projects [28], their research is very limited.

3.3.2 Moisture content monitoring systems

Monitoring moisture content in concrete is important for controlling reinforcement corrosion, as a significant drop in electrical resistivity indicates the vulnerability of the concrete to corrosion. The Multi-Ring Electrode (MRE) system is a new technology that can be used to monitor moisture content, and it measures electrical resistance and provides a profile across the sensor depth. The resistivity readings are converted to moisture profiles using concrete-specific calibrated curves [29, 30]. This technology is installed before concrete placement in new structures and drilled and anchored with mortar in existing structures. The sensors need to be connected to a measuring device which records data automatically. Moisture content governs the initiation and progression of reinforcement corrosion, and reducing it to below 40% can stifle corrosion. The MRE is beneficial because it provides electrical resistance measurements in case NDT methods are not used.

3.3.3 Chloride content monitoring systems

New non-destructive methods have been developed to continuously monitor chloride concentration in concrete. One of these methods is using potentiometric sensors or Ion Selective Electrodes (ISE), which can determine free chlorides in RC. The system consists of an ISE sensor and a reference electrode that measures the change in potential between the two, allowing for the estimation of chloride activities and subsequently, the determination of chloride concentration using the chloride activity coefficient. This method can be used in existing structures, especially in inaccessible areas. The ISE sensors are commercially available and have been used in various studies to detect chlorides non-destructively in concrete [27, 31]. They have also been tested in laboratories, in which they were found to successfully measure chloride activity [32]. Some of the sensors include but are not limited to Ag/AgCl-ISE and the ERE 20 reference electrodes.

4. CONCLUSIONS, REMARKS AND FUTURE TRENDS

Reinforcement corrosion poses a significant challenge to the durability of RC structures, often going unnoticed in visual inspections and leading to costly repairs. To address this issue, monitoring technologies are needed to detect corrosion damage throughout the lifespan of RC bridges and enable proactive maintenance. The Struman BMS currently relies mainly on visual inspection, but it needs to incorporate corrosion monitoring methods to detect damage earlier. While progress has been made in developing NDT and remote monitoring methods, further refinement is necessary to effectively incorporate them into the BMS for condition assessments. By incorporating various monitoring methods, including cover depth and chloride measurements, HCP measurement, LPR, and other corrosion onset sensors, the Struman BMS can provide a comprehensive condition assessment, reduce maintenance and repair costs, and improve the speed and scope of condition assessment. It is recommended to use multiple monitoring methods in conjunction to effectively detect and quantify relevant defects in reinforcement corrosion damage.

REFERENCES

[1] J. X. Yan, "A Survey of the State of Bridge Management in Canada," Concordia University, 2008.

[2] T. Mbanjwa, "An Investigation of the Relationships between Inventory and Inspection Data of RC Bridges and RC Culverts in the Western Cape Province.," The University of Cape Town, South Africa, 2014.

[3] H. W. Song and V. Saraswathy, "Corrosion monitoring of reinforced concrete structures - A review," *Int. J. Electrochem. Sci.*, vol. 2, no. 1, pp. 1–28, 2007.

[4] R. Rodrigues, S. Gaboreau, J. Gance, I. Ignatiadis, and S. Betelu, "Reinforced concrete structures: A review of corrosion mechanisms and advances in electrical methods for corrosion monitoring," *Constr. Build. Mater.*, vol. 269, no. 121240, p. 121240, Feb. 2021.

[5] D. Luo, Y. Li, J. Li, K. S. Lim, N. A. M. Nazal, and H. Ahmad, "A recent progress of steel bar corrosion diagnostic techniques in RC structures," *Sensors (Switzerland)*, vol. 19, no. 34, pp. 1–30, 2019.

[6] M. Daniyal and S. Akhtar, "Corrosion assessment and control techniques for reinforced concrete structures: a review," *J. Build. Pathol. Rehabil.*, vol. 5, no. 1, pp. 1–20, 2020.

[7] NDT James Instruments Inc., "Gecor 8™ - Corrosion analysis equipment," 2021. https://www.ndtjames.com/Gecor_8_p/c-cs-8.htm (accessed Oct. 15, 2021).

[8] P. Bucan, "Catalogue for products related to corrosion monitoring in concrete.," *FORCE Technology*, 2004. https://forcetechnology.com/en/services/probes-and-measuring-equipment-for-corrosion-monitoring-of-steel-reinforcement.

[9] Giatec Scientific Inc., "iCOR® - Wireless NDT corrosion detection," 2021. https://www.giatecscientific.com/products/concrete-ndt-devices/icor-rebar-corrosion-rate/ (accessed Oct. 17, 2021).

[10] S. Lee, N. Kalos, and D. H. Shin, "Non-destructive testing methods in the U.S. for bridge inspection and maintenance," *KSCE J. Civ. Eng.*, vol. 18, no. 5, pp. 1322–1331, 2014.

[11] S. Lee and N. Kalos, "Bridge inspection practices using non-destructive testing methods," *J. Civ. Eng. Manag.*, vol. 21, no. 5, pp. 654–665, 2015.

[12] Y. Ballin, H. Beushausen, M. Alexander, and R. Amtsbuchler, *Fulton's Concrete Technology*, Ninth Edit. Midrand, South Africa: Cement and Concrete Institute, 2009.

[13] D. Li, S. Zhang, W. Yang, and W. Zhang, “Corrosion monitoring and evaluation of reinforced concrete structures utilizing the ultrasonic guided wave technique,” *Int. J. Distrib. Sens. Networks*, no. 827130, pp. 1–9, 2014.
[14] Y. Kawasaki, T. Wakuda, T. Kobarai, and M. Ohtsu, “Corrosion mechanisms in reinforced concrete by acoustic emission,” *Constr. Build. Mater.*, vol. 48, pp. 1240–1247, 2013.
[15] H. Macdonald, *Marine Concrete Structures – Design, Durability and Performance*, vol. 2017, no. v25i2. Cambridge: Woodhead Publishing, 2016.
[16] S. A. Dabous, S. Yaghi, S. Alkass, and O. Moselhi, “Concrete bridge deck condition assessment using IR Thermography and Ground Penetrating Radar technologies,” *Autom. Constr.*, vol. 81, pp. 340–354, 2017.
[17] A. Zaki, M. A. M. Johari, W. M. A. W. Hussin, and Y. Jusman, “Experimental Assessment of Rebar Corrosion in Concrete Slab Using Ground Penetrating Radar (GPR),” *Int. J. Corros.*, no. 5389829, pp. 1–11, 2018.
[18] M. Solla, S. Lagüela, N. Fernández, and I. Garrido, “Assessing rebar corrosion through the combination of nondestructive GPR and IRT methodologies,” *Remote Sens.*, vol. 11, no. 14, 2019.
[19] T. Omar and M. L. Nehdi, “Remote sensing of concrete bridge decks using unmanned aerial vehicle infrared thermography,” *Autom. Constr.*, vol. 83, pp. 360–371, 2017.
[20] T. Omar and M. L. Nehdi, “Condition assessment of reinforced concrete bridges: Current practice and research challenges,” *Infrastructures*, vol. 3, no. 3, pp. 1–23, 2018.
[21] S. Baek, W. Xue, M. Q. Feng, and S. Kwon, “Nondestructive Corrosion Detection in RC Through Integrated Heat Induction and IR Thermography,” *J. Non-destructive Eval.*, vol. 31, pp. 181–190, 2012.
[22] M. Raupach and P. Schießl, “Macrocell sensor systems for monitoring of the corrosion risk of the reinforcement in concrete structures,” *NDT E Int.*, vol. 34, no. 6, pp. 435–442, 2001.
[23] SENSORTEC GmbH, “Specification of the Anode Ladder Corrosion Sensor,” Munich, Germany, 2009.
[24] M. Raupach, “Corrosion monitoring using a new sensor for installation into existing structures,” in *Durability of Building Materials and Components 8*, M. A. Lacasse and D. J. Vanier, Eds. Ottawa ON, KIA 0R6, Canada: National Research Council Canada, 1999, pp. 365–375.
[25] J. Harnisch, C. Dauberschmidt, G. Ebell, and T. F. Mayer, “The new DGZfP Specification B12 " Corrosion Monitoring of Reinforced Concrete Structures "," in *SMAR 2019 - Fifth Conference on Smart Monitoring Assessment and Rehabilitation of Civil Structures*, 2019, pp. 1–8.
[26] SENSORTEC GmbH, “Corrosion Sensor: Expansion Ring Anode,” 2013.
[27] G. Per, “Integrated Monitoring Systems for Durability Assessment of Concrete Structures,” Denmark, 2002.
[28] C. Y. Gong *et al.*, “Long-term field corrosion monitoring in supporting structures of China Xiamen Xiangan Subsea Tunnel,” *Acta Metall. Sin. (Engl Lett)*, vol. 30, no. 4, pp. 399–408, 2017.
[29] T. F. Mayer, C. Gehlen, and C. Dauberschmidt, “Corrosion monitoring in concrete,” in *Techniques for Corrosion Monitoring*, Second Edi., L. Yang, Ed. Munich, Germany: Elsevier Ltd., 2021, pp. 380–405.
[30] Sensortec GmbH, “Moisture Sensor - Multiring Electrode (MRE),” Munich, Germany, 2013.
[31] R. Bäßler, J. Mietz, M. Raupach, and O. Klinghoffer, “Corrosion Risk and Humidity Sensors for Durability Assessment of Reinforced Concrete Structures,” in *SPIE*, 2000, no. August, pp. 1–11.
[32] U. Angst, B. Elsener, C. K. Larsen, and Ø. Vennesland, “Potentiometric determination of the chloride ion activity in cement based materials,” *J. Appl. Electrochem.*, vol. 40, no. 3, pp. 561–573, 2010.

YCRETS 2023
YOUNG CONCRETE RESEARCHERS, ENGINEERS & TECHNOLOGISTS SYMPOSIUM
CEMENT & CONCRETE SA

A structural reliability-based approach to prestressed concrete design

Zander Snel (1), Nico P.J. de Koker (1) and Celeste Viljoen (1)

(1) Department of Civil Engineering, Stellenbosch University

Abstract

The design of a prestress configuration for flexure is governed by the serviceability limit state of cracking. Structural design standards provide guidelines for design of prestressed concrete by specification of allowable stresses and a set of partial factors applicable for the different limit states considered. The calibration of partial factors for a target reliability level is generally only performed for the ultimate limit state, whereas all partial factors for the verification of the serviceability limit state are set equal to unity in the Eurocode suite of design standards. This study demonstrates that these partial factors are not reliability-based which results in sub-optimal reliability performance. The reliability performance of these factors is contrasted against the reliability performance of a set of partial factors for SLS design of prestressed concrete elements calibrated using the design value method described by the Eurocodes in EN 1990:2002. The developed set of partial factors presents an improvement of the current state of the art with the potential for optimised durability of designs.

Keywords: Prestressed concrete, Serviceability limit state, Structural reliability, Durability

1. INTRODUCTION

Modern design standards are based on the limit states design philosophy which is frequently calibrated using the theory of structural reliability. These standards provide a procedure for design of prestressed concrete elements by specification of allowable stresses and a set of partial factors applicable for the different limit states considered. The allowable stress limits are to be satisfied at transfer of prestress force and during service. For an appropriately scaled cross section, these allowable stresses can be written as four stress inequalities which delimit a domain of feasible prestress configurations expressed graphically as a Magnel diagram [1].

Partial factors are calibrated based on the associated statistical characteristics of the different loading and resistance parameters for a specified target reliability level. The calibration of partial factors for a target reliability level is generally only performed for the ultimate limit state, whereas all partial factors for verification of the serviceability limit state are set equal to unity in the Eurocode suite of design standards [2]. Variable uncertainty is, therefore, addressed only by the specified characteristic values and may result in a greater

tolerable probability of failure in design than is specified by the target reliability level. This specification is especially a concern when structural design is governed by the serviceability limit state, as for prestressed concrete design, as it may lead to unsatisfactory structural performance.

In this paper the reliability performance of the prestressed concrete serviceability limit state design procedure of the Eurocodes[3] and a set of partial factors calibrated using the design value method (DVM) are contrasted. A single span concrete girder bridge with composite prestress concrete sections is assumed as the reference structure. An analysis model is developed to evaluate the reliability along the boundaries of the Magnel diagram.

2. FUNDAMENTAL STRUCTURAL RELIABILITY BACKGROUND

Structural reliability concerns the probabilistic measure of structural safety. To ensure safety in design, a margin of safety is provided which is quantified by means of a performance function. The performance function for the SLS is defined as $g(\boldsymbol{x}, \boldsymbol{a}) = L - E$ where $\boldsymbol{x}$ and $\boldsymbol{a}$ are vectors of random variables and deterministic parameters respectively [4] and L and E are the limiting design value and load effects respectively. The reliability of a structure is expressed probabilistically in terms of a probability of failure which denotes the probability of $g(\boldsymbol{x}, \boldsymbol{a}) < 0$. When multiple limit states are significant in determining the probability of failure (as for prestressed concrete) the probability of failure is determined as the probability of violation of the union of the limit states ($\bigcup_i g_i(\boldsymbol{x}, \boldsymbol{a}) < 0$). The probability of failure is then determined as,

$$p_f = p\left(\bigcup_i g_i(\boldsymbol{x}, \boldsymbol{a}) < 0\right) = \int_{\bigcup_i g_i(\boldsymbol{x},\boldsymbol{a})<0} f_{\boldsymbol{X}}(\boldsymbol{x}) d\boldsymbol{x} \tag{1}$$

where $f_{\boldsymbol{X}}(\boldsymbol{x})$ is the multivariate probability density of $\boldsymbol{X}$ [4]. The probability of failure is frequently rewritten as an associated reliability index $\beta = -\Phi^{-1}(p_f)$. The exact closed-form solution of Eq 1 is rarely achievable. In this study Eq 1 is integrated by employing the Monte Carlo method. This method generates sampling sets of each of the random variables based on their associated distributions. Using these sampling sets, many realisations of the performance function are determined from which the number of failures are counted to determine the probability of failure.

3. PROBABILISTIC ANALYSIS MODEL

To evaluate the reliability performance of the SLS design procedure a probabilistic analysis model is developed.

3.1 Reference Structure

The reference structure selected for the analysis model is a 3-meter-wide single span, simply supported concrete girder bridge. The bridge has a span length of 20 meters and is comprised of three equally spaced precast beams with a cast in situ deck forming composite

prestressed concrete sections. The precast beam profiles are based on the geometry of standardised AASHTO I-beam profiles[5]. The geometry to be considered at transfer and service stresses for the generation of the Magnel diagram is provided in Figure 1.

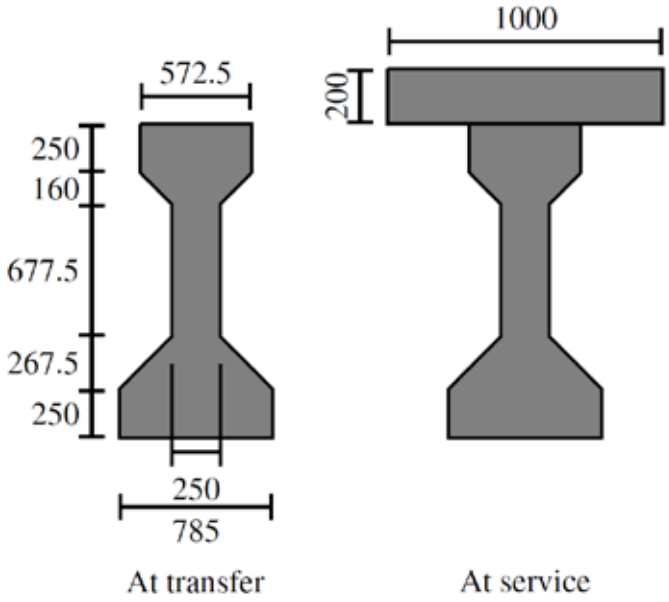

Figure 1: Cross section used in the study (units in mm)

The reference structure is to be designed for traffic loading in accordance with Load Model 1 (LM1) specified in EN 1991-2:2003[6]. Accounting for transverse load distribution, the worst case characteristic applied midspan bending moment per beam for the 20m span length is 2959 kN.m. A C50/60 concrete class described in EN 1992-1-1:2004 [3] is adopted for which the characteristic compressive strength at a 7-day concrete age at transfer is 40.94 MPa. The stress limits at transfer and service as described in EN 1992-1-1:2004 [3] are used. To determine the load effects owing to self-weight of the composite section, the nominal density of concrete is assumed equal to 24 kN/m^3. Further, it is assumed that the precast sections are post-tensioned and the total time-dependent prestress losses are 25% of prestress force at transfer.

3.2 Reliability Verification

The reliability performance of prestressed concrete can be evaluated by the definition of four performance functions based on the four stress inequalities to be satisfied. These performance functions are,

$$g_1(\boldsymbol{x}, \boldsymbol{a}) = \sigma_{t,t} - \left[\frac{P_t}{A_b} + \frac{P_t e}{Z_{top,b}} + \frac{\theta_{E,M} M_b}{Z_{top,b}}\right] \tag{2}$$

$$g_2(\boldsymbol{x}, \boldsymbol{a}) = \left[\frac{P_t}{A_b} + \frac{P_t e}{Z_{bot,b}} + \frac{\theta_{E,M} M_b}{Z_{bot,b}}\right] - \sigma_{c,t} \tag{3}$$

$$g_3(\boldsymbol{x},\boldsymbol{a}) = \left[\frac{\eta P_t}{A_b} + \frac{\eta P_t e}{Z_{top,b}} + \frac{\theta_{E,M}M_b + \theta_{E,M}M_F}{Z_{top,b}} + \frac{\theta_{E,M}M_L}{Z_{top,cb}}\right] - \sigma_{c,s} \quad (4)$$

$$g_4(\boldsymbol{x},\boldsymbol{a}) = \sigma_{t,s} - \left[\frac{\eta P_t}{A_b} + \frac{\eta P_t e}{Z_{bot,b}} + \frac{\theta_{E,M}M_b + \theta_{E,M}M_F}{Z_{bot,b}} + \frac{\theta_{E,M}M_L}{Z_{bot,cb}}\right] \quad (5)$$

In the above performance functions M_b, M_F and M_L are the moments generated by precast beam self-weight, cast in situ deck self-weight and traffic loading respectively. To integrate Eq 1 for a given prestress configuration, Monte Carlo simulations generating 5×10^7 trials of each of the four performance functions is performed. A trial is deemed to have failed if any of the performance functions are violated. The random variables defining the above performance functions are characterised by the probabilistic models and population parameters in Table 1.

Table 1: Probabilistic models of basic variables

Variable, X	Unit	Distribution	Mean, μ_x	CoV, δ_x	Reference
Self-weight	kN/m^3	Normal	24	0.04	[7]
Dimensions	mm	Normal	Varies	0.03	[8]
Initial compressive strength, $f_{cm,i}$	MPa	Log-normal	58.08	0.18	[9]
Ultimate compressive strength, $f_{cm,u}$	MPa	Log-normal	70.94	0.18	[9]
Concrete tensile strength, f_{ct}	-	Log-normal	$1.05f_{ctm}$	0.15	[10]
Prestress loss, ΔP_t	-	Normal	$0.25P_t$	0.3	[11]
Prestress force, P_t	kN	Normal	Varied	0.015	[12]
Maxima traffic load effect (50-y), M_L	kN.m	Gumbel	2655	0.061	[8]
Eccentricity, e	mm	Normal	Varied	0.015	[12]
Moment Model Uncertainty, $\theta_{E,M}$	-	Log-normal	1.0	0.1	[11]
Length, L	m	-	-	-	-

4. PARTIAL FACTOR CALIBRATION

The *fib* Model Code 2010 [13] and EN 1990:2002 [2] detail an approach for developing partial factors known as the design value method (DVM). This method is frequently used for determining partial factors for the ultimate limit state. To enable the use of the design value method to determine partial factors for SLS, a significant assumption is made that the sensitivity factors as developed by König and Hosser [14] are applicable for the serviceability limit state. These sensitivity factors assume the resistance (or limiting design value for the case of SLS) and load effect terms to have comparable coefficients of variation which may not necessarily be the case for SLS prestressed concrete design.

The target reliability for irreversible serviceability is specified in EN 1990:2002 [2] as $\beta_{t,SLS} = 1.5$ for a 50-year reference period. Making use of the design value method, the partial factors for SLS design of prestressed concrete structures are evaluated for a target reliability index of 1.5. These calculations are not detailed in this paper but are based on the equations provided in the *fib* Model Code 2010 [13]. This provides a set of partials factors aimed at satisfying the target reliability as a minimum. This set of partial factors is provided in Table 2.

Table 2: Partial factors for irreversible SLS target reliability (rounded off conservatively)

Variable	Partial Factor	Value
Concrete compressive strength	γ_c	0.92≈0.95
Concrete tensile strength	γ_{ct}	1.14≈1.15
Prestress force	γ_p	Favourable: 0.99≈1.0 Unfavourable: 1.01≈1.0
Prestress loss	γ_{pl}	Favourable: 0.85 Unfavourable: 1.13≈1.15
Permanent actions	γ_g	Favourable: 0.98 Unfavourable: 1.03
Model uncertainty	γ_{Ed}	Favourable: 0.95 Unfavourable: 1.05
$\gamma_G = \gamma_{Ed} \times \gamma_g$	γ_G	Favourable: 0.93≈0.9 Unfavourable: 1.08≈1.1
Variable actions	γ_q	0.95
$\gamma_Q = \gamma_{Ed} \times \gamma_q$	γ_Q	0.99≈1.0

5. RESULTS

Based on the loading and resistance parameters of the reference structure, the Magnel diagram delimiting the feasibility domain is generated. Dividing the feasibility domain into a grid of points and evaluating the reliability index at each point provides an indication of the performance of the design method. The lowest reliability indices are achieved at the boundaries of the Magnel diagram's feasibility domain with increasing reliability as distance from the boundaries increases. For the composite beam configuration used, only three of the four limit states (and their associated Magnel diagram equations) have significance in defining the feasibility domain for the relevant range of eccentricities. These boundaries are the compressive and tensile stress limit states at transfer, which together forms the Magnel diagram boundary with the lowest absolute value of $1/p_t$, and tensile stress limit state at service, which forms the Magnel diagram boundary with greatest absolute value of $1/p_t$. The figures below detail the reliability achieved along the boundaries of the Magnel diagram.

Figure 2(a) demonstrates the reliability performance of the design procedure specified in the Eurocodes. Use of partial factors equal to 1.0 for all the variables defining the limiting design value and action effect with the resistance factors, r_{sup} and r_{inf}, results in inconsistent and unsatisfactory reliability performance. The boundaries formed by the tensile stress limit states at transfer and service yields reliability performance below the target, $\beta_{t,sls} = 1.5$. Figure 2(a) also shows a diminishing reliability performance of the tensile stress limit state at transfer boundary as the eccentricity decreases. In contrast the boundary formed by the compressive stress limit state at transfer provides a reliability performance which significantly exceeds the target.

Figure 2(b) demonstrates the reliability performance when using the partial factors calibrated using the design value method. The use of these factors significantly improves the control of achieved reliability along the boundaries of the Magnel diagram when compared to

the results when using the Eurocode prescribed factors. The boundaries formed by the compressive stress limit state at transfer and tensile stress limit state at service yield similar reliability performance, $\beta \approx 1.6$, which satisfies the target. However, the reliability achieved by the boundary formed by the tensile stress limit state at transfer fails to achieve the target reliability and also demonstrates a reduction in calculated reliability as the eccentricity decreases.

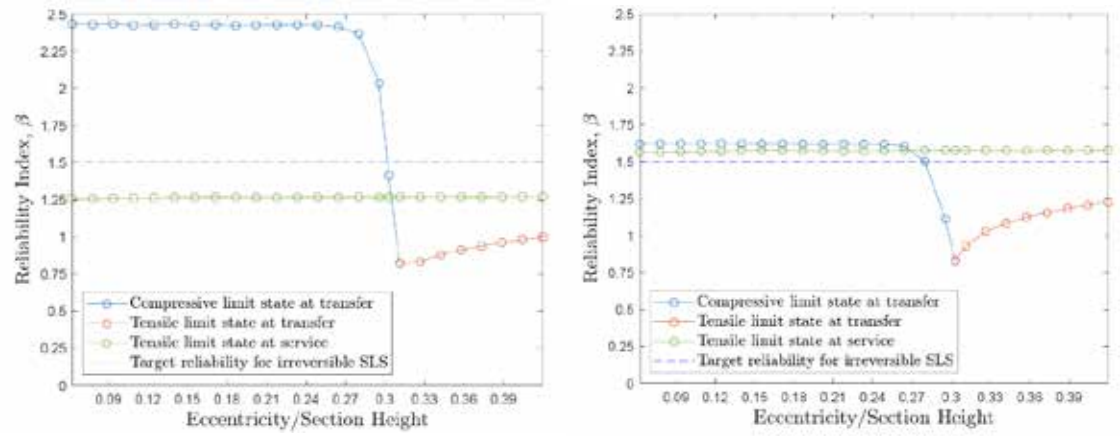

(a) Eurocode Factors (b) DVM partial factors

Figure 2: Reliability performance of Magnel diagram boundaries

6. DISCUSSION

The significance of the tensile stress limit state at transfer attaining a reliability level lower than the target depends on the interpretation of the reference period of 50-years associated with the target reliability. It could be argued that transfer is an instantaneous event and as a result it should be associated with a lower target reliability. However, this study makes the case that the random variables defining the limit states at transfer are not time-dependant and therefore specifying the same target reliability for transfer and service is appropriate.

When using the developed set of partial factors, the failure to meet the reliability level of the tensile stress limit state at transfer indicates that this limit state is sensitive to variations of some of the random variables which are not captured by the partial factors. Further, it is clear that as eccentricity decreases the reliability achieved at the boundary reduces which shows that the sensitivity to these random variables increases with a decrease in eccentricity. This phenomenon is explored by determining the direction cosines, or sensitivity factors, of the design point which describe the sensitivity of the reliability index to the variations of the different random variables. It is found that the tensile stress limit state at transfer is highly sensitivity to geometric variations. This can be acknowledged by the introduction of a factor accounting for geometric uncertainties γ_{Rd2} in determining the partial factor for concrete tensile strength. Caspeele *et al*. [8] provides a value of $\gamma_{Rd2} = 1.10$ for concrete geometry in line with the JCSS Probabilistic Model Code [11]. The partial factor for concrete tensile strength is then determined as $\gamma_{Ct} = \gamma_{Rd} \times \gamma_{ct}$ where the model uncertainty factor for

material properties is $\gamma_{Rd} = \gamma_{Rd1} \times \gamma_{Rd2} = 1.10$. For a target reliability index for the irreversible serviceability limit state of $\beta_t = 1.5$, $\gamma_{Ct} = 1.10 \times 1.14 \approx 1.25$. Using the partial factors provided in Table 2 and γ_{Ct}, the reliability performance of the Magnel diagram boundaries is determined and plotted for the range of eccentricities as shown in Figure 3.

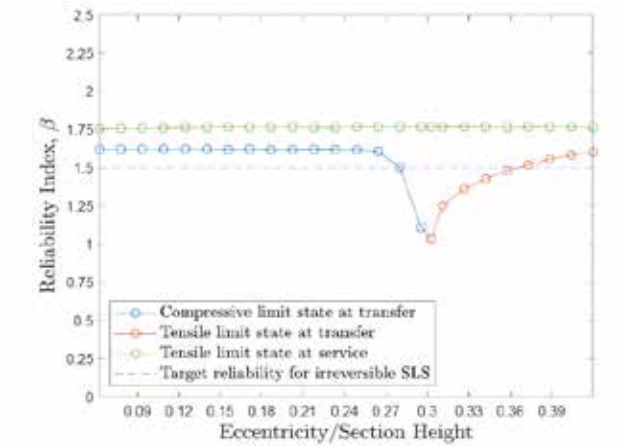

Figure 3: Reliability performance of Magnel Diagram boundaries for DVM partial factors with updated partial factor for concrete tensile strength

Figure 3 illustrates that use of the partial factor γ_{Ct} leads to a significant improvement of the reliability performance of the boundary of the Magnel diagram enforced by the tensile stress limit state at transfer. At maximum practical eccentricity, the boundary of the Magnel diagram developed by the tensile stress limit state at transfer has satisfactory reliability performance. However, the reliability performance still decreases with a reduction in eccentricity due to the change in the balance of the limit state sensitivity to random variables, resulting in geometric deviations becoming more significant.

A characteristic of the reliability performance of the Magnel diagram demonstrated by Figures 2 and 3 is that there is a steep drop in the achieved reliability along the boundaries defined by the tensile and compressive stress limit state at transfer at eccentricities approaching the eccentricity at which the two boundaries intersect. This steep drop in achieved reliability can be explained by considering that the analysis model inspects a grid of points within the feasibility domain. At each grid point, a Monte Carlo analysis generates many trials with each trial being associated with a sampling set of the vector of random variables. The four limit states are evaluated for each trial and if one of the limit states fail, the trial is deemed to have failed. In this way the probability of failure demonstrates the union of the four failure modes. At prestress design configurations located on the feasibility domain close to where the two boundaries intersect (which includes those points on the boundaries nearing this point), two different failure mechanisms become significant and the likelihood that the Monte Carlo simulations fail by either exceeding the tensile or compressive stress limits increase. As a result, the total number of failures increases on the boundaries approaching these points leading to a greater failure probability and lower reliability index.

The reliability performance deficit of design configurations located on the Magnel diagram near where the Magnel diagram boundaries intersect is concerning. However, this deficit cannot be treated directly with the partial factor framework without significantly increasing the reliability achieved along the boundaries. Increasing the reliability achieved along the boundaries above the target is unfavourable as these target reliability indices have been derived to minimise the economic cost in general for a specific structural class. It is prudent to rather recommend that these locations along the boundaries of the Magnel diagram should be avoided and a design at the maximum practical eccentricity is to be selected.

7. CONCLUSIONS

The partial factors developed in this study using the design value method (DVM) provide a significant improvement on the current state of the art provided in the Eurocodes (EC). Comparing Figure 2(a) to Figure 3 shows enhanced reliability performance at the compressive stress limit state at transfer ($\beta_{EC} = 2.45$ vs $\beta_{DVM} = 1.6$), tensile stress limit state at transfer ($\beta_{EC} = 1.0$ vs $\beta_{DVM} = 1.6$) and tensile stress limit state at service ($\beta_{EC} = 1.25$ vs $\beta_{DVM} = 1.75$) with values closer to the target $\beta_{\mathrm{t,SLS}} = 1.5$.

REFERENCES

[1] A. E. Naaman, *Prestressed Concrete Analysis and Design: Fundamentals*, 3rd ed. Michigan: Techno Press 3000, 2012.

[2] CEN, *Eurocode - Basis of structural design*. Brussels: European Committee for Standardization, 2002.

[3] CEN, *Eurocode 2: Design of concrete structures - Part 1-1: General rules and rules for buildings*. Brussels: European Committee for Standardization, 2004.

[4] A. M. Hasofer and N. C. Lind, “Exact and invariant second-moment code format,” *J. Eng. Mech. Div.*, vol. 100, no. 1, pp. 111–121, 1974.

[5] AASHTO, *AASHTO LRFD Bridge Design Specifications*, 8th ed. 2017.

[6] CEN, *Eurocode 1: Actions on structures - Part 2: Traffic loads on bridges*. Brussels: European Committee for Standardization, 2003.

[7] JCSS, *Probabilistic Model Code Part 2- Load Models*. Joint Committee on Structural Safety, 2001.

[8] R. Caspeele, R. Steenbergen, and M. Sykora, *fib Bulletin 80: Partial factor methods for existing concrete structures*. Lausanne, 2016.

[9] P. Tanner, C. Lara, and R. Hingorani, “Structural Safety-a struggle with uncertainties,” *Hormigón y Acero*, vol. 58, no. 245, pp. 59–78, 2007.

[10] N. L. Tran and C.-A. Graubner, “Uncertainties of concrete parameters in shear capacity calculation of RC members without shear reinforcement,” 2018.

[11] JCSS, *Probabilistic Model Code Part 3- Resistance Models*. Joint Committee on Structural Safety, 2001.

[12] C. Caprani, M. Mayer, and K. e Siamphukdee, “Reliability analysis of a Super-T prestressed concrete girder at serviceability limit state to AS 5100:2017,” *Aust. J. Struct. Eng.*, vol. 18, no. 2, 2017.

[13] *fib*, *Fib Model Code for Concrete Structures 2010*. Lausanne: Ernst & Son, a Wiley brand, 2011.

[14] G. König and D. Hosser, “The simplified level II method and its application on the derivation of safety elements for level I.,” Paris, France, 1982.

YCRETS 2023
YOUNG CONCRETE RESEARCHERS, ENGINEERS & TECHNOLOGISTS SYMPOSIUM
CEMENT & CONCRETE SA

The development of a vermiculite based 3D printable fire-resistant concrete and an assessment of its fresh state and mechanical properties

Kyle B. Stebbing and Algurnon S. Van Rooyen

Stellenbosch University, Department of Civil Engineering, South Africa

Abstract

3D Printed Concrete (3DPC) is in the preliminary stages of implementation and is considered a large part of the 4th industrial revolution (4IR). Currently there is sparse 3DPC research focusing on insulation properties such as sound and heat. This research focuses on the development of a lightweight vermiculite-based fire-resistant 3DPC. Vermiculite is a mica-like mineral consisting of shiny porous flakes. The flaky structure results in vermiculite having high lubricating characteristics, allowing it to be used as a fire-resistant material. Various grades of vermiculite were tested resulting in the use of micron grade vermiculite for the 3DPC trial mixes. Fresh state tests were performed with the best mix having a mini-slump of 170mm and a dynamic shear reduction factor of 0.72. Mechanical tests resulted in a compressive strength of 4.88 MPa and a tensile strength of 0.56 MPa tested at 7 days.

Keywords: 3DPC, Expanded Vermiculite, 4IR, Fire-resistant

1. INTRODUCTION

The world is on the precipice of the 4th industrial revolution (4IR). The goal of 4IR is to create adaptive networks through the digitization of industrial processes. Implementing 4IR technology creates an environment in which mechanized automation operates and shares information without the need for human interaction, improving efficiency [1]. Although the construction industry would greatly benefit, it is still slow to implement these technologies. One of these 4IR technologies showing great potential is 3D printed concrete (3DPC) which offers benefits such as a substantial reduction in construction time, waste minimisation, lowered cost of elements compared to traditional construction methods and environmentally friendlier when recycled construction materials are used [2]. 3DPC technology holds the advantage over traditional concrete by not requiring formwork during construction. However, it requires complex rheological parameters making it notoriously difficult to develop.

Rheological parameters are paramount to successfully 3DPC and requires that thixotropy, constructability, printability and workability be considered. 3DPC mixes need to optimally balance these requirements to achieve success [3]. Thixotropy is the most important parameter and materials exhibiting thixotropy have the consistency of dough at rest and flows readily when energy is applied through perturbation, thus having a distinct difference

between dynamic and static yield stress. For 3D printing, the bottom layer requires a sufficiently developed static yield stress to maintain its shape and carry the weight of subsequent layers printed on top. The compressive stress in the bottom layer is directly proportional to the number and height of successive layers. When the compressive stress in the bottom layer exceeds the uniaxial yield stress, the layer will deform which leads to collapse [4]. Yield stress also directly relates to the pumping of concrete as pressure is applied to the concrete to facilitate flow. Only once the static yield stress is exceeded does the material start to flow, thereafter the dynamic yield stress is maintained. A low dynamic stress places less strain on the motor of the pump, while also reducing the chance of water separating from the mix. A high static yield stress results in a stiff concrete with better buildability, as it requires more energy to flow. By determining the dynamic shear reduction factor, the ratio of the average yield stress over the peak yield stress, an indication of the thixotropic nature of the concrete can be achieved. In general, the higher the factor the more thixotropic the material. Due to these factors, concrete with an optimal balance between high static and low dynamic yield stresses is required for effective 3DPC [3]. An indication of the printability of concrete can be found using the mini-slump test where researchers have reported successful 3D printable mixes in the slump range of 150 to 190 mm, dependent on the mix constituents [8].

Researchers developing 3DPC found that replacing large aggregates with finer material such as sands, clays, and lightweight aggregates (LWA) provided better rheological properties but required higher cement volumes, increasing cost. The use of finer material lead to excessive shrinkage and cracking, requiring shrinkage reducing admixtures and fibre reinforcement to be incorporated and the higher cost of cement is offset through the use of supplemental cementitious materials (SCM's) such as fly ash, silica fume limestone filler, and blast furnace slag are used [2].

To design a fire-resistant concrete the use of non-combustible thermal insulators is key. The primary focus is to obtain higher volumes of air-solid interfaces, low heat transfer and low radiation at high temperatures, which can be achieved by using porous materials [5]. LWA are porous in nature, therefore, their use could improve the thermomechanical behaviour of cementitious materials [6]. This research focuses on expanded vermiculite (EV) which is a mica-like mineral that consists of shiny porous flakes and is produced by heating raw vermiculite to 1000°C. The flaky structure results in high lubricating characteristics, allowing it to be used as a fire-resistant material and a lightweight filler for heat insulation [7]. EV's notable properties are a low thermal conductivity (0.04 – 0.14 W/m K), good sound absorption coefficient (0.7 – 0.8 at 1kHz), high melting point (1240 – 1430°C), non-toxic and chemically inert [7]. A study conducted on the high-temperature performance of self-compacting mortars (ScM) containing EV concluded that introducing EV showed a reduced loss of compressive strength at higher temperatures compared to the control ScM [5]. The use of EV in concrete increases porosity and sound insulation while decreasing the density, thermal conductivity, and mechanical strength [7]. However, the primary challenge of using EV in the mix is an increased water absorption rate due to the porous nature of EV, which affects the workability, open time and shrinkage of the concrete.

EV sees study as an addition to various concretes and shows a versatility in potential uses, however, there is no research coupling EV with 3DPC. Stellenbosch University (SU) developed a 3DPC mix that conforms to the rheological requirements necessary for 3DPC [3]. This paper aims to extend the existing body of knowledge by developing a lightweight 3D printable EV

concrete, based on the SU 3DPC mix, with potential practical applications in the fire safety sector. In this investigation, the absorption rates of the different grades of EV are tested. Mini-slump flow tests are conducted on mixes with unsaturated-, saturated-, and silane treated EV, to evaluate slump loss and find a solution to the absorption issue. Rheology, and early age mechanical tests (tensile- and compressive strength) are performed on the most viable mixes.

2. EXPERIMENTAL DESIGN

2.1 Experimental Programme Rationale

Materials used to fire-rate buildings are expensive. EV is currently used in various forms to protect against fire due to its low thermal conductivity. EV has been used in bricks, however, there is no research coupling EV with 3DPC. Developing a 3DPC containing EV could save costs used on protecting buildings from fire post-construction, by pre-fabricating or in-situ printing fire-rated EV concrete.

2.2 Mix Design

2.2.1 Materials

EV mixes were designed using CEM II 52.5N Portland cement with relative density of 3.14 as binder and fly ash (FA) and silica fume (SF), both with a relative density of 2.2 as cement extenders. For filler, silica sand with relative density 2.64 and maximum particle size of 0.3 mm and graded EV is used. Potable tap water is used for mixing and the superplasticiser (SP) CHRYSO®Fluid Premia 310 is used.

2.2.2 Mix design procedure

In this investigation the EV concrete mix designs are done based on conservation of mass and setting the total volume as 1000 litres. Table 1 gives the concrete mix compositions used in this investigation. Mix 1 enables a comparison between saturated and unsaturated EV, mix 2 determines the effectiveness of silane treated EV, mix 3 is the standard SU 3DPC mix [2] and mix 4 and 5 are based on mix 3.

Table 1: EV concrete mix compositions in kg per 1000 L

Mix	w/c	Cement	FA	SF	Sand	EV	Water	SP
1	0.7	357	-	-	771	27.7	250	-
2	0.5	412	-	-	165	82.4	206	-
3	0.45	579	165	83	1167	-	261	12.24
4	0.57	546	165	83	584	142	313	25.6
5	0.625	474	165	83	467	170	296	25.6

2.3 Experimental Testing

2.3.1 Sieve test

Sieve tests were performed on four different grades of EV according to BS EN 993 standards. The tests are performed using sieves of various sizes, a catching bowl and a vibratory machine. The sieves aperture sizes are 0.075 mm, 0.15 mm, 0.3 mm, 0.6 mm, 1.18 mm, 2.36 mm, and 4.75 mm. The sieves are weighed and stacked from smallest to largest aperture in the vibratory machine, 100g of vermiculite is placed on the 4.75 mm sieve and the

lid is placed on top. The vibratory machine is turned on for 10 minutes to allow enough time for the vermiculite to be accurately sieved. The sieves are weighed to determine the weight of the vermiculite retained.

2.3.2 EV absorption rates

Absorption rate tests of the fine-, superfine-, and micron grade EV were performed by submersing 400g of EV in water for 24hrs and measuring the weight gain. The increase in mass of the sample was recorded at intervals during the 24hr period. It was determined that the EV's absorptive properties would limit its use in 3DPC. To solve the absorption problem, trial mixes were performed with unsaturated, saturated and treated EV. The saturated EV was soaked in water and the treated EV was coated with a hydrophobic chemical. Relative densities were calculated from the mix designs as the pycnometer test proved unsuitable and gave inaccurate results.

2.3.2 Fresh state tests

The fresh state tests performed were mini-slump and rheology. The mini-slump is determined by placing a cone on a hydraulic turntable and filling the cone with the mix. The cone is removed and the handle is turned, raising and dropping the turntable. This is repeated 15 times after which the average diameter of the concrete is measured, indicating the flowability of the mix. This test is performed over 30 minutes at 15 minute intervals. Thereafter the rheology is tested using the German ICAR Rheometer. The rheometer is set up by inserting the vane and calibrating the rheometer. The bucket is filled with 20L of concrete, the rheometer is inserted and stress growth tests are performed. The test is run for 60s after which a rest period of 10s is observed and the test is then repeated. This process is repeated for rest periods of 30s, 60s, 90s, 120s, 10 mins, 20 mins and 30 mins. The rheometer test outputs applied torque readings which are used to determine the yield stress given as Equation 2.1.

$$T = \frac{\pi D^3}{2}\left(\frac{H}{D} + \frac{1}{3}\right)\tau \qquad \text{Equation 2.1}$$

Where T is the applied torque (Nm), D is the vane diameter (m), H is the vane height (m) and τ is the yield stress (Pa).

2.3.3 Mechanical tests

To test the mechanical properties of the mix, the concrete must be in a hardened state. This is achieved by casting the concrete into moulds and allowing it to cure for 24 hours. Once hardened it can be removed and cured for the desired duration. For this investigation 7-day strength was tested, the result of which is roughly 70% of the final strength. To determine the mechanical properties the concrete's compressive and tensile strength was tested using a Zwick/Roell Z250 materials testing machine. The machine applies force to the samples until failure and gives the maximum force they are able to withstand. The compressive stress test requires cubes to be crushed and the tensile strength test requires cylinders to be split. This testing process was done for 3 - 100x100x100mm cubes and 3 cylinders of each mix to obtain an average. The densities of the concrete mixes were calculated by measuring the weight of the samples, dividing it by the volume of the samples and taking the average.

3. RESULTS

3.1 EV Test Results

The sieve test results of the different grades of EV is presented in Figure 1. The 3D printer nozzle has a 4 mm aperture; therefore, the large grade cannot be used as it has a particle size of 8mm. The medium grade has a smooth S-curve grading which is close to the ideal Fuller curve [3], however, it would need to be sieved to remove the 5% of particles larger than 4.75 mm. The medium grade was removed from consideration as sieving would not be feasible for large scale use. As can be seen, the micron grade has the smoothest grading.

Figure 1: Sieve Analysis of EV Gradings

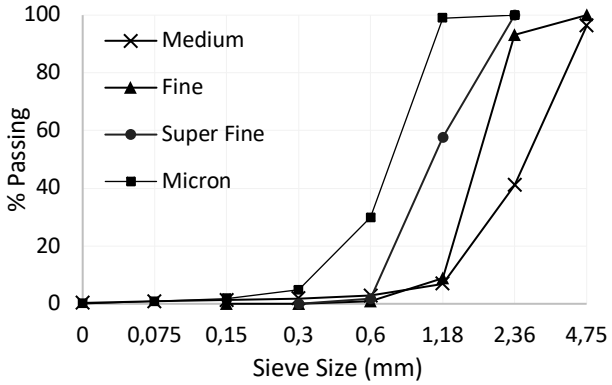

To achieve an improved S-curve grading for the filler, silica sand was combined with the micron vermiculite. The silica sand grading is shown in Figure 2 and the combined filler grading along with the ideal Fuller grading is shown in Figure 3.

Figure 2: Silica Sand Grading

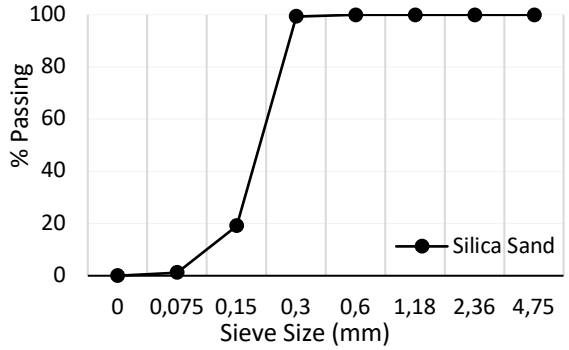

Figure 3: Combined Filler & Fuller

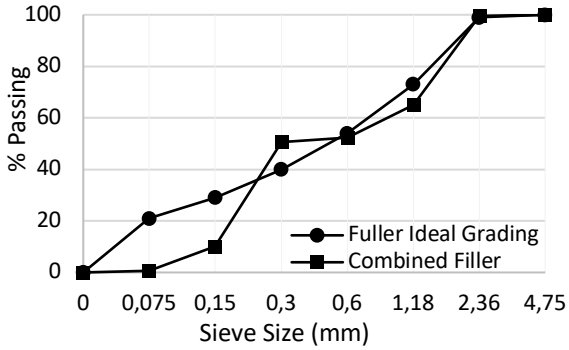

The relative density was determined to be 0.145, 1,11 and 0.644 for the unsaturated, saturated and treated vermiculite. Figure 4 shows the rate of absorption of the micron, superfine, and fine grade of EV. The micron grade absorbs the least amount of water, however, in its initial hour of submersion it soaks up the most water. This is likely due to the particles being smaller thereby allowing the EV to have more surface area in contact with the water. The smaller particles also mean less pores, therefore the micron EV soaks up the least

water. Based on these results along with the sieve analysis it was decided that the micron EV shows the most promise for incorporation into a 3DPC mix.

Figure 4: Comparative EV Absorption

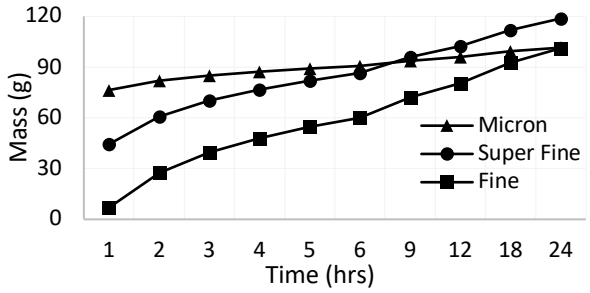

3.2 Fresh State Test Results

The results from the mini-slump tests, on the unsaturated-, saturated-, and silane treated EV mixes are shown in Figure 5. The additional water of the saturated EV affects workability of the mix. The mini-slump results show a rapid decrease in slump which is not ideal for 3DPC. It should be noted that as the EV becomes saturated it sinks, however, this process is not uniform and as such it is not possible to achieve partially saturated EV in this manner. The process to achieve fully saturated EV takes between 36 and 48 hrs. For these reasons as well as large scale reproducibility it was decided that this method of treatment is ineffective. The unsaturated EV has better mini-slump results, however, there is still a notable decrease in slump over time. Additionally, unsaturated EV soaks up the water, thereby not allowing the cement to hydrate effectively, as well as affecting the workability of the mix. Mix 2 was developed to determine the capabilities of treated EV. As can be seen the mini-slump remains constant which means the mix will not dry out, resulting in a mix that retains workability, consistency and cohesion over time.

Figure 5: Mini-Slump of EV Treatments

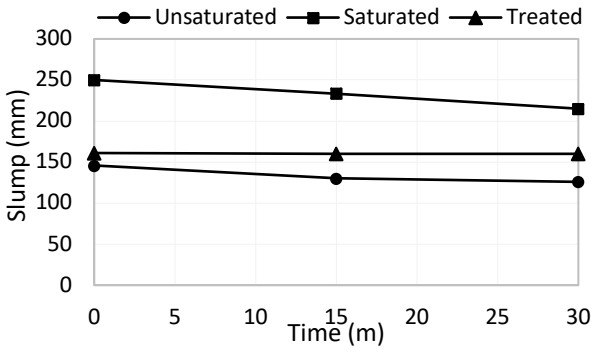

Mini-slump and rheology tests were performed on mix 4 and 5. They had a slump of 170 mm and 145 mm respectively. Mix 4 has better mini-slump results. Table 2 shows the stress growth test results. Both mixes demonstrate sufficient difference between their peak and minimum yield stresses to be good candidates for 3D printing. The average dynamic yield stress is taken between the rest periods of 30s and 120s and the peak yield stress is taken at

0s. Therefore the dynamic shear reduction factor is 0.72 and 0.65 for mix 4 and 5 respectively. Mix 4 would be considered to be more thixotropic. Mix 4 has a lower difference between the peak and minimum yield stress, most likely due to the higher slump.

Table 2: Peak and Minimum Yield Stresses Between Rest Periods

Rest Period (s)	0	10	30	60	90	120
Mix 4						
Peak Yield Stress (Pa)	1218	973	931	881	818	794
Min Yield Stress (Pa)	877	782	694	639	589	534
Mix 5						
Peak Yield Stress (Pa)	2589	1788	1739	1695	1640	1575
Min Yield Stress (Pa)	1663	1542	1444	1384	1320	1268

3.3 Mechanical Test Results

The mechanical test results of Mix 4 and Mix 5, conducted at an early age of 7 days, is presented in Table 3. Mix 5 has a compressive and tensile stress half of that which mix 4 exhibits, while only containing 10% more EV. Upon demoulding a few samples of Mix 5 crumbled confirming that the mix lacks cohesion and is inferior to mix 4. Mix 4 and 5 have a density of 1466 kg/m³ and 1318 kg/m³ respectively. Mix 4 was printed to test its 3DP capabilities, shown in Figure 6. Significant buildability was demonstrated with 27 - 10mm layers being printed before the process was halted due to bulging of the lower layers. This could be improved by a slight reduction in slump. Furthermore, fibres and a viscosity modifier should be incorporated to improve the cohesion of the mix.

Table 3: Average compressive- (σ_c) and average tensile stress (σ_T) in MPa of Mixes 4 and 5

Description.	Mix 4 σ_c	Mix 4 σ_T	Mix 5 σ_c	Mix 5 σ_T
Average	4.88	0.56	2.36	0.27
Std	0.217	0.067	0.165	0.053

Figure 6: Mix 4 3D printed.

4. CONCLUSION

In this investigation the development of a 3D printable lightweight EV-based fire-resistant concrete is reported. Sieve analyses and absorption rate tests of the eligible grades of EV were conducted. Mini-slump tests were performed to evaluate the printability and slump retention

of unsaturated-, saturated-, and silane treated EV concrete mixes. Finally, early age mechanical tests were done on the EV mixes developed and the best mix was printed. The following conclusions can be drawn:

- Sieve analyses results revealed that micron EV in combination with silica sand closely resembles the Fuller-Thompson curve, which is the ideal grading curve for 3DPC.
- Absorption tests show that micron EV had the steadiest absorption rate and that treated micron EV is best for incorporation in EV based 3DPC.
- Rheology and mini-slump tests showed both final mixes having thixotropic properties. However, the 50% EV mix showed superior fresh state properties over the 60% EV mix.
- A significant difference between the dynamic and static yield stress was noted for both viable mixes, indicating a high probability of printability.
- Mechanical test results showed that the 50% EV mix was far superior to the 60% EV mix, while only being 150kg/m³ denser.
- The 50% EV mix was printed and achieved 27 – 10mm layers.

In conclusion, silane treated micron EV showed the best results for including EV in 3DPC. The 50% EV mix showed improved fresh state and mechanical properties over the 60% EV mix and has great potential for 3D printable EV concrete. For mix improvement it is recommended that fibres and a viscosity modifier be incorporated to improve the cohesion and buildability.

5. REFERENCES

[1] Alaloul, W.S., Liew, M.S., Zawawi, N.A.W.A. and Kennedy, I.B., 2020. Industrial Revolution 4.0 in the construction industry: Challenges and opportunities for stakeholders. *Ain shams engineering journal*, *11*(1), pp.225-230.

[2] Souza, M.T., Ferreira, I.M., de Moraes, E.G., Senff, L. and de Oliveira, A.P.N., 2020. 3D printed concrete for large-scale buildings: An overview of rheology, printing parameters, chemical admixtures, reinforcements, and economic and environmental prospects. *Journal of Building Engineering*, *32*, p.101833.

[3] Kruger, P.J., 2019. Rheo-mechanics modelling of 3D concrete printing constructability (Doctoral dissertation, Stellenbosch: Stellenbosch University).

[4] Zhang, C., Hou, Z., Chen, C., Zhang, Y., Mechtcherine, V. and Sun, Z., 2019. Design of 3D printable concrete based on the relationship between flowability of cement paste and optimum aggregate content. Cement and Concrete Composites, 104, p.103406.

[5] Benli, A., Karatas, M. and Toprak, H.A., 2020. Mechanical characteristics of self-compacting mortars with raw and expanded vermiculite as partial cement replacement at elevated temperatures. Construction and Building Materials, 239, p.117895.

[6] Liu, J., Zhuge, Y., Ma, X., Liu, M., Liu, Y., Wu, X. and Xu, H., 2022. Physical and mechanical properties of expanded vermiculite (EV) embedded foam concrete subjected to elevated temperatures. *Case Studies in Construction Materials*, *16*, p.e01038.

[7] Rashad, A.M., 2016. Vermiculite as a construction material–A short guide for Civil Engineer. Construction and Building Materials, 125, pp.53-62.

[8] Tay, Y.W.D., Qian, Y. and Tan, M.J., 2019. Printability region for 3D concrete printing using slump and slump flow test. Composites Part B: Engineering, 174, p.106968.

YCRETS 2023
YOUNG CONCRETE RESEARCHERS, ENGINEERS & TECHNOLOGISTS SYMPOSIUM
CEMENT & CONCRETE SA

Optimising the mix design of earth blocks using recylced clay brick aggregate

Karel van Rooyen (1), Griffin Surendra (1) Janina P. Kanjee (1) and Ryan A. Bradley (1)

(1) School of Civil and Environmental Engineering, University of Witwatersrand

Abstract

This study focuses on the production of compressed stabilised earth blocks (CSEBs) incorporating waste in the form of crushed recycled masonry clay bricks. The primary aim is to optimise the mix design of earth blocks by improving the particle size distribution of the constituent soil. Herein, the effect of modifying a soil deficient in fine particles, i.e., a poorly graded soil, is considered. The earth blocks were produced with soil classified as SW (USCS), obtained from a construction site located on the premises of the University of Witwatersrand, Johannesburg. Waste clay bricks were obtained from a local demolition site and were, subsequently, crushed and separated according to particle size. The earth blocks were produced with a constant 5% cement, by mass, with different amounts of waste materials substituted for soil, i.e., crushed masonry brick incorporated at 20%, 30% and 40% by dry mass. The compressive strength, water absorption, and wetting and drying deformation tests were conducted after 28 days of curing to assess the performance of the earth blocks. In all cases, the addition of waste clay brick particles resulted in increased compressive strength of CSEBs. The optimum addition of waste material was observed at 30%, which yielded a compressive strength of 2.9 MPa. The water absorption and the wetting and drying deformations were only affected with waste additions in excess of 30% to the soil mixture. It can be concluded that incorporating recycled crushed masonry clay brick particles in the production of CSEBs resulted in an improvement of the soil grading as well as the mechanical properties of the units.

Keywords: Earth blocks, masonry clay bricks, construction waste, sustainability, recycling

1. INTRODUCTION

Addressing the insufficient availability and quality of affordable housing is a critical concern for the expanding population of South Africa. Utilising local soil and waste to produce good quality bricks is one low-cost solution that may help in tackling the problem. The South African state of waste report indicates that there are 55 million tonnes of waste in the country, with 8% coming from construction and demolition waste, amounting to roughly 4.4 million tonnes [1]. As more buildings are constructed and demolished due to industrialisation, waste materials such as clay masonry bricks are becoming more abundant. However, by finding uses for these materials, we can encourage better sustainability by reducing the amount of waste

in landfills [2]. This can be achieved by incorporating recycled construction waste into the production of new construction materials, thus reducing the demand for natural resources.

Compressed earth blocks are made from inorganic subsoil. These blocks can be made by mechanically compressing damp soil in a mould and then leaving them to air dry. Stabilisation with a chemical binder like Portland cement or lime can increase the strength and durability of the blocks and make them more water resistant [3].

This study aims to explore the potential of using recycled clay masonry brick aggregate in the production of earth blocks. To achieve this, the mix design of the soil is optimised by carefully considering the particle size distribution of the soil and adding recycled clay masonry bricks to fill the missing particle sizes, thereby creating a more well-graded soil. Through this process, we aim to investigate how modifying the soil grading affects the properties of the blocks. By using this approach, we can potentially contribute towards addressing the housing shortage in South Africa, while simultaneously promoting sustainability and reducing waste.

2. MATERIALS AND TEST METHODS

2.1 Characterisation of Inorganic Subsoil Used in Earth Blocks

Soil located more than 1 meter below the surface and free from organic materials was sourced from a construction site, located at The University of the Witwatersrand, for use in the production of earth blocks. The soil was sieved through an 8-10mm aperture size to remove large rocks and other unwanted debris, such as organic materials. A sieve analysis was then conducted according to SANS 1083 [4] to determine the particle size distribution and identify any missing particle sizes. The soil was also classified using the Unified Soil Classification System (USCS), and it was found to be SW, which is well-graded sands and gravelly sands with little or no fines.

Furthermore, the Atterberg limits of the soil were determined and are presented in Table 1. According to Burroughs [5], the most suitable soils for earth block production should have a plasticity index (PI) of less than 15%, sand content of less than 64%, and clay and silt content between 20% and 35%. Based on the broad criteria outlined by Burroughs [5], the soil obtained from the construction site is lacking in fines content but is otherwise suitable for the production of earth bricks.

Table 1: Soil characteristics of inorganic subsoil used in Earth Blocks

LL (%)	PL (%)	PI (%)	Fines (%)	Sand (%)	Gravel (%)	USCS
27	22	4	1	60	39	SW

2.2 Optimised Soil Grading Curve of Inorganic Subsoil Used in Earth Blocks

The soil grading was optimised by determining the maximum density grading using Equation 1 (which is the size cumulative distribution function). The resulting curves are plotted in Figure 1.

$$P(d) = \left(\frac{d}{d_{max}}\right)^{n} \quad (1)$$

Where: d = particle diameter being considered
d_{max} = maximum particle diameter in the mixture
n = exponent (0.33–0.5), which adjusts the curve for fineness or coarseness.

To optimise the particle size distribution of the soil, crushed clay masonry rubble bricks (CMRB) were added in varying proportions. This was done to adjust the particle distribution curve so that it would align as closely as possible with the optimisation Fuller curves. Specifically, the particle sizes between 1.18mm and 0.075mm were targeted for an increase, with proportions of 20%, 30%, and 40% of the total soil mass utilised.

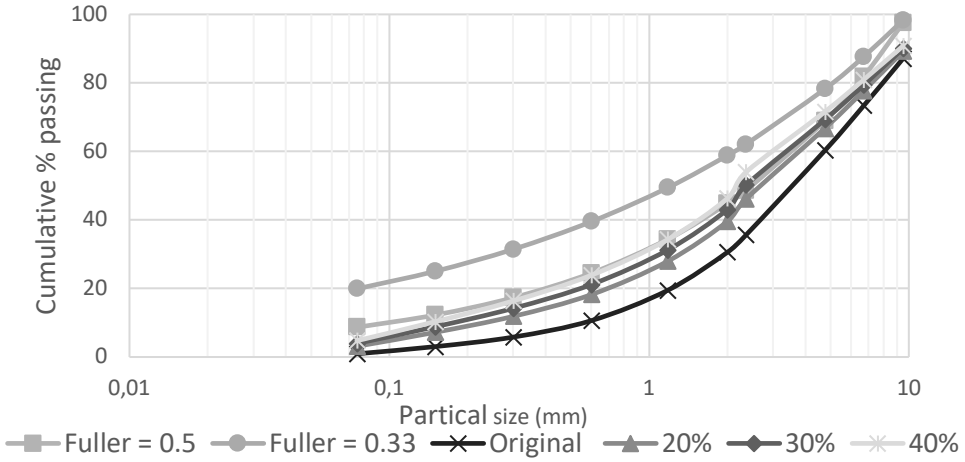

Figure 1: Optimised soil grading curves incorporating crushed clay masonry rubble bricks in proportions based on maximum density grading

2.3 Compressed Stabilised Earth Blocks (CSEB)

2.3.1 Clay masonry rubble bricks (CMRB) as fine particle addition in earth blocks

Recycled clay masonry rubble bricks were sourced from a local demolition site, crushed and used in the production of the earth blocks. Prior to crushing the bricks, excess mortar and paint (physical impurities) were removed from the CMRB using a hammer and chisel. The CMRB were then mechanically crushed to produce particle size varying from 1.18mm to the pan (<0.075mm).

2.3.2 Stabiliser used in the production of earth blocks

To bind the earth blocks, 42.5R Portland cement was used. Literature has shown an optimal cement content of 5 – 12%; however, a decision has been made to use the lowest amount of 5% as the overall objective is to reduce cost and be more sustainable.

2.3.3 Production of compressed stabilised earth blocks (CSEB)

Five different earth block mixes were investigated, and Table 2 provides a summary of the details of the mix design. Three earth blocks per mix were used for each test type to get an average result. To prepare the Earth block mixture, soil was mixed in a pan-mixer and water was subsequently added by sprinkling over the top to avoid “balling” of the material. The water content was determined to be 18%. For the production of each blocks, approximately

6kg of material was loaded into a Hydraform M7E380V block-making machine and pressed at 10MPa (or 100 bar) from the bottom up. A masonry unit with size 250×140×90 mm was adopted in the present study.

Table 2: Compressed stabilised earth blocks proportions

Mix no.	Label	Stabiliser	CMRB
Mix 1	0C0	0% Cement	0%
Mix 2	5C0	5% Cement	0%
Mix 3	5C20	5% Cement	20%
Mix 4	5C30	5% Cement	30%
Mix 5	5C40	5% Cement	40%

2.3.4 Curing of compressed stabilised earth blocks (CSEB)

The compressed stabilised earth blocks were moist cured by spraying water on them using a watering canister at the same time each day for 28 days.

2.4 Testing Approach

2.4.1 Compressive strength

The compressive strength of Compressed Stabilized Earth Blocks (CSEB) is a crucial mechanical characteristic that determines their suitability for construction. The compression strength test is the most widely used method for evaluating this parameter, as noted by Fetra [6]. Both the 28-day wet and dry compressive strength tests were performed. The blocks used for the wet compression test were submerged in water for 24-hours on 27th day of curing before being crushed. The blocks were loaded using a Amsler compression machine, which has a maximum loading capacity of 2 000 kN.

2.4.2 Water absorption

Measuring moisture content is critical, and the parameter is influenced by the clay and cement content in the soil. To determine the moisture content, the weights of the earth blocks were measured in their cured state at 28 days. Subsequently, the blocks were placed in an oven at 70°C for 24 hours to dry out, and were then allowed to stabilize for an hour before being weighed again. To evaluate the ability of the blocks to absorb water, the units were submerged in water for 24 hours, and any excess water was removed with a cloth before weighing. To ensure that accurate saturation conditions were achieved, the blocks were weighed within a minute of being removed from the water. Equation 2 was used to calculate the moisture content in both the cured and wet states.

$$Moisture\ content\ (\%) = \frac{(M_W - M_0)}{M_0} X\ 100 \quad (2)$$

Where: M_w - mass of the saturated block
M_o - mass of the oven dry block

2.4.3 Deformation

Wet and dry deformations are useful parameters because they reveal the extremities of dimensional changes under certain conditions. To measure dimensional deformation, both drying and wetting conditions were evaluated after 28 days. A digital vernier caliper was used to measure the length, width, and height of the blocks. For the drying shrinkage assessment, dimensional changes were recorded for the cured earth blocks at 28 days. The blocks were then placed in an oven at 70°C for 24 hours to dry out and were allowed to stabilize for an hour before being measured again.

To assess wetting shrinkage, the dimensional changes were measured after the dry earth blocks were submerged in water for 24 hours. The blocks were then removed from the water, excess water was removed with a cloth, and they were measured again. Equations 3 & 4 were used to calculate both wetting and drying deformations.

$$Wetting\ deformation = W - D \quad (3)$$

$$Drying\ deformation = D - W \quad (4)$$

Where: D - oven dry length
W - wet length
C - length in cured state

3. RESULTS AND DISCUSSION

3.1 Compressive Strength of Compressed Stabilised Earth Blocks

In general, the compressive strength is observed to be higher in dry specimens compared to the wet specimen. This results can be attributed to development of pore water pressure which decreases the contact forces between particles and also the effective stress in wet specimens. The largest reduction is strength, due to wetting, corresponds to the 5C40 specimens (Figure 3), which may be explained by the adsorptive nature of clay particles. This aspect is discussed further in section 3.2.

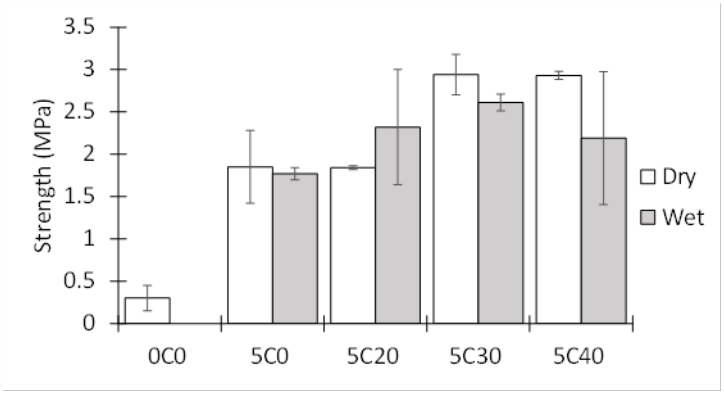

Figure 2: Compressive strength of compressed stabilised earth blocks incorporating 20%, 30% and 40% of the total soil mass as CMRB as fines aggregates at 28 days

From Figure 3, for the dry CSEBs, there is a drastic increase in compressive strength is observed from 0% cement to 5% cement being added. This is due to the hydration of Portland cement leading to the formation of calcium silicate hydrates particles, contributing to the hardening of the CSEB. Compared to the 5C0 mix there was a 0.01 MPa decrease, 1.09 MPa increase and 1.08 MPa increase for 5C20, 5C30 and 5C40 mixes respectively.

It is notable that there was no compressive strength recorded for 0% cement wet specimens as these specimens dissolved in the water baths due to there being no binder present. For the wet CSEBs, there is a gradual increase in compressive strength from 5% cement + soil to 30% waste addition and then a decrease in compressive strength of the 40% waste mixture. This observation indicates that the optimum percentage of CMRB to incorporate is 30% for both dry and wet blocks. There lies a discrepancy within the 5C20 specimen group as the wet compressive strength is higher than the dry strength, which is opposed to the expected trend observed for the other specimens. A larger sample size would better elucidate such discrepancies in future studies.

3.2 Water Absorption of Compressed Stabilised Earth Blocks

A general trend can be seen that the wet state blocks have a higher water content percentage than the cured state blocks due to them being submerged in water.

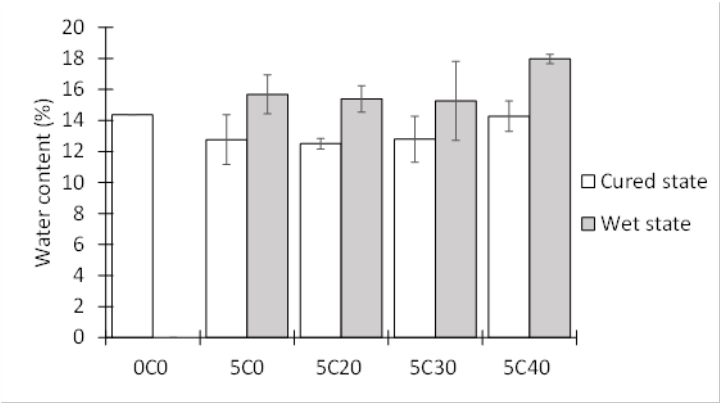

Figure 3: Water content % of compressed stabilised earth blocks incorporating 20%, 30% and 40% of the total soil mass as CMRB as fines aggregates at 28 days

The cured state blocks experienced no more than 2% change in water content when comparing the 5C20, 5C30 and 5C40 specimens to the 5C0 CMRB. For the wet state blocks, the water content percentage remained fairly constant for the first three 5% cement subgroups but increased by approximately 2% in water content for the 5C40 specimens. This shows that CMBR added between 20 and 30 % does not affect water absorption but is affected by adding waste in excess of 30%. This is possibly due to water being absorbed by the high amount of clay content from the clay masonry bricks added. Kesegic [7] noted the problem of using recycled clay bricks as an aggregate in concrete is that it has high water absorption. Zhu[8] agrees with this and noted that the porosity increased resulting in an increase in water absorption.

3.3 Deformation of Compressed Stabilised Earth Blocks

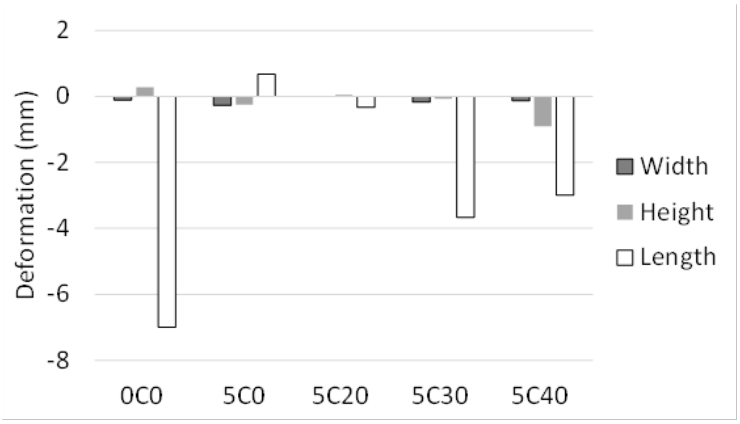

Figure 4: Drying deformation of compressed stabilised earth blocks incorporating 20%, 30% and 40% of the total soil mass as CMRB as fines aggregates at 28 days

There is a decrease in width, height and specifically the length for majority of the CSEBs for drying deformations with addition of CMRBs.

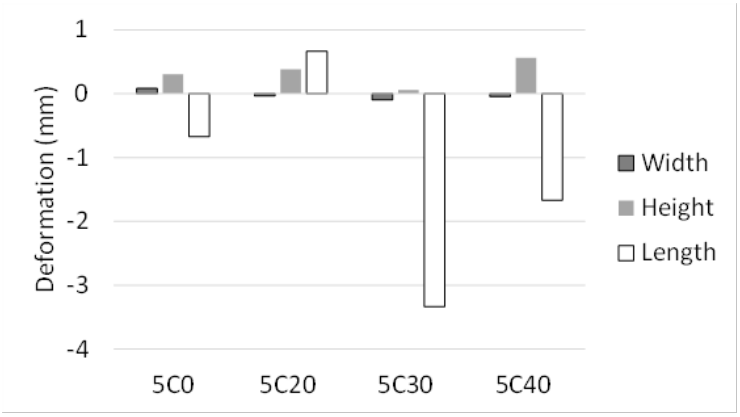

Figure 5: Wetting deformation of compressed stabilised earth blocks incorporating 20%, 30% and 40% of the total soil mass as CMRB as fines aggregates at 28 days

There is a decrease in length for bricks 5C30 and 5C40. A further investigation is needed to provide a clear and plausible explanation for these results.

4. CONCLUSIONS

This research project examined incorporating recycled CMRBs in the production of earth blocks. The mix design was optimised by giving attention to the particle size distribution of the soil. The effects of modifying the soil grading by adding recycled clay masonry bricks for the missing particle sizes forming a more well-graded soil were investigated. The properties tested include compressive strength, water absorption and deformation. The results are summarised below:

- There was an increase in compressive strength from the mixes containing CMRB compared to the mix with no CMRB addition. This is possibly due to the particle packing

theory being applied which increased the density and also due to the pozzolanic activity of the calcined clay brick powder. The optimum mixture for a 5% cement content earth block was found to be 30% of CMRB addition which yielded a compressive strength of 2.94 MPa: a roughly 50 % increase in strength over the control specimen.

- The CSEBs with 20% and 30% of CMRBs were not significantly affected by water absorption. The results, however, do show that water absorption and strength reduction were greatest for the 5C40 specimens. The results indicate possible durability issues with high concentration of CMRB replacement, which warrants further study.

In summary, the results suggest that recycled CMRB has the potential to be used as a constituent in optimising the mix design of compressed stabilised earth blocks, resulting in improved mechanical properties of the units. However, further testing is necessary to assess the long-term mechanical and durability properties of earth blocks incorporating CMRB.

REFERENCES

[1] Remade.co.za. (2022) [online] Available at: https://remade.co.za/wp-content/uploads/2020/01/South-Africa-State-of-Waste-Report.pdf [Accessed 15 March 2022].

[2] Batayneh, M., Marie, I. and Asi, I. (2007) Use of selected waste materials in concrete mixes. // Waste Management. pp 1870-1876. [online] Available at: Use of selected waste materials in concrete mixes – ScienceDirect

[3] Adam, E. and Agib, A. (2001) Compressed stabilised earth block manufacture in Sudan, UNESCO, Paris, France. [online] Available at: Compressed stabilised earth block manufacture in Sudan - UNESCO Digital Library

[4] SANS 1083:2006., 2006. Aggregate from natural sources. Aggregates for concrete, Pretoria: South African Bureau of Standards.

[5] Burroughs, S. (2008) Soil Property Criteria for Rammed Earth Stabilization. Journal of materials in civil engineering. Vol 20. Issue 3. pp 264-273. [online] Available at: Soil Property Criteria for Rammed Earth Stabilization | Request PDF (researchgate.net)

[6] Fetra, V.R., Ismail, A.R. and Ahmad M.A. (2010) A brief review of Compressed Stabilized Earth Brick (CSEB). 2010 International Conference on Science and Social Research (CSSR 2010), 2010, pp. 999-1004. [online] Available at: A brief review of Compressed Stabilized Earth Brick (CSEB) | IEEE Conference Publication | IEEE Xplore

[7] Kesegic, I., Netinger, I. and Bjegovic, D. (2008) Recycled clay brick as an aggregate for concrete: Overview. Technicki Vjesnik. Vol 15. Issue 3. pp 35-40. [online] Available at: (PDF) Recycled clay brick as an aggregate for concrete: Overview (researchgate.net)

[8] Zhu, L. and Zhu, Z. (2020) Reuse of Clay Brick Waste in Mortar and Concrete. [online] Hindawi. Available at: https://www.hindawi.com/journals/amse/2020/6326178/

YCRETS 2023
YOUNG CONCRETE RESEARCHERS, ENGINEERS & TECHNOLOGISTS SYMPOSIUM
CEMENT & CONCRETE SA

The effect of nanographene on conventional concrete using a variety of application techniques

Abraham E. van Wyk (1), Carla van Wyk (1) and Riaan Combrinck (1)

(1) Department of Civil Engineering, Stellenbosch University

Abstract

Nanographene was identified by Andre Geim and Konstantin Novoselov in 2004 and was labeled as a "wonder material". Nanographene applied to conventional concrete has shown potential to drastically improve concrete's mechanical performance. Although nanographene added to concrete has exceptional properties the practical application thereof has proven to be difficult. Thus, there is a notion in the concrete industry that this wonder material does not perform so wonderful in concrete. This study aims to address challenges relating to nanographene application in conventional concrete. This is done by treating conventional concrete ingredients with a variety of nanographene application techniques to improve its mechanical performance. This study concluded that nanographene does improve the mechanical performance of conventional concrete, but only for some of the application techniques. These applications techniques are described in detail in this study.

Keywords: Mechanical performance, Nanographene, Concrete, Application techniques

1. INTRODUCTION

Population growth and rapid urbanization have caused pressure on existing urban infrastructure. The pressure exhorted on urban infrastructure let to the demand for building and developments to escalate. These developments need durable, low cost, and accessible materials to implement solutions. Material compositions such as concrete are commonly used in the built environment because of its accessibility and high strength properties with regards to compression. Conventional concrete consists of four constituent materials namely water, sand, aggregate and cement [1]. The need for infrastructure development has brought forth a great demand for these constituent materials.

The demand for these materials brings a variety of benefits but also problems. Unfortunately, some of concrete's age-old problems is still to be resolved. Problems such as the negative effects cement has on the environment and concrete's weak tensile capabilities. For most of the time, steel is incorporated in concrete to improve concretes tensile capability. Both the cement and steel industries are energy hungry during production. These two industries contribute to 16% of the global carbon dioxide emissions released on an annual basis [2, 3]. Carbon dioxide (CO_2) is classified as the main accelerator in the greenhouse effect which drives global warming [3]. This is a tremendous obstacle for the cement and steel industry to overcome as more and more pressure is enforced to comply with Net Zero Emission by 2050. Thus, the need to reduce CO_2 emissions increases by the day.

This study focusses on potential solutions and application techniques that can reduce the CO_2 emissions released by the cement and steel industry. Globally the most cement and steel are used in the built environment [4, 5]. One of the key viable solutions would be to reduce the amount of cement and steel used. The majority of cement and steel used in the built environment is used in concrete structures [4, 5]. By drastically increasing the mechanical performance of concrete, the cement content and steel quantity used in concrete can be reduced. If the desired concrete performance can be achieved with less cement and less steel, the negative environmental impact can be greatly reduced.

Nanomaterials have opened new possibilities for concrete enhancement and alteration. Nanomaterials such as nanographene is a light and extremely strong material that can dramatically affect the mechanical performance of concrete [6]. Only a small amount is needed because of the particle size and large surface area of nanographene [7]. Although nanographene added to concrete has exceptional properties the practical application thereof is difficult. The dispersion of nanographene has proven to be the greatest challenge since the non-sixed graphene flakes flocculates and has hydrophobic tendencies. The dispersion of a nano particles in a cementitious matrix plays an important role to enhance its mechanical performance [8]. Johnson et al. [9] found that ultrasonication is a possible solution to disperse nanographene in a mixture. Sonication is a process in which sound energy is applied to a mixture to agitate the particles in the mixture and cause dispersion. Sonication is costly and not viable on large scale [9]. Thus, a more cost effective, commercially viable dispersion method was developed through high mechanical shearing.

A study by Van Wyk [10] identified which type of dispersion agents allows for the best dispersion of nanographene using mechanical shearing. Furthermore, attention was placed on how the degree of dispersion influenced the performance of concrete. Van Wyk assessed the influence the degree of the dispersion on the fresh properties, mechanical properties, and durability properties of concrete. Experimental analysis showed that a higher the degree of dispersion resulted in a positive enhancement of concrete's mechanical and durability performance.The combined dispersion action of a polymetric (Polycarboxylate Ether) and a surfactant (Lignosulfonate) admixture resulted in the highest degree of dispersion of nanographene. This led to superior mechanical and durability performance enhancement compared to the other tested admixtures. Unfortunately, van Wyk's research still did not improve the reference mixture. Thus, nanographene was seen as an expensive and ineffective addition to concrete.

Concrete is strong in compression but weak in tension [1]. One of the reasons for concrete being weak in tension is because of the weak interface bond between the aggregate and mortar [11, 12]. The Interfacial Transition Zone (ITZ) is where tensile failure of concrete occurs. Concrete is described as a heterogeneous material which means it is diverse in character and constituents [1]. Concrete is not uniform in composition due to the difference in stiffness of materials. Cement, water, and sand which is thoroughly blended forms mortar and can be described as a homogenous material [1]. When adding large aggregate or stone to mortar, concrete is formed [1]. Thus, when concrete forms the material transitions from a more homogenous state to a near heterogeneous state due to difference in stiffness between aggregate and mortar. The aggregate and mortar subsequently form a type of cold joint because of the difference in stiffness and composition. A cold joint is described as a difference in consistency between to materials which causes weak adhesion between materials [13]. Therefore, a weak bonding between aggregate and mortar transpires which causes concrete to mostly mechanically fail at the ITZ between the mortar and the stone.

This study aims to develop a variety of nanographene application techniques to improve the mechanical performance of conventional concrete by densifying the mortar matrix as well as the ITZ. Little to no research has been done on the majority of nanographene application techniques developed in this study.

2. EXPERIMENTAL FRAMEWORK

2.1 Nanographene Application Techniques

This study focusses on two mechanisms which can potentially improve the mechanical performance of conventional concrete using nanographene application techniques (NGAT). These two mechanisms are the densification of the mortar matrix and ITZ.

Three NGAT's were implemented to densify the mortar matrix. 1) Nanographene pre-dispersed in a superplasticiser (PCE_LIG_NG) and then added to fresh concrete. 2) Nanographene pre-dispersed in a super absorbent polymer (SAP_NG) and then added to fresh concrete. 3) Nanographene pre-dispersed in a grinding aid (GA) and used to treat cement (TC) with nanographene using a ball mill (TCGA_NG). The pre-dispersion time and intensity of the nanographene was determined by van Wyk's research [10]. A separate reference mixture without nanographene was mixed and tested for each of the three techniques to make results comparable. When nanographene is pre-dispersed in a solution or admixture, it is referred to as a nanographene dispersion agent (NGDA).

There were three NGAT's implemented to densify the ITZ. 1) Wet coating aggregate (WCA) with a NGDA and then use the nanographene coated aggregate to mix in the concrete. 2) Dry coating aggregate (DCA) without pre-dispersing the nanographene and then using the nanographene coated aggregate to mix in the concrete. 3) Wet coating aggregate with a nanographene dispersion agent (Tylose_NG) and then applying a thin material film to the surface of the aggregate. Figure 1-3 illustrates the experimental procedure of the NGAT, WCA_NG.

Figure 1: Pre-dispersion of NGDA (Tylose_NG)

Figure 2: Implementation of pre-dispersed NGDA

Figure 3 : Aggregate coated with pre-dispered NGDA

Three different material film approaches were used. The first approach was to apply a cementitious (WCAC_NG) film to the surface of the aggregate. The second approach was to apply a sand (WCAS_NG) film to the surface of the aggregate. The third approach was to apply a combined cementitious and sand (WCACS_NG) film to the surface of the aggregate.

The multi-particle coated aggregate was then used to mix in the concrete. The amount of material (cement, sand, or combined) that was used to apply the thin film to the surface of the aggregate was deducted from the base mix constituents. A separate reference mixture without nanographene was mixed and tested for the WCA technique to make results comparable.

2.2 Concrete Mix Design

Fifteen different mixtures were prepared in this study as shown in Table 1. Each mixture contained the same amount water, cement, sand, and stone. For the base mix, a water to cement ratio of 0.6, a target strength of 35MPa with a slump of 92.5mm were achieved.

A CEM II/A-L 52.5 N cement from Portland Cement (PPC) was used for all the mixes [14]. A coarse natural pit sand, known locally as Malmesbury sand, with a 13mm Greywacke coarse aggregate from Lafarge quarry in Eersterivier were used for all mixes. The relative density (RD) of the Malmesbury sand was 2.63, the fines modulus (FM) was 3.24, and the dust content (<0.075mm) was 4.6%. The nanographene was sourced from First Graphene Ltd. PUREGRAPH®50 and PUREGRAPH®50 AQUA was used for this study [15, 16]. A dosage of 0.07% of the cement weight was used based on recommendation from literature [17]. A dosage of 1% of the cement weight was used for the admixtures, solutions and grinding aids. CHRYSO ADA 25EL grinding aid (GA) was used as a NGDA to treat the cement. Tylose H 6000 YP2 (Hydroxyethyl cellulose) acts as a rheology and viscosity modifier and was used as a NGDA to wet coat the aggregate. The mixes that used an admixture (PCE_LIG) and Super Absorbent Polymer (SAP) was formulated from raw ingredients.

Table 1: Concrete mix constituents and proportions

		NGAT mix names						
Constituents (kg/m^3)	**REF**	**TCGA_NG**	**TC_NG**	**WCA_NG**	**DCA_NGF**	**DCA_NGA**	**PCE_LIG_NG**	**SAP_NG**
Water	209	209	209	209	209	209	209	209
Cement	348	348	348	348	348	348	348	348
Sand	911	911	911	911	911	911	911	911
Aggregate	900	900	900	900	900	900	900	900
Tylose	-	-	-	10,03	-	-	-	-
PCE_LIG	-	-	-	-	-	-	3,48	-
SAP	-	-	-	-	-	-	-	3,48
GA	-	3,48	-	-	-	-	-	-
PG®50	-	0,24	0,24	0,24	0,24	-	0,24	0,24
PG®50_AQUA	-	-	-	-	-	0,82	-	-

2.3 Tests

The slump test was determined in accordance with SANS 5861-1 (2006) and was used to measure the flowability of conventional concrete. At least two slump measurements were conducted, respectively.

The compressive strength of 100mm cubes were determined in accordance with SANS 6253 (2006). Four cubes per concrete mixture were tested after 7 days and on 28 days of curing in the water baths controlled at 23℃ temperature. The force (in Newton) applied at the time of failure was then recorded.

The tensile splitting capacity of 100mm cubes were determined in accordance with SANS 5863 (2006). Four cubes per concrete mixture were tested after 28 days of curing in the water baths. A constant stress of 0.03 ±0.01MPa/s was applied up until the point of failure. Equation 1 illustrates the tensile splitting capacity (MPa) calculated using F, force at failure (N), and a, cube width (mm).

$$f_{cu} = \frac{2F}{\pi a^2} \quad (1)$$

3. RESULTS AND DISCUSSION

Table 2 shows the slump measurements after mixing as well as the compressive strength, and tensile splitting capacity of all fifteen mixes at 7 days and 28 days of curing. Each application technique is compared to its respected reference mix as illustrated in Table 2.

The slump results indicated a decrease in flowability when PUREGRAPH®50 (flake) was not pre-dispersed and used in concrete. There was a slight decrease in flowability when the PUREGRAPH®50 AQUA (agglomerate) was used in concrete. The slump results indicate that the flowability remains similar when nanographene was pre-dispersed in an admixture or solution and then added to concrete.

The application techniques, DCA_NGF and DCA_NGA, indicated a 25mm and 5mm decrease in flowability, respectively. DCA_NGF and DCA_NGA increased the compressive strength after 7 days of curing with 2.6% and 3.1% respectively and by 4.3% and 2.8% after 28 days of curing respectively. DCA_NGF indicated a decrease of 9.9% in the tensile splitting capacity while DCA_NGA indicated an increase of 11,4% in the tensile splitting capacity after 28 days of curing. Deflection measurements from the tensile splitting test for DCA_NGF and DCA_NGA was 1,01mm and 0,82mm respectively.

The application techniques, TCGA_NG, WCA_NG and WCACS_NG, indicated a 15mm, 17,5mm and 50mm increase in flowability, respectively. TCGA_NG, WCA_NG and WCACS_NG decreased the compressive strength after 7 days of curing with 8.5%, 15.8% and 16.2% respectively and by 5.5%, 4.2% and 9.1% respectively after 28 days of curing. TCGA_NG decreased the tensile splitting capacity by 22.0% while WCA_NG and WCACS_NG indicated an increase of 2,9% and 4.8% respectively after 28 days of curing. Deflection measurements from the tensile splitting for TCGA_NG, WCA_NG and WCACS_NG was 0,74mm, 0,82mm and 0,79mm respectively.

The application techniques, WCAC_NG and WCAS_NG, indicated a 27.5mm and 15mm decrease in flowability, respectively. WCAC_NG and WCAS_NG increased the compressive strength after 7 days of curing with 6.5% and 2.8% respectively and by 4.0% and 5.4% respectively after 28 days of curing. WCAC_NG and WCAS_NG increased the tensile splitting capacity after 28 days of curing with 15,0% and 13,1% respectively. Deflection measurements from the tensile splitting test for WCAC_NG and WCAS_NG was 0,78mm and 0,84mm respectively.

The application techniques, PCE_LIG_NG and SAP_NG, indicated a 5mm increase and 5mm decrease in flowability, respectively. PCE_LIG_NG and SAP_NG decreased the compressive strength after 7 days of curing with 3,3% and 4,2% respectively, but increased the compressive strength after 28 days of curing with 8,2% and 3,4% respectively. Both PCE_LIG_NG and SAP_NG indicated a decrease of 0,7% in the tensile splitting capacity after 28 days of curing. Deflection measurements from the tensile splitting test for PCE_LIG_NG and SAP_NG was 0,81mm and 0,91mm respectively.

Table 2: Flowability, compression, and tensile results

	Flowability	Compression				Tensile		
Mix	Slump (mm)	7-Days (kN)	%>OR<	28-Days (kN)	%>OR<	28-Days (kN)	Deflect (mm)	%>OR<
REF_MIX	92,5	300,90	Ref	352,70	Ref	2,63	0,81	Ref
DCA_NGF	67,5	308,80	2,6%	368,50	4,3%	2,37	1,01	-9,90%
DCA_NGA	87,5	310,10	3,1%	362,60	2,8%	2,93	0,82	11,40%
TC_NGF	65	311,20	3,4%	374,50	6,2%	2,68	0,82	1,90%
TCGA_REF	107,5	341,70	Ref	370,60	Ref	2,73	0,73	Ref
TCGA_NG	122,5	312,50	-8,5%	350,10	-5,5%	2,13	0,74	-22,00%
WCA_REF	87,5	294,50	Ref	332,80	Ref	2,38	0,82	Ref
WCA_NG	105,0	248,10	-15,8%	318,90	-4,2%	2,45	0,75	2,90%
WCACS_NG	137,5	246,70	-16,2%	302,40	-9,1%	2,50	0,79	4,80%
WCAC_NG	115,0	313,70	6,5%	346,10	4,0%	2,74	0,78	15,00%
WCAS_NG	72,5	302,80	2,8%	350,80	5,4%	2,69	0,84	13,10%
PCE_LIG_REF	165,0	342,60	Ref	399,00	Ref	2,86	0,74	Ref
PCE_LIG_NG	170,0	331,40	-3,3%	366,40	-8,2%	2,88	0,81	0,70%
SAP_REF	85,0	367,30	Ref	417,00	Ref	2,61	0,81	Ref
SAP Ref_NG	80,0	382,60	4,2%	431,20	3,4%	2,63	0,91	0,70%

The application techniques, TC_NGF and DCA_NGA, prove to facilitate the best overall improvement in mechanical performance of conventional concrete. This improvement is visible in the 28 day compressive strength and tensile splitting capacity results. The application technique where cement was treated with nanographene in flake form (TC_NGF) showed the best improvement in compressive strength with an increase of 6,2%. It is known that finer materials (<0,075mm) such as ground limestone, slag and fly ash fill pours and voids in concrete, resulting in increased strength [1]. Thus, nanographene flake is believed to have had the same effect and facilitated the densification of the mortar matrix which enhanced the compression performance of the concrete.

The application technique where the surface of the aggregate was dry coated with nanographene in aqua form (DCA_NGA), showed the best improvement in tensile splitting capacity with an increase of 11,4%. It is believed that the increase is due to a high coating efficiency the agglomerated nanographene had on the surface of the aggregate. This high coating efficiency is facilitated by a smearing action caused by the agglomerated nanographene. It is believed that this smearing action also enhances the ability of the nanographene to remain on the surface of the aggregate when introduced into a robust mixing environment. This allows for the nanographene to densify the ITZ and not be diluted into the mortar paste. Therefore, the nanographene is focussed at the ITZ and enhances the tensile splitting capacity of conventional concrete.

Several application techniques as shown in Table 2 drastically decreased the mechanical performance of conventional concrete. The results indicate that a major decrease in mechanical performance occurred when nanographene was pre-dispersed (TCGA_NG, WCA_NG and WCACS_NG) in a dispersion agent. It is believed that the viscosity and the chemical composition of the dispersion agent does influence the degree of dispersion. The degree of dispersion relates to how long nano particles remain in suspension after separation through dispersion methods. The goal is to separate the nanographene from each other and keep the particles in suspension before adding to concrete. Van Wyk proved that the higher the degree of dispersion, the higher the higher the mechanical performance of conventional concrete [10]. Therefore, more research needs to be done on the factors that influences the application of nanographene pre-dispersed in a dispersion agent.

Only a few application techniques improved the mechanical performance beyond the performance of the base mix (REF_MIX). Figure 1 shows the percentage improvement in mechanical performance when NGAT's implemented are compared to the base mix (Ref mix). The results indicate that a specific application technique, DCA_NGA, showed a small improvement in the compression performance and a significant improvement tensile performance of conventional concrete. Therefore, DCA_NGA can be used specifically to densify the ITZ and improve the tensile performance of conventional concrete.

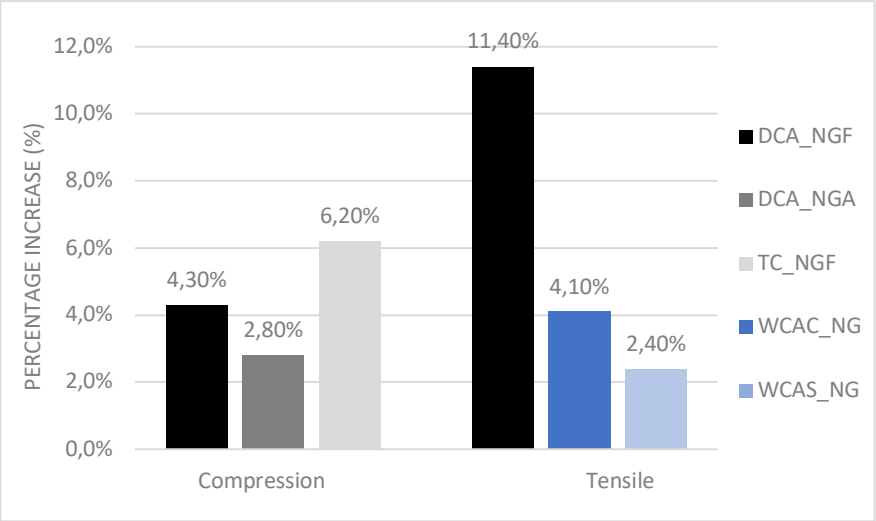

Figure 1: Percentage Increase in mechanical performance compared to the base mix (REF_MIX)

4. CONCLUSIONS

The main conclusions from this study are as follows:

- There are indications that when nanographene is not pre-dispersed in a dispersion agent, the flowability of the concrete decreases. Rheology testing needs to be done to confirm this phenomenon.
- Conventional admixtures and solutions increase the compression performance of conventional concrete far greater than nanographene. Although it should be kept in mind that the admixtures were added at dosages more than 100 times that of the nanographene.
- There is more research to be done on the factors that have an impact on the application of nanographene pre-dispersed in a dispersion agent. This includes the dosage of nanographene used.
- Nanographene improved the tensile performance of almost every concrete mix compared to its respected reference mix.
- The nanographene application technique (NGAT), DCA_NGA, slightly improved the compression performance of conventional concrete. It outperformed all other concrete mixes with respect to tensile performance. Thus, this NGAT is seen as a viable option to improve the mechanical performance of conventional concrete, especially in tension.

The application of nanographene in concrete remains challenging and more research needs to be done before it can be applied to the construction industry. Several application

techniques in this study shows promise. More research on especially the impact these nanographene application techniques has on the rheology and durability of the concrete is needed.

ACKNOWLEDGEMENTS

The following people are acknowledge for their support during this study. Barry Jollife, for introducing the world of Nanographene and supplying the nanographene and raw chemicals. Concrete and admixture specialists, Darius Herbs and Alexander Smith from Nanoproof. Paul Botha from Fine Bubble Technologies (Pty).

REFERENCES

[1] Alexander, K.M., Wardlow, J. and Gilbert, D., "*Fulton's concrete technology TENTH EDITION", 2021*. Cement & Concrete SA.
[2] McKinsey & Company, 2020. *Decarbonization challenge for steel Hydrogen as a solution in Europe*.
[3] Badel, A. et al., "Concrete needs to lose its colossal carbon footprint. *Nature", 2021.* Volume 597, pp. 593-594
[4] IEA, *Cement*, 2022. http://www.Cement – Analysis - IEA/ [Accessed 07 April 2023].
[5] WSA, 2023. *Steel in building and Infrustructure*. http://www.Buildings and infrastructure - worldsteel.org/ [Accessed 07 April 2023].
[6] T. S. Qureshi and D. K. Panesar, "Nano reinforced cement paste composite with functionalized graphene and pristine graphene nanoplatelets," *Compos B Eng*, vol. 197, Sep. 2020, doi: 10.1016/j.compositesb.2020.108063.
[7] P. Demo, A. Sveshnikov, Š. Hošková, D. Ladman, and P. Tichá, "Physical and Chemical Aspects of the Nucleation of Cement-Based Materials," 2012.
[8] A. H. Korayem, N. Tourani, M. Zakertabrizi, A. M. Sabziparvar, and W. H. Duan, "A review of dispersion of nanoparticles in cementitious matrices: Nanoparticle geometry perspective," *Construction and Building Materials*, vol. 153. Elsevier Ltd, pp. 346–357, Oct. 30, 2017. doi: 10.1016/j.conbuildmat.2017.06.164.
[9] D. W. Johnson, B. P. Dobson, and K. S. Coleman, "A manufacturing perspective on graphene dispersions," *Current Opinion in Colloid and Interface Science*, vol. 20, no. 5–6. Elsevier Ltd, pp. 367–382, Oct. 01, 2015. doi: 10.1016/j.cocis.2015.11.004.
[10] C. Van Wyk, "Nanographane dispersed in admixtures to enhance concrete performance" Final year project, Stellenbosch University, 2022.
[11] R. Liu, H. Xiao, J. Liu, S. Guo, and Y. Pei, "Improving the microstructure of ITZ and reducing the permeability of concrete with various water/cement ratios using nano-silica," *J Mater Sci*, vol. 54, no. 1, pp. 444–456, Jan. 2019, doi: 10.1007/s10853-018-2872-5.
[12] V. Nežerka, P. Bílý, V. Hrbek, and J. Fládr, "Impact of silica fume, fly ash, and metakaolin on the thickness and strength of the ITZ in concrete," *Cem Concr Compos*, vol. 103, pp. 252–262, Oct. 2019, doi: 10.1016/j.cemconcomp.2019.05.012.
[13] İ. Bekem Kara, "Experimental Investigation of the Effect of Cold Joint on Strength and Durability of Concrete," *Arab J Sci Eng*, vol. 46, no. 11, pp. 10397–10408, Nov. 2021, doi: 10.1007/s13369-021-05400-5.
[14] PPC Limited, "PPC Limited," *PPC Limited*, 2023. https://www.ppc.africa/ [Accessed 09 Feb 2023].
[15] First Graphene Ltd, *PureGRAPH-datasheet_v1-02, 2021*. http://www.PureGRAPH-datasheet_v1-02.pdf (firstgraphene.net)/[Accessed 07 April 2023].
[16] V. D. Ho, T. G. Tg, T. Ozbakkaloglu, A. Goodwin, C. McGurkin, R. U. Karunagaran, D. Losic., "Investigating the reinforcing mechanism and optimized dosage of pristine graphene for enhancing mechanical strengths of cementitious composites," *RSC Adv*, vol. 10, no. 70, pp. 42777–42789, Nov. 2020, doi: 10.1039/d0ra07639b.

Clear vision is essential for environmentally responsible practices.

Become a member – be part of the future

CEMENT & CONCRETE SA

www.cemcon-sa.org.za